Vol. 299, No. 2, December 30, 1994 ISSN 0003-2670

ANALYTICA CHIMICA ACTA

An international journal devoted to all branches of analytical chemistry

ELSEVIER

ANALYTICA CHIMICA ACTA

Scope. *Analytica Chimica Acta* publishes original papers, rapid publication letters and reviews dealing with every aspect of modern analytical chemistry. Reviews are normally written by invitation of the editors, who welcome suggestions for subjects. Letters can be published within **four months** of submission. For information on the Letters section, see inside back cover.

Submission of Papers

Americas

Prof. Harry L. Pardue
Department of Chemistry
1393 BRWN Bldg, Purdue University
West Lafayette, IN 47907–1393
USA

Tel:(+1-317) 494 5320
Fax:(+1-317) 496 1200

Computer Techniques

Prof. J.T. Clerc
Universität Bern
Pharmazeutisches Institut
Baltzerstrasse 5, CH-3012 Bern
Switzerland

Tel:(+41-31) 6314191
Fax:(+41-31) 6314198

Prof. Sarah C. Rutan
Department of Chemistry
Virginia Commonwealth University
P.O. Box 2006
Richmond, VA 23284-2006
USA
Tel:(+1-804) 367 7517
Fax:(+1-804) 367 8599

Other Papers

Prof. Alan Townshend
Department of Chemistry
The University
Hull HU6 7RX
Great Britain

Tel:(+44-482) 465027
Fax:(+44-482) 466410

Prof. Willem E. van der Linden
Laboratory for Chemical Analysis
Department of Chemical Technology
Twente University of Technology
P.O. Box 217, 7500 AE Enschede
The Netherlands
Tel:(+31-53) 892629
Fax:(+31-53) 356024

Prof. Paul Worsfold
Dept. of Environmental Sciences
University of Plymouth
Plymouth PL4 8AA
Great Britain

Tel:(+44-752) 233006
Fax:(+44-752) 233009

Submission of an article is understood to imply that the article is original and unpublished and is not being considered for publication elsewhere. *Anal. Chim. Acta* accepts papers in English only. There are no page charges. Manuscripts should conform in layout and style to the papers published in this issue. See inside back cover for "Information for Authors".

Publication. *Analytica Chimica Acta* appears in 18 volumes in 1995 (Vols. 297–314). *Vibrational Spectroscopy* appears in 2 volumes in 1995 (Vols. 8 and 9). Subscriptions are accepted on a prepaid basis only, unless different terms have been previously agreed upon. It is possible to order a combined subscription (*Anal. Chim. Acta* **and** *Vib. Spectrosc.*).
Our p.p.h. (postage, packing and handling) charge includes surface delivery of all issues, except to subscribers in the U.S.A., Canada, Australia, New Zealand, China, India, Israel, South Africa, Malaysia, Thailand, Singapore, South Korea, Taiwan, Pakistan, Hong Kong, Brazil, Argentina and Mexico, who receive all issues by air delivery (S.A.L.–Surface Air Lifted) at no extra cost. For Japan, air delivery requires 25% additional charge of the normal postage and handling charge; for all other countries airmail and S.A.L. charges are available upon request.

Subscription orders. Subscription prices are available upon request from the publisher. Subscription orders can be entered only by calendar year and should be sent to: Elsevier Science B.V., Journals Department, P.O. Box 211, 1000 AE Amsterdam, The Netherlands. Tel: (+31-20) 4853 642, Telex: 18582, Telefax: (+31-20) 4853 598, to which requests for sample copies can also be sent. Claims for issues not received should be made within six months of publication of the issues. If not they cannot be honoured free of charge. Readers in the U.S.A. and Canada can contact the following address: Elsevier Science Inc., Journal Information Center, 655 Avenue of the Americas, New York, NY 10010, U.S.A. Tel: (+1-212) 633 3750, Telefax: (+1-212) 633 3990, for further information, or a free sample copy of this or any other Elsevier Science journal.
Advertisements. Advertisement rates are available from the publisher on request.

US mailing notice – Analytica Chimica Acta (ISSN 0003-2670) is published 3 times a month (total 54 issues) by Elsevier Science B.V. (Molenwerf 1, Postbus 211, 1000 AE Amsterdam). Annual subscription price in the USA US$ 3677.75 (valid in North, Central and South America), including air speed delivery. Second class postage paid at Jamaica, NY 11431. *USA Postmasters*: Send address changes to Anal. Chim. Acta, Publications Expediting, Inc., 200 Meacham Av., Elmont, NY 11003. Airfreight and mailing in the USA by Publication Expediting.

ANALYTICA CHIMICA ACTA

An international journal devoted to all branches of analytical chemistry

(Full texts are incorporated in CJELSEVIER, a file in the Chemical Journals Online database available on STN International; Abstracted, indexed in: Aluminum Abstracts; Anal. Abstr.; Biol. Abstr.; BIOSIS; Chem. Abstr.; Curr. Contents Phys. Chem. Earth Sci.; Engineered Materials Abstracts; Excerpta Medica; Index Med.; Life Sci.; Mass Spectrom. Bull.; Material Business Alerts; Metals Abstracts; Sci. Citation Index)

VOL. 299 NO. 2 CONTENTS DECEMBER 30, 1994

(Continued overleaf)

Contents (continued)

ELSEVIER

Analytica Chimica Acta 299 (1994) 145–163

ANALYTICA CHIMICA ACTA

A potentiometric iodide (and other) ion sensor based on a conducting polymer film electrode Part II. effect of electrode conditioning and regeneration techniques

Ahmed Galal [a], Z. Wang [1,b], A.E. Karagözler [b], Hans Zimmer [b], Harry B. Mark, Jr. [b,*], Paul L. Bishop [c]

[a] *Department of Chemistry, College of Science, University of Cairo, Giza, Egypt*
[b] *University of Cincinnati, Department of Chemistry, Cincinnati, OH 45221-0172, USA*
[c] *University of Cincinnati, Department of Civil and Environmental Engineering, Cincinnati, OH 45221-0071, USA*

Received 14 April 1994; revised manuscript received 26 July 1994

Abstract

A novel potentiometric halide sensor electrode for iodide, based on the entrapment of iodide/iodine/triiodide into a poly(3-methylthiophene) conducting polymer, had previously been developed using a potentiostatic technique for film formation. The effect of film thickness (with the film thickness controlled by the amount of charge passing in the electrolytic cell during the polymerization) has been studied. Also, the effects of various pre- and postconditioning parameters on the electrode performance and life time were examined and compared. The life time of the electrode was extended up to one year by storing its sensing tip in a newly designed cap. The cap consisted of two chambers linked with a special orifice; the first contained iodine adsorbed on silica or alumina and the second housed the electrode tip. The linear dynamic range of the new sensor electrode was 1×10^{-7}–5×10^{-1} M iodide and the detection limit was 1×10^{-8} M iodide. The working temperature range, response time and working pH range of the electrode are 0–50°C, 17–20 s and 2–11, respectively. The potential for bromide, chloride, and sulfite selective electrodes based on these conducting polymer films are also presented and compared to those obtained for iodide. Moreover, the effect of changing the type of conducting polymer using poly(3-methylthiophene), poly(*N*-methylpyrrole) or poly(aniline) are given and compared.

Keywords: Sensors; Potentiometry; Halide selective electrodes; Conducting polymers

1. Introduction

Studies of the electrochemical behavior of electrodes modified with polymeric materials are one of the most rapidly growing and advancing areas of modern electrochemistry. The behavior of electrodes modified with conducting poly(thiophene) films have also been of great interest [1]. This is due to both the stability of poly(thiophene) films produced electrochemically and to their interesting electrochromic and conducting properties. The selective response of this class of polymers towards dissolved ions has made them useful in

* Corresponding author.

[1] Present address: Hebei Institute of Light Industry and Chemical Engineering, Shijiazhuang China.

SSDI 0003-2670(94)00333-5

various applications as a new "generation" of ion sensors. Ohnuki et al. [2] reported that selective film permeation of H^+, Br^-, and Fe^{2+} was observed in some polymer coated electrodes. Poly(o-phenylenediamine) coated electrodes were also applied in voltammetric [3] and pH measurements [4]. The "unique" advantage of the electrochemical synthesis of the polymer films is that this procedure leads directly to the conductive polymers in a single-step process. Moreover, electrosynthesis of polymers also results in a "self-doped" film which incorporates a supporting electrolyte ion into the polymer [5]. The property of doping of the conducting polymers can be exploited in various ways from an analytical chemistry application point of view. For example, a polymer can be doped with an electroactive substance, which subsequently attains a thermodynamic equilibrium between the doping species and one in solution phase, forming the basis of a selective potentiometric electrode system. However, actual applications using these particular conducting polymers, such as poly(methylthiophene), poly(*N*-methylpyrrole) and poly(aniline), is rather limited [6].

The selective potentiometric response for chloride [6a] and perchlorate [6b] ions using poly(pyrrole), and for the selective response to iodide ion [6d] based on poly(*N*,*N*-dimethylaniline/poly(*o*-chloroaniline) dual-layer coated conducting film electrodes, are among the few studies cited in the literature on the application of conducting polymers in potentiometry. Our group has been studying [7] the electrosynthesis [7a–d,f–i], spectroscopic characterization [7e] and application [7l–q] of some conducting polymers.

In a previous work [7o], we reported the construction and properties of an iodide-selective electrode based on a poly(3-methylthiophene) conducting polymer film. This electrode suffered from short life times, up to a maximum of fifteen days, but possessed a relatively high selectivity coefficients towards most interfering anions. Also, some technical data, such as film thickness, working temperature range, etc. were not reported. In this study, we also introduce the design of a new cap for the storage of this electrode which resulted in extending its life time to more than a year. In addition, more data for this electrode concerning preparative and operating conditions are presented. The effect of changing the type of the conducting polymer used in the fabrication of this type of I^--selective electrode is given and the responses are compared. Moreover, the efforts towards the fabrication of electrode sensors for other anions are discussed.

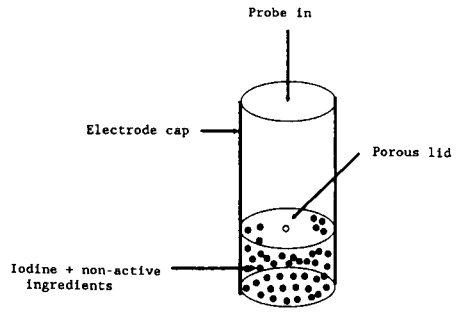

Fig. 1. Design of cap used for the activation/preservation of the iodide selective electrode.

2. Experimental

2.1. Electrode construction

The fabrication of the electrode has been described previously [7o]. Fig. 1 shows a schematic diagram of the "storage" cap used for the electrode preservation. Electrochemical polymerizations were carried out with a three electrode cell where the working electrode was graphite of 2.544 cm^2 apparent surface area (Model Paroz-series 2003 Gr A 91EE075, AMP Inc., Cincinnati, OH). All the potentials in the polymerization and other measurements were referenced to an Ag/AgCl (3 M KCl) electrode. The auxiliary electrode was a $2 \times 2\ cm^2$ or a $4 \times 4.2\ cm^2$ platinum sheet. All the sensor electrodes were pretreated prior to the electropolymerization step as follows: The electrode was mechanically polished using metallurgical papers of successive grades 600 to 1200, and then the surface was treated by rubbing with filter paper, and finally with a fine tissue paper using an alumina/water suspension (10 μm) until no visible scratches were observed. Prior to immersion in the cell, the electrode was rinsed with distilled water, dried, and then thoroughly "degreased" in methanol. Finally, the electrode was rinsed with conductivity water, the solvent employed in the electropolymerization experiment, dried, and immediately put to use.

2.2. Electrolytic cells

All electrochemical measurements were performed in a conventional 100-ml flat bottom (Pyrex) glass cell which was fitted with five ground glass joints.

2.3. Chemicals and solvents

Tetrabutylammonium tetrafluoroborate (Aldrich, Milwaukee, WI), tetraethylammonium (Sigma, St. Louis, MO), hexylammonium tetrafluoroborate (Southwest Analytical Chemicals, Austin, TX), and lithium tetrafluoroborate, hexafluorophosphate, perchlorate, trifluoromethane sulfonate (Sigma) were used as supplied except for those experiments where samples were prepared for elemental or ESCA analyses. In such cases, the aforementioned electrolytic salts were recrystallized from a methanol/water mixture. Potassium and sodium salts of chloride, bromide, iodide, nitrate and sulfite (Aldrich) were used as supplied. All other salts, buffer solutions, HPLC-grade solvents, and reagents were purchased from Fisher Scientific. However, solvents used in the electropolymerization were distilled, purified as described in standard methods [8] and kept over molecular sieves, type A4, for at least 48 h prior to use. Aqueous solutions were prepared by dissolving a pre-weighed sample in conductivity water. The conductivity water was prepared from triple-distilled water which was subsequently passed through a Nanopure 4C-unit (Fisher). The water prepared in this way had a specific conductivity of 1×10^{-17} to 1×10^{-18} S/cm. It should be noted that the conductivity increases when the water is left open to the atmosphere due to the dissolution of carbon dioxide. This water, which is known as "equilibrium water", was used only for rinsing purposes. All glassware and electrolytic cells were cleaned with a chromic–sulfuric mixture prepared by grinding chromium oxide with sulfuric acid or by using a cleaning mixture of alcoholic potassium hydroxide bath (either method yielded the same results). The cell was then washed with distilled water, equilibrium water, conductivity water, and was finally dried.

2.4. Electropolymerization

The conducting polymer films were electrochemically grown potentiostatically at 1.75 V on pretreated graphite surfaces (Paco Graphite, Decatur, TX). The electrosynthesis was achieved in a cell containing 50 mM 3-methylthiophene or *N*-methylpyrrole and 100 mM Bu_4NBF_4 in acetonitrile. The poly(aniline) polymer film was prepared from a solution containing 100 mM aniline in 1 M sulfuric acid. These films were then undoped by subjecting the working electrode to an applied potential of -0.2 V in the same synthesis solution for 45 min, where the current decreases to a 0.001 μA value within 5 min. The electrode was then removed from the synthesis cell, rinsed with acetonitrile, alcohol and water. The electrode was "activated" for subsequent use as a selective electrode for iodide, bromide, chloride and sulfite by one of the following methods; (i) the electrode was immersed in a cell containing aqueous solutions of 0.1 M KI, or KBr, or KCl, or K_2SO_3, and was subjected to a positive potential (determined by the oxidation potential of the anion of interest) in order to redope the film with the anion of interest. The electrode was then rinsed thoroughly with water; (ii) The electrode was alternatively "activated" by exposing its surface to one of the following gases: I_2, Br_2, Cl_2, or SO_2; the electrode was then rinsed with water and dried; or (iii) the "activation" was a combination of the electrochemical doping and the chemical treatment mentioned in (i) and (ii), respectively. The variation of the method of "activation" resulted in large differences in the potentiometric performance of the electrode.

2.5. Potentiometric measurement

Potential measurements were made with an Orion Model 601A ionalyzer using an Orion Model 90-02 double-junction reference electrode with a 10% KNO_3 solution in its outer chamber. As the ion selective electrodes respond to ionic activity, and as the readout is to be proportional to the analyte concentration, it is important that the activity coefficient, which relates these factors, is kept constant. In this respect, all the studied solutions contained 1×10^{-3} M KNO_3 as an ionic strength adjuster (except in the experiments where the interferences and the pH effect were investigated). These measurements were normally carried out at 23 ± 0.5°C (except in the temperature range response measurements). Cyclic and double potential step experiments were performed using a BAS-100 instrument (BAS, West-Lafayette, IN).

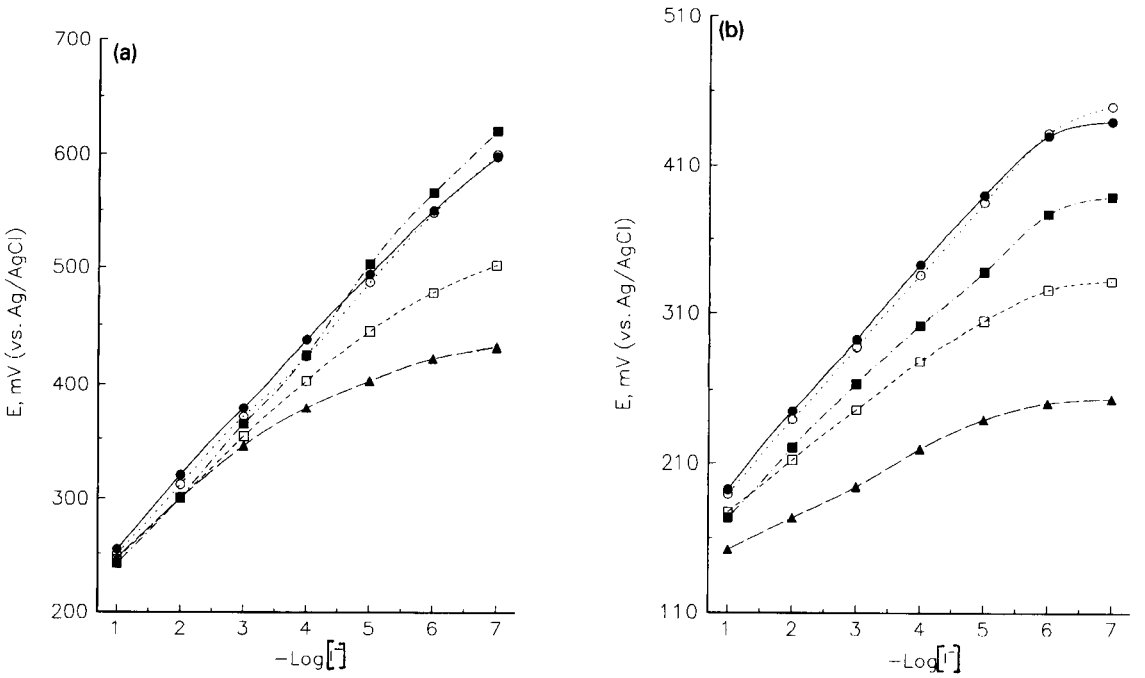

Fig. 2. Effect of doping potential on the response of 1000 thick film electrode of (a) PMT and (b) PA. 0.70 V (●), 0.80 V (○), 0.90 V (■), 1.00 V (□), 1.50 V (▲).

3. Results and discussion

3.1. Effect of electrode preconditioning parameters on electrode response

(i) Effect of doping potential.

The oxidation potential of I^-, Br^-, Cl^-, and SO_3^- solutions at the polymer film electrode was determined by a differential pulse voltammetry experiment. The doping (or more accurately, the activating) potentials were then applied using a potential slightly more positive than the oxidation "peak" potential determined from the differential pulse voltammetry experiment (ca. 50 mV). The effect of the doping potential on the response of the conducting polymer ion-selective electrode (CPISE) was studied for the poly(3-methylthiophene) (PMTCPISE) and the poly(aniline) (PACPISE) films. Figs. 2A and 2B. show the effect of the doping potential on the response of 1000 Å thick film electrodes of (PMT) and (PA), respectively. The effect of the applied potential for the doping step was found to depend on the nature of the doping ion and the type of the film under investigation. For example, Fig. 3A depicts the effect of the doping potential on the response of a 1000 Å thick PMTCPISE (doped in 1×10^{-1} M KI solution for 45 s). It is evident that the films doped at a potential ≥ 1.2 V did not produce an acceptable linear dynamic calibration range. The films doped at potentials of +0.70, +0.80, or +1.00 V, on the other hand, produced calibration curves with a larger linear dynamic range (10^{-1}–10^{-7} M) and with correlation coefficients of 0.998, 0.999, and 0.998, respectively. Although the correlation coefficients of the calibration curves obtained for the electrode doped at +0.70, +0.80, and +1.00 V were comparable, the slopes obtained were different. For that doped at +0.80 V, the slope was 58.54 mV per decade. This is close to the expected value of 58.7 mV per decade (at 23°C). However, for the other two doping potentials the slopes were 57.42 and 64.54 mV per decade, respectively. All ensuing experiments were performed using films doped at +0.8 V for iodide ion determination. The relation between the doping potential and the "Nernstian" slope obtained from the calibration curves measured with the PMTCPISE for the determination of iodide is illustrated in Fig. 3A. It shows that the slope decreases significantly for films doped at potentials > +1.00 V. This phenomenon is probably a result of oxidative

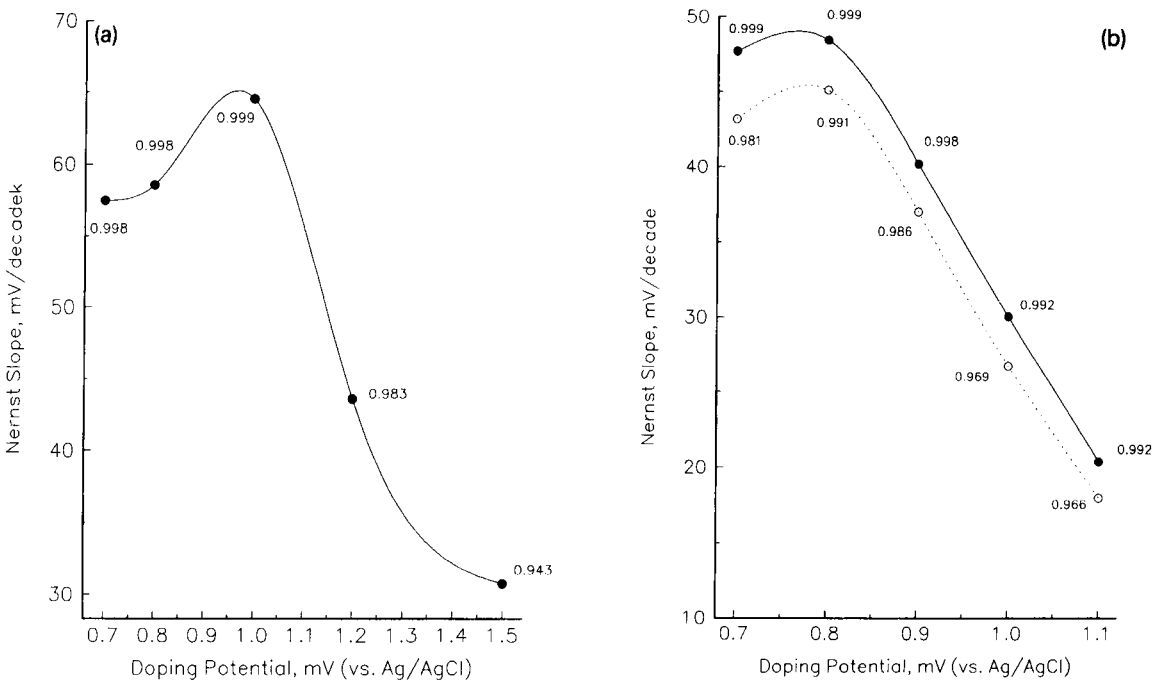

Fig. 3. The relation between doping potential and Nernst slope of the calibration for (a) PMT (film thickness 1000); and (b) PA: concentration range 1×10^{1} to 1×10^{-6} M (●), 1×10^{1} to 1×10^{-7} M (○). The correlation coefficient values are indicated for each calibration data.

effects caused by the iodine (I_2 gas) evolution at the film surface at the higher doping potentials. This will result in physical deterioration of the film. The oxidation peak potential of iodide at the PMT surface appeared at +0.97 V, as determined by the differential pulse voltammetric experiments. Similar behavior was also observed in the case of the PACPISE. However, the slope of the calibration curves were 20, 40, 48, and 46 mV/decade, with a conspicuous deviation from linearity at concentrations $\geq 10^{-6}$ M of iodide as depicted in Fig. 3B. Fig. 3B illustrates the relationship between the doping potential and the Nernst slope of the calibration curves. The slopes of the calibration curves decreased for films doped at potentials > +0.80 V. The magnitude of the doping potential at which the PACPISE response decreases occurs at less positive potentials than that of the PMTCPISE. A possible explanation for this behavior is attributed to the less positive oxidation potential for iodide at the PA film (ca. 682 mV, as measured from the DPV experiments). In general PMT electrodes had better analytical performance compared to PA and poly(*N*-methylpyrrole) (PNMP) as shown in Tables 1–3

(ii) Effect of polymer film thickness

The effect of film thickness on the potentiometric response of the modified PMTCPISE and PACPISE electrodes is illustrated in Figs. 4A and 4B, respectively. For the PMTCPISE, the correlation coefficients and slope values are given in Tables 1–3 for two different concentration ranges and indicate that all five electrodes (films grown at a constant deposition potential of +0.8 V, and with thicknesses corresponding to apparent 250, 500, 1000, 1500, and 2000 Å, respectively) exhibit acceptable calibration plots, with the 1000 Å thick film having the closest slope value to the expected Nernstian slope. The PACPISE, on the other hand, exhibited a different trend; thin films of 500 Å thickness had closer to Nernstian behavior than those for greater thickness, as shown in Tables 1–3. Fig. 5 illustrates the effect of film thickness on the performance of the PMTCPISE and the PACPISE, respectively. The optimum slope and correlation coefficients for the calibration curves for the PMTCPISE and PACPISE are 58.55 mV/decade, and 1.00; and 51.18 mV/decade, and 0.997, for films having 1000 and 500 Å thickness, respectively. This can be explained in terms of the difference in the morphology of the film (the

Table 1
(A) Effect of various preconditioning parameters on the correlation coefficients (R) and slope (S) of calibration graphs for different concentration ranges for PMTCPISE

Parameter	Value	Concentration range (M)			
		10^{-1}–10^{-5}		10^{-1}–10^{-6}	
		R	S	R	S
Film thickness (Å)	250	0.996	57.86	0.995	57.33
	500	0.999	57.43	0.997	56.78
	1000	1.000	58.54	0.999	56.89
	1500	0.999	54.43	0.999	57.45
	2000	0.999	48.57	1.000	56.31
Dopant concentration (M)	10^{-3}	0.999	56.10	0.999	54.5
	10^{-2}	1.000	57.35	0.999	53.64
	10^{-1}	0.998	58.81	1.000	58.54
	10	1.000	48.55	0.955	42.54
Doping period (s)	30	1.000	57.98	1.000	58.54
	60	0.999	58.67	0.999	58.71
	120	0.999	56.78	0.999	55.46
	240	1.000	45.62	0.989	40.57
Doping potential (mV)	700	0.999	58.56	0.998	57.43
	800	1.000	60.20	1.000	58.54
	1000	1.000	59.21	0.999	64.54
	1200	0.992	51.01	0.984	43.57
	1500	0.981	44.32	0.944	30.75

Table 2
Effect of various preconditioning parameters on the correlation coefficients (R) and slope (S) of calibration graphs for different concentration ranges for PACPISE

Parameter	Value	Concentration range (M)			
		10^{-1}–10^{-5}		10^{-1}–10^{-6}	
		R	S	R	S
Film thickness (Å)	250	1.000	52.14	0.998	48.86
	500	0.999	51.67	0.997	51.18
	1000	0.997	49.04	0.990	45.11
	1500	0.995	48.11	0.990	40.82
	2000	0.997	42.21	0.995	38.04
Dopant concentration (M)	10^{-3}	0.999	54.11	0.999	41.50
	10^{-2}	0.999	50.88	0.997	42.14
	10^{-1}	1.000	55.51	0.991	45.11
	10	0.985	45.16	0.966	34.39
Doping period (s)	30	0.999	50.34	0.991	45.11
	60	0.998	50.12	0.998	44.00
	120	1.000	40.98	0.982	33.86
	240	0.998	32.45	0.927	29.89
Doping potential (mV)	700	0.999	47.71	0.981	43.14
	800	1.000	48.46	0.991	45.11
	1000	0.998	40.20	0.985	36.98
	1200	0.992	30.06	0.969	26.75
	1500				

difference in morphology between thin and thick films) [7n,q].

(iii) Effect of dopant concentration.

The effect of concentration of iodide in the doping solution was investigated using electrodes having 1000 Å thickness films of PMT and PA, respectively. All dopant concentration studies were conducted on films doped at +0.8 V for 45 s. As can also be observed in Figs. 6A and 6B and Tables 1 and 2, increasing the dopant concentration results in a decreasing value of the linear dynamic range for the PMTCPISE and PACPISE. This deviation can probably be attributed to the increased oxidation of the electrode surface with the increase in the iodide ion concentration.

(iv) Effect of doping period

For a given film thickness of 1000 Å and a dopant solution concentration of 0.1 M KI, the effect of the doping period on the linear dynamic range and the slope of the calibration curve of the PMTCPISE and the PACPISE were also investigated. For this given set of conditions, the optimum doping period was found to be in the range of 30 to 60 s, for both types of films, as illustrated by Figs. 7A and 7B, and Tables 1 and 2.

The data presented so far indicate that in order to obtain an iodide selective electrode from the conduct-

Table 3
Effect of various preconditioning parameters on the correlation coefficients (R) and slope (S) of calibration graphs for different concentration ranges for PPCPISE

Parameter	Value	Concnetration range (M)			
		10^{-1}–10^{-5}		10^{-1}–10^{-6}	
		R	S	R	S
Film thickness (Å)	500	0.901	35.21	0.865	24.16
	1500	0.893	30.45	0.774	22.28
Dopant concentration (M)	10^{-2}	0.945	29.70	0.843	25.67
	10^{-1}	0.798	34.89	0.679	29.45
Doping period (s)	60	0.923	32.55	0.832	20.34
	120	0.945	28.38	0.712	19.05
Doping potential (mV)	700	0.967	38.90	0.756	30.48
	1000	0.877	34.22	0.652	26.83

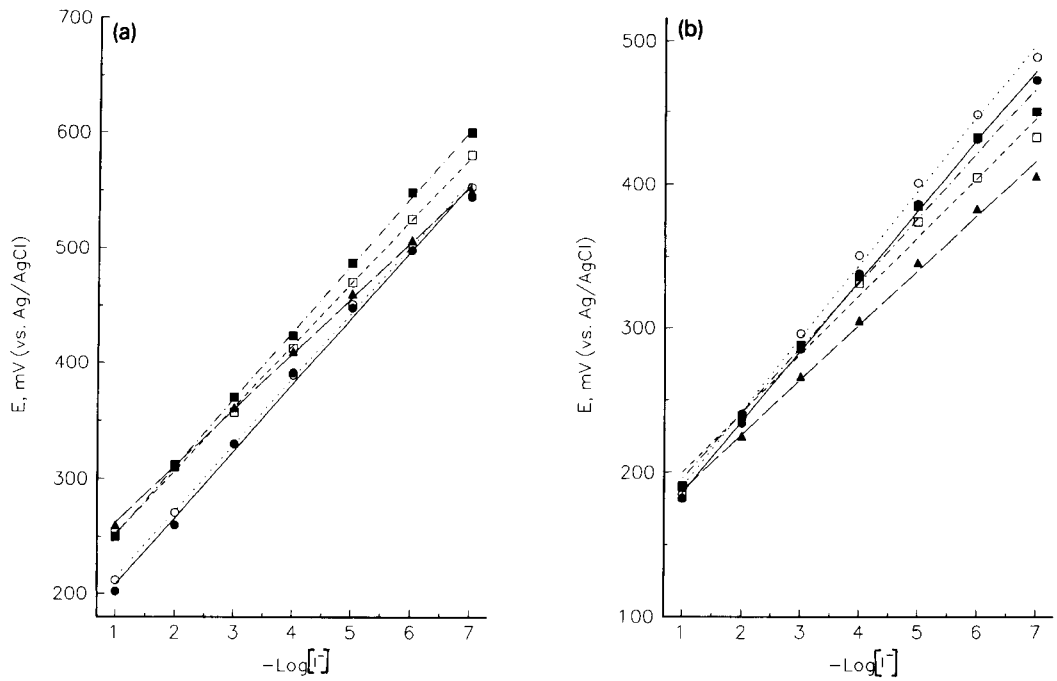

Fig. 4. Effect of polymer film thickness on the potentiometric response of (a) PMT and (b) PA: 250 (●), 500 (○), 1000 (■), 1500 (□), 2000 (▲).

ing polymer films with a wide linear dynamic range and a near Nernstian slope, there must be an optimum amount of iodide/iodine incorporated into the film matrix (which should have, in turn an ideal thickness). However, the amount of iodide/iodine should be restricted to the minimum amount required to generate a surface redox potential within the polymer film. Exceeding such level of doping proved to be destructive to the physical integrity of the film resulting in an inferior response. Thus, as the film thicknesses are increased, the concentration of the dopant required for an optimum electrode performance also increased as illustrated in Figs. 8 and 9. However, for PMTCPISE films with a 2000 Å thick film, the effect of doping periods between 30–240 s seems to be insufficient. The PACPISE shows a comparable trend in the case of films of 500 Å thickness. The relationship between the film thickness, the doping period, and the Nernst slope of the PMTCPISE for the determination of iodide ion is represented in Fig. 9. It can be seen that a large variation exists in the values measured for the slope as the film thickness changes. The increase in the film thickness leads to a noticeable drop in the value of the slope. However, for films of ≥ 1000 Å thick, the increase in doping time did not change the Nernst slope. This appears to confirm the previously mentioned destructive effect of excessive exposure of the films to iodine evolution throughout the doping process. Fig. 8 shows the potential response of PMTCPISE with different film thicknesses towards various iodide ion concentration of the doping solution. Optimum response is found to occur for 1000 Å thick films doped for a period of 30 s in the 0.1 M KI/0.1 M $NaNO_3$ at +0.8 V.

(v) Effect of exposure time to iodine vapor

In this section, the effect of changing the method of activation of the ISE is discussed. As mentioned earlier in the experimental section (electrode preparation), an alternative method for the activation of the polymer was employed; the film was "exposed" to iodine vapors for a given period of time. The exposure of the surface was made possible using the "modified" cap shown in Fig. 1. The cap contained iodine adsorbed on activated alumina or silica gel. This cap was used for "storage" or when the electrode was not in use in order to retain the "activity" and the response of the film for extended periods of time. The effect of the exposure time on the response of the PMTCPISE is illustrated in

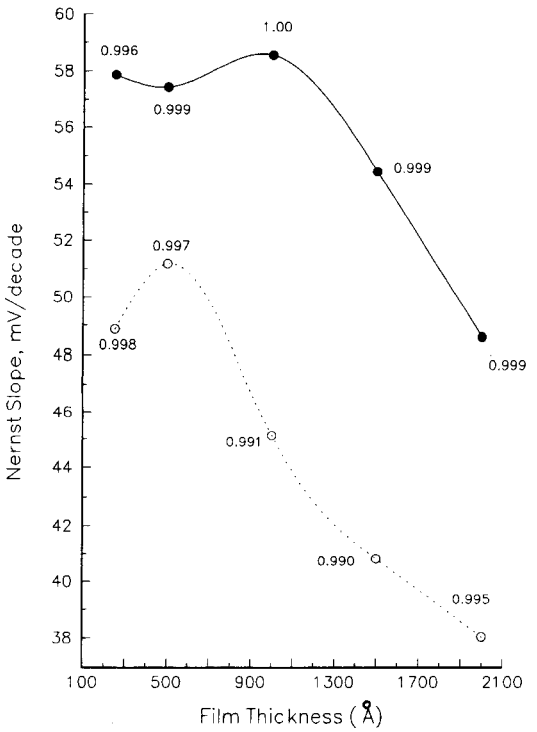

Fig. 5. Effect of polymer film thickness on the Nernstian slope of PMT (●) and PA (○). The correlation coefficient values are indicated for each calibration data.

Fig. 10. The amount of iodine used was 0.0500 g, which was thoroughly mixed with 1.2000 g of silica gel or activated alumina. A diaphragm that contains 10 peripheral and one central orifices of 1 mm diameter each was used to separate the electrode tip from the iodine/alumina containing compartment. The cap-chamber capacity is 1.3 cc and was filled with the doping mixture just prior to the preconditioning step. The previous conditions were found optimum for the electrode response. As can be learned from Fig. 10, the exposure of the PMT film to the iodine vapor for 30 s exhibited near Nernstian behavior and a larger linear dynamic range (1×10^{-7} to 1×10^{-1} M) than for films exposed for a period of time between 60 to 120 s. The previously observed damaging effect which results from prolonged periods of exposure to iodine under electrolysis conditions was also observed in the iodine vapor exposure study.

Thus, the calibration curves obtained for films doped for periods >120 s showed a deviation from linearity in the calibration curves for concentrations $\leq 1\times10^{-5}$ M iodide analyte and had lower slopes and correlation coefficients, as can be seen from Fig. 11 and Table 4. Films preconditioned using a combination (hybrid) of the two methods showed superior characteristics over those preconditioned using only one method. A comparison of the three activation procedures are given in Table 5. The most important advantages of the "hybrid" method of activation were observed in the lifetime of the electrode, reduced interference by other ions, and improved (near Nernst) slopes for long exposure periods to the analyte solution, as can be seen from Fig. 11.

3.2. *Electrode reproducibility and response time*

During the course of this study a large number of electrodes had been prepared to test the reproducibility of the potential response with electroactivation parameters. In order to determine the reproducibility of electrode preparation, the data were examined for a set of electrodes that had been prepared under the same conditions. Table 6 shows the reproducibility of electrode measurements for (a) the electrodes having 1000 Å thick films, doped electrochemically with 1×10^{-1} M KI + 1×10^{-1} M $NaNO_3$ at +0.8 V, and (b) for those both electrochemically doped and also exposed to iodine vapors for 60 s as described above. The data in Table 6, which were extracted from thirty seven measurements obtained over a period of nine months, show a reasonable degree of precision in electrode preparation, as demonstrated by the standard deviation of the potential values for a given analyte concentration. The uniformity of the electrode preparation is also demonstrated as shown in Fig. 12 for those films prepared using the "hybrid" technique.

The response time of the electrodes studied in this work was reported as the time required for the potential to come to a final steady value of ±1 mV/min. Replicate measurements using the same electrode showed a considerable variation of $\pm28\%$. This parameter was examined for the electrodes responding to both concentration increases and decreases. The experimental procedures for the determination of this parameter were as follows: (i) the two electrodes, the indicator (CPISE) and the reference were connected to a strip-chart recorder, (ii) then immersed in a solutions containing the KI of different concentrations and 1×10^{-3} M $NaNO_3$, and (iii) the time between the time at which the immersion of the iodide-selective electrode and a

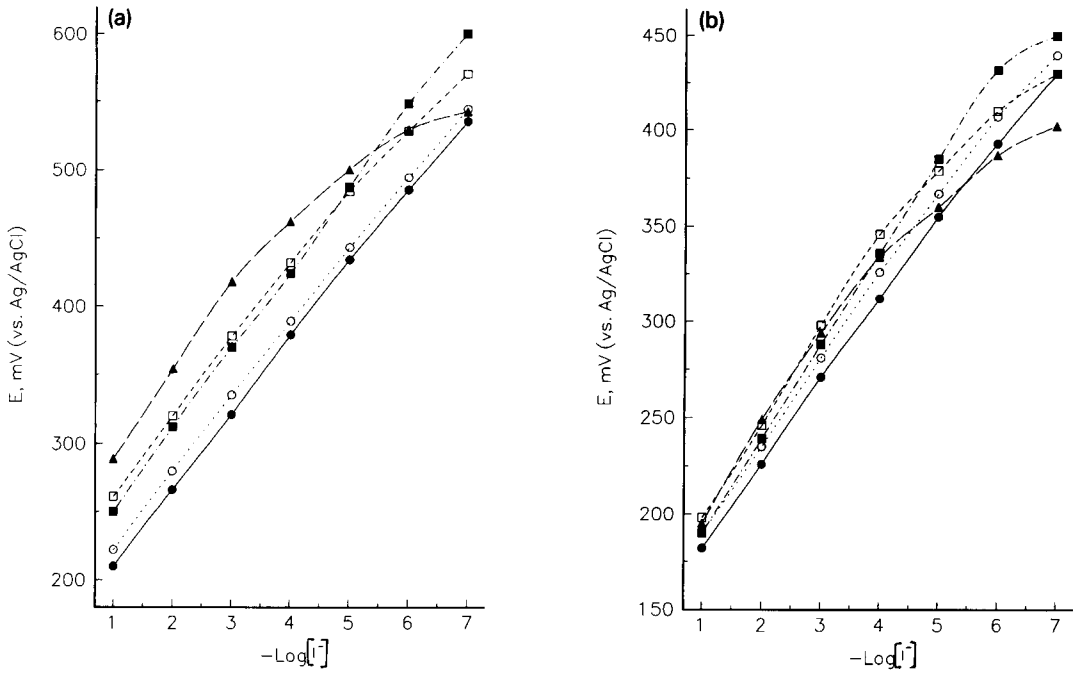

Fig. 6. Effect of iodide concentration used for doping on the potentiometric response of (a) PMT and (b) PA: 1×10^{-3} M (●), 1×10^{-2} M (○), 1×10^{-1} M (■), 5×10^{-1} M (□), 1×10^{1} M (▲).

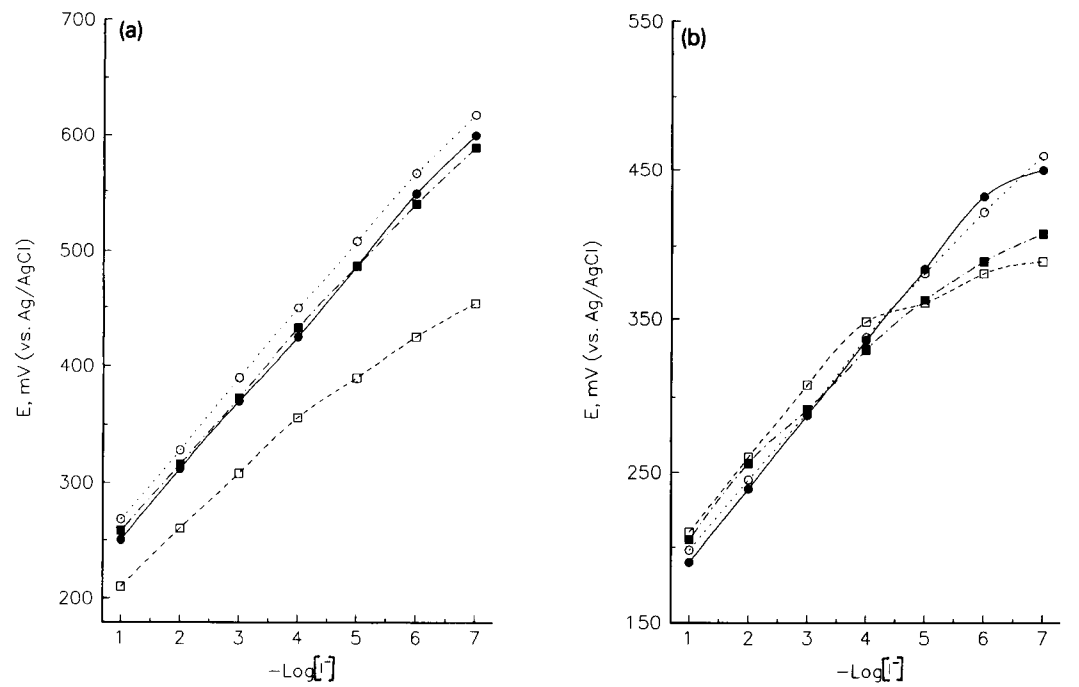

Fig. 7. Effect of doping period for 1000 thick film on the potentiometric response of (a) PMT and (b) PA: 30 s (●), 60 s (○), 120 s (■), 240 s (□).

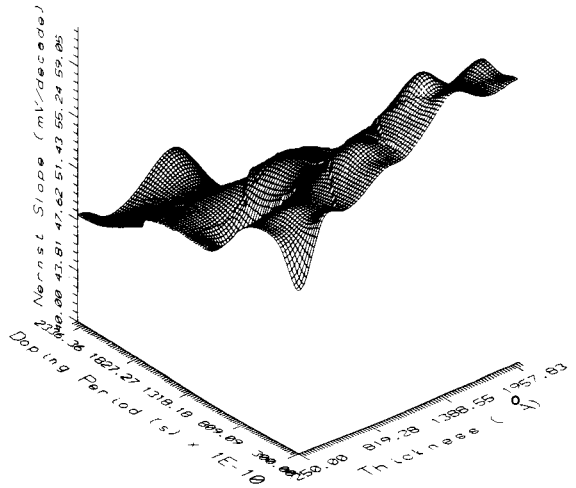

Fig. 8. Potential response of PMT electrode of different thicknesses towards various iodide ion concentrations.

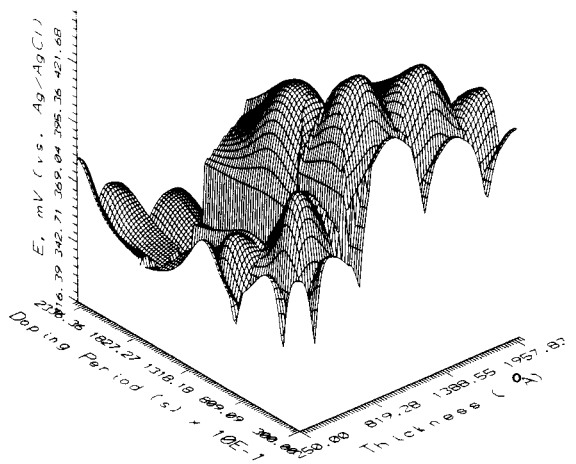

Fig. 9. Relation between film thickness, doping period, and the Nernst slope of the PMT electrode for the determination of iodide ions.

new potential plateau reached was taken as the response time. The results for the response time at the PMTCPISE and the PACPISE prepared by (a) the electrochemical doping, or (b) the hybrid-electrochemical-chemical doping are given in Table 5. For concentrations $\geq 1\times10^{-5}$ M KI, the response time was in the range of 21 to 26 s with a standard deviation of ± 2.45 for electrodes preconditioned using method (a), and 17 to 20 s with a standard deviation of ± 0.67 for method (b), for a set of 14 electrodes each. A significant decrease of the response time of the CPISE preconditioned using method (b) was observed for iodide ion solutions with concentration $\leq 1\times10^{-6}$ M. The electrodes preconditioned via method (a) showed

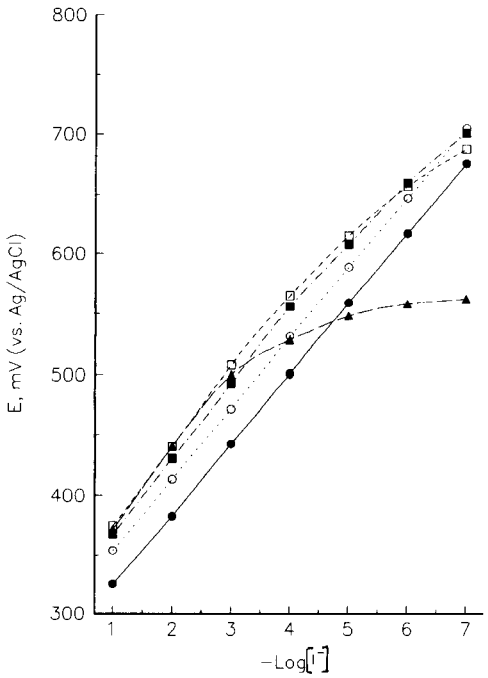

Fig. 10. Effect of exposure time of the PMT electrode to the iodine vapor on the response to iodide ion of different concentrations. 60 s (●), 90 s (○), 120 s (■), 300 s (□), 600 s (▲).

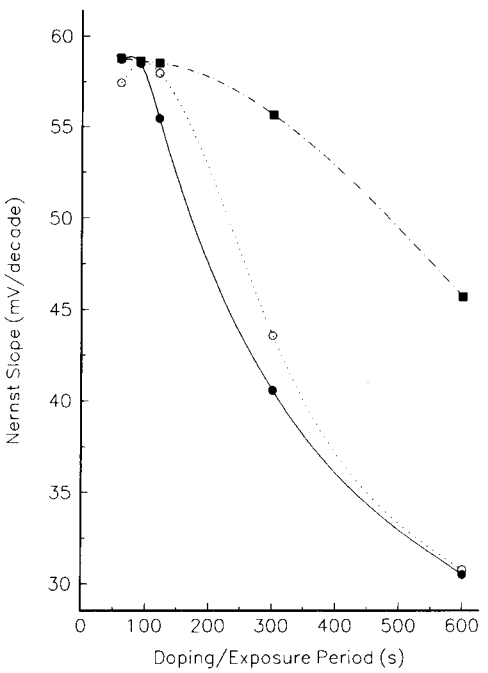

Fig. 11. Effect of exposure time on the Nernst slope of the PMT electrode response in the determination of iodide ions. Method of preparation: electrochemical (●), chemical (○), hybrid (■).

Table 4
Effect of exposure time of the PMTCPISE to the iodine vapor on the response to the iodide ion solutions

Exposure time (s)	Concentration range (M) 10^{-1}–10^{-4}	
	R	*S*
60	1.000	58.50
90	1.000	58.50
120	0.996	56.21
300	0.985	52.86
600	0.860	30.50

a response time of ca. 47 to 54 s for the dilute solutions of iodide, and those prepared using method (b) displayed values of ca. 26 to 34 s. The response time for some commercial iodide ion selective electrodes have been reported as follows: (i) Radiometer America, Inc. reported that the response time of their ion-selective electrodes in general varies from 10 s to several minutes, depending on the concentration of the iodide ion, the composition of the sample, etc.; (ii) Orion Research, Inc. reported that 99% of their iodide selective electrodes responded in one minutes or less; (iii) Corning/Fisher Scientific reported simply <30 s response times for their ion selective electrodes. All the previously mentioned commercially available electrodes reported their values without mentioning any concentration range for the iodide ion. Thus the iodide ion selective electrode based on conducting polymer films showed comparable or superior response time characteristics over these commercially available ones.

3.3. *Stability of potential measurements*

The effect of subsequent runs on the measured potential of a given electrode for identical analyte concentration was also examined for electrodes preconditioned using (a) the electrochemical and (b) the hybrid elec-

Table 5
Effect of preconditioning parameters on the characteristics of the PMTCPISE in the determination of iodide

Parameter	Value		
	Electrochemical	Chemical	Hybrid [a]
Film thickness (Å)	1000	1000	1000
	R(0.999),*S*(56 .78)	*R*(1.000),*S*(57.31)	*R*(1.000),*S*(58.31)
Dopant concentration (M)	10^{-1} I^-	Sat. I_2	Sat. I_2, 10^{-1} I^-
	R(1.000),*S*(58 .54)	*R*(1.000),*S*(58.75)	*R*(1.000),*S*(59.23)
Doping period (s)	60	120	60, 120
	R(0.999),*S*(58 .71)	*R*(1.000),*S*(59.23)	*R*(0.999),*S*(58.62)
Doping potential (mV)	800	–	800
	R(1.000),*S*(58 .54)		*R*(0.999),*S*(58.62)
Lifetime (days)	15	23	>120
Selectivity coefficient			
Cl^-	2.57×10^{-3}	3.55×10^{-3}	1.21×10^{-4}
Br^-	4.71×10^{-3}	2.33×10^{-3}	4.56×10^{-4}
NO_3^-	5.62×10^{-3}	1.66×10^{-4}	2.78×10^{-5}
ClO_4^-	2.12×10^{-3}	3.51×10^{-4}	5.16×10^{-5}
SCN^-	3.78×10^{-3}	5.67×10^{-4}	1.04×10^{-4}
$H_2PO_4^-$	4.61×10^{-4}	1.24×10^{-4}	4.66×10^{-5}
SO_4^{2-}	3.66×10^{-4}	2.71×10^{-4}	5.29×10^{-5}
CO_3^{2-}	2.79×10^{-3}	3.84×10^{-4}	1.34×10^{-4}
$S_2O_3^{2-}$	6.88×10^{-3}	2.33×10^{-3}	6.77×10^{-4}
OH^-	2.30×10^{-1}	4.10×10^{-1}	1.18×10^{-1}
CN^-	8.34×10^{-1}	6.45×10^{-1}	2.11×10^{-1}
Response time (s)	21–26, σ(2.45)	20–25, σ(1.65)	17–20, σ(0.67)
Temperature range (°C)	0–80	0–80	0–80

[a] In the hybrid method both electrochemical and chemical doping were used. The electrode was kept all the time in a cap containing the activating agent.

trochemical/chemical techniques. For a given electrode, potentials were measured over a period of four months in which the electrode was left (i) standing in air, (ii) in distilled/deionized water, (iii) 1×10^{-1} M KI solution, or (iv) in the previously described regeneration cap in Fig. 1 containing iodine between measurements. Each electrode was equilibrated first in stirred deionized water prior to the next set of measurements. Comparison of Figs. 13a and 13b shows: (i) For an electrode doped electrochemically (A) the calibration curves were shifted to less positive potentials on subsequent measurements. An electrode doped chemically/electrochemically (B) showed an insignificant change in the calibration curves; (ii) after a two weeks period, the slopes of the calibration curves showed a departure from the expected Nernst value of 58.7 mV/decade for electrode (A), while the slopes of the calibration curves for electrode (B) remained practically the same; and (iii) a change in the linear dynamic range, which was reduced to 1×10^{-1} to 1×10^{-6} M KI after the first day of preparation for electrode (A); On the other hand, electrode (B) maintained the same dynamic range of ca. 1×10^{-1}--1×10^{-7} M for the whole testing period. It was concluded from the above studies that the electrodes kept in the cap (containing the iodine) gave the best results relative to reproducibility and long term stability. These conclusions can also be drawn from in Fig. 14, where the slopes of the calibration curves for electrode type (B) kept in air were compared to that kept in the cap within the same time period.

3.4. Selectivity coefficients

As no electrode is entirely selective towards the ions specified, the presence of other ions can seriously impair electrode performance. Such interferences can take several forms, depending on the type of electrode material used and on the method of surface activation. The electrode behavior can be represented by an equation first used by Nicolsky [9] for the glass electrode showing a mixed response to hydrogen and sodium ions, which can be adopted for the study of the interference effects on the CPISE:

$$E = \text{constant} \pm k \log(C_i + k_{ij}C_j) \quad (1)$$

or for the case of other halides as:

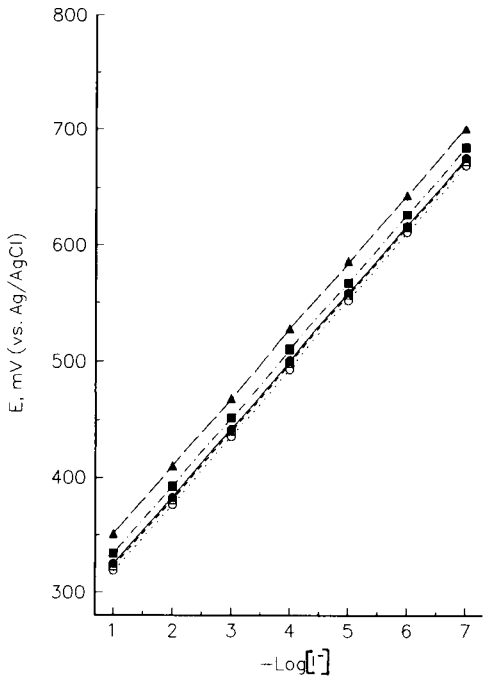

Fig. 12. Uniformity of preparation of PMT electrodes preconditioned with the hybrid method. Electrode 1 (○), 2 (□), 3 (■), 4 (●), 5 (▲).

Table 6
Uniformity of electrode preparation. Comparison between electrodes preconditioned electrochemically, and using the hybrid technique

Concentration (M)	Electrochemical doping		"Hybrid" doping	
	E, Mean (mV)	σ_n (mV)	*E*, Mean (mV)	σ_n (mV)
1×10^{-1}	254	6.53	323	2.45
1×10^{-2}	315	7.19	382	2.29
1×10^{-3}	376	6.95	439	2.54
1×10^{-4}	435	6.82	501	5.49
1×10^{-5}	490	10.87	559	5.78
1×10^{-6}	540	21.25	618	5.52
1×10^{-7}	553	21.67	676	5.49

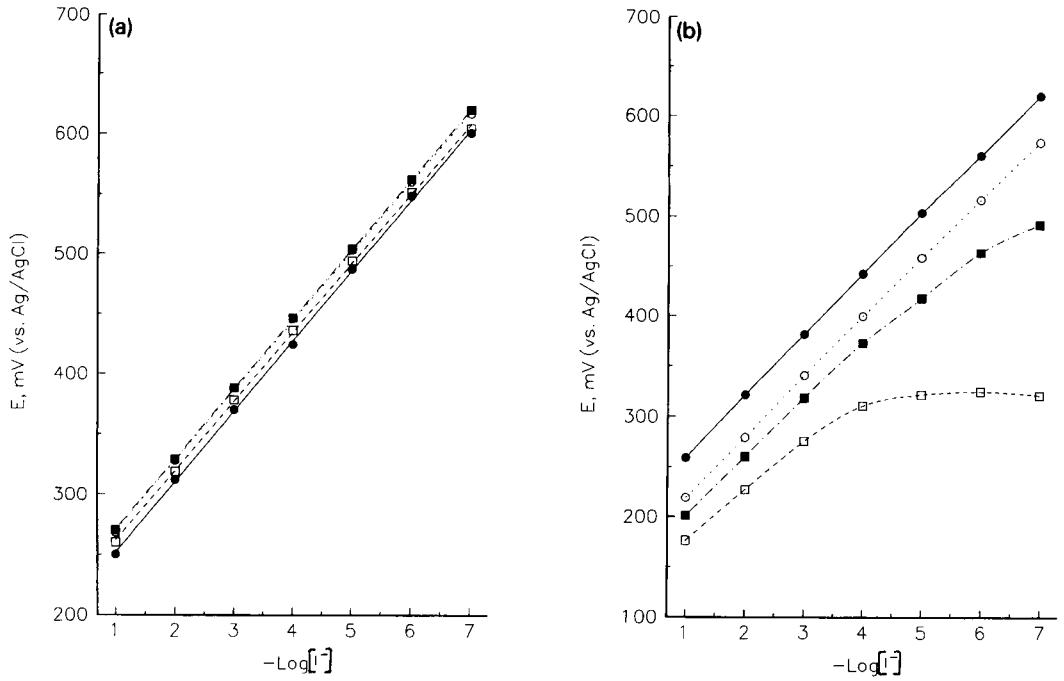

Fig. 13. Stability of potential measurements of (a) PMT and (b) PA: 1 day (●), 7 days (○), 30 days (■), 120 days (□).

$$E = \pm\frac{RT}{zF}\ln\left[a_i + \sum_j k_{ij}^{Pot} a_j\right] + \text{constant} \qquad (2)$$

where i and j are two similarly charged ions, k_{ij} is the selectivity coefficient, and k_{ij}^{Pot} is the ratio of the solubility products and activity coefficients.

The selectivity coefficients of the CPISE for the commonly encountered anions were determined by the commonly used method adopted by Srinivasan and Rechnitz [10], known by the "fixed interference method". The results for common interfering anions are summarized in Table 5, which shows that for the large majority of anions the selectivity coefficients are of the order of 1×10^{-3} or smaller. The poorer selectivity coefficients observed with the CN^- and OH^- can be explained in terms of the following reactions [11]:

$$I_2 + 2OH^- \rightleftharpoons IO^- + I^- + H_2O \qquad (3a)$$

$$3IO^- \rightleftharpoons 2I^- + IO_3^- \qquad (3b)$$

Hence the concentration of iodine in the film will decrease with a concomitant increase of iodide in the aqueous phase. From Eq. 3 it follows that electrode potential will shift to lower values as a result of the above reaction, and this will be reflected as an interfer-

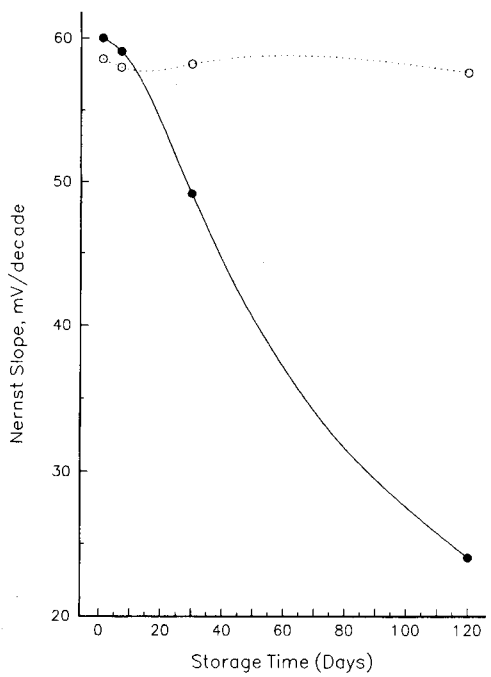

Fig. 14. Nernst slopes of the calibration curves for PMT electrode preconditioned by the hybrid method and kept in the cap (○) and left in the air (●).

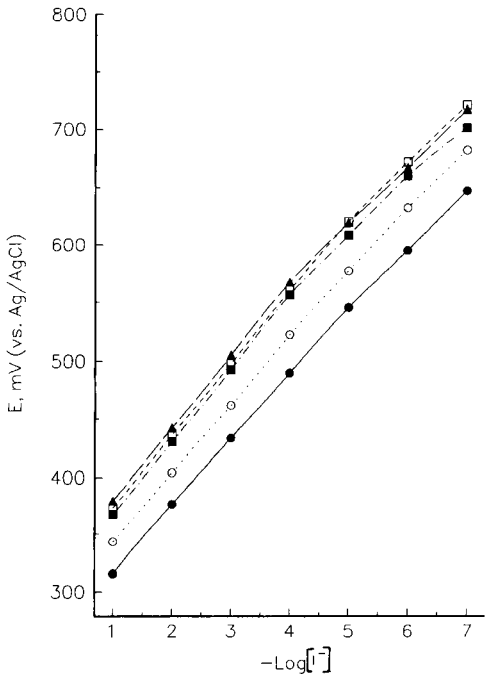

Fig. 15. Temperature effect on the potentiometric response of PMT electrode preconditioned using the hydrid method. 0°C (●), 10°C (○), 20°C (■), 50°C (□), 80°C (▲).

ence. Similarly, the cyanide effect can be accounted for by the following reaction [12]:

$$I_2 + CN^- \rightleftharpoons ICN + I^-$$

It can also be expected that any redox system which can reduce iodine or oxidize iodide would interfere with the measurements.

3.5. Effect of temperature on the CPISE

The theoretical temperature coefficient value is 0.198 mV/decade/K [13]. The effect of temperature on the performance of the CPISE was examined for the electrodes preconditioned using the "hybrid" method. The temperature coefficients calculated from the data obtained in Fig. 15 are on the order of c.a 0.09 to 0.15 mV/decade/K. Working temperatures > 80°C proved to be detrimental to the life time of the electrode.

3.6. The nature of the response of the CPISE

The oxidation of iodide in aqueous solutions on solid electrodes has been widely investigated. For instance, iodide gives two voltammetric anodic waves on a platinum electrode, the first of which corresponds to the oxidation of iodide to iodine and the second to the oxidation of iodine to iodate [14]. On a pyrolytic graphite electrode three waves are found, which have been attributed to the successive oxidation of iodide to iodine, I^+ and iodate [15]. I^- may be oxidized to either I_2 or I_3^- in the same potential region [16]:

$$I_3^- + 2e^- = 3I^-; \quad E^\circ = 0.545 \text{ V}$$

$$I_{2(s)} + 2e^- = 2I^-; \quad E^\circ = 0.535 \text{ V}$$

Therefore, on oxidation of I_2 may occur initially; then, with subsequent reaction with I^-, I_3^- formation may take place in relatively concentrated ($> 2.5 \times 10^{-3}$ M) I^- solutions [17]. We do not have direct evidence as to what type or in what ratio the oxidation products exist inside the polymer matrix. However, analogous to work concerning the oxidation of iodide at an electrodeposited poly(carbazole) film electrode [18], it tentatively was suggested that iodine is fixed on the polymeric electrode and at the same time I_3^- is formed in the diffusion layer. The formation of I_3^- seems essential for electroneutrality of the oxidized film. Alternatively it is suggested that a substantial fraction of I_3^- leaches out to the water during the equilibration of the electrode prior to the potential measurements. Assuming that iodine predominantly prevails on the polymer, the potential of the electrode can then be expressed by the following relationship:

$$E = E^{\circ\prime} + \left(\frac{RT}{2F}\right) \ln \frac{(a_{I_2})_f}{(a_{I^-})_w^2} \qquad (3)$$

where (aI_2) denotes activity in the polymer film and $(aI^-)_w$ denotes the activity in the aqueous phase. For dilute solutions, the activity terms can be replaced by concentration terms, so that at 25°C:

$$E = E^{\circ\prime} + 0.0296 \log[I_2]_f - 0.0592 \log[I^-]_w \qquad (4)$$

From Eq. 4, it follows that the potential of this electrode depends on the concentration of iodine in the polymer film and on the concentration of iodide in both film and aqueous phase. If, however, $[I_2]_f$ can be kept constant, Eq. 4 converts to:

$$E = \text{constant} - 0.0592 \log[I^-] \qquad (5)$$

at 25°C. A liquid-state iodide selective electrode based on a carbon rod impregnated with iodine from an

organic phase was described by Ruzicka and Rald [19]. The data regarding the longevity and stability tests of the PMTCPISE, which are represented in Figs. 13a and 13b, indicate that the electrode potential drifts to lower values (for those electrochemically doped or preconditioned with use) and the rate of drop decreases with each new set of measurements and time. The drift of the potential to lower values can be interpreted as the leaching out of I_2 from the polymer body. As indicated in Fig. 13a, this process apparently continues until a stable value for $[I_2]_f$ is reached or, alternatively it slows down to the extent that Eq. 5 holds for all practical purposes. The electrode performance is unfortunately altered at that stage and the slope deviates from the expected Nernstian value. The electrodes preconditioned using the "hybrid" method, on the other hand, and kept in the cap containing iodine as the active agent displayed more stability and longevity, as shown in Fig. 13b.

Electrochemically produced iodine can adsorb on unmodified graphite electrodes [20]. Therefore, it has been suggested that a simple iodide-treated graphite electrode can function in the same way as a polymer-coated iodine/iodide-doped electrode, and the need for a polymer coating can be questioned. However, uncoated graphite electrodes activated with the same procedures as described for the polymer-coated ones showed a response but with non-Nernstian slopes. Moreover, iodine-doped-graphite electrodes proved to be unstable and have a noticeable decrease in response upon repetitive measurements. The method employed by Dong and co-workers [6a,6b] and [21] was also examined and compared to ours. The polymer electrode was undoped at -0.2 V for 45 min, then was subjected to different final potential values varying in the range of 0 to $+0.8$ V for 5 to 30 min in 0.1 M KI solution before subjecting the electrode to potentiometric assays. The precision of the potential readings with the electrodes preconditioned using this method was poor, and the average lifetime of the electrode was only 1 to 2 days.

3.7. Chloride, bromide, and sulfite-chemical sensor based on conducting poly-3-methylthiophene

The selective determination of chloride, bromide and sulfite using a poly(3-methylthiophene)-modified electrode was investigated in order to demonstrate the multifaceted nature of this class of conducting polymer as an ion-selective probe. Three different techniques were used for the "preconditioning/activation" of the polymer film for a given anion. (i) The first method adopted the same procedures as reported by Dong et al. [6a,6b] for PNMP preconditioning. Thus, the PMT was formed potentiostatically as described above; the film was "undoped" at a negative potential of -0.20 V for 45 min; this was followed by immersing the electrode in solutions containing varying concentrations of the "doping" anion (0.01–1.00 M Cl^-, Br^- or SO_3^{2-}) for 5 h (and for varying periods of time between 1 to 3 days). (ii) The polymer film was alternatively activated by the electrochemical method described in the Experimental section of this paper. (iii) The third method depends on the use of a supporting electrolyte containing the anion under investigation (i.e. Cl^-, Br^-, or SO_3^{2-}) during the electrosynthesis step. In this case the following precautions were taken in order to ensure only the incorporation of the anion of interest in the film; the supporting electrolyte used was of a high purity grade, the final synthesis potential was $+1.80$ V in all cases, and the electrode was rinsed in an aqueous solution containing the counter anion.

Best results were obtained for films activated using a combination of the first and third methods. For example, for a chloride ion selective electrode, a typical preparation method was as follows: The polymer film (1000 Å thick) is formed potentiostatically from a solution containing 0.05 M monomer/0.10 M Bu_4NCl in acetonitrile. The electrode is rinsed with acetone, dried, then rinsed with a solution containing 0.1 M KCl, and finally immersed in the KCl solution for 3 days. The electrodes were thoroughly rinsed with distilled water prior to the potentiometric measurements. Representative potential response of the Cl^-, Br^-, and SO_3^{2-}-doped poly(3-methylthiophene) film electrodes are given in Figs. 16a, 16b, and 16c, respectively. The data in Figs. 16a, 16b, and 16c revealed that the chloride, bromide, and sulfite-selective-conducting polymer-based electrodes prepared by the above method have common features. These can be summarized as follows: (i) the linear dynamic range is limited (1×10^{-1} to 1×10^{-5} M concentration), (ii) the slope is in the range of 45 to 48 mV/decade, and (iii) the detection limits are in the order of $1.2–8.9\times10^{-6}$ M. Moreover, their average lifetime was in the range of 2

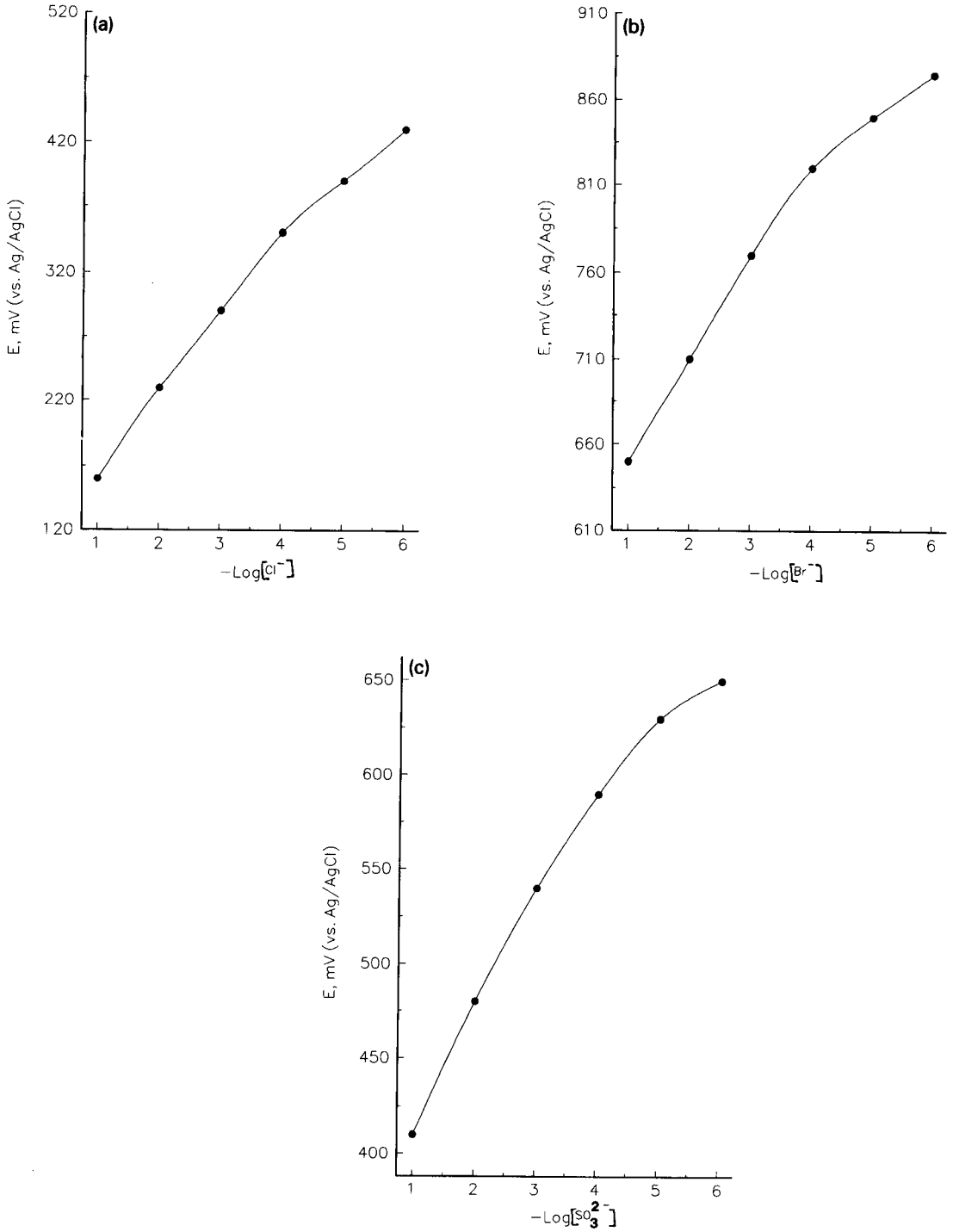

Fig. 16. Representative potentiometric response of PMT electrode towards (a) Cl^-, (b) Br^-, (c) SO_3^{2-}

to 3 days. The longevity of the electrode could only be extended upon keeping the electrode immersed in a 0.1 M solution of the ion under investigation.

The "superior" performance of the conducting polymer film which was preconditioned for the potentiometric detection of iodide ion over those devised for other anions could be explained in terms of the nature of interaction of the film with the species under investigation. Thus, absorption of gaseous iodine by films of poly(thiophene) was found to be fully reversible, the doping process appeared to be similar to the case of conventional semiconductors, and I_2, the electrically active dopant, behaves as an acceptor [22]. Moreover, Kim and Reiss [22] suggested the following equilibria to be associated with the iodine-polymer film interaction:

$$I_2(\text{gas}) = I_2(\text{PT})$$

$$2I_2(\text{PT}) = I^+(\text{PT}) + I_3^-(\text{PT})$$

$$I^+(\text{PT}) = I(\text{PT}) + e^+(\text{PT})$$

$$2I(\text{PT}) = I_2(\text{PT})$$

$$I_3^-(\text{PT}) + I_2(\text{PT}) = I_5^-(\text{PT})$$

It can be concluded that the I_2, I^+, I, I_3^-, and I_5^- are all present in the polymer film at some given concentration ratios. The equilibrium established between the I^- in solution and species in the polymer gives rise to the observed potentiometric response. It is important to note that the renewal of the film response by its exposure to the iodine vapor in the cap suggests this. These peculiar reversible iodine-polymer interactions are probably not found with other anions. Therefore, the inclusion of I_2/I^- would lead to physically change film morphology.

3.8. *pH effects*

The ion selective electrode is affected by large hydrogen or hydroxyl ion activities, and the analyte under investigation may react with them. The iodide electrode, for example, responded over a limited pH range of 3.0 to 10.0 for 1×10^{-2} M I^- and 4.0 to 9.0 at the 1×10^{-4} M concentrations. The poor response beyond these limits could be explained as follows: at high pH values it responds to the hydroxyl ion (cf. the selectivity coefficient for hydroxyl ion in Table 5), while, at low pH, iodide (similar to fluoride) and hydrogen ions react to form undissociated hydrogen iodide. Fig. 17 shows the effect of pH on the PMTCPISE performance is displayed.

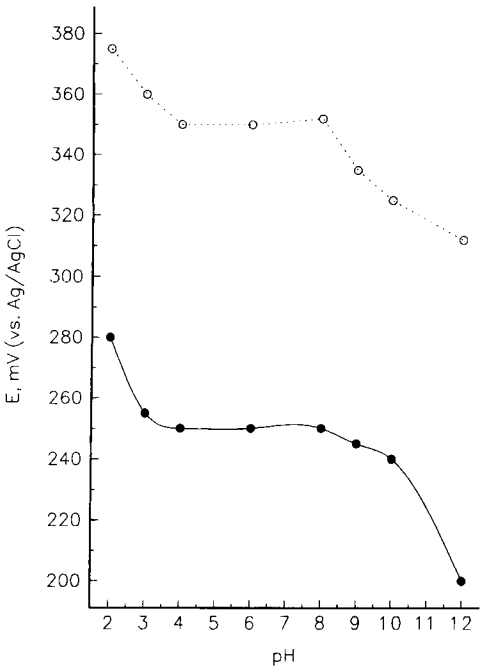

Fig. 17. pH effect on the potentiometric response of PMT electrode towards iodide. Iodide ion concentrations: 1×10^{-4} (○), 1×10^{-2} (●).

4. Conclusions

In conclusion, the "hybrid" technique used for the "preconditioning" of the electrode proved to extend the lifetime of the iodide selective electrode. The working temperature range, the selectivity coefficients, and response time of this sensor electrode are comparable to those commercially available. The preparation of bromide, chloride or sulfite selective electrodes was successful, however, extended lifetimes for such electrodes was difficult. The "unique" response of iodine-doped poly(3-methylthiophene) electrode towards iodide and its superior behavior over that of poly(aniline) or poly(*N*-methylpyrrole) is explained in terms of the specific interaction of iodine with the poly(3-alkylthiophene). In a paper by Winokur et al.

[23], the authors demonstrated that poly(3-alkylthiophenes) undergo continuous structural transformations upon doping with iodine vapor. In their discussion [23], the authors showed that an unusual reorganization can occur in the doped phases of alkyl-substituted conducting poly(thiophenes). Therefore, the iodine-induced structural changes in the poly(3-methylthiophene) may be different than that of other polymers. Moreover, the chloride, bromide and sulfite interactions with the polymer films can be explained similarly.

Acknowledgements

This research was partially supported by the American Microproducts Corporation, Cincinnati, OH; the Superfund Basic Research Program from the National Institute of Environmental Health Sciences and the Department of Chemistry of the University of Cincinnati. One of us, A.G. would like to thank Profs. S.A. Darwish and M.W. Khalil, of the College of Sciences, University of Cairo, for their continuous support.

References

[1] (a) J. Wang and R. Li, Anal. Chem., 61 (1989) 2809; (b) N. Atta, A. Galal, A.E. Karagözlar, G.C. Russell, H. Zimmer and H.B. Mark, Jr., Biosensors Bioelectron., 6 (1991) 333; (c) L. Campanella, T. Ferri, M. Majone, T. Mihic, M.V. Russo, A.M. Salvi, in P.A. Williams and M.J. Hudson (Eds.), Recent Developments in Ion Exchange, Elsevier, Amsterdam, 1987, pp. 315–321; (d) M. Josowicz, J. Janata, K. Ashley and S. Pons, Anal. Chem., 59 (1987) 253; (e) A.E. Karagözler, O.Y. Ataman, A. Galal Z.L. Xue, H. Zimmer and H.B. Mark, Jr., Anal. Chim. Acta, 248 (1991) 163; (f) J.G. Redepening, Trends Anal. Chem., 6 (1987) 18; (g) M.D. Imisides, G.G. Wallace and E.A. Wilke, Trends Anal. Chem., 7 (1988) 143.

[2] Y. Ohnuki, H. Matsuda, T. Ohsaka and N. Oyama, J. Electroanal. Chem., 158 (1983) 55.

[3] W.R. Heineman, H.J. Wieck and A.M. Yacynych, Anal. Chem., 52 (1980) 345.

[4] I. Rubinstein, Anal. Chem., 56 (1984) 1135.

[5] (a) A.G. MacDiarmid and A.J. Heeger, in W.E. Hatfield (Ed.), Molecular Metals, Plenum, New York, 1979; (b) A.F. Diaz, K.K. Kanazawa and G.P. Gardini, J. Chem. Soc. Chem. Commun., (1979) 635.

[6] (a) S. Dong, Z. Sun and Z. Lu, Analyst, 113 (1988) 1525; (b) Z. Lu, Z. Sun and S. Dong, Electroanalysis, 1 (1989) 271; (c) L. Camperella, T. Ferri, M. Majone, T. Mihic, M.V. Russo and A.M. Salvi, in P.A. Williams and M.J. Hudson (Eds.), Recent Developments in ion Exchange, Elsevier, Amsterdam, 1987, pp. 315–321; (d) J. Yano and T. Tanaka, Chem. Lett., (1988) 1943.

[7] (a) L.L. Davidson, C.V. Pham, H. Zimmer, H.B. Mark, Jr. and D.J. Ondrus, J. Electrochem. Soc., 135 (1988) 1406; (b) D.D. Cunningham, L.L. Davidson, H.B. Mark, Jr., C.V. Pham and H. Zimmer, J. Chem. Soc., Chem. Commun., (1987) 1021; (c) A. Galal, E.T. Lewis, O.Y. Ataman, H.B. Mark, Jr. and H. Zimmer, J. Polym. Sci. Polym. Chem. Ed., 27 (1989) 1891; (d) R. Shabana, A. Galal, H.B. Mark, Jr., H. Zimmer, S. Gronowitz and A.B. Hörnfeldt, J. Chem. Soc. Chem. Commun., (1988) 988; (e) D.D. Cunningham, A. Galal, C.V. Pham, E.T. Lewis, A. Burkhardt, L.L. Davidson, A. Nkansah, O.Y. Ataman, H. Zimmer and H.B. Mark, Jr., J. Electrochem. Soc., 135 (1988) 2750; (f) C.V. Pham, R.S. Macomber, H.B. Mark, Jr. and H. Zimmer, J. Org. Chem., 49 (1984) 5250; (g) A. Burkhardt, M.Sc. Thesis, University of Cincinnati, Cincinnati, OH, 1987; (h) C.V. Pham, A. Burkhardt, R. Shabana, D.D. Cunningham, H.B. Mark, Jr. and H. Zimmer, Phosphorus, Sulfur and Silicon, 46 (1989) 153; (i) H. Zimmer, R. Shabana, A. Galal, H.B. Mark, Jr., S. Gronowitz and A.-B. Hörnfeldt, Phosphorus, Sulfur and Silicon, 42 (1989) 171; (j) R. Shabana, A. Amer, H.B. Mark, Jr. and H. Zimmer, Phosphorus, Sulfur and Silicon, 53 (1990) 299; (k) A. Amer, A. Burkhardt, A. Nkansah, R. Shabana, A. Galal, H.B. Mark, Jr. and H. Zimmer, Phosphorus, Sulfur and Silicon, 42 (1989) 63; (l) R. Shabana, A. Galal, H.B. Mark, Jr., H. Zimmer, S. Gronowitz and A.-B. Hörnfeldt, Phosphorus, Sulfur and Silicon, 48 (1990) 239; (m) Z. Xue, A.E. Karagözler, O.Y. Ataman, A. Galal, A. Amer, R. Shabana, H. Zimmer and H.B. Mark, Jr., Electroanalysis, 2 (1990) 1; (n) N.F. Atta, A. Galal, A.E. Karagözler, H. Zimmer, J.F. Rubinson and H.B. Mark, Jr., J. Chem. Soc. Chem. Commun., 19 (1990) 1347; (o) A.E. Karagözler, O.Y. Ataman, A. Galal, Z. Xue, H. Zimmer and H.B. Mark, Jr., Anal. Chim. Acta, 248 (1991) 163; (p) N.F. Atta, A. Galal, A.E. Karagözler, G.C. Russell, H. Zimmer and H.B. Mark, Jr., Biosensors Bioelectron., 6 (1991) 331; (q) A. Galal, N.F. Atta, J.F. Rubinson, H. Zimmer and H.B. Mark, Jr., Anal. Lett., 26 (1993) 1361.

[8] J.A. Riddick, W.B. Bunger and T.D. Sakano, in Organic Solvents: Physical properties and Methods of Purification, 4th edn., Wiley, New York, 1986.

[9] B.P. Nicolsky, Acta Physicochim., URSS, 7 (1937) 507.

[10] K. Srinivasan and G.A. Rechnitz, Anal. Chem., 41 (1969) 1203.

[11] J. Ruzicka and K. Rald, Anal. Chim. Acta, 53 (1972) 1.

[12] I.M. Kolthoff and R. Belcher, Volumetric Analysis, Vol. II, Interscience, New York, 1957, p. 302.

[13] R.J. Simpson, in A.K. Covington (Ed.), Ion-Selective Electrode Methodology, Vol. I, CRC Press, Boca Raton, FL, 1980, p. 54.

[14] G. Raspi, F. Pergola and D. Cozzi, J. Electroanal. Chem., 15 (1967) 35.

[15] G. Dryhurst and P.J. Elving, Anal. Chem., 39 (1967) 607.

[16] A.J. Bard (Ed.), Encyclopedia of Electrochemistry of the Elements, Vol. I, Marcel Dekker, New York, 1973.

[17] E.C. Toren, Jr. and C.P. Driscoll, Anal. Chem., 38 (1966) 872.

[18] R.N. O'Brien and K.S.V. Santhanam, Electrochim. Acta, 34 (1989) 493.
[19] J. Ruzicka and K. Rald, Anal. Chim. Acta, 53 (1972) 1.
[20] K. Kinoshita, in Carbon Electrochemical and Physicochemical Properties, Wiley, New York, 1988, p. 41.
[21] S. Dong, Z. Lu and Z. Sun, Chim. Sci. Bull., 35 (1990) 612.
[22] (a) D. Kim and H. Reiss, J. Phys. Chem., 89 (1985) 2728; (b) H. Reiss and D. Kim, J. Phys. Chem., 90 (1986) 1973.
[23] M.J. Winokur, P. Nansley, J. Moulton, P. Smith and A.J. Heeger, Macromolecules, 24 (1991) 3812.

ELSEVIER

Analytica Chimica Acta 299 (1994) 165–170

ANALYTICA CHIMICA ACTA

Microbiosensor based on an integrated thermopile

Bin Xie [a], Michael Mecklenburg [a], Bengt Danielsson [a,*], Ove Öhman [b], Fredrik Winquist [c]

[a] *Pure and Applied Biochemistry, Chemical Center, University of Lund, Box 124, S-22100 Lund, Sweden*
[b] *Pharmacia Biotech AB, BL 5-3, S-75182, Uppsala, Sweden*
[c] *Laboratory of Applied Physics, Linköping University, S-58183 Linköping, Sweden*

Received 20 April 1994; revised manuscript received 7 July 1994

Abstract

A microbiosensor based on an integrated thermopile was designed and fabricated on a quartz chip. The thermopile, which was manufactured by doping boron in polysilicon together with aluminium, provided a potential output of ca. 2 mV/K. A silicone rubber membrane was used to form and seal the microchannel. The total column volume was 20 μl. Glucose oxidase and catalase were co-immobilized on spherical CPG beads (controlled pore glass) and in turn charged into the microchannel. Using 1 μl sample volumes, a linear range of 2 to 25 mM glucose was obtained using a flow rate of 105 μl/min. The relative standard deviation for 100 glucose samples (10 mM) was 5%.

Keywords: Biosensors; Flow injection; Thermal biosensor; Integrated thermopile; Glucose; Micromachining

1. Introduction

Thermal biosensors have been applied extensively in biochemical analysis since the early 1970s. Recently, determination of glucose, L-lactate and urea in one microliter whole blood samples was demonstrated using a miniaturized flow injected thermal biosensor [1,2]. The improved sensitivity and linear range of the oxidase reactions was primarily due to the miniaturization of the sensor using conventional machining technology.

Micromachining and microelectronic technologies are powerful tools for miniaturizing sensors and have been increasingly employed for the fabrication of microbiosensors [3–9]. They have not only facilitated the extensive miniaturization of biosensors, but also allowed the fabrication of transducers on microchips. In our previous study, a microbiosensor based on multiple thin-film thermistors was fabricated on a quartz chip by etching and doping polysilicon. This sensor was applied to the simultaneous determination of multiple analytes [10]. Although this method bears promise for analysis of multiple metabolites in blood, the sensitivity is inadequate in many cases. This is partly due to the lower temperature coefficient of the film thermistors, as compared with the bead thermistors employed in the miniaturized sensors.

Alternatively, thermocouples or thermopiles based on the Seebeck effect have been applied in biosensors [11,12]. In principle, the thermocouples have a high rejection ratio for common-mode thermal noise and do not require a well-matched reference, as is the case in thermistor based systems. In addition, advancements in micromachining and microelectronic technologies

* Corresponding author.

SSDI 0003-2670(94)00346-7

make the integration of the thermocouples on silicon chips easy to perform. As a result, it is possible to construct thermopiles with high potential output and small size.

Here, we present the design and fabrication of a flow injected thermopile microbiosensor on a quartz chip. In order to demonstrate the feasibility of this device for determining the concentration of metabolites in whole blood, one microliter glucose samples were analyzed employing this integrated thermopile-based biosensor.

2. Experimental

2.1. Chemicals and materials

Glucose oxidase (GOD, E.C. 1.1.3.4, types X-S, from *Aspergillus niger*, 166 U mg^{-1}) and catalase (E.C. 1.11.1.6, from beef liver, 19900 U mg^{-1}) were purchased from Sigma (St. Louis, MO). All other reagents were of analytical grade. The quartz chip with integrated thermopile was manufactured at Phamarcia Biotech (Uppsala). Propylamino-derivatized CPG (controlled-pore glass beads, particle diameter: 125–140 μm, pore diameter: 50 nm) was obtained from Steinachglas (Steinach).

2.2. Preparation of the enzyme matrix

In this study, spherical CPG beads were used as support material in the microchannel because they provide a large surface area for enzyme immobilization and low pressure in the micro-flow system. A phosphate-buffered saline solution (PBS) was employed as the running buffer and in the preparation of the glucose samples. This buffer was prepared by dissolving the following components: 8.0 g of NaCl, 0.2 g of KCl, 1.44 g of Na_2HPO_4, 0.24 g of KH_2PO_4, 2.2 g of NaF and 1 g of EDTA in 1 l of distilled water. The pH of the solution was 7.0.

Glucose oxidase and catalase were coimmobilized on the CPG beads and subsequently charged into the microchannel of the sensor. The procedure was carried out as follows: the propylamino-CPG was activated with 2.5% glutaraldehyde in 0.1 M sodium phosphate buffer (pH 7.0) at room temperature for 1 h under reduced pressure, then washed exhaustively on a Büchner funnel with distilled water and finally stored in water at 4°C. Glucose oxidase (500 U) and catalase (13,000 U) were added into 500 mg wet, activated CPG suspended in 1 ml buffer. The coupling was allowed to proceed overnight on a shaker at 4°C. Prior to packing the microchannel, the CPG beads with immobilized enzymes were thoroughly washed with buffer.

2.3. Biosensor chip

The thermopile is based on the Seebeck effect, that is $\Delta V = n a_{ab} \Delta T$, where ΔV is the voltage output of one thermocouple; n stands for the number of thermocouples; ΔT is the temperature difference between the hot junction and the cold junction and a_{ab} is the relative Seebeck coefficient which is dependent upon the composition of the material and upon the working temperature. For small temperature ranges, the Seebeck coefficient a_{ab} can be considered to be constant. Thus, the voltage output of the thermocouple is proportional to the temperature difference, ΔT. A thermopile was constructed by connecting a number of thermocouples in series. Thus, the thermopile has a much larger voltage output than a single thermocouple for the same temperature difference, since the output from the thermopile is equal to the sum of the outputs from each thermocouple. When the cold junction is maintained at a constant temperature and the hot junction is placed near the place of the exothermic enzyme reaction, the detection of the output voltage from the thermopile is directly related to the substrate concentration.

The integrated thermopile (1.6×10 mm) was manufactured by a method similar to that described by Obermeier and Kopystynski [13]. In our case, a quartz chip ($25.2 \times 14.8 \times 0.6$ mm) was used as a substrate instead of a silicon wafer in order to reduce the heat conductivity of the chip. A 0.5 μm thick layer of polysilicon was deposited using LPCVD (low-pressure chemical vapour deposition) onto the quartz substrate. The layer was boron doped using ion implantation and then annealed in N_2 at 950°C for 30 min. Next, the layer was patterned by wet chemical etching using negative photoresist as an etch mask. Metallization was accomplished through aluminium vapour deposition and an additional photolithographic patterning procedure. As a final step, the chip was annealed at 200°C for 30 min. The chip surface was covered by a 30 μm thick layer of polyimide membrane to electrically insulate the

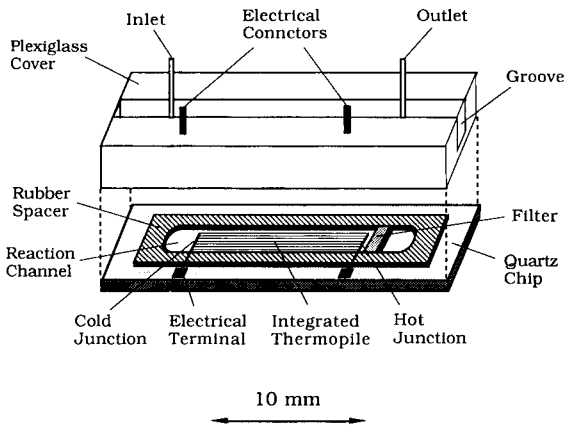

Fig. 1. Schematic diagram of the thermal microbiosensor based on an integrated thermopile fabricated on a quartz chip. The groove in the Plexiglas cover reduces the heat capacity of the reaction channel. Glucose oxidase immobilized onto CPG beads was charged into the channel (not shown here).

transducer from flow liquid. The voltage output per degree of the integrated thermopile was about 2 mV/K at 22°C.

On the chip, a silicone rubber membrane (0.32 mm thick) was used to form the microchannel ($17.5 \times 3.6 \times 0.32$ mm) and to seal between the chip and the plexiglass cover. The inlet and outlet stainless steel tubings, as well as the electrical connectors, were mounted on the cover (Fig. 1). The entire unit was held together with a screw mounted polyacetal (Delrin™, DuPont) holder (not shown here). This construction was rather bulky but was required in order to facilitate repeated access to the sensor chip. The CPG beads were charged into the microchannel by sucking them in from the outlet end. The beads were stopped at the hot junction using a filter made from a minute piece of Kleenex tissue. Two thirds of the channel from the hot junction was filled with the enzyme containing beads. The remainder was filled with the same beads without any enzyme in order to reduce the heat carry-over to the cold junction.

2.4. Experiment set-up

The flow injected measurement system included a peristaltic pump (Alitea pump unit C-4V from Ventur Tekniska, Sweden), a sample valve suitable for 1 μl sample volume (type C14W, VIGI AG, Valco Europe, Switzerland), a pre-heat sink, the sensor device, a potential amplifier (constructed at our institute) and a chart recorder. As the glucose samples were injected into the microchannel, the temperature difference between the cold and the hot junctions of the thermopile was measured while the exothermic enzyme reaction took place. According to the Seebeck effect, the resulting temperature difference effected the voltage change which was in turn detected by the amplifier. At maximal amplification, a temperature change of 10^{-4}°C could be detected. This corresponded to 0.2 μV based on a Seebeck effect of 2 mV/K. In this study, all experiments were conducted using 1 μl sample volumes in PBS buffer at a flow rate of 105 μl/min, unless stated otherwise.

3. Results and discussion

The thermometric determination of glucose employed glucose oxidase and catalase reactions, that is

$$\text{glucose} + O_2 \xrightarrow{\text{glucose oxidase}} \text{gluconic acid} + H_2O_2 + \Delta H_1$$

$$H_2O_2 \xrightarrow{\text{catalase}} H_2O + \tfrac{1}{2}O_2 + \Delta H_2$$

where ΔH_1 and ΔH_2 are the thermal output for glucose oxidase and catalase reactions, respectively. Catalase was employed to reduce hydrogen peroxide formed in the glucose oxidase reaction. This reaction scheme provides additional heat generated by the reduction of H_2O_2 (100 kJ per mol/l) as well as the partial regeneration of O_2. This extends the linear range of the glucose assay and eliminates the presence of harmful H_2O_2.

3.1. Sensitivity and linear range

Often, flow injection analysis demands the employment of large sample volumes in order to obtain adequate sensitivity and linear range. However, in glucose analyses, increasing the sample volume does not always result in an increase in sensitivity and linear range. This is primarily due to the limited oxygen supply. The linear range is limited by the amount of immobilized enzyme available and by the amount of dissolved oxygen present in the buffer.

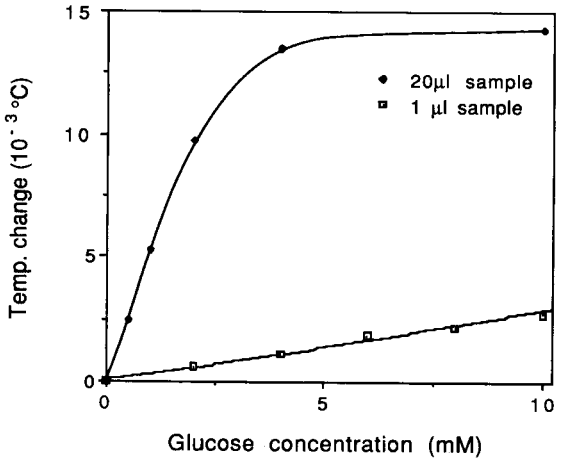

Fig. 2. Effect of the sample volume on the sensitivity and the linear range of the glucose oxidase reaction.

The sample volume was optimized to provide a balance between sensitivity and linear range in order to adequately measure physiological glucose concentrations. The effect of the sample volume on the sensitivity and the linear range of the microbiosensor was investigated. In this study, glucose samples ranging in concentration from 1 to 10 mM were determined using 1 and 20 μl sample volumes (Fig. 2). As can be seen, increasing the sample volume from 1 to 20 μl resulted in a proportional increase in the thermal response at concentrations below 2 mM glucose. Above 2 mM, the response increased nonlinearly and gradually reached a steady-state. When 1 μl sample volumes were employed, the response peak heights were reduced, while the linear range was extended. Fig. 3 shows actual thermal responses from injections of 1 μl glucose samples ranging in concentration from 5 to 30 mM. The response profiles do not show extended tailing, which indicates that the heat exchange between the cold and hot junctions was insignificant, despite the fact that they were electrically connected.

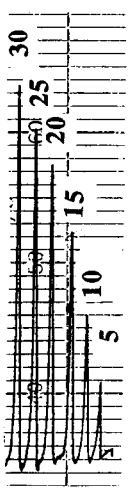

Fig. 3. Thermal responses of the integrated thermopile based biosensor for samples of 5 to 30 mM glucose. One microliter sample volumes and a flow rate of 105 μl/min were used.

The calibration curve in Fig. 4 shows that the employment of 1 μl sample volumes extends the linear range of the glucose measurements up to 25 mM, as compared with 2 mM using 20 μl sample volume. This 10 fold increase in linear range corresponds well with the results obtained from other thermistor based miniaturized biosensors, in which the linear ranges of glucose assays are also extended about 10 times as the sample volumes are reduced from 20 μl down to 1 μl [1,14]. This indicates that the relationship between the linear range and the sample volume is independent of the type of transducer employed, which implies that this sample volume effect may be universally applicable. This extension in linear range makes it possible for the thermopile based biosensor to measure glucose in most diabetes patients. However, when 1 μl sample volumes were used, the resolution obtained using this system was only 1–2 mM as compared with 0.1–0.2 mM range obtained using thermistor-based systems. This was primarily attributed to an increase in electrical interference with the thermopile circuit as compared to the thermistor-based systems.

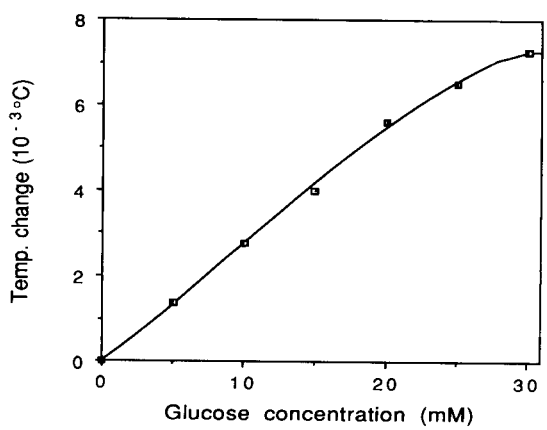

Fig. 4. Calibration graph of the glucose determination with the integrated thermopile based biosensor.

3.2. Effect of flow rate

The catalytic efficiency of the immobilized enzymes and the heat leakage in the column are highly flow rate dependent. Too high a flow rate results in inefficient glucose catalysis due to the reduction in substrate residence time in the microchannel. Too low a flow rate, on the other hand, increases the heat leakage. The effect of varying the flow rates at various glucose concentrations, 2 to 20 mM, was investigated. The results from Fig. 5 show that flow rates ranging between 76 and 105 μl/min did not significantly affect the sensitivity below 15 mM glucose. Above this concentration, however, the linearity differed significantly. This was attributed to an increase in heat leakage from the enzyme channel. When the flow rate was increased to 135 μl/min, a general decrease in sensitivity over the entire concentration range was observed. This was presumably due to the incomplete catalysis of the glucose. The small difference between the calibration curves at 105 and 76 μl/min indicated that this sensor has excellent catalytic efficiency and minimal heat leakage.

3.3. Operational stability

Electrical noise was the factor which limited the sensitivity in this system most strongly. This interference could be due to the high impedance of the integrated thermopile which was required to match the impedance of the amplifier (more than 10^7 ohm). This high impedance destabilized the measurement system. These effects were reduced by placing the entire sensor in a well grounded aluminium box.

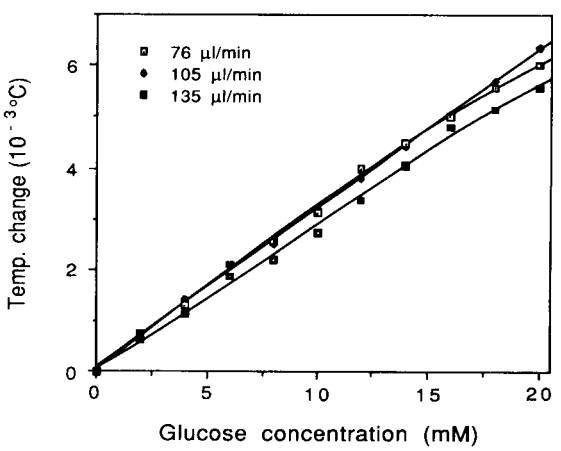

Fig. 5. Effect of the flow rate on the thermal response for different concentrations of glucose. Flow rates of 76, 105 and 135 μl/min were used.

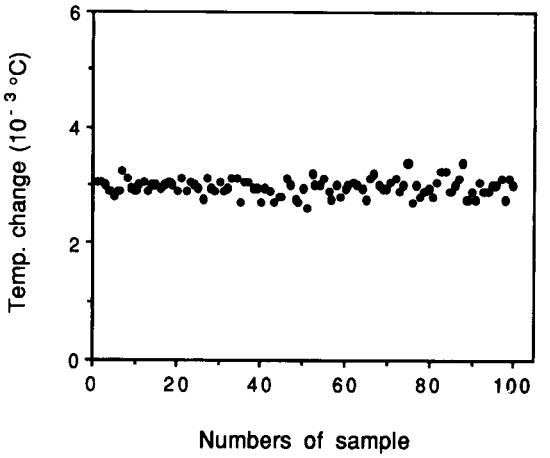

Fig. 6. Reproducibility of the glucose determination with the microsensor. 100 samples of 10 mM glucose in 1 μl buffer were continuously injected using a flow rate of 105 μl/min.

Chemical effects, such as enzyme stability and nonspecific heat produced from the mixing reactions were also investigated. At room temperature (23°C), the enzyme column was stable for more than two weeks. In terms of nonspecific heat, the salt concentration in buffer caused the baseline to shift but did not affect the sensitivity of the determinations.

The thermopile detector was less sensitive to flow rate changes than the conventional thermistor based biosensors where sudden changes in the flow rate immediately result in a drastic destabilization of the baseline, despite the fact that the reference and measurement thermistors are closely matched. This result indicates that thermopiles do indeed improve the common-mode temperature rejection ratio of the flow injected thermal biosensor.

The operational stability of the biosensor was further evaluated by performing multiple determinations. Over 100 glucose injections were analyzed (Fig. 6). A relative standard deviation of 5% was obtained. This precision could be improved if the stability of the measurement system was improved. This could be achieved by appropriately shielding the device.

4. Conclusions

A microbiosensor based on an integrated thermopile was designed and fabricated on a quartz chip employing

micromachining and microelectronic technologies. This sensor was applied to the determination of glucose concentrations in the 2 to 25 mM range, using 1 μl sample volumes. The results show that this device is capable of measuring blood glucose concentrations required in clinical analysis. Even greater sensitivities could be obtained if the electric and magnetic interference could be efficiently isolated using a simple, small Faraday cage. More importantly, this study demonstrates that integrated thermopiles are a viable alternative to thermistor transducers. In addition, the potential output from thermopiles can be further increased by integrating additional thermocouples. Furthermore, employment of the integrated thermopile could eliminate the need for complicated thermostating schemes which in turn facilitates the further miniaturization of these biosensors.

Miniaturization of sensor devices makes additional reduction in sample volumes possible. This also reduces the amount of reagents required. Silicon based devices provide a flexible and inexpensive method for producing sensing devices. Advancements in the field of microfabrication and microelectronics will provide even greater opportunities in the future.

Acknowledgements

This work was supported by grants from the National Swedish Board for Technical Development (NUTEK).

References

[1] B. Xie, U. Hedberg, M. Mecklenburg and B. Danielsson, Sensors Actuators, B15 (1993) 141.
[2] B. Xie, U. Harborn, M. Mecklenburg and B. Danielsson, Clin. Chem., (1994) accepted for publication.
[3] K. Yokoyama, K. Sode, E. Tamiya and I. Karube, Anal. Chim. Acta, 218 (1989) 137.
[4] H. Suzuki, Fujitsu Sci. Tech. J., 25 (1989) 52.
[5] F. Gardies, N. Jaffrezic-Renault, C. Martelet, H. Perrot, J.M. Valleton and S. Alegret, Anal. Chim. Acta, 231 (1990) 305.
[6] G. Urban, H. Kamper, A. Jachimowicz, F. Kohl, H. Kuttner, F. Olcaytug, P. Goiser, F. Pittner, T. Schalkhammer and E. Mann- Buxbaum, Biosensors Bioelectron., 6 (1991) 275.
[7] M. Koudelka, F. Rohner-Jeanrenaud, J. Terrettaz, E. Bobbioni-Harsch, N.F. De Rooij and B. Jeanrenaud, Biosensors Bioelectron., 6 (1991) 31.
[8] B. Xie, B. Danielsson, P. Norberg, F. Winquist and I. Lundström, Sensors Actuators, B6 (1992) 127.
[9] I. Karube, K. Yokoyama and E. Tamiya, Biosensors Bioelectron., 8 (1993) 219.
[10] B. Xie, M. Mecklenburg, B. Danielsson, O. Öhman, P. Norlin and F. Winquist, Analyst, (1994) in press.
[11] P. Bataillard, E. Steffgen, S. Haemmerli, A. Manz and H.M. Widmer, Biosensors Bioelectron., 8 (1993) 89.
[12] M.J. Muehlhauer, E.J. Guilbeau and B.C. Towe, Anal. Chem., 61 (1989) 77.
[13] E. Obermeier and P. Kopystynski, Sensors Actuators, A30 (1992) 149.
[14] B. Xie, F. Winquist and B. Danielsson, Sensors Actuators, B16 (1993) 443.

ELSEVIER

Analytica Chimica Acta 299 (1994) 171–177

ANALYTICA CHIMICA ACTA

Analytical application of membranes with covalently bound glucose oxidase

E.G. Entcheva [a], L.K. Yotova [b,*]

[a] *Bioengineering Department, Technical University, Sofia 1756, Bulgaria*

[b] *Department of Biotechnology, Technological University of Sofia, Blvd.Kl. Ohridsi 8, Sofia 1756, Bulgaria*

Received 1 September 1993; revised manuscript received 12 July 1994

Abstract

Biosensor membranes with glucose oxidase, covalently bound to acetylcellulose carriers activated with urea, were prepared and tested in order to evaluate their application in measuring the glucose concentration in blood serum and plasma. A computer-interfaced measurement and research system was used to obtain data about the characteristics of the constructed biosensors. Stability (less than 7.5% change in sensitivity for 20 days by overnight storage at 25°C), biocompatibility (2.2–2.4% loss of sensitivity after 10 blood samples) and acceptable correlation with conventional methods were found to be the main advantages of the biosensors thus obtained.

Keywords: Biosensors; Biosensor membranes; Glucose oxidase

1. Introduction

The development of precise and fast means for glucose measurements in biological fluids is of extreme importance for contemporary medicine. Methods using enzyme electrodes turned out to be rapid and reliable [1]. Different membranes and immobilization techniques were used in the construction of such biosensors. Most successful in aspects of stability and reproducibility are the sensors with covalent enzyme immobilization [2].

A method for covalent binding of enzymes to different cellulose carriers was described previously [3], and includes activation of the cellulose matrix by using urea and formaldehyde. The derivative obtained contains active hydroxymethyl groups, which can bind the amino acid residues of proteins. This method was successfully used to prepare multi-enzyme membranes for biosensors [4] on a cellulose cheese-cloth matrix and the resulting membranes were suitable for use in measuring the concentrations of glucose and saccharose both in fermentation broths and food products.

A modification of this method was used for covalent binding of enzymes to synthetic membranes [5] and also for producing membranes for optical pH sensors [6] with covalent immobilized indicators Phenol Red and Congo Red.

The purpose of the present investigation is to use the urea derivative of acetylcellulose carriers, obtained according to the above method for immobilization of glucose oxidase with previously oxidized carbohydrate moiety. The characteristics of the membranes produced were investigated and their application in the design of enzyme electrodes for clinical practice was evaluated. A computerized measurement system was used to test

* Corresponding author.

SSDI 0003-2670(94)00350-5

the constructed biosensors for determination of glucose in blood serum and plasma. The results were compared with those given by routine methods.

2. Experimental

2.1. Apparatus

An amperometric O_2 sensor with Ag/AgCl anode and Pt cathode (1 mm) was used and placed in an electrolytic cell with 1 M KCl solution and PTFE membrane. The sensor was made by the Bioengineering Department, Technical University (Sofia). Its parameters are as follows: current in quiescent solution, 7 nA and response time, $t_{95\%} = 18$ s.

The measurement system includes a current-to-voltage converter, in which the reference voltage $U_{ref} = -0.7$ V relative to the cathode is also incorporated. Another unit of the measurement block is the analog-to-digital converter (ADC, range 0–5.12 V) with 3 sub-ranges and a conversion time of 100 μs. The above-mentioned blocks are incorporated on a peripheral printed circuit board for an IBM-compatible PC.

Several modes of operation are provided by the program: calibration by steady state (calibration curve CC1) or maximum slope (calibration curve CC2) values; measurement (by CC1 or by CC2); biosensor technical characteristics determination: range and sensitivity (with preset non-linearity error), response time and stability; statistical analysis of the results.

The computerized research system, built at the Bioengineering Department (TU Sofia), is keyboard controlled, works in dialogue mode, visualizes transition curves on the graphic screen in the process of measurement, displays calibration curves and diverse information in connection with the above functions and stores measurement results for later processing.

2.2. Reagents

Glucose oxidase (EC 1.1.3.4.) from *Penicillium chrysogenum* was supplied by the plant for Microbial Preparations in Peshtera, Bulgaria. This commercial preparation of glucose oxidase was further purified as follows: the enzyme was dissolved in distilled water and subjected to ultrafiltration at 4°C until elimination of the low-molecular-weight substances had occurred, and then lyophilized. Peroxidase (EC 1.11.1.7.) from horse radish 245 E/mg was obtained from Reanal (Hungary). Glucose (anhydrous) was supplied by Chemapol (Czech Republic), urea, 4-aminophenazone and phenol by Merck. 0.1 M phosphate buffer, pH 6.0, was used. Dialysing membranes (type 20/32, pore size 24 Å) were supplied by Serva and ultrafiltration cellulose acetate membranes (UF-CA, pore size 100 Å) by the Plant for Membrane Technologies, Plovdiv (Bulgaria). Transparent triacetylcellulose membranes were used for the production of granules, obtained by treating waste film tapes as described previously [7]. All other chemicals were of reagent grade or better.

2.3. Treatment of cellulose carriers

The ultrafiltration cellulose acetate membranes were previously hydrolyzed in order to de-esterify the acetyl groups. Separate pieces of membranes with a diameter of 18 mm were treated in 0.1 M KOH for 24 h [8]. The urea derivative was then prepared by oxidation of the cellulose membranes with 0.25 M sodium periodate at 22 ± 2°C and pH 5.0 for 2 h in the darkness and further treatment with 15% (w/w) urea for 14 h in the presence of 0.9% (v/v) sulfuric acid at 60°C according to Ref. [9]. The membranes were washed with water in a Buchner funnel until the rinsing showed a neutral reaction. The resulting urea derivative of the ultrafiltration cellulose acetate membranes contained 3.2% nitrogen.

2.4. Immobilization of glucose oxidase with oxidized carbohydrate residues

The oxidation of carbohydrate residues of glucose oxidase with periodic acid 0.04 mM in 0.05 M acetate buffer (pH 5.0) was provided according to the method of Zaborsky and Ogletree [9].

The binding of the enzyme to activated cellulose membrane was performed in 0.1 M acetate buffer, pH 3.8, for 18 h at 4°C with careful magnetic stirring. Then the samples were carefully washed with distilled water until no absorbance was observed at 280 nm. The activity of the enzyme used to perform the binding was 50 E/mg.

Granules from triacetylcellulose were obtained according to Ref. [8]. 2 g of granules with size 0.08–

Table 1
Catalytic properties of membranes with covalently bound glucose oxidase

Membrane	Amount of bound protein (mg g^{-1} carrier)	Activity (U cm^{-2})	Relative activity (%)	pH_{opt}
(1) Dialysis membrane with cell granules	34	9.0	45	5.8(5.8) [a]
(2) Ultra- filtration membrane	19.8	8.64	45	5.8(5.8)

[a] The figures in parentheses refer to the free enzyme.

0.1 mm were activated and treated with oxidized glucose oxidase according to the above-mentioned method for the ultrafiltration membrane.

2.5. *Determination of enzyme activity*

The activity of the immobilized enzyme was determined by a batch method using Trinder reagent, according to Ref. [10]. One unit of glucose oxidase activity was taken to be that amount of enzyme which causes the release of 1 μM of hydrogen peroxide per 1 min at a temperature of 25°C and at pH 6.0.

The amount of bound protein was determined using a modified Lowry method [11].

2.6. *Construction of biosensors*

The biosensors were prepared as follows. Biosensor with type 1 membrane: 4 mg acetylcellulose granules with immobilized glucose oxidase are placed on a piece of dialysis membrane with diameter $d = 18$ mm. The membrane is fastened to the operating surface of the sensor by means of an O-ring; biosensor with type 2 membrane: a circular piece of ultrafiltration cellulose acetate membrane with immobilized glucose oxidase and $d = 18$ mm is fastened to the sensor as described above.

In both cases the biosensor is placed for about 5–6 h in a 0.1 M phosphate buffer to establish diffusion channels and stabilize readouts.

2.7. *Blood glucose determination. Analyzed specimen.*

All measurements were performed as the biosensor was dipped into a measuring cell, filled with 3 ml 0.1 M phosphate buffer, pH 6, at 25°C. The liquid in the measuring cell was continuously stirred by a magnetic stirrer; 0.2 ml samples were injected into the cell with an automatic micropipette; intensive water rinsing was applied after each measurement.

Measurements were performed using the following fluids. Control lyophilized serum Precipath U (Boehringer Mannheim); icteric serum (treated by anticoagulant heparin, centrifuged), supplied by the Clinical Laboratory at the Second Surgery (MA Sofia); blood plasma (the samples were taken using heparinized glass capillary tubes and were transferred to Beckman Microfuges), supplied by the Clinical Laboratory, 22nd Polyclinic Sofia. The specimen were taken from patients with normal blood glucose levels and also from patients with pathological levels up to 20 mmol/l.

3. Results and discussion

3.1. *Catalytic properties of membranes with covalently bound glucose oxidase*

The characteristics of the bound enzyme are given in Table 1. The immobilized glucose oxidase manifested good relative activity and no change of its pH optima, compared to the values for the free enzyme. Obtained membranes were very stable. When stored at 4°C for a year there was no detectable change in enzyme activity.

These results can be interpreted based on the influence of the immobilization procedure on the bound enzyme. As known glucose oxidase is a glycoprotein, which is composed of 16% carbohydrate residues per 150,000 molecular weight units [12]. Some previous investigations showed that this enzyme has been bound successfully to granulated synthetic carriers [9], Sepharose [13] or alkylamine glass beads [14] by means of oxidized carbohydrate residues.

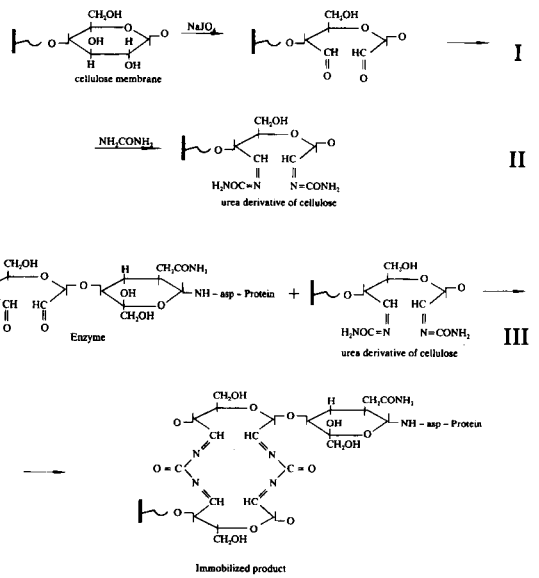

Scheme 1. Possible reaction scheme. (I) Activation of cellulose carriers with 0.25 M sodium periodate and (II) with 15% (w/w) urea. (III) Condensation of oxidized enzyme with the activated carriers.

A possible scheme for the reaction is shown in Scheme 1. In the experiments it was found that it is possible to achieve covalent binding of the enzyme with oxidized carbohydrate residues to the activated urea derivative of cellulose membranes at low pH values. A highest degree of condensation and highest value of relative activity was achieved at pH 3.8–4.0.

This novel approach for covalent binding of glucose oxidase to urea derivatives of cellulose membranes tends to show higher values of activity and bound protein, compared with our previous investigations with this enzyme bound by chemical modification of its amino acid residues to polysaccharide membranes, activated with urea and formaldehyde [4].

3.2. *Technical characteristics of the biosensors*

The calibration curves CC1 and CC2 for the two constructed biosensors by measuring in aqueous glucose solution are given in Fig. 1. After processing the calibration curves, the values for the technical characteristics of the biosensors were obtained as presented in Table 2.

The linear range and determination limit values in the table refer to the sample concentration. The bulk-to-sample concentration ratio was 1:15 for the measurement system. Both biosensors cover the physiological range and enable measuring pathologically high glucose level samples.

It is obvious from the table, that the biosensor with membrane type 1 has a wider linear range, in return for lower sensitivity. The biosensor with membrane type 2 is more sensitive and faster because of the better diffusional properties of the industrially prepared membrane carrier.

Both biosensors have relatively short reaction times and enable fast measurements when using the maximum slope method.

The precision of the biosensors was evaluated by calculation of the coefficients of variations (C.V.) after measuring 20 consecutive samples of lyophilized control serum with a mean value of 12 mmol/l glucose. Both sensors manifested similar precision.

Stability of the investigated biosensors was very high, comparable with that of the enzyme electrodes

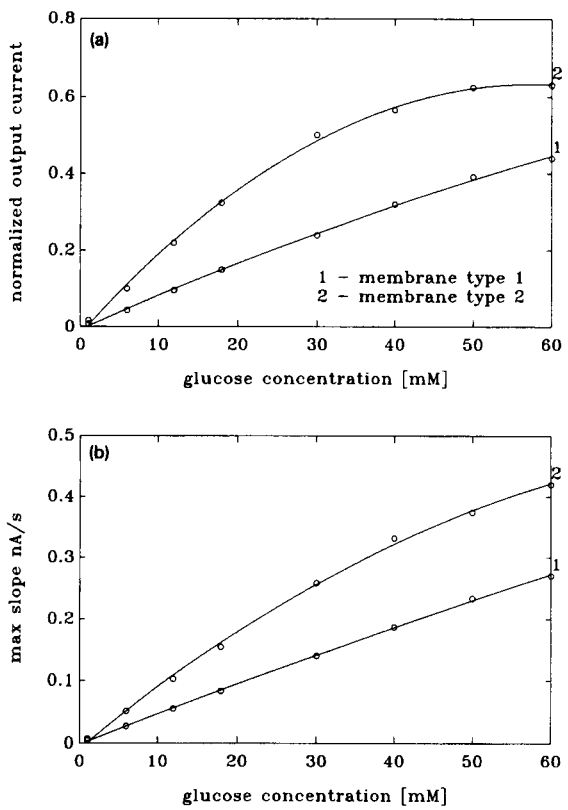

Fig. 1. Membrane comparison: (a) calibration curves CC1 (steady state values); (b) calibration curves CC2 (maximum slope values). 1 = Membrane type 1; 2 = membrane type 2.

Table 2
Technical characteristics of the biosensors

Characteristic	Biosensor 1		Biosensor 2	
	CC1	CC2	CC1	CC2
Linear range(mmol/l) (2% non-linear error)	52	60	27	36
Determination limit [a] (mmol/l)	0.8		0.5	
Response time [b] (at 5 mmol/l)	t_{lag} = 28 s t_{inf} = 42 s $t_{95\%}$ = 18 0 s		t_{lag} = 13 s t_{inf} = 23 s $t_{95\%}$ = 95 s	
Precision (C.V.)	2.5%	2.7%	2.4%	2.68%
Stability 1 [c] (change, %)	6.2%	7.4%	5.7%	7%
Stability 2 [d] (change, %)	2.2%		2.4%	

[a] Signal-to-noise ratio, 100:1.
[b] Average values for the lag time, the inflection point moment and the 95% of steady state moment, obtained from 20 D-glucose measurements.
[c] Loss of sensitivity (%) between the 5th and the 25th day of D-glucose measurements, by overnight storage at 25°C in a phosphate buffer.
[d] Loss of sensitivity (%) after measurement of 10 blood (icteric serum) samples.

with chemical binding from [15]. The absence of conformational changes in the enzyme activation center accompanying the oxidation of carbohydrate residues of glucose oxidase results in high enzyme activity after immobilization, which guarantees diffusion control of the biosensor activity and insensitivity towards enzyme deactivation.

Data obtained for the sensitivity reduction percentage after measuring 10 blood samples (icteric serum) show good biocompatibility and weak influence of blood components over the enzyme stability.

3.3. *Measurements in real biological fluids*

A main problem when measuring in real media is the biosensor selectivity. In the biosensors constructed, because of the −0.7 V potential applied across the cathode, the problem of blood components, which interfere the reaction is not acute, as they are mainly easily oxidizable substances (ascorbic acid, paracetamol, dopamine, etc.). On the other hand it is important to overcome the influence of the O_2 absolute level in the blood samples and its possible variations. In this case the reaction limitation by the co-substrate O_2 (because of its lower concentration in blood) is avoided by means of the bulk-to-sample ratio applied, which is also necessary for obtaining the desired first-order kinetics.

Diffusion control contributes to the reduction of additional effects of pH and temperature. In addition, a high ionic strength buffer is used to reduce the pH influence, and the temperature variations of 2°C are accounted for in the output current normalization.

The other problem when measuring biological fluids is the effect of the media on the diffusion properties of the membrane and the stability of the latter. All specimen were preliminary centrifuged and treated with anticoagulants in order to reduce possible effects of blood cells clogging on the membrane. Furthermore, intensive stirring and water rinsing after each measurement were applied to remove colloidal species responsible for the clogging. The dilution of the samples also contributes to reduce such blocking effects.

The obtained results for the analyzed biological fluids are shown in Fig. 2 for biosensor 1, and in Fig. 3 for biosensor 2. On the x-axis glucose values of the specimen are shown, preliminarily determined by the hexokinase glucose-6-phosphate dehydrogenase method for the icteric serum and by the Beckman oxygen rate method (Beckman Glucose Analyzer 2) for blood plasma, respectively, or given by the producer for the control serum. The measured values (y-axis) were obtained using the corresponding calibration curves for aqueous glucose solution, which are shown as well.

Several facts were observed for both biosensors. The values of the calibration curves CC1 and CC2 for the aqueous glucose solution were always lower than those for the analyzed real biological fluids with the same

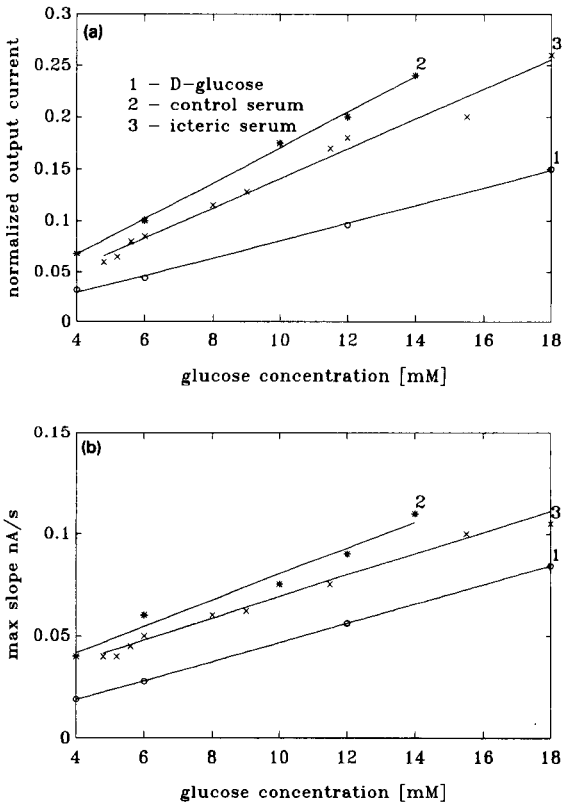

Fig. 2. Measurements in real media. Biosensor with membrane type 1: (a) steady state values for analyzed biological fluids, (b) maximum slope values for analyzed biological fluids. 1 = D-Glucose solution; 2 = control lyophilized serum; 3 = icteric serum.

glucose concentration. One of the reasons for this is perhaps the fact that clinical laboratories use special calibration solutions with parameters nearer to blood samples. The proximity of data obtained for the control lyophilized serum and the icteric serum (Fig. 2) shows that the control serum is more adequate for calibration than the water solution of glucose. An additional rise of the measured glucose level may be caused by the eventual presence of residual viable red blood cells, which could exchange oxygen with the enzyme in our experiments, but those cells do not interfere the hexokinase method used to determine the glucose concentration in the icteric serum. The deviation of the data for blood plasma from those obtained with the Beckman rate method is smaller (Fig. 3). The reason for this lies perhaps in the same measurement principle (oxygen consumption rate) and consequently identical interferents. The deviations on the maximum slope curves (Fig. 2b and Fig. 3b) for both sensors are in percentage smaller than those on the steady state curves, which means this method is more insensitive towards interferents, leading to additive shifts.

Similar results were obtained using both biosensors, with the second being more sensitive. The steady state method was found to be more stable and accurate, the maximum slope method is faster and excludes the influence of additive interferents.

3.4. Experiments with two diffusion-limiting membranes

Because of the very good stability of the immobilized enzyme and of the sensors by measurements in aqueous glucose solutions, we consider the loss of sensitivity in biological fluids (2.2–2.4% after 10 blood samples) as a result of the increased boundary layer thickness (and following worsened diffusion properties) in greater extent than as a result of the reduced enzyme activity.

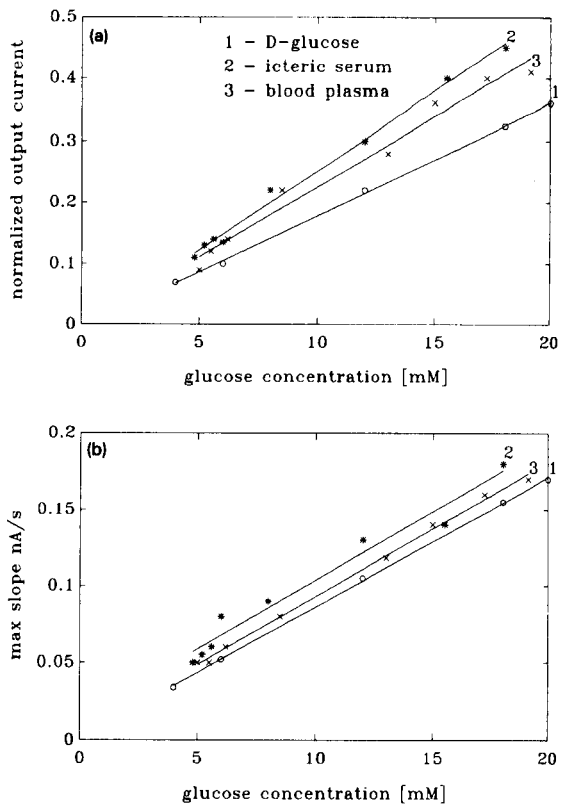

Fig. 3. Measurements in real media. Biosensor with membrane type 2: (a) steady state values for analyzed biological fluids, (b) maximum slope values for analyzed biological fluids. 1 = D-Glucose solution; 2 = icteric serum; 3 = blood plasma.

Table 3
Correlation analysis

Media	Number of measurements	Comparison between	Regression equations	Correlation coefficients
Icteric serum	$n=25$	x = hexokinase method,	CC1: $y=1.7x+0.5$	$r_{xy}=0.992$
		y = measurements using biosensor 1	CC2: $y=1.5x+0.98$	$r_{xy}=0.9874$
Icteric serum	$n=21$	x = hexokinase method	CC1: $y=1.42x+0.06$	$r_{xy}=0.9943$
		y = measurements using biosensor 2	CC2: $y=1.2x+0.112$	$r_{xy}=0.9912$
Blood plasma	$n=16$	x = Beckman rate method	CC1: $y=1.3x-0.2$	$r_{xy}=0.9651$
		y = measurements using biosensor 2	CC2: $y=1.1x-0.25$	$r_{xy}=0.9508$

In this connection the idea for the two diffusion-limiting membranes with different permeability, the second (possessing higher permeability) being changeable [16], was used. We performed some experiments with the second type biosensor (with cellulose acetate membrane, which is more convenient for this purpose) covering it with a dialysing membrane and changing the latter after every five measurements, assuring relatively unique mounting conditions. As shown in [16] the general penetration ratio undergoes no substantial change (and the sensitivity of the sensor as well) even by variations in the penetration ratio of the other more permeable changeable membrane. The results confirmed our hypothesis and better stability was obtained (3.4% total coefficient of variations for 170 blood samples by slightly increased response time).

Our results were compared with results obtained from measuring the same samples using two of the most widely applied methods for the analysis of glucose in blood samples: the hexokinase method and the Beckman rate method.

Correlation analysis yielded the results in Table 3. As a whole the correlation of data obtained from biosensor measurements with the data obtained from the reference methods was very good (correlation coefficients from 0.95 to 0.9943).

In conclusion, the membranes with covalently bound glucose oxidase possessed high activity and stability. Inexpensive and easily-available reagents were used for their preparation. The constructed biosensors manifested good stability and biocompatibility, and the results from measurements in blood serum and plasma were in acceptable correlation with those obtained by conventional methods. Combined with measurements for the reduction of the effects of interferences, reliable sensors for practical exploitation could be obtained.

References

[1] Fr.W. Scheller, D. Pfeiffer, F. Schubert, R. Renneberg and D. Kirstein, in A.P.F. Turner, I. Karube and G.S. Wilson (Eds.), Biosensors – Fundamentals and Applications, Oxford University Press, 1987, p. 315.
[2] L.D. Bower, Anal. Chem., 58 (1986) 513A.
[3] M.A. Krysteva and S.R. Blagov, J. Appl. Biochem., 6 (1984) 367.
[4] M.A. Krysteva and L.K Yotova, J. Chem. Technol. Biotechnol., 54 (1992) 13.
[5] M.A. Krysteva, B.I. Schopova, L.K. Yotova and M. Karasavova, Biotechnol. Appl. Biochem., 13 (1991) 106.
[6] Y. Kostov, St. Tzonkov, L. Yotova and M.A. Krysteva, Anal. Chim. Acta, 280 (1993) 15.
[7] M.A. Krysteva, G.A. Peev and L.K. Yotova, Acta Biotechnol., 7 (1987) 93.
[8] L.F. Chen and G.S. Tsao, Biotechnol. Bioeng., 18 (1976) 1507.
[9] O.R. Zaborsky and S. Ogletree, Biochim. Biophys. Res. Commun., 61 (1974) 210.
[10] J. Endo, M. Tabata, S. Okada and T. Murashi, Clin. Chim. Acta, 95 (1979) 411.
[11] G.R. Schacterlle and L.R. Pollak, Anal. Biochem., 51 (1973) 654.
[12] J.H. Pazur, K. Kleppe and A. Cepure, Arch. Biochem. Biophys., 111 (1965) 351.
[13] M. Hsiao and G.P. Royer, Arch. Biochem., 198 (1979) 379.
[14] T. Murashi and M. Terada, Biochemie, 62 (1980) 581.
[15] A. Cincu, V. Magearu, N. Cincu and G. Radu, Rev. Roum. Biochim., 26 (1989) 9.
[16] H. Katayama, Y. Yoshida and T. Osaka, U.S. Pat., 4 923 586 (1990).

ELSEVIER

Analytica Chimica Acta 299 (1994) 179–187

ANALYTICA CHIMICA ACTA

Flow-through type calcium ion selective optodes based on novel neutral ionophores and a lipophilic anionic dye

Hideaki Hisamoto [a], Kazuhiko Watanabe [a], Eriko Nakagawa [a], Dwi Siswanta [a], Yushi Shichi [b], Koji Suzuki [a,*]

[a] *Department of Applied Chemistry, Keio University, 3-14-1 Hiyoshi, Kohoku-ku, Yokohama 223, Japan*
[b] *Surface Analysis Section, Research Department, Nissan ARK, Ltd., Natsushima-cho, Yokosuka 237, Japan*

Received 17 May 1994; revised manuscript received 12 July 1994

Abstract

Flow-through type calcium ion selective optodes based on novel neutral ionophores and a lipophilic anionic dye were developed. The novel calcium ion selective neutral ionophores designed and synthesized were double-armed diazacrown ether compounds possessing glycolic amides as the binding arms. Cation sensing material was prepared by coating pellicular-type ODS (octadecylsilica) beads with a lipophilic organic liquid which incorporates a novel neutral calcium ionophore and a lipophilic anionic dye of the diphenyl amine type. These beads were packed in a flow-through optical cell, and the Ca^{2+} measurement was performed to measure the absorbance change of the sensing beads at 516 nm. The best optode tested exhibited a good response to calcium ions in the concentration range from 10^{-7} M to 10^{-1} M with 0.05 M Tris–HCl of pH 7.0 as the flowing buffer solution. This optode showed excellent Ca^{2+} selectivity of over 10^{-4} in selectivity coefficient values ($k_{i,j}^{opt}$; i = primary ion (Ca^{2+}); j = interfering ion) against Na^+, K^+ and Mg^{2+} which are primary interferents for human serum analysis. Sensor response theory, response time, selectivity, and application to the determination of calcium ion concentration in human serum were also discussed together with experimental results.

Keywords: Ion-selective electrodes; Calcium; Neutral ionophores; Lipophilic anionic dye

1. Introduction

Accurate determination of calcium ion without the interference of other ions (Na^+, K^+, Mg^{2+}, etc.) is important in the biomedical and clinical fields, because calcium ion has physiological action useful for medical diagnostics [1,2]. At present, in order to determine calcium ion in human blood or serum, ion-selective electrodes (ISEs) have been most commonly used [3–14].

Recently, we reported a highly selective calcium ion electrode based on the neutral ionophore of a double-armed macrocyclic compound. This ionophore is a diazacrown ether derivative having two diglycolic amide side chains that form a 1:1 complex with Ca^{2+} [15]. On the other hand, we prepared a sensitive chromophore (color changeable anionic dyes of diphenyl amine type: LAD and LAD-3, Fig. 1) and applied them to the Li^+- and K^+-selective optodes [16,17]. These dyes give a reversible absorbance change in the visible region by the deprotonation–protonation at the secondary amine group of the dye molecule in the neutral pH region.

* Corresponding author.

SSDI 0003-2670(94)00351-3

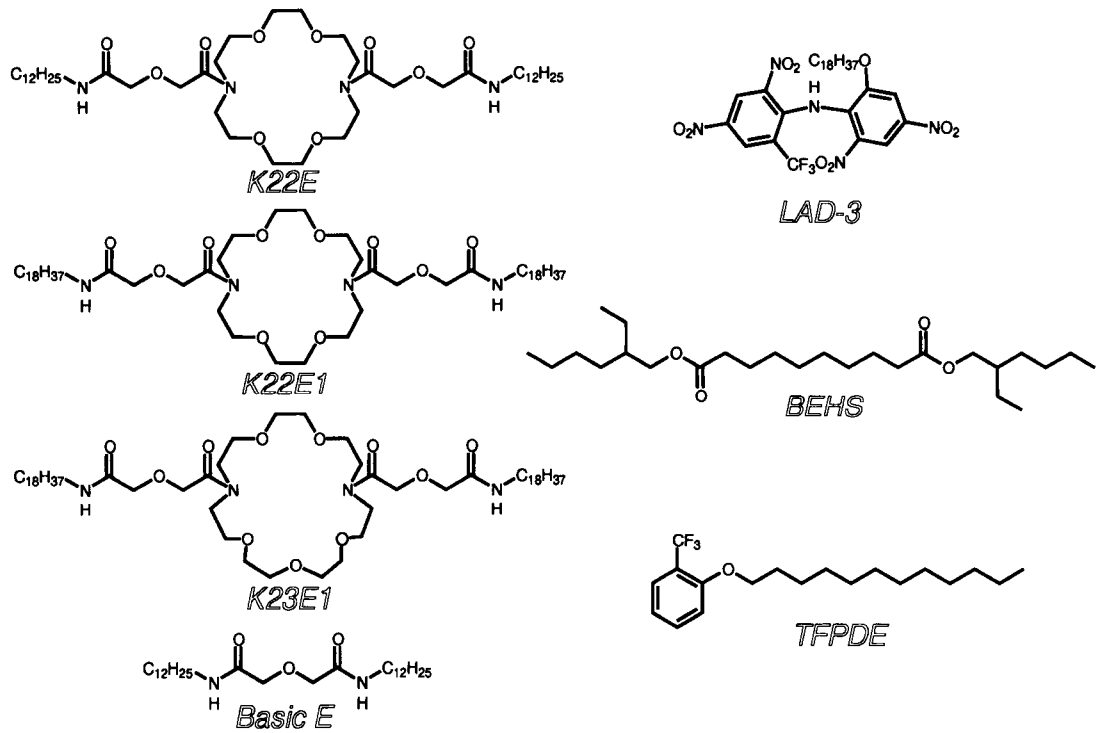

Fig. 1. Chemical structures of ionophores (K22E, K22E1, K23E1, and Basic E), a lipophilic anionic dye (LAD-3), and lipophilic organic liquids (BEHS and TFPDE).

Here we report a novel flow-through type highly sensitive and selective calcium ion optode which utilizes the novel neutral Ca^{2+} ionophore and the lipophilic anionic dye. The optical response principle of this type of optode is based on the following ion-pair formation reaction.

$$i^{2+} + S_o + 2AH_o = SiA_{2,o} + 2H^+ \quad (1)$$

where S is a calcium ion selective neutral ionophore, the subscript o denotes the organic phase, i^{2+} is the ion to be sensed (Ca^{2+} in this case), AH is a lipophilic anionic dye, and S_iA_2 is the complex formed by S_i^{2+}, and A^-. Based on this reaction, the calcium ion concentration can be determined by measuring the absorbance change caused by the deprotonation of the indicator dye which acts as a counter ion when the cation–ionophore complex (S_i^{2+}) is formed in the organic phase. The calcium ion-selective optodes developed were the flow-through type which were prepared by packing pellicular ODS (octadecylsilica) beads in which they are coated with a lipophilic organic liquid incorporating the calcium ionophore and the anionic dye. The use of this ion sensing bead component for the optode has some advantages such as a short analytical time due to the fast color change, and high response sensitivity due to the large sensing area. In addition, the optical sensing probe can be easily assembled with a small amount of sensing beads. This optode exhibited a high Ca^{2+} selectivity of over 10,000 against biologically important cations such as Na^+, K^+, Mg^{2+}, etc., and the Ca^{2+} concentration in human serum was successfully determined with the optode. In addition, sensor response theory and important sensor characteristics such as response time, and selectivity were also discussed together with the experimental results of the prepared optodes.

2. Experimental

2.1. Reagents

Reagents of the highest grade commercially available were used for the synthesis of the novel calcium ionophores and the preparation of the aqueous test electrolytes. Distilled and deionized water had resistivity

values of more than 1.5×10^7 Ω cm at 25°C. The pellicular ODS bead was purchased from Merck (Darmstadt; Perisorb RP-18; 30–40 μm particle size, approx. 2 μm surface modified layer having *n*-octadecyl group). The serum samples were supplied from Ortho Diagnostics (Raritan, NJ).

2.2. Preparation of Ca^{2+} sensing beads

The chemical structures of the ionophores, a chromophore (a dye), and the lipophilic organic liquids used for the sensing components are shown in Fig. 1. The procedures for the synthesis of the calcium ionophores (K22E, K22E1, K23E1, and Basic E), chromophore (LAD-3) and *o*-trifluoromethylphenyl dodecyl ether (TFPDE) used as the lipophilic organic liquid were described elsewhere [15,16]. The Ca^{2+}-sensing lipophilic organic liquid was prepared by dissolving the neutral ionophore and the color changeable dye (LAD-3) in the lipophilic organic liquid of BEHS (bis-(2-ethylhexyl)sebacate) or TFPDE in a 10-ml glass vessel. The Ca^{2+}-sensing ODS beads were prepared by only mixing the pellicular ODS beads in order to coat the Ca^{2+}-sensing organic liquid on the bead surface in the glass vessel. Basically, two kinds of Ca^{2+}-sensing bead components were prepared. One was prepared with 2.8×10^{-6} mol neutral calcium ionophores, 5.6×10^{-6} mol LAD-3, 93 mg TFPDE, and 200 mg ODS beads. The other was prepared with 2.8×10^{-6} mol neutral calcium ionophores, 5.6×10^{-6} mol LAD-3, 80 mg BEHS, and 300 mg ODS beads.

2.3. Structure of the flow-through type Ca^{2+} optode

The structure of the Ca^{2+} optode was the same as the previously reported lithium ion selective optode [16]. For the flow-through system, 0.05 M Tris–HCl buffer solution adjusted to pH 7.0 was pumped at 1.0 ml/min in flow-rate using the pulse-free liquid delivery pump (Jasco Trirotor 2) attached to the flow system. All sample solutions were prepared with 0.05 M Tris–HCl buffer solution adjusted to pH 7.0 and introduced to the flow system through liquid chromatographic injector having a 2-ml injection loop.

2.4. Determination of lipophilicities of membrane components

The lipophilicities of the synthesized neutral calcium ionophores, a lipophilic anionic dye, and lipophilic organic liquids, log $P_{o/w}$, ($P_{o/w}$ = distribution coefficient between organic liquid and water) were determined using the R_F values of the reversed-phase thin-layer chromatography (RP-TLC) according to the method reported by Dinten et al. [18]. The RP-TLC used contained octadecylsilane-modified reversed-phase silica plates (KC18F; Whatman, Maidstone), cut to 18×20 cm and developed chromatographically with ethanol–water (90:10) as the mobile phase.

2.5. Serum sample measurement

The determination of the Ca^{2+} concentration in the serum samples were carried out as follows. The serum samples were diluted 1:10 with 0.05 M Tris–HCl buffer solution (pH 7.0) and filtered with a PTFE membrane filter (Ekicrodisk 13CR, Gelman Science, Tokyo). The diluted serum samples were then introduced to the flow system equipped with the Ca^{2+} optode.

3. Results and discussion

3.1. Response characteristics of the optode based on a neutral ionophore and a lipophilic anionic dye

The response principle of the optodes based on neutral ionophores and anionic dye can be described on the basis of the thermodynamic equilibrium of the chemical species between the lipophilic phase and sample solution phase. We have already proposed the optical detection system based on an ion-pair extraction model which is related to the association of the ion–ionophore complex and deprotonated lipophilic anionic dye [16]. The scheme for the reaction of the chemical species at the interface between the aqueous sample phase and the lipophilic sensor phase is shown in Fig. 2 which demonstrates the response mechanism of the prepared optode. The ion concentration can be determined by measuring the absorbance change of the lipophilic dye species [16]. Based on the stoichiometry of the ion–ionophore complex (p:m-type complex for ion–ionophore complex is assumed) and the charge

number of analyte ion, this equilibrium can be generally expressed as Eq. 2, which is a general formalism involving Eq. 1 as the case for Ca^{2+} detection.

$$pi^{z+} + mS_o + nAH_o = S_m i_p A_{n,o} + zpH^+ \quad (2)$$

where S is a neutral ionophore, i^{z+} is the primary cation having a charge number of z, AH is the lipophilic anionic dye, and $S_m i_p A_n$ is the produced ion pair species. Subscript o denotes the organic phase. When the ion-pair extraction equilibrium constant and activities are defined as K and a, respectively, the activity of the optically important chemical species, $S_m i_p A_n$, in the organic phase can be represented by Eq. 3 [16].

$$a_{S_m i_p A_{n,o}} = \frac{K a^p_{i^{z+}} (a^{tot}_S - m a_{S_m i_p A_{n,o}})^m (a^{tot}_{AH} - n a_{S_m i_p A_{n,o}})^n}{a^n_{H+}} \quad (3)$$

Further, the detection light mode of these optodes is the diffuse reflection mode. Thus, the introduction of Kubelka-Munk's equation (Eq. 4) [19] leads to the theoretical response Eq. 5 of the optode.

$$f(r) = \frac{(1-10^{-A})^2}{2\times 10^{-A}} = \frac{a_{S_m i_p A_{n,o}}}{\Psi} \quad (4)$$

$$a^p_{i^{z+}} = \frac{a^n_{H+}\, \Psi f(r)}{K(a^{tot}_S - m\Psi f(r))^m (a^{tot}_{AH} - n\Psi f(r))^n}$$
$$(a^{tot}_S > m\Psi f(r) \geq 0,\ a^{tot}_{AH} > n\Psi f(r) \geq 0) \quad (5)$$

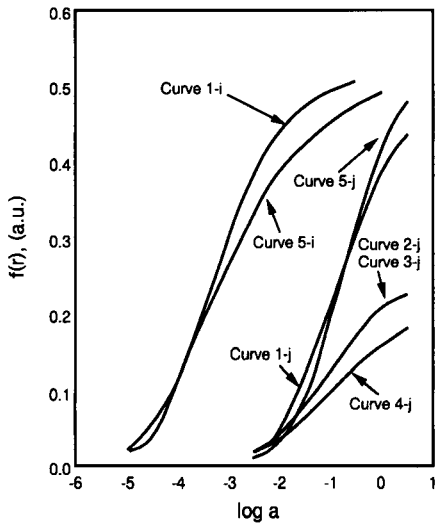

Fig. 3. Theoretical response curves obtained with five typical cases summarized in Table 1 using Eq. 5.

where f(r) is the Kubelka-Munk factor measured as the sensor response in the absorbance mode and Ψ represents an instrumental factor.

The theoretical response of the optode is then expressed by the curves in Fig. 3, where all curves were obtained by introducing the typical realistic values summarized in Table 1 into Eq. 5. These values were determined from the responses of our previously reported optodes [16]. In this case, the response curves in Fig. 3 demonstrate five typical cases (cases 1–5) as indicated in Table 1 where they were calculated in consideration of their stoichiometries of the optically

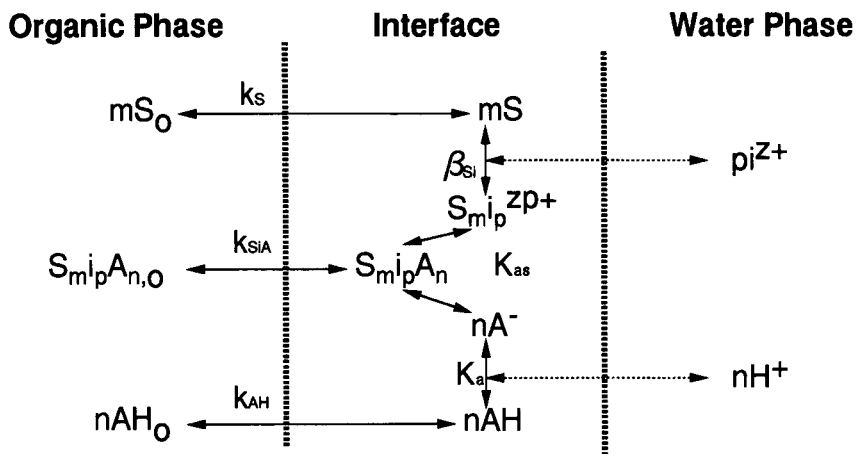

Fig. 2. Ion-extraction system for explaining the response of cation selective optode: S, neutral ionophore; AH, anionic dye of the protonated form; i^{z+}, ion to be sensed (z, charge number). The subscript o represents the organic phase. For factors and coefficients, see Results and discussion.

important chemical species, $S_m i_p A_n$, for the primary ion (i^{z+}) and $S_m j_p A_n$ for the interfering ion (j^{z+}). For example, when both the primary ion (i^{z+}) and the interfering ion (j^{z+}) have the same charge number and same stoichiometry for the complex formation of $S_m i_p A_n$ or $S_m j_p A_n$ species, the response of the optode can be represented as Eqs. 6a and 6b using the basic Eq. 5.

$$a_i = \frac{a_{H+}\Psi f_i(r)}{K_i(a_S^{tot} - \Psi f_i(r))(a_{AH}^{tot} - \Psi f_i(r))} \quad (6a)$$

$$a_j = \frac{a_{H+}\Psi f_j(r)}{K_j(a_S^{tot} - \Psi f_j(r))(a_{AH}^{tot} - \Psi f_j(r))} \quad (6b)$$

where subscripts, i and j represent the factors relating the cation i and j ($i \neq j$), respectively. For case 1 in Table 1, the stoichiometry of the chemical species ($S_m j_p A_n$) is the same as $S_m i_p A_n$ ($m = p = n$). The curves based on these species, which were obtained using Eqs. 6a and 6b, then give the same shapes as demonstrated by curves 1-i and 1-j in Fig. 3. In this case, the response curve simply shifts parallel along the abscissa ($\log a_i$ or $\log a_j$) depending on the values of K_i and K_j (case 1 in Table 1). The typical experimental response obtained with the optode based on K22E and LAD-3 is shown in Fig. 4. The response curves for Ca^{2+}, Ba^{2+} and Mg^{2+}, which correspond to the above discussed case 1, exhibited similar response curve shapes as theoretically explained (see Figs. 2 and 3). On the contrary, the curve shape varies with the difference in the charge or stoichiometry of the chemical species of $S_m i_p A_n$ or $S_m j_p A_n$, where the response curves for the primary and interfering ions have different complex stoichiometry (cases 2 and 4 in Table 1) or different charge number (cases 3, 4 and 5 in Table 1). The typical experimental response curves for Ca^{2+} and K^+ are shown in Fig. 4 which correspond to case 5 (see curves 5-i and 5-j in Fig. 3), and the shapes of these curves are different. The response curve for K^+ showed a slightly steeper slope than the response curves for the divalent ions such as Ca^{2+} or Ba^{2+}. It is noticed that

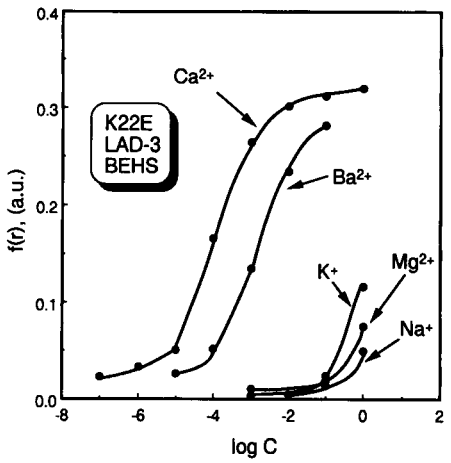

Fig. 4. Response curves for typical cations (Na^+, K^+, Mg^{2+}, Ca^{2+}, and Ba^{2+}) obtained with the optodes based on K22E and LAD-3.

Table 1
Typical examples for calculating the theoretical response curves of the optode when typical optically important chemical species (ion-ionophore complex-anionic dye) were formed

Case	Primary ion i^{z_1+}			Interfering ion j^{z_2+}			a_S^{tot}	a_{AH}^{tot}	a_{H+}	K_i	K_j	Φ	Response curve [a] in Fig. 3
	m_1	z_1		m_2	z_2								
1	1	1	(SiA)	–	–		0.035	0.035	10^{-7}	10^{-2}	–	0.069	Curve 1-i
	–	–		1	1	(SjA)	0.035	0.035	10^{-7}	–	$10^{-4.5}$	0.069	Curve 1-j
2	1	1	(SiA)	–	–		0.035	0.035	10^{-7}	10^{-2}	–	0.069	Curve 1-i
	–	–		2	1	(S_2jA)	0.035	0.035	10^{-7}	–	10^{-3}	0.069	Curve 2-j
3	1	1	(SiA)	–	–		0.035	0.035	10^{-7}	10^{-2}	–	0.069	Curve 1-i
	–	–		1	2	(SjA_2)	0.035	0.035	10^{-7}	–	10^{-10}	0.069	Curve 3-j
4	1	1	(SiA)	–	–		0.035	0.035	10^{-7}	10^{-2}	–	0.069	Curve 1-i
	–	–		2	2	(S_2jA_2)	0.035	0.035	10^{-7}	–	$10^{-8.5}$	0.069	Curve 4-j
5	1	2	(SiA_2)	–	–		0.035	0.070	10^{-7}	10^{-8}	–	0.069	Curve 5-i
	–	–		1	1	(SjA)	0.035	0.070	10^{-7}	–	10^{-5}	0.069	Curve 5-j

[a] The calculated theoretical response curves are shown in Fig. 3. Curves 1-i and 5-i represent the theoretical response curves for a primary ion of the respective cases. Curve 1-j to 5-j represent the theoretical response curves for an interfering ion of the respective cases. The bracket represents complex type formed with the ionophore (S), cation (i or j), and anionic dye (A).

these differences affect not only the response curve shape but also the limiting sensitivity as demonstrated by the curves in Fig. 3. Exceptionally, the same shapes are obtained for cases 2 and 3 in Table 1 (see curves 2-j and 3-j in Fig. 3), where they have the same values of the parameters (a_S^{tot}, a_{AH}^{tot}, Ψ, and a_{H+}) but only differ in stoichiometry of the ion–ionophore complex (1:1 or 2:1) or charge number (j^+ or j^{2+}). The detection limit depends mostly on the K_i value (see Eq. 6a), which is the ion-pair extraction constant of the chemical species, $S_m i_p A_n$. The highest and lowest response curves are given for the case where the optically response species ($S_m i_p A_n$) are $S_i A$ ($m=n=1$, i is a monovalent cation; see curve 1-i or 5-j in Fig. 3) or $S_2 i A_2$ ($m=n=2$, i is a divalent cation; see curve 4-j in Fig. 3), respectively. The response characteristics based on the theory in relation to the optically important chemical species in the bulk optode sensing phase have never been thoroughly discussed. This subject is quite important in order to understand the response characteristics and ion selectivity feature (see the following section) of the ion-selective optode using ion-complex species such as an ionophore and a chromophore.

3.2. *Selectivity coefficient of the optode based on a neutral ionophore and a lipophilic anionic dye*

The theoretical equations for calculating the optical ion selectivity coefficient ($k_{i,j}^{opt}$) of the optode are generally expressed as the following Eqs. 7a or 7b [16].

$$k_{i,j}^{opt} = \frac{f_1(r)(a_S^{tot} - m_1\Psi f_2(r))^{m_1}(a_{AH}^{tot} - n_1\Psi f_2(r))^{n_1}}{f_2(r)(a_S^{tot} - m_1\Psi f_1(r))^{m_1}(a_{AH}^{tot} - n_1\Psi f_1(r))^{n_1}} \quad (7a)$$

$$\left(= \frac{a_H^{n_1} + K_i(a_S^{tot} - m_2\Psi f_1(r))^{m_2}(a_{AH}^{tot} - n_2\Psi f_1(r))^{n_2}}{a_H^{n_2} + K_i(a_S^{tot} - m_1\Psi f(r))^{m_1}(a_{AH}^{tot} - n_1\Psi f_1(r))^{n_1}} \right) \quad (7b)$$

where m_1 and m_2 are the stoichiometric numbers in relation to the ion–ionophore complexes for the primary (i) and interfering ion (j), respectively, and n_1 and n_2 are charge numbers of the ion–ionophore complexes for the primary (i) and interfering ion (j), respectively. Eqs. 7a and 7b are the basic equations for calculating the selectivity coefficient of the optode from measured absorbances for the primary ion ($f_1(r)$) and interfering ion ($f_2(r)$). These equations indicate that if the stoichiometric numbers and the charge numbers for the primary ion and interfering ion are different, the determined ion selectivity coefficients depend on the response absorbance values used for the calculation. Based on the conditions of the five typical cases indicated in Table 1 and their theoretical response curves shown in Fig. 3, the variation in the ion selectivity coefficients ($k_{i,j}^{opt}$) as a function of the measured absorbance, which relates to the activity of the measuring ion, can be demonstrated by the curves in Fig. 5. The variation in the ion selectivity coefficient, which depends on the activity of the measured ion, is a classical problem in the ion-selective electrode method, especially the coefficients determined by the separate solution method (SSM) [20]. The same problem exists for the optode as shown by the curves in Fig. 5. The selectivity coefficients obviously depend on the activity of the measured ion and the type of interfering ion except for case 1 in Table 1, where the primary ion has the same charge and the same complex type as those of the interfering ion. Especially, the factors calculated for cases 2–4 in Table 1 vary considerably with the measured ion activity as demonstrated in Fig. 5. This problem is caused by the difference in the response curve shapes for a primary ion and an interfering ion. Thus, evaluation of the ion selectivity of the optode by using the fixed interference method (FIM) is more acceptable and reliable [16].

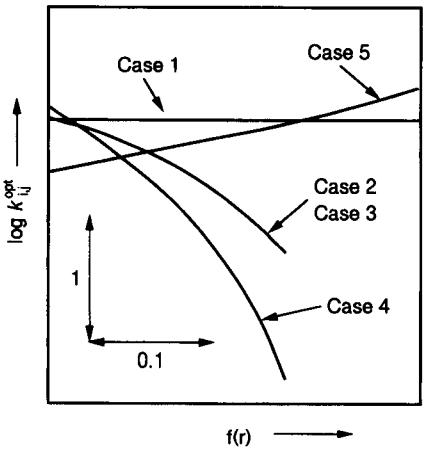

Fig. 5. Relationship between arbitrary absorbance (A or $f(r)$) and selectivity coefficients calculated by the separate solution method (Eq. 7) using the theoretical response curves shown in Fig. 2.

3.3. Response of the optodes based on Ca^{2+} selective neutral ionophores and a lipophilic anionic dye (LAD-3)

Fig. 6 shows the response curves for Ca^{2+} obtained with the optodes based on a novel calcium ion selective ionophore (K22E1 or K23E1) and a lipophilic anionic dye (LAD-3) which is dissolved in different lipophilic organic liquids (TFPDE or BEHS). The measured absorbance (f(r)) was obtained on the basis of the blank absorbance, ($f_B(r)$) for 0.05 M Tris–HCl buffer solution (pH 7.0) as the flowing solution. This blank absorbance, $f_B(r)$ can be negligible by using a double-beam spectrophotometer equipped with a reference optode ($f_B(r)=0$) which had the same structure as that of the Ca^{2+} optode but not containing the Ca^{2+} selective ionophore and LAD-3 in the coating liquid of the sensing beads [16]. The optode based on LAD-3 and the non-macrocyclic compound, Basic E(N,N'-didodecyl-3-oxapentanediamide), which has two dodecyl groups introduced on both ends of the base diglycolic amide group, exhibited no response to Ca^{2+} as well as other alkali metal and alkaline earth metal ions. Though the potentiometric ion-selective electrode based on this compound and *o*-nitrophenyl octyl ether (o-NPOE) exhibited high calcium ion selectivity (log $k_{i,j}^{pot}=-3.5$ for Na^+, and -4.1 for Mg^{2+}) [15], this compound probably forms a weak complex with Ca^{2+}. Therefore, the response mechanism of the optode is

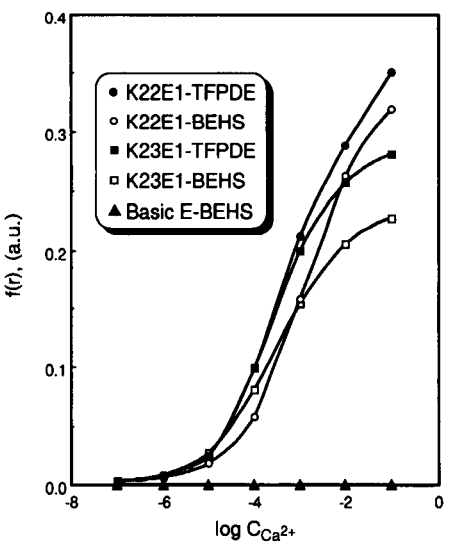

Fig. 6. Response curves for Ca^{2+} obtained with the optodes based on neutral Ca^{2+} ionophores and LAD-3.

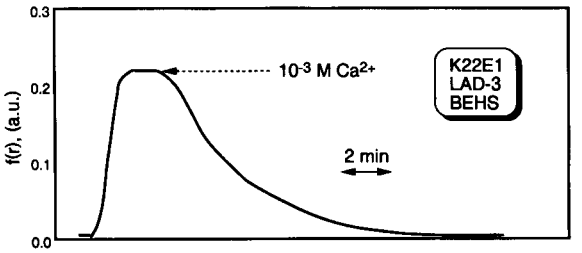

Fig. 7. Response profile of the optode based on K22E1, LAD-3 and TFPDE.

obviously different from that of the potentiometric liquid membrane electrode using the same neutral ionophore. The optodes based on the armed-azacrown derivatives K22E, K22E1, and K23E1 with TFPDE or BEHS as the lipophilic organic liquid exhibited a response to Ca^{2+} concentrations in a wide range of over five orders of magnitude. Especially the optode based on K22E1 and LAD-3 dissolved in TFPDE responded to Ca^{2+} concentrations in the range from 10^{-7} to 10^{-1} M, which involves the high sensitivity range of 5×10^{-5} to 10^{-2} M Ca^{2+}. The optodes based on the novel neutral ionophores K22E1 or K23E1 with TFPDE exhibited higher sensitivity to Ca^{2+} than those with BEHS. The value for the ion-pair extraction equilibrium constant, K, depends on the polarity of the organic liquid incorporating the ionophore and the dye. The more polar organic liquid gives larger K values, so that the higher sensitivity was obtained with the optode based on TFPDE compared to that based on BEHS which is a low polarity organic liquid.

Fig. 7 shows the typical response profile for 10^{-3} M Ca^{2+} of the optode based on K22E1 and LAD-3 dissolved in TFPDE. Similar response profiles were also obtained with the optodes based on other sensing bead components. The 95% response time of this optode was approximately 2 min after the injection of the sample solution including 10^{-3} M Ca^{2+}. The time required for one sample was about 10 min for 10^{-4} M Ca^{2+} and ca. 20 min for 10^{-1} M Ca^{2+} where a 100% response is recorded and includes the required time back to the blank absorbance value. Concerning the reproducibility of the response of the optodes based on K22E1, LAD-3, and TFPDE, the relative standard deviations for five response measurements to 1×10^{-3} M and 1×10^{-5} M Ca^{2+} were 0.6% and 0.8%, respectively.

Table 2 summarizes the selectivity coefficients of the Ca^{2+} optodes based on K22E, K22E1, and K23E1, in which five kinds of optodes were prepared with the

different organic sensing layer components. They all exhibited excellent Ca^{2+} selectivities against Li^+, Na^+, K^+, and Mg^{2+} ($\log k_{i,j}^{opt} \leq$ ca. -4) which exist in human serum electrolytes. There was no significant difference between the selectivity coefficients of the five prepared optodes and their ion selectivities are the best among all Ca^{2+} optodes developed to date [21–23]. The required selectivity coefficients of the optode for the measurement of Ca^{2+} concentration in human serum are also indicated in Table 2. These required values were calculated based on a maximum interference of 1% in the 0.1 mM Ca^{2+} measurement in which the co-existing electrolytes were assumed to be 3 mM Li^+, 150 mM Na^+, 5 mM K^+, and 0.8 mM Mg^{2+} that are the same as the upper ion concentration limit of normal human serum [1]. The ion selectivities of the five kinds of optodes all satisfied these required values. For a practical Ca^{2+} measurement, all ion-sensing components of the optodes require high lipophilicity which is an important factor for the reproducibility of the sensor response as well as for a long sensor lifetime. The required lipophilicity value of the neutral ionophores for the measurements in the aqueous sample solutions is reported as 10.0 in log $P_{o/w}$ values which guarantees a lifetime of at least 30 days with continuous use (24 h a day) of the optode in a flow-through system [18]. The log $P_{o/w}$ values for K22E, K22E1, and K23E1 are 10.1, 14.4, and 14.6, respectively, and the values for the lipophilic organic liquids used for the ion-sensing organic layer component are 10.0 and 10.3 for TFPDE and BEHS, respectively. Thus, the five kinds of optodes listed in Table 2 satisfy all the required lipophilicity values ($\log P_{o/w} \geq 10.0$).

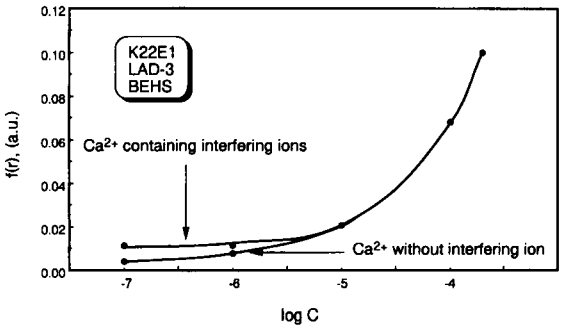

Fig. 8. Calibration curves for Ca^{2+} obtained with the optode based on K22E1, LAD-3 and BEHS with and without interfering ions similar to the human serum sample (interfering ion composition: 3 mM Li^+, 150 mM Na^+, 5 mM K^+, 0.8 mM Mg^{2+}).

3.4. Measurement of Ca^{2+} concentration in human serum using a Ca^{2+} optode

The measurement of Ca^{2+} concentration in human serum was performed using the flow-through type optode based on K22E1, LAD-3, and BEHS. Fig. 8 shows the calibration curve for Ca^{2+} obtained with the aqueous solution containing the interfering ions which had compositions similar to the upper normal level of human serum (3 mM Li^+, 150 mM Na^+, 5 mM K^+,

Table 2
Selectivity coefficients ($k_{i,j}^{opt}$ [a]; i = primmary ion, j = interfering ion) of the optodes based on various calcium ionophores and LAD-3 (at 0.1 M for each cation with 0.05 M Tris–HCl, pH 7.0)

Organic sensing layer [e] components		log $k_{i,j}^{opt}$ [b]					
		j = Li^+	Na^+	K^+	NH_4^+	Mg^{2+}	Ba^{2+}
K22E	BEHS	−4.1	−4.3	−4.0	−4.2	−4.2	−0.8
K22E	TFPDE	−3.9	−4.1	−4.0	−4.7	−3.8	−1.8
K22E1	BEHS	−4.0	−4.5	−4.1	−4.3	−4.0	−2.5
K22E1	TFPDE	−4.2	−4.9	−4.3	−4.7	−4.4	−2.8
K23E1	TFPDE	−4.0	−4.8	−4.1	−4.4	−4.0	−1.7
Required [c]		−2.5 [d]	−4.2	−2.7		−1.9	

[a] For calculations, see Results and discussion.
[b] i = Ca^{2+}.
[c] Required selectivity coefficients for a maximum interference of 1% by other cations (worst case, with following total concentrations; Li^+, 3 mM; Na^+, 150 mM; K^+, 5 mM; Mg^{2+}, 0.8 mM; and Ca^{2+}, 1.0 mM. 10-fold dilution).
[d] Therapeutic level.
[e] Abbreviations of the compounds, see Fig. 1.

0.8 mM Mg^{2+}). As shown in Fig. 8, the response curve of the optode for the serum sample is in perfect accord with the response curve for Ca^{2+} samples without any interfering ions in the Ca^{2+} concentration range over 1×10^{-5} M. The Ca^{2+} concentration in the normal serum sample solutions was found to be 2.51 ± 0.01 mM using this optode and the calibration curve shown in Fig. 7 with a relative standard deviations for five measurements was 0.40%. For this case, the expected value was 2.50 ± 0.10 mM. The sensor sensitivity and selectivity was almost constant for two weeks. Further lifetime measurements were not performed.

In this report, we demonstrated highly sensitive and selective Ca^{2+} optodes based on a novel neutral Ca^{2+} ionophore and a lipophilic anionic dye of the diphenyl amine type. Based on the principal described in Eq. 2, many kinds of ion-selective optodes could be developed using other excellent ion-selective neutral ionophores and chromophore (lipophilic dye).

Acknowledgements

This work was partially supported by the Asahi Glass Foundation, Kurata Research Fund and Iketani Foundation.

References

[1] D. Ammann, Ion-selective Microelectrodes, Springer Verlag, Berlin, 1986, 144.
[2] M. Shibagaki, Question and Answer of Water-Electrolyte, Chugai igakusha, Tokyo, 5th edn., 1987, 165.
[3] U. Schefer, D. Ammann, E. Pretsch, U. Oesch and W. Simon, Anal. Chem., 58 (1986) 2282.
[4] P. Gehrig, B. Rusterholz and W. Simon, Chimia, 43 (1989) 377.
[5] J.D.R. Thomas, Anal. Proc. (London), 22 (1985) 356.
[6] W. Simon, D. Ammann, M. Oehme and W.E. Morf, Ann. N.Y. Acad. Sci., 307 (1978) 52.
[7] G.J. Moody and J.D.R. Thomas, Ion-Sel. Electrode Rev., 1 (1979) 3.
[8] E. Pretsch, D. Ammann, H.F. Osswald, M. Guggi and W. Simon, Helv. Chim. Acta, 63 (1980) 191.
[9] J. Petranek and O. Ryba, Anal. Chim. Acta, 128 (1981) 129.
[10] D. Ammann, W.E. Morf, P. Anker, E. Pretsch and W. Simon, Ion-Sel. Electrode Rev., 5 (1983) 3.
[11] K. Kimura, K. Kumami, S. Kitazawa and T. Shono, J. Chem. Soc., Chem. Commun., 44 (1984) 2.
[12] T. Okada, H. Sugihara and K. Hiratani, Anal. Chim. Acta, 307 (1986) 186.
[13] S.A.H. Khalil, G.J. Moody, J.D.R. Thomas and J.L.F.C. Lima, Analyst, 611 (1986) 111.
[14] N. Nishino, T. Kamizuru, Y. Sano, T. Nakashima, H. Karakawa and T. Fujimoto, Peptide Chem., (1989) 365.
[15] K. Suzuki, K. Watanabe, Y. Matsumoto, M. Kobayashi, S. Sato, D. Siswanta and H. Hisamoto, submitted for publication.
[16] K. Watanabe, E. Nakagawa, H. Yamada, H. Hisamoto and K. Suzuki, Anal. Chem., 65 (1993) 2704.
[17] K. Suzuki, H. Ohzora, K. Tohda, K. Miyazaki, K. Watanabe, H. Inoue and T. Shirai, Anal. Chim. Acta, 237 (1990) 155.
[18] O. Dinten, U.E. Spichiger, N.A. Chaniotakis, P. Gerrig, B. Rusterholz, W.E. Morf and W. Simon, Anal. Chem., 63 (1991) 596.
[19] P. Kubelka and F. Munk, Z. Tech. Phys., 12 (1931) 593.
[20] IUPAC Recommendation for Nomenclature of Ion-Selective Electrodes, Pure Appl. Chem., 48 (1976) 129.
[21] B.P.H. Schaffer and O.S. Wolfbeis, Anal. Chim. Acta, 217 (1989) 1.
[22] W.E. Morf, K. Seiler, B. Rusterholz and W. Simon, Anal. Chem., 62 (1990) 738.
[23] T. Rosatzin, P. Holy, K. Seiler, B. Rusterholz and W. Simon, Anal. Chem., 64 (1992) 2029.

ELSEVIER

Analytica Chimica Acta 299 (1994) 189–194

ANALYTICA CHIMICA ACTA

Determination of hydrazines by capillary zone electrophoresis with amperometric detection at a platinum particle-modified carbon fibre microelectrode

Weihong Zhou, Liang Xu, Mingjia Wu, Lijuan Xu, Erkang Wang *

Laboratory of Electroanalytical Chemistry, Changchun Institute of Applied Chemistry, Chinese Academy of Sciences, Changchun 130022, China

Received 6 May 1994; revised manuscript received 15 July 1994

Abstract

A novel modified electrode dispersed with ultrafine platinum particles on the surface of a 30-μm carbon fibre microelectrode was investigated as an amperometric detector in capillary zone electrophoresis (CEEC) for determining hydrazines. The unique characteristic of the Pt particle-modified carbon fibre microelectrode is its excellent stability. Hydrazines were separated and detected by CEEC with the modified microelectrode with detection limits down to the femtomole level.

Keywords: Amperometry; Electrophoresis; Hydrazines

1. Introduction

Hydrazines are widely used in some industrial applications as catalysts, corrosion inhibitors, emulsifiers and reducing agents. Hydrazine is very important in pharmacology because it has been recognized as a carcinogenic and hepatotoxic substance, which affects liver and brain glutathione. Consequently, drug regulatory authorities are becoming increasingly aware of the need to control the levels of hydrazones in isoniazid and other hydrazide drugs and in their formulations. Therefore, sensitive methods are needed for their determination.

Amperometric detection is a powerful technique for monitoring easily oxidizable species. Unfortunately, hydrazine compounds exhibit such a large overpotential towards electrooxidation at ordinary carbon surfaces that they cannot be determined by this method. The development of methods for the determination of hydrazines based on liquid chromatography–electrochemistry (LCEC) has been reported [1–8]. Previous efforts to enhance the amperometric detection of hydrazines included the application of a pre-anodized glassy carbon electrode [1]. Chemically modified electrodes (CMEs) offer a promising way to minimize overpotential effects. Various CMEs have been constructed and applied in the LCEC of hydrazines sensing, including cobalt phthalocyanine (CoPC)-modified carbon paste elec-

* Corresponding author.

SSDI 0003-2670(94)00326-2

trodes [2,3] and inorganic mixed-valent Prussian Blue [4] (PB) and its analogous ruthenium cyanide [5] film-coated electrodes. A cobalt tetraphenylporphyrin-modified electrode [6] with heat treatment (HCME), an oxymanganese film-modified electrode [7] (MnCME) and a vitamin B_{12}-adsorbed glassy carbon electrode [8] have recently been prepared and used in the flow-injection amperometric detection of hydrazines.

A diverse range of CMEs have been applied to both flow-injection and liquid chromatographic (LC) systems. Few reports of the use of CMEs in capillary electrophoresis with electrochemical detection (CEEC) have appeared, even though CEEC has attracted increasing attention [9]. With off-column detection in CEEC, usually a 2–30-μm o.d. carbon fibre microelectrode (CFE) is manipulated inside the capillary bore. To modify a carbon fibre is difficult because of its inherently small dimensions. Colon et al. [10] tried two types of copper-modified carbon fibre electrodes, but the copper material was stripped from the carbon fibre after subsequent scans, producing unstable responses. O'Shea and Lunte [11] reported some good results with cobalt phthalocyanine and immobilized glucose oxidase-modified carbon paste microelectrodes.

In this work, a novel modified electrode dispersed with ultrafine platinum particles on the surface of a 30-μm carbon fibre microelectrode was investigated in CEEC. The unique characteristic of the Pt particle-modified carbon fibre microelectrode is its excellent stability. Hydrazines were separated and detected by CEEC with the modified microelectrode.

2. Experimental

2.1. Apparatus

The power supply (Jiuqiang Bioelctric, Beijing) provided a 0–30 kV d.c. high voltage. An uncoated fused-silica capillary (50 μm i.d.) was obtained from Yongnian Optical Fiber Factory (Hebei). To isolate the high-voltage field, the capillary has to be separated into two parts, a separation capillary and a detection capillary. A Nafion tube was used to link these two parts. The Nafion joint was made as described by O'Shea et al. [12]. This joint was immersed in a buffer reservoir, where the cathodic electrode of the power supply was also immersed. The joint permits ion movement but not bulk electrolyte flow, thus allowing electrochemical detection to be performed without adverse effects from the electrical field. Both the Nafion joint and electrochemical cell were shielded in an aluminium box to reduce external noise. An El-400 dual microelectrode potentiostat (Ensman Instrumentation, USA) was used as an amperometric detector. A Model 056 recorder (Hitachi) was used.

The electrochemical cell is similar to that described by Wallingford and Ewing [9]. The microelectrode was mounted on an X–Y–Z micromanpulator (laboratory-built) and positioned in the electrochemical detection cell. With the aid of an optical microscope, the microelectrode was aligned and inserted in the capillary column. The cell was operated in a two-electrode configuration, with a laboratory-built Ag/AgCl reference electrode.

2.2. Capillary conditioning

New fused-silica capillaries were treated by flushing with 0.1 M NaOH solution before use and then with doubly distilled water and the corresponding separation electrolyte. Before each run, the capillary was flushed with the separation electrolyte. The capillary was filled with water for overnight storage.

2.3. Electrode preparation

The microcylindrical carbon fibre electrodes were constructed with 30-μm diameter carbon fibre. One end of a 1–1.5-cm piece of the fine fibre was attached to a piece of Cu wire (10 cm $\times$ 200 μm diameter) by means of Ag epoxy, providing electrical connection. A glass capillary (1.7 mm o.d.) (Shanghai Brain Institute, Chinese Academy of Science) was pulled with a vertical pipette puller (Shanghai Institute of Physiology, Chinese Academy of Science), resulting in two capillary pieces with a microtip at one end of each. The tip of the glass micropipette was gently cut to allow passage of the fine carbon fibre. The carbon fibre was carefully introduced into the glass capillary through the end opposite to the microtip exposing 2–3 mm of the fibre. The open end of the glass capillary was filled

with epoxy using a syringe. After being allowed to cure at room temperature, the fibre was cut with a scalpel to give an exposed length of 1–2 mm.

After pretreatment, the carbon fibre electrode (CFE) was cycled in the potential range +0.3–1.3 V in 2.5×10^{-3} M K_2PtCl_4–0.1 M K_2SO_4 solution. A Pt(IV) complex was formed on the electrode surface by coordination with the oxygen atom of the oxide functional group on the carbon fibre. The platinum complex on the surface of the carbon fibre can be converted into Pt by cycling the electrode between −0.25 and +1.45 V in 0.1 M H_2SO_4. This procedure is a unique method for dispersing ultrafine platinum particles on the surface of carbon fibre. The method [13] is different from the common deposition technique, which employs the electroreduction of platinum salt from the solution.

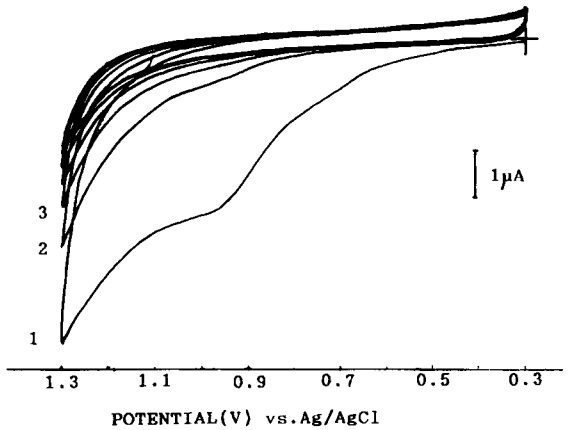

Fig. 1. Cyclic voltammograms of 2.5×10^{-3} M K_2PtCl_4 on a 30-μm i.d. CFE in 0.1 M K_2SO_4. Scan rate, 100 mV s^{-1}. E (V) vs. Ag/AgCl.

2.4. Cyclic voltammetry

Cyclic voltammetric experiments were performed with a laboratory-made potentiostat in a conventional three-electrode system cell, using a carbon fibre working electrode in conjunction with an Ag/AgCl reference electrode and a platinum wire counter electrode.

2.5. Reagents

Analytical-reagent grade hydrazine sulphate (HZ) was obtained from Beijing Institute of Chemicals and 1,2-dimethylhydrazine (DMHZ) from Merck. Stock solutions (0.1 M), prepared with doubly distilled water, were stored in the dark at 4°C. All other reagents were of analytical-reagent grade; doubly distilled water was used for the preparation of all solutions.

3. Results and discussion

3.1. Cyclic voltammetry of K_2PtCl_4 and formation of Pt particles at CFE

Cyclic voltammograms for 2.5×10^{-3} M K_2PtCl_4 on CFE were obtained in a solution of 0.1 M K_2SO_4 in the potential range +0.3–1.3 V. An irreversible anodic peak can be observed, as shown in Fig. 1 at +1.05 V. It is very interesting that the anodic peak for the oxidation of $PtCl_4^{2-}$ complex decreases gradually from cycle to cycle and finally reaches a steady state. Considering the oxide functional groups of an electrochemically activated carbon fibre, it is reasonable to suggest that oxygen atoms of the functional group may serve as one of the two axial ligands when the planar complex of Pt(II) is oxidized to form the octahedral complex of Pt(IV). The surface complex may hinder the electrooxidation of the Pt(II) complex by occupying the active site in the compact double layer, thus decreasing the apparent electrode area. As a result, the anodic peaks were shifted to higher potentials along with a decrease in peak current, as shown in Fig. 1.

The surface complex on the electrode can be converted into platinum particles on cathodization. After reaching the steady state as in Fig. 1, CFE can be activated electrochemically by cycling the electrode in the potential range from −0.2 to +1.45 V in 0.1 M H_2SO_4. The Pt(IV) complex on the surface of CFE can be reduced to Pt or Pt(II) complex with a cathodic scan. After cycling for about 2 min in the H_2SO_4, the typical steady state for the activated Pt-coated CFE was achieved as shown in Fig. 2.

3.2. Pt particle-modified CFE

The characteristics of the Pt particles on a CFE was evaluated by cyclic voltammetry. Fig. 3 shows

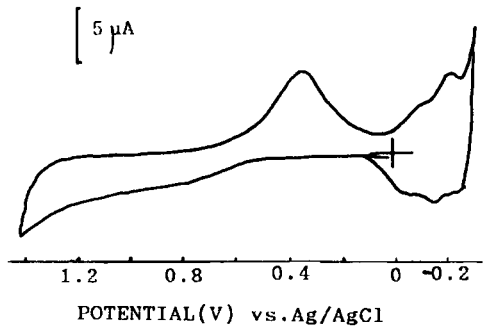

Fig. 2. Cyclic voltammograms of Pt-coated CFE in 0.2 M H_2SO_4. Scan rate, 500 mV s^{-1}. E (V) vs. Ag/AgCl.

the cyclic voltammograms obtained for (A)a bare electrode and (B)a Pt particle-coated electrode, both immersed in (a) a 4 mM phosphate buffer (pH 4.42) blank solution and (b) a 4 mM phosphate buffer (pH 4.42) solution containing hydrazine sulphate. The cyclic voltammograms of hydrazine sulphate in the 4 mM phosphate buffer show that no oxidation peak was obtained with the bare carbon fibre microelectrode in the potential range 0.0 – 1.2 V (curve A, b), whereas a defined oxidation peak with a potential of 0.60 V was observed with the Pt particle-coated carbon fibre microelectrode.

The current–time recordings obtained at (A) a bare CFE (B) a Pt particle-coated CFE are shown in Fig. 4. The oxidation current at the modified CFE was much larger than that at the bare CFE. The catalytic current observed was proportional to hydrazine concentration. The Pt particle-modified carbon fibre microelectrode exhibits a highly stable catalytic capability towards hydrazines in batch and flow systems. For example, virtually no changes in the peak potential and current on cyclic voltammograms for 1 mM hydrazine at the microelectrode were observed on scanning between 0.0 and 1.20 V at 100 mV s^{-1} during several hundred cycles. The behaviour was same from electrode to electrode.

The long-term stability of the electrode was investigated. The modified surface maintains long-term catalytic activity and is highly suitable for the electrochemical detection of hydrazine compounds in acidic and neutral solutions. As shown in Fig. 4C, an electrode that had been stored in the atmosphere for 2 weeks still gave highly reproducible catalytic responses.

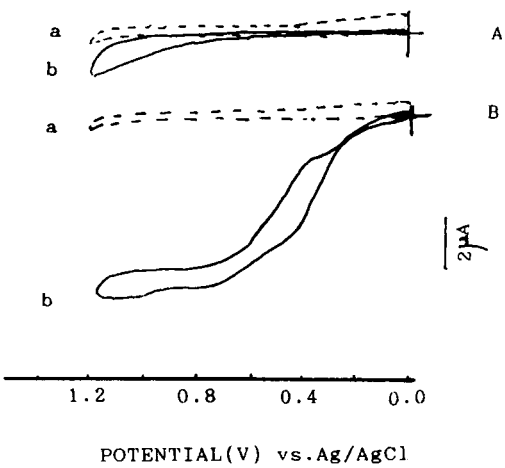

Fig. 3. Cyclic voltammograms of hydrazine sulphate at (A) carbon fibre microelectrode and (B) Pt particle-coated carbon fibre microelectrode in 4 mM phosphate buffer (pH 4.42) Scan rate, 100 mV s^{-1}; electrode diameter, 30 μm. (a) Blank solution; (b) containing 1 mM hydrazine sulphate solution.

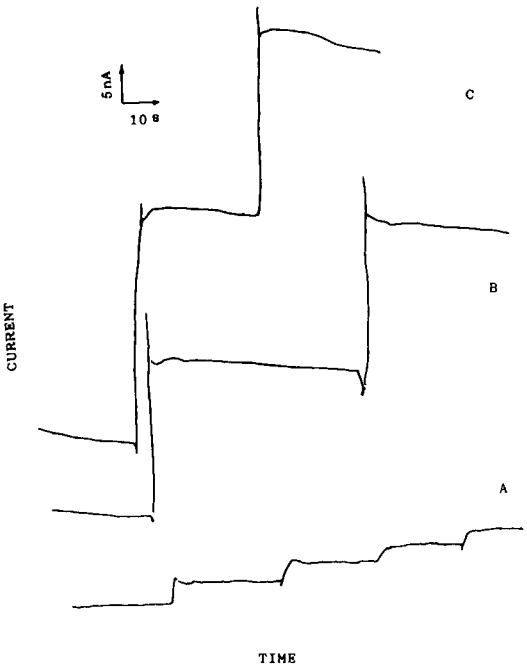

Fig. 4. Current–time recordings obtained at (A) a bare CFE (B) a, Pt particle-coated CFE and (C) as (B) but after standing for 2 weeks with increased HZ concentration of 2×10^{-6} M in 4 mM phosphate buffer (pH 6.96) solution. Operating potential, 1.0 V.

3.3. CZE

Fig. 5 shows the hydrodynamic voltammograms (HDVs) of hydrazines on a Pt particle-coated carbon fibre microelectrode under neutral conditions. Hydrazine exhibited plateau-shaped HDVs on the modified surface, reaching its maximum level at around 0.6 V. DMHZ, however, showed S-shaped HDVs, levelling off at 1.0 V. The sensitivity of current measurements follows the order HZ > DMHZ, consistent with their cyclic voltammetric behaviour. The amine group might be responsible for these differences. No apparent currents was obtained on a bare carbon fibre microelectrode surface up to 1.0 V under the same solution conditions. Based on the compromise among high sensitivity, selectivity and low background current, 1.0 V was selected for subsequent CE amperometric detection.

Well defined and resolved electropherograms were obtained and are shown in Fig. 6 for an operating potential applied at 1.0 V. Regression analysis for HZ over the concentration range $1 \times 10^{-4} - 1 \times 10^{-2}$ M (based on an injection volume of 27 nl, corresponding to 2.73–273 pmol) resulted in a correlation coefficient of 0.990 ($n = 6$). Regression analysis for DMHZ over the range of 15–350 pmol resulted in a correlation coefficient of 0.989 ($n = 5$).

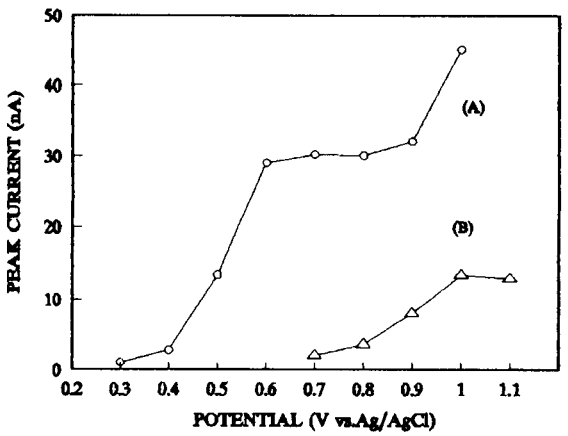

Fig. 5. Hydrodynamic voltammograms of 0.01 M each of (A) HZ and (B) DMHZ at a Pt particle-coated carbon fibre microelectrode. Capillary, 50 μm i.d.; separation capillary, 33 cm long; detection capillary, 1.7 cm long; injection by electromigration, 5 s at 12.4 kV; separation voltage, 12.4 kV; buffer, 4 mM phosphate (pH 6.96).

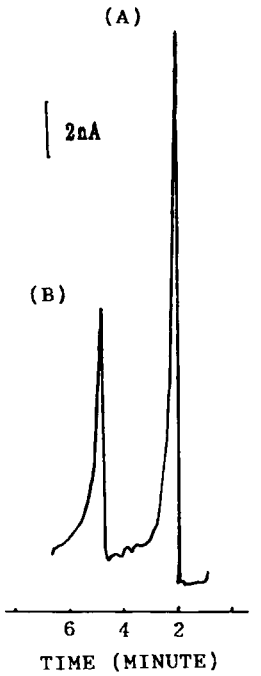

Fig. 6. Electropherogram of (A) HZ (5×10^{-3} M) and (B) DMHZ (2.5×10^{-2} M). Separation potential, 12.2 kV, 10 μA; injection, 12.2 kV for 10 s; electrochemical detection at 1.0 V; electrode, 30-μm i.d. Pt particle-coated carbon fibre microelectrode; capillary, 50 μm i.d.; separation capillary, 33 cm long; detection capillary, 1.7 cm long; 4 mM phospate buffer at pH 6.96.

The slopes of the curves obtained were 6.9 nA mM^{-1} for HZ and 0.188 nA mM^{-1} for DMHZ. Based on a signal-to-noise ratio of 3, the detection limits were found to be 90 fmol for HZ and 500 fmol for DMHZ. The relative standard deviation for the current response of 20 consecutive injections of 1×10^{-3} M HZ was calculated to be 2.2%.

Sample introduction was accomplished using an electromigration system and the volume injected was calculated in the continuous fill mode by recording the time required for the sample to reach the detector. In order to obtain reproducible results, it is important to maintain the electrode at the same position in relation to the outlet of the capillary. The electrodes had to be replaced mainly because of breakage, caused by accidental movements of the electrode or the capillary. The same microelectrode has been used without any special treatment for a period up to 2 weeks with more than 100 runs, and

no change in the character was observed during this period.

4. Conclusion

The Pt particle-modified carbon fibre microelectrode studied is easy to prepare and has excellent stability. This modified electrode offers high sensitivity for the detection of hydrazines. This method should be extremely useful for detecting hydrazines in real samples, e.g., the detection of traces of hydrazine in isoniazid and its formulations has been done in this laboratory.

Acknowledgement

This project was supported by the National Natural Science Foundation of China.

References

[1] K. Ravichandran and R.P. Baldwin, Anal. Chem., 55 (1983) 1782.
[2] K.M. Korfhage, K. Ravichandran and R.P. Baldwin, Anal. Chem., 56 (1984) 1514.
[3] J. Wang, T. Golden and R. Li, Anal. Chem., 60 (1988) 1642.
[4] W. Hou and E. Wang, Anal. Chim. Acta, 257 (1992) 275.
[5] J. Wang and Z. Lu, Electroanalysis, 1 (1989) 517.
[6] W. Hou, J. Hua and E. Wang, Chin. Sci. Bull., 36 (1991) 785.
[7] Z. Taha and J. Wang, Electroanalysis, 3 (1991) 215.
[8] J. Zhou and E. Wang, Electroanalysis, 4 (1992) 473.
[9] R.A. Wallingford and A.G. Ewing, Anal. Chem., 60 (1988) 258.
[10] L.A. Colon, R. Dadoo and R.N. Zare, Anal. Chem., 65 (1993) 476.
[11] T.J. O'Shea and S.M. Lunte, Anal. Chem., 66 (1994) 307.
[12] T.J. O'Shea, R.D. Greenhagen, S.M. Lunte and C.E. Lunte, J. Chromatrgr., 593 (1992) 305.
[13] L. Xu, F. Li and S. Dong, J. Electroanal. Chem., in press.

ELSEVIER

Analytica Chimica Acta 299 (1994) 195–208

ANALYTICA CHIMICA ACTA

Systematic comparison of data-processing options for kinetic-based single-component determinations of non-catalysts Part 1. Review, systematic classification, mathematical descriptions, performance characteristics and perspectives

Michael D. Love, Harry L. Pardue *

Department of Chemistry, 1393 Brown Bldg., Purdue University, West Lafayette, IN 47907-1393, USA

Received 28 April 1994; revised manuscript received 26 July 1994

Abstract

This paper addresses several aspects of the applications of kinetic-based methods for single-component determinations of non-catalysts. One goal is to review many of the different approaches to these kinetic-based determinations. A second goal is to organize many of these different approaches into a systematic classification scheme. A third goal is to present mathematical descriptions that help to differentiate among the different approaches. A fourth goal is to differentiate among important features of the different approaches with emphasis on the ruggedness of the different options. In this context, ruggedness is defined as the ability of a method to resist changes in experimental variables. It is concluded that available options can be grouped into one or more of four general categories in this regard, namely those with no ability to resist changes in experimental variables, those that resist such changes via temporal optimization, those that can be used in modes that compensate for changing variables extrinsically and those that have built-in (intrinsic) variable compensation. A fifth goal is to place the many different options to kinetic-based determinations into a somewhat broader and more consistent perspective than may have been done previously. In particular, an aim is to identify similarities among measurement and data-processing options applied to transient (kinetic) aspects of chemical, physico-chemical and physical processes.

Keywords: Kinetic methods; Data-processing options; Non-catalysts; Single-component determination

1. Introduction

Kinetic-based determinations can be traced to the previous century [1]. Although these kinetic-based methods frequently offer advantages relative to methods based on equilibrium responses [2–5] they also tend to be less rugged than equilibrium-based determinations because transient responses tend to depend more on experimental conditions than equilibrium responses [6]. Recognizing these problems, several authors have developed and reported measurement and data-processing methods designed to improve the ruggedness of kinetic-based determinations. With few exceptions [7,8], most studies have focused on just one approach which makes it difficult to compare relative merits of the different variable-compensating options.

Based on these observations, a study was undertaken to compare performance characteristics of a variety of kinetic measurement and data-processing options [9].

* Corresponding author.

SSDI 0003-2670(94)00362-9

Table 1
Classification and performance features of measurement/data-processing options for single-component kinetic-based determinations of non-catalysts: unmodified-signal options

	Temporal optimization	Variable compensation	
		Intrinsic	Extrinsic
(A) Signal-based calculations			
(1) Direct-computation			
(a) One-point/fixed-time	?	No	Yes
(b) Two-point/fixed-time	Yes	No	Yes
(c) Multipoint			
(i) Three-point/fixed time	NA [a]	Yes	NA [a]
(ii) Four-point/fixed time	NA	Yes	NA
(iii) Partial sums	NA	Yes	NA
(2) Indirect-computation			
(a) Linear extrapolation			
(i) Semi logarithmic	NA	Yes	NA
(ii) Semi exponential	NA	Yes	NA
(b) Non-linear curve-fitting			
(i) First-order model	NA	Yes	NA
(ii) Variable-order model	NA	Yes	NA
(iii) Empirical model	NA	Yes	NA
(B) Other measurement objective			
(1) Direct computation			
(a) Variable-time option			
(i) One-point	No	No	Yes
(ii) Two-point	No	No	Yes
(b) Signal-stat option	Possible	Possible	Possible
(2) Indirect-computation			
(a) Signal-stat option	NA	Yes	

[a] Not applicable.

Results of that study are to be published in a short series of papers. This first paper in the series reviews a variety of data-processing approaches reported to date with emphasis on similarities and differences among concepts and mathematical models used in the different options.

2. Classification of options

Many different features can be used as the basis for classifying different measurement and data-processing approaches to kinetic-based determinations [2–5,9,10]. The first feature used in this classification scheme involves the choice between the use of unmodified or modified forms of detector signals in the data-processing step. In this context, options based on simple mathematical operations such as logarithmic or exponential conversions are included in a group identified as *unmodified-signal options* whereas options involving calculus-based operations such as differentiation and integration are included in the group called *modified-signal options* because it may or may not be possible to retrieve the actual detector signal.

2.1. Unmodified-signal options

Measurement and data-processing approaches included in the unmodified-signal option are summarized in Table 1. Approaches within this general option can be further subdivided depending upon the quantity measured and used to compute concentration (herein called the *measurement objective*). In most applications the detector signal itself is the measurement objective. However, in some procedures, the detector signal is used only as an indicator that some events have taken

Table 2
Classification and performance features of measurement/data-processing options for single-component kinetic-based determinations of non-catalysts: modified-signal options

	Temporal optimization	Variable compensation	
		Intrinsic	Extrinsic
(A) Rate-based options			
(1) Direct-computation			
(a) One-rate option	Yes	No	Yes
(b) Two-rate option	NA	Yes	NA [a]
(2) Indirect-computation			
(a) Linear extrapolation			
(i) Rate extrapolation	NA	Yes	NA
(ii) Semilogarithmic	NA	Yes	NA
(b) Non-linear extrapolation			
(i) Michaelis–Menten model	NA	Yes	NA
(B) Integrated-signal options			
(1) Direct-computation			
(a) One-integral option	?		
(b) Two-integral option	Probably	No	Probably
(2) Indirect-computation			
(a) Linear extrapolation			
(i) Successive integration	NA	Yes	NA
(b) Non-linear extrapolation			
(i) First-order model	NA	Yes	NA
(ii) Mixed-order model	NA	Yes	NA

[a] Non applicable.

place and some other variable such as reaction time or reagent volume is measured and used to compute concentration. These two approaches are grouped in Table 1 as *signal-based calculations* and as *other measurement objective.*

Within each of these groupings there are two other choices that are called *direct-computation* and *indirect-computation* options. In the direct-computation option, the measured variable (detector signal or other measurement objective) is used with a suitable closed-form mathematical function or calibration plot or equation to quantify analyte concentration directly. In the indirect-computation option, the detector signal or other measurement objective are not used directly to compute concentration; rather some other quantity is derived from these directly measured variables and used to compute concentration. A typical example of the indirect-computation option involves the use of linear or non-linear curve-fitting methods to extrapolate measured signals to infinite time in order to obtain a derived quantity (eg. equilibrium signal) that is used to compute the concentration.

Other features of the classification scheme, such as the number of data points or linear vs. non-linear extrapolation, are discussed later in connection with more specific examples.

2.2. *Modified-signal option*

Measurement and data-processing options included in the modified-signal option are summarized in Table 2. The most common modifications of signals are time-based differentiation (*rate-based options*) and time-based integration (*integrated-signal options*). Each of these more general options includes direct-computation and indirect-computation options as discussed above, as well as several other features such as the number of rates or integrals and linear vs. non-linear extrapolations. These and other features are discussed in more detail below.

3. Selected performance characteristics

The classification scheme in Tables 1 and 2 is a convenient way to compare two important performance characteristics of the various options, namely *temporal optimization* [11] and *variable compensation* [5,12]. Although these terms have been used somewhat interchangeably in the literature, there are subtle but important differences between them. Temporal optimization involves the use of a carefully selected measurement time or time interval at which effects of variables are minimized. On the other hand, variable compensation involves the use of data-processing procedures that reduce or eliminate effects of changes in variables [5,12]. A temporally optimized method will be optimized for only one set of conditions; if conditions differ from the expected situation then the method will no longer be optimized. On the other hand, with variable-compensation methods, variables can change over quite large ranges without affecting the results. Thus it is important to differentiate between these two features.

The variable-compensation feature can be further subdivided into two groups. Some data-processing options are inherently designed to compensate for changes in experimental variables; these options provide *intrinsic variable compensation.* Some data-processing options do not have built-in capability to compensate for changes in variables but can be used in ways to provide variable compensation; these options provide *extrinsic variable compensation.*

Tables 1 and 2 indicate which of these characteristics are associated with each of the data-processing options included in the table. Considering the two-point/fixed-time option as an example, it has been shown that it can be used in a temporally optimized mode [9,13]. Although this option does not provide any intrinsic variable compensation, it can be used to provide extrinsic variable compensation by using rate constants determined independently for each sample to calculate concentration [9]. These and other features are discussed in more detail for other options later in this paper.

4. Mathematical descriptions

Mathematical descriptions of the different options follow the groupings summarized in Tables 1 and 2. Although most of the mathematical descriptions are applicable to a wide variety of situations, some simplifying assumptions are included for sake of simplicity.

First, the treatment is restricted to single-component determinations of non-catalysts. Second, unless stated otherwise, it is assumed that each analyte is a reactant in a first-order reaction and that the progress of the reaction is monitored by changes in the concentration of a product of the reaction. Third, it is assumed that the measured signal varies linearly with product concentration as follows

$$S_t = S_0 + bC_t \tag{1}$$

in which S_t is the measured signal, S_0 is a background signal, b is a sensitivity factor and C_t is the time-dependent concentration that is monitored. Finally, unless stated otherwise, it is assumed that measured signals change monotonically with time.

4.1. Unmodified-signal options/signal-based computations

This group includes options without either optimization or variable compensation, with optimization, with extrinsic variable compensation and with intrinsic variable compensation.

The primary mathematical relationship upon which all the first-order options are based is

$$S_t = S_0 + bC_a^0[1 - \exp(-kt)]$$
$$= S_0 + \Delta S_\infty[1 - \exp(-kt)] \tag{2}$$

in which some symbols are defined above, C_a^0 is the initial analyte concentration, k is a pseudo-first-order rate constant, t is time and ΔS_∞ is the total signal change from $t=0$ until the reaction (process) is complete. Differences among the alternative options depend primarily upon the way this relationship is used.

This group is further subdivided into two major subgroupings, namely *direct-computation* and *indirect-computation options.* Examples of each group are discussed below.

4.1a. Direct-computation options

In this group of options, the detector signal is used directly to compute the concentration. The concentration is determined directly from the measured values of the detector signal by using either a closed-form mathematical equation or a calibration plot or equation.

One-point/fixed-time option

In a one-point/fixed-time method, the detector signal is measured at some fixed point in time after the reaction (process) is initiated. An early example of a one-point/fixed time option involved the determination of "diastase" (amylase) based on the determination of the amount of substrate, starch, that reacted during a fixed time period [1]. That procedure and other similar ones of the same era were awkward and time consuming; however, the principles of the measurement/data-processing steps were the same as modern versions of this general approach [10]. In such procedures applied to first-order reactions, the background signal, S_0, is assumed to be zero, and analyte concentration is determined from a single proportionality of the form

$$C_a^0 = S_t/\{b[1-\exp(-kt)]\} \quad (3)$$

in which the calibration constant, $1/\{b[1-\exp(-kt)]\}$, was evaluated by using calibration standards or calibration plots. The one-point option cannot compensate for background (blank) signals and it cannot detect unexpected changes in kinetic behavior. Any change in variables that would affect the rate constant would also affect the calibration constant and computed concentration. The one-point/fixed-time option is seldom used now because it does not compensate for changing backgrounds.

Two-point/fixed-time option

The two-point/fixed-time option is perhaps the most widely used approach for kinetic determinations [5,7,10]. In this approach, two signal values, S_1 and S_2, are measured at two points in time, t_1 and t_2, and the difference, $\Delta S_t = S_2 - S_1$, is used to compute the concentration. The mathematical description for a first-order process is easily shown to be

$$C_a^0 = \Delta S_\infty / b$$
$$= \Delta S_t/\{b[\exp(-kt_1) - \exp(-kt_2)]\} \quad (4a)$$

In the most common applications of this approach, the calibration factor in the denominator of the right-most term is determined by using calibration standards. This option compensates for background signals but, like the one-point option, cannot detect unexpected changes in kinetic behavior. This approach offers no intrinsic compensation for variables that influence the rate constants. Extrinsic variable compensation can be obtained by using independently determined values of the rate constant for each sample and using these in Eq. 4a to compute the concentration [9].

A temporally optimized approach to the two-point/fixed-time option has been described [13]; a slightly modified version [9] is described here. By rearranging Eq. 4a to be explicit in the signal difference, ΔS_t, taking the first derivative with respect to the rate constant, setting the result equal to zero, collecting terms and setting the ratio, $t_2/t_1 = R$, the result can be rearranged into the form

$$t_1 = (1/k)(\ln R)/(R-1) \quad (4b)$$

in which $R = t_2/t_1 > 1$. Thus, for any value of k and R, it is easy to calculate a continuum of optimized values of t_1 (Eq. 4b) and $t_2 = Rt_1$. This temporally optimized approach requires prior knowledge of the rate constant and is effective only for small changes in the rate constant.

Multipoint options

Multipoint options are defined as options that use three or more data points in the data-processing step. At least three direct-computation options have been reported. Although reported independently, the first two options are special cases of the third.

Three-point/fixed-time option. By measuring three values of signal, S_1, S_2, S_3, at three points in time such that $\Delta t = t_2 - t_1 = t_3 - t_2$, it is possible to compute both the rate constant and the total signal change, ΔS_∞, that would be expected if the reaction (process) were to proceed to completion [14]. The rate constant is given by

$$k = -(1/\Delta t)\ln[(S_3 - S_2)/(S_2 - S_1)] \quad (5a)$$

By making use of some rules of logarithms and exponents ($n \ln x = \ln x^n$ and $\exp(\ln x) = x$), equations for ΔS_∞ presented earlier [14] can be simplified to

$$\Delta S_\infty = (S_3 - S_1)/\{[(S_3 - S_2)/(S_2 - S_1)]^{t_1/\Delta t} - [(S_3 - S_2)/(S_2 - S_1)]^{t_3/\Delta t}\} \quad (5b)$$

For this and other approaches discussed elsewhere in this paper, the analyte concentration can be computed as the equilibrium signal change divided by the sensitivity, $C_a^0 = \Delta S_\infty / b$, (see Eqs. 1 and 4a). This approach provides intrinsic compensation for variables that affect rate constants.

Four-point/fixed-time option. The four-point/fixed-time option [15] requires measurements of four signals, S_0, S_1, S_2, S_3, at four points in time such that t_1-$t_0 = t_2 - t_1 = t_3 - t_2 = \Delta t$, where S_0 is measured at $t = 0$. Like the three-point option, this option can be used to compute the signal change expected if the reaction were to go to completion. The quantitative relationship is

$$\Delta S_\infty = S_1 + [(S_2 - S_1)^2/(2S^2 - S_1 - S_3)] - S_0 \qquad (6)$$

Again, because the computed maximum signal change is independent of the rate constant, this approach provides intrinsic compensation for variables that affect rate constants. Operationally, it differs from the three-point option in that a value of the background signal, S_0, is required.

Partial-sums option. The partial sums option [16,17] is a straight-forward method to compute both the first-order rate constant and the equilibrium signal change. In this method three sets of signal values are obtained and summed. Each set must contain the same number, p, of data points with the same spacing, Δt, between successive points. Three sums, Σ_1, Σ_2, Σ_3, of signals, S_t, are computed over ranges of $t = 0$ to t_{p-1}, t_p to t_{2p-1} and t_{2p} to t_{3p-1}, respectively. It can be shown that the rate constant is given by

$$k = -\ln[(\Sigma_3 - \Sigma_2)/(\Sigma_2 - \Sigma_1)]/p\Delta t \qquad (7a)$$

Using the same symbols given above, in which Σ_1 is the sum from $t = 0$ to t_{p-1}, the maximum signal is given by

$$\Delta S_\infty = \{1 - [(\Sigma_3 - \Sigma_2)/(\Sigma_2 - \Sigma_1)]^{1/p}\}(\Sigma_2 - \Sigma_1) / \{1 - [(\Sigma_3 - \Sigma_2)(\Sigma_2 - \Sigma_1)]\}^2 \qquad (7b)$$

This approach permits direct computation of the maximum signal change, ΔS_∞, that is independent of the rate constant and accordingly provides intrinsic variable compensation.

It is easy to see by inspection of Eqs. 5a and 7a that the three-point/fixed-time option is a special case of the partial-sums option. In the former case, $p = 1$; in the latter case, $p \geq 1$.

4.1b. *Indirect-computation options*

In these options, some quantities derived from measured values of detector signal are used to compute the concentration. Selected examples are discussed below.

Linear extrapolations

Two of the three options involve semilogarithmic extrapolations between the measured signal and time and the other involves semiexponential extrapolation.

Semilogarithmic extrapolations. The classic approach used to determine rate constants is to measure several values of the signal, S_t, including the equilibrium signal, S_∞, at several points in time and to plot ln $(S_\infty - S_t)$ vs. t. The slope of such a plot is equal to $-k$ and the intercept is equal to ln S_∞. The primary value of this option is to obtain the rate constant.

A procedure described originally by Guggenheim [18] involves a semilogarithmic extrapolation of data that has been used primarily to determine rate constants but can also be used to determine the equilibrium signal change, ΔS_∞, and analyte concentration. In this approach, two or more paired sets of signals, S_i and $S_{i+\Delta t}$, are measured at times, t_i and $t_{i+\Delta t}$. Starting with Eq. 2, it is easy to develop the relationship

$$\ln(S_{i+\Delta t} - S_i) = -\mathrm{k}t_i + \ln\{\Delta S_\infty[1 - \exp(-k\Delta t)]\} \qquad (8)$$

For several pairs of data, the rate constant is obtained from the slope of a plot of $\ln(S_{i+\Delta t} - \mathrm{S_i})$ vs. t_i and the equilibrium signal change can be obtained from the intercept. Because the rate constant can be determined for each sample, this option can provide compensation for variables that affect rate constants. Accordingly, this approach can provide intrinsic variable compensation.

Semiexponential extrapolation. The approach described by Kezdy [19] and Swinbourne [20] also makes use of several pairs of data as described above for the Guggenheim method. However, unlike the method of Guggenheim, this approach involves a semiexponential extrapolation. Starting with Eq. 2, it is easy to develop the relationship

$$S_i = S_{i+\Delta t}[\exp(k\Delta t)] + S_\infty[1 - \exp(k\Delta t)] \qquad (9)$$

For several pairs of data, the slope of a plot of S_i vs. $S_{i+\Delta t}$ should be linear with slope equal to $\exp(k\Delta t)$. Thus, the rate constant can be obtained from the slope and the maximum signal, S_∞, can be obtained from the intercept. Like the Guggenheim method, this approach can provide *intrinsic variable compensation* via a two-step computational process.

There are some similarities and differences between these latter two approaches. With both options, data points need not be equally spaced in time but the spacing, Δt, between pairs of points, must be the same for all pairs. Because the Guggenheim option involves a non-linear (logarithmic) transformation of the signal, data should be weighted by the factors, $1/(S_i - S_{i+\Delta t})^2$, for least-squares fits. Because the Kezdy–Swinbourne treatment does not involve any non-linear transformation of the data, no weighting is required. Whereas the Guggenheim approach yields the signal change, ΔS_∞, directly, the Kezdy–Swinborne approach does not, meaning that an independent measure of S_0 must be obtained for the latter method.

Non-linear curve-fitting options

Several extrapolation options based on non-linear curve-fitting procedures have been described [12,21–24]. This option is identified herein as the *curve-fitting/predictive option* because measured data are used with suitable kinetic models and a curve-fitting process such as linear or non-linear least-squares or the Kalman filter [22,24] to predict the signals that would be measured if the reaction (process) were monitored to completion. Selected examples involving different kinetic models are described briefly here; all these options can yield intrinsic variable compensation.

First-order model. The first-order version of the curve-fitting/predictive option is implemented by fitting a first-order model such as Eq. 2 to experimental data [8,12]. In this case, the object of the curve-fitting process would be to obtain best-fit values of S_0, ΔS_∞ and the rate constant, k. Thus, in a single data-processing step, it is possible to compensate intrinsically for variables that affect rate constants.

It has also been shown [9] that the curve-fitting predictive option can be adapted to other approaches including those described by Cornell (partial sums [16,17]), Guggenheim [18], Kezdy and Swinbourne [19,20] and the successive-integration option described later.

Variable-order model. Although the previous option will compensate for variables that affect rate constants, it will not compensate for variables that affect reaction order. This subsection describes an option that permits inherent compensation not only for variables that affect rate constants but also for variables that affect reaction order [23]. For a reaction with order n, the rate can be represent by

$$-\mathrm{d}C/\mathrm{d}t = kC^n \qquad (10a)$$

It can be shown [23] that the time-dependent signal is given by

$$S_t = S_\infty - [k_s(n-1)t + (\Delta S_\infty)^{1-n}]^{1/(1-n)} \qquad (10b)$$

in which k_s is a signal-based rate constant. By fitting this model to data that follow reaction orders other than zero and unity, it is possible to obtain best-fit values of S_∞, ΔS_∞, k_s and n, thus permitting intrinsic compensation for variables that affect both rate constants and reaction order.

Empirical model. To this point it has been assumed that a theoretical model for the process of interest is available. For some very complex processes it is not always possible to develop a reliable theory in a reasonable period of time. In such cases, it may be necessary to use an empirical model. Also, to this point it has been assumed implicitly that the process being monitored is a chemical reaction. As noted earlier, that is not a necessary condition. An example is cited here that illustrates both these situations.

The example involves an application of the curve-fitting-predictive option to liquid chromatography [25]. Data from the leading edges of chromatographic peaks are used with a suitable mathematical model and curve-fitting procedure to predict the steady-state signal expected if sufficient sample were added to saturate the chromatographic column. It was shown that the predicted saturation signals are virtually independent of sample volume and flow-rate over two-fold ranges of both variables. By comparison, dependencies of both peak-height and peak-area methods on these variables were 10 to 100-fold larger than for the predictive steady-state option.

4.2. *Unmodified-signal option/other measurement objectives.*

As noted earlier, the most distinguishing feature of this group of options is that the detector signal is used only as an indicator that some events have taken place and some other variable such as reaction time or reagent volume is measured and used to compute the concentration. This feature is analogous to titration options for equilibrium-based methods in the manner in which

detector signal and other measurement objectives are used. It differs from titration procedures in the sense that the events detected do not correspond to equivalent points between reactant and analyte. Both direct-computation and indirect-computation options are considered here.

4.2a. Direct-computation options

Two different options in this group have been identified. In one option, the measurement objective is the time interval, Δt, required for the reaction (process) to proceed to a predetermined extent; this group has been called *variable-time methods* [26,27]. In the other option, the detector signal is used to indicate when a property (e.g. pH) has changed outside some predetermined narrow limits and a reagent (e.g. acid or base) is added to return the property to within the desired limits. The quantity of reagent needed to maintain the measured property within the desired limits is measured and used to compute the analyte concentration. The most common version of this group is the *pH-stat option*; however, the concept is general and the generalized version is identified herein as the *signal-stat option.*

Variable-time options

Two versions of this option are identified here, namely one-point and two-point options.

One-point/variable-time option. In this option, the quantity measured was the time interval between the start of a reaction and some predetermined point in the reaction, usually completion. An early example of this option involved a "stop-watch method" for the determination of iodine based on the catalysis by iodine of the reaction between thiosulfate and nitrous acid [28]. The time from start to finish was measured and used to compute iodine concentration. An extension of this approach involved the famous Kolthoff–Sandell procedure for iodine based on catalysis of the cerium(IV)/arsenic(III) reaction [29].

Two-point/variable-time option. In this option, the measurement objective is the time interval between two predetermined signal values [30,31]. The time interval is used to compute concentration. This option has been discussed extensively for chemical reactions [10,26,28]; however, although it has some interesting features, it is seldom used in practice. Some interesting physical and physico-chemical analogues have been developed. A purely physical analogue involves the determination of viscosity by measuring the time required for a small spherical object to fall a fixed distance in the fluid of interest [32]. A physico-chemical analogue involves a flow-injection approach in which the measured quantity is the time required for the detector signal to change between two predetermined points on a response profile [33–36]. Like the chemical analogues [10,26–28], these latter options do not require a knowledge of the relationship between concentration and detector signal and the dynamic range can be extended by control of reagent concentration [35].

Signal-stat option

The most common version of this option is the pH-stat in which acid or base is added as needed to maintain a constant pH [37]. An important feature of this approach is that some critical property of a reaction system is controlled at a near constant value. Although applied principally for control of pH, the concept should be applicable to the control of any reactant such as a coenzyme in an enzymatic reaction.

The quantity measured and used to compute the concentration is the amount of reagent added to maintain the property constant. Usually the concentration being controlled is a reactant or product in the reaction. Therefore, the time-dependent addition of reagent reflects the time course of the reaction. Usually multiple additions of reagent are required so that a multipoint response curve is available. If the reaction is first-order (or any other order) the data for reagent vs. time will reflect this. Although the two-point/fixed-time option is usually used with pH-stat applications, virtually any of the data-processing options discussed in this paper can be applied to such data with all the advantages and limitations associated with each option.

4.2b. Indirect-computation option

It should be both possible and advantageous to apply the curve-fitting predictive option to multipoint data from a signal-stat procedure and obtain intrinsic variable compensation.

4.3. Modified-signal options

Two groups of modified-signal options are discussed here, namely *rate-based* and *integrated-signal options.*

It is important to differentiate between the integrated-signal option and the integrated form of the rate equation. The unmodified-signal options discussed earlier make use of the integrated form of the rate equation. The integrated-signal options utilize the *double integral* of the rate equation with respect to time.

4.3a. Rate-based options

The rate-based options are grouped into direct-computation and indirect-computation categories.

Direct-computation options

Two groupings of direct-computation, rate-based options, namely *one-rate and two-rate options*, have been identified.

One-rate option. The one-rate option is one of the most popular approaches to kinetic determinations [5,7,10]. In this approach, the rate of signal change is measured (or computed) and related to analyte concentration. Assuming that the analyte is the rate determining reactant in a first-order reaction, the relationship can be represented as:

$$V_t = \mathrm{d}S/\mathrm{d}t = bkC_a^0 \qquad (11a)$$

in which $\mathrm{d}S/\mathrm{d}t$ is the velocity, V, of signal change, b is the sensitivity factor in Eq. 1, k is a first-order rate constant and C_a^0 is the initial analyte concentration. Calibration standards are usually used to obtain a calibration constant representing the proportionality factor, bk. In such procedures, changes in any variable (e.g. temperature, pH, enzyme activity) that would affect the rate constant would produce an error in the determined concentration. Thus, the usual application of the one-rate option does not provide any compensation for variables that affect rate constants.

One way to reduce effects of variables is to use temporal optimization by making rate measurements at a point in time at which the effects of changes in the rate constant have a minimum effect on the determined value of analyte concentration. Previous studies [11,38–40] have shown that the optimum time is related to the rate constant as follows

$$t_{opt} = 1/k \qquad (11b)$$

Obviously, use of this option requires prior knowledge of the value of the rate constant. This approach does not compensate for changes in the rate constant; it reduces effects of those changes.

Another way to reduce effects of variables that affect rate constants is to determine the apparent value of the rate constant for each sample, and to use the determined value to compute analyte concentration. Appropriate manipulation of the first-order expression shows that the total signal change when all reactant has reacted is given by

$$\Delta S_\infty = V_t/k \exp(-kt) \qquad (11c)$$

The total signal change, ΔS_∞, is proportional to initial analyte concentration ($\Delta S_\infty \propto C_a^0$). Thus, the determined value of k can be used to compute analyte concentration by using either Eq. 11a or 11c. Either procedure would provide extrinsic variable compensation.

Two-rate option. In this option, two rates, V_1 and V_2, determined at two points in time, t_1 and t_2, are used to compute the concentration [41]. Appropriate manipulation of the first-order expression in Eq. 11c for two rates yields

$$\Delta S_\infty = [V_1(t_2 - t_1)/\ln(V_1/V_2)](V_1/V_2)^{t_1/(t_2-t_1)} \qquad (12)$$

Thus, the equilibrium signal change, which is proportional to the analyte concentration, can be computed from the two rates. The two-rate option provides intrinsic variable compensation.

Indirect-computation options

Both linear and non-linear extrapolation procedures have been applied to rate data yielding a variety of options with intrinsic variable compensation. The linear-extrapolation options are based on the assumption of first-order kinetics; the non-linear extrapolation does not require first-order behavior and has been applied to reactions that follow Michaelis–Menten kinetics.

Linear-extrapolation options. The first option depends upon the fact that, for a first-order process, a plot of $\mathrm{d}S/\mathrm{d}t$ vs. S_t is linear and extrapolates to S_∞ when $\mathrm{d}S/\mathrm{d}t = 0$ [42]. The determined value of S_∞ should be independent of the rate constant and variables that affect it; accordingly, this rate-extrapolation option gives intrinsic variable compensation provided an independent value of S_0 is measured.

A second option, which is a rate analogy of the Guggenheim method, involves a semilogarithmic extrapolation [9]. Writing Eq. 11c for two rates, V_i and $V_{i+\Delta t}$

at two times, t_i and $t_{i+\Delta t}$, rearranging to be explicit in the rates, subtracting the second from the first, and rearranging yields

$$\ln(V_i - V_{i+\Delta t}) = -kt_i + \ln\{k\Delta S_\infty[1-\exp(-k\Delta t)]\} \quad (13)$$

If several pairs of rates are determined at times, t_i and $t_{i+\Delta t}$, then the slope of a plot of $-\ln(V_i - V_i\Delta t)$ vs. t_i should be proportional to the rate constant and the intercept should be related to the equilibrium signal change. The value of the rate constant determined in this way can be used with the numerical value of the intercept and the second term on the right side of Eq. 13 to compute the signal change, ΔS_∞, which is proportional to initial analyte concentration. Alternatively, the rate constant could be used with one or more of the rates to compute ΔS_∞ by using Eq. 11a or 11c. Either approach would yield intrinsic variable compensation.

Non-linear extrapolation option. Both linear-extrapolation options described above apply only to first-order processes. The non-linear-extrapolation option described here should be applicable to a variety of options; application to a Michaelis–Menten model is described here. Starting with the rate form of the Michaelis–Menten equation, it is easily shown that the rate, V_t, at some time t, is related to the maximum signal change, ΔS_∞, and the signal change ΔS_t at time t as follows [43,44]

$$V_t = V_{max}(\Delta S_\infty - \Delta S_t)/[K_m + (1/b)(\Delta S_\infty - \Delta S_t)] \quad (14)$$

in which V_{max} is the maximum velocity, K_m is the Michaelis–Menten constant and other symbols have been defined above. Multiple data for signal vs. time were used to compute the rate and the signal change, $\Delta S_t = S_t - S_0$, at each of several points in time. Then Eq. 14 was fit to these values of V_t and ΔS_t by an iterative process that yielded values of V_{max}, K_m and ΔS_∞ that gave the best fit of the model to the data for each sample. Because the computed value of ΔS_∞ corresponded to best-fit values of V_{max} and K_m, this approach provided inherent compensation for variables that affected these reaction parameters. Results for the enzymatic determination of uric acid were virtually independent of the amount of an inhibitor (xanthine) of uricase added to sample solutions [43]. An added advantage of the approach is that calibration plots of ΔS_∞ vs. concentration remain linear well beyond the range for which initial rates become independent of substrate concentration.

4.3b. *Integrated-signal options*

The integrated-signal options have been implemented by both direct-computation and indirect-computation procedures. All these options make use of multiple data points. However, some options utilize only one integral, some utilize two integrals and some utilize multiple integrals.

Direct-computation options

Direct-computation options have been implemented with both one-integral and two-integral options.

One-integral option. A single-integral option has been described [45], evaluated for a variety of applications and compared to conventional rate and two-point/fixed-time methods [46,47]. In this approach, signal vs. time data are integrated over a single fixed-time interval and the resulting integral is related to analyte concentration. For a variety of kinetic models, the integral is proportional to analyte concentration. Principal advantages of the approach are that it reduces effects of random noise and it is applicable to a variety of kinetic responses without prior knowledge of the kinetic behavior as long as it is the same among standards and samples. In fact, it has been shown to be applicable to time-dependent responses with maxima and minima [48]. As described in these papers, this particular approach does not permit compensation for systematic changes in variables that affect rate constants nor has temporal optimization been attempted.

Two-integral options. An early integration method was designed to determine the slopes of linear (pseudo zero-order) responses [49–51]. In this approach, the signal was integrated during two equal time periods, $\Delta t = t_2 - t_1 = t_4 - t_3$ separated by an interval, $\Delta t' = t_3 - t_2$. It was shown that the difference between the two areas, $\Delta A = A_2 - A_1$, was related to the rate of signal change, $V_s = dS/dt$, as follows

$$V_s = \Delta A/[\Delta t'\Delta t + \Delta t]^2 \quad (15a)$$

For the special situation involving integration of two adjacent segments of the response, $t_2 = t_3$ and $\Delta t' = 0$ so that the expression reduces to

$$V_s = \Delta A/(\Delta t)^2 \quad (15b)$$

This approach has the advantage of reducing effects of random signal noise via the integration process. As implemented in these early studies, this approach does not provide either intrinsic or extrinsic variable compensation nor was temporal optimization attempted, although the latter should be possible.

Indirect-computation options

Both linear-extrapolation and nonlinear- extrapolation options have been implemented with integrated data. Both groups of options make use of multiple integrals.

Linearized-extrapolation option. One approach identified here as *successive integration* [9,52] is a linearization procedure that can be illustrated for first-order processes by writing the first-order equation in the form

$$S_t = S_\infty - (S_\infty - S_0)\exp(-kt) \tag{16a}$$

Integration of both sides and rearranging yields

$$\exp(-kt) = k(A_t - S_\infty t)/(S_\infty - S_0) \tag{16b}$$

in which A_t is the area corresponding to the integral of signal vs. time. Substitution into Eq. 16a yields

$$S_t = -kA_t + kS_\infty t + S_\infty \tag{16c}$$

The area, A_t, can be obtained by using the trapezoidal rule. A fit of this linearized model to data for S_t, A_t, and t should yield best-fit values of k and S_∞ [52]. The equilibrium signal change can be calculated if an independently measured value of S_0 is available. The resulting value of the equilibrium absorbance can be used to compute concentration values that are independent of variables that affect rate constants. Accordingly, this approach provides intrinsic compensation for variables that affect rate constants.

Non-linear-extrapolation options. Two versions of the non-linear-extrapolation option are presented here, one involving a first-order process and one involving a combined zero-order/first-order process.

In an extension of the curve-fitting predictive method to atomic absorption data obtained via an electro-thermal atomizer, it was found that the time-dependent area, Q_t, could be represented by a first-order relationship [53]. Accordingly, the equation

$$Q_t = Q_0 + (Q_\infty - Q_0)[1 - \exp(-kt)] \tag{17}$$

was fit to data for area vs. time to obtain best-fit values of Q_0, Q_∞ and k. Values of $\Delta Q_\infty = Q_\infty - Q_0$ evaluated in this way should have low dependencies on atomization conditions. This was confirmed for atomization temperatures from 2200 to 2600°C [53], demonstrating inherent variable compensation for this approach.

A different application involves an enzyme-based electrode used in a thin-layer cell such that all the substrate in a small volume of solution normal to the surface of the reactor/sensor system decreased toward a small steady-state value [54]. It was hypothesized that integration of the current corresponding to depletion of substrate in the small fixed volume of solution near the reactor surface should yield a charge, Q_∞, proportional to the amount, and therefore concentration of substrate. Because the concentration is determined from the total amount of substrate reacting in a fixed volume, it should be independent of variables that affect the kinetic behavior and should have a linear range much larger than results based on steady-state responses for which the linear range is limited by the effective Michaelis constant.

A mathematical treatment of the system showed that the charge vs. time data could be represented by a combined zero-order/first-order model of the form

$$Q_t = k_0 C_b t + k_2 C_b[1 - \exp(-k_3 t)] \tag{18a}$$

in which C_b is the bulk substrate concentration and k_0, k_2, and k_3 are combinations of rate constants (see Eq. 12 in [54]). Because the bulk concentration was proportional to the maximum charge, the equation was used in the form

$$Q_t = \beta_0 Q_\infty t + \beta_1 Q_\infty[1 - \exp(-kt)] \tag{18b}$$

in which β_0 and β_1 are variables incorporating the rate constants and the sensitivity factor relating charge and concentration. By fitting this combined zero-order/first-order model to data for Q_t vs. t, it was possible to obtain best-fit values of β_0, β_1, k and Q_∞. Accordingly, Q_∞ values determined in this way should have low dependencies on variables that affect the rate processes and should have extended linear ranges relative to steady-state based results. The latter expectation was fully confirmed; the former only partially. The linear range for the curve-fitting option was much wider than that for the steady-state option which exhibited curvature toward the concentration axis consistent with Michaelis–Menten behavior of initial-rate results. The

curve-fitting option exhibited substantially smaller dependency on pH than the initial-rate option. Additional work is needed to exploit the full potential of this general approach.

5. Discussion

Most of the different options described above can be used either in temporally optimized modes or in modes that provide either extrinsic- or intrinsic-variable compensation. However, in most options the mathematical justifications are based on first- or pseudo-first-order behavior. This includes all the fixed-time options, the two-rate option, the partial-sums option, and the options adapted from Guggenheim and Kezdy–Swinbourne. An important advantage of the curve-fitting predictive option is that it is applicable to a wide variety of kinetic models [12,20–25,52–60]. The two primary requirements are that a suitable model be found and that the predicted signal be independent of the variables of interest. The only example examined to date for which significant (10 to 100-fold) variable compensation has not been achieved involved the application to an ion-selective electrode [59]. As expected, temperature compensation was not achieved because equilibrium potentials depend on temperature; however, it is probable that effects of other variables that affect the kinetic response but not the equilibrium potential can be reduced.

There is a tendency to focus at least implicitly on kinetic responses that change monotonically with time. However, that is not a necessary requirement. Several examples have been discussed above in which peak-shaped kinetic responses have been used [25,48,53,57,58]. Another group which is discussed only indirectly above involves non-equilibrium steady-state responses. There are many examples such as the responses from membrane-based sensor systems such as the oxygen electrode [58] and enzyme-based electrodes [54]. For these and many other examples, the steady-state response that is measured usually corresponds to situations in which two or more rate processes are counter-balancing one another. It is important to recognize this fact because results based on such non-equilibrium steady-state responses tend to have much larger variable dependencies than equilibrium-based results. Moreover, it has been shown that measurement/data-processing options developed originally for more conventional types of kinetic responses can improve the ruggedness of methods based on these types of responses [54,56].

Also, there is a tendency to associate kinetic analyses almost exclusively with determinations based on the kinetic behavior of chemical reactions. Despite this perception, it is important to realize that there are some strong correlations among methods based on transient aspects of chemical reactions and transient aspects of physical and physico-chemical processes. For example, just as the transient responses of chemical processes tend to depend more on experimental conditions than equilibrium responses, the transient responses of physico-chemical and physical processes tend to depend more on experimental conditions than equilibrium responses. Consequences of this behavior are also similar. For example, to obtain similar degrees of reliability with kinetic-based and equilibrium-based determinations, it usually is necessary to control conditions within tighter tolerances for kinetic-based than equilibrium-based determinations. As examples, just as it is necessary to control variables such as temperature and pH within tight limits for determinations based on kinetics of chemical reactions, it also is necessary to control variables such as sample volume and flow-rate within tight tolerances for chromatographic methods based on transient responses (e.g. peak heights).

There are also analogies among data-processing approaches used with the different processes. For example, the fixed-time measurement approach used with chemical reactions is analogous to peak-height measurements in chromatography or flow injection; both involve measurement of detector signal at a fixed point in time of a transient response. Similarly, there is a close analogy between the variable-time approach as applied to chemical reactions [30,31] and the time-based methods used with flow-injection systems [33–36]; both groups involve the measurement of the time required for a process to change between predetermined points and use of the measured time to compute concentration. There also is a strong analogy between the integrated-signal approach applied to chemical reactions [45–51] and peak-area approaches applied to chromatography [25], flow-injection [57] and other types of transient responses; all involve the measurement and use of integrals of transient detector signals.

There are potential advantages to making these correlations. From a disciplinary point of view, it is important that we recognize systematic patterns rather than viewing the area as a collection of unrelated methods. From a pragmatic point of view, it is important to recognize these similarities because approaches developed to solve problems in one area can be adapted to solve analogous problems in other areas. For example, although most of the variable-compensating measurement and data-processing approaches described above were developed with chemical reactions in mind, it has been shown that similar advantages can be realized by applying similar procedures to physico-chemical and physical processes such as liquid chromatography [25], electrothermal atomizers [53], enzyme-based reactor-sensor systems [54], flow-injection [57], membrane-based detectors [58], ion-selective electrodes [59,61,62] and laser ionization [63]. Similarly, the integrated-signal (peak-area) option developed initially for chromatography has been extended to chemical reactions [45–51] with analogous advantages.

This paper is restricted to single-component determinations for a variety of reasons. However, it is important to note that the variable-compensating feature of the curve fitting approach [12] has been extended to other kinetic models suitable for mixtures [64,65]. Additional information about multicomponent methods is available in some of the more general references given above [2–6] and in an excellent review [66] published recently.

We believe the classification scheme presented herein is sufficiently general to accommodate all these seemingly dissimilar methodologies.

Acknowledgements

This research was supported in part by Grant GM 13326-25/26 from the National Institutes of Health.

References

[1] W. Roberts, Proc. Roy. Soc. London, 32 (1881) 145.
[2] H.B. Mark, Jr. and G.A. Rechnitz, Kinetics in Analytical Chemistry, Wiley Interscience, New York, 1968.
[3] H.A. Mottola, Kinetic Aspects of Analytical Chemistry, Wiley Interscience, New York, 1988.
[4] D. Perez-Bendito and M. Silva, Kinetic Methods in Analytical Chemistry, Ellis Horwood, Chichester, 1988.
[5] H.L. Pardue, Anal. Chim. Acta, 216 (1989) 69.
[6] H.A. Mottola and H.B. Mark, Jr., Anal. Chem., 58 (1986) 264R.
[7] P.D. Wentzel and S.R. Crouch, Anal. Chem., 58 (1986) 2855.
[8] B.L. Bacon and H.L. Pardue, Clin. Chem., 35 (1989) 360.
[9] M.D. Love, Comparison of Performance Characteristics for Different Data-Processing Methods for Kinetic Determinations, Ph.D. Thesis, Purdue University, West Lafayette, IN, 1992.
[10] H.L. Pardue, Clin. Chem., 23 (1977) 2189.
[11] S.A. Engh and F.J. Holler, Anal. Chem., 60 (1988) 545.
[12] G.E. Meiling and H.L. Pardue, Anal. Chem., 50 (1978) 1611.
[13] J.E. Davis and B. Renoe, Anal. Chem., 51 (1979) 526.
[14] R.C. Harris and E. Hultman, Clin. Chem., 29 (1983) 2079.
[15] R. Christie Smith, Philos. Mag. J. Sci., 1 (1926) 496.
[16] R.G. Cornell, Biometrics, 18 (1962) 104.
[17] R.G. Cornell and J.A. Speckman, Biometrics, 23 (1967) 717.
[18] E.A. Guggenheim, Philos. Mag. J. Sci., 2 (1926) 538.
[19] F.J. Kezdy, J. Kaz and A. Bruylants, Bul. Soc. Chim. Belge, 67 (1958) 687.
[20] E.S. Swinbourne, J. Chem. Soc., (1960) 2731.
[21] R.L. Czervionke, G.F. Johnson, N.F. Nujuayhid and R.D. Feld, Clin. Chem., 32 (1986) 1648.
[22] C.A. Corcoran and S.C. Rutan, Anal. Chem., 60 (1988) 1146.
[23] J.A. Larsson and H.L. Pardue, Anal. Chim. Acta, 224 (1989) 289.
[24] S.C. Rutan, C.P. Fitzpatrick, J.W. Skoug, W.E. Weiser and H.L. Pardue, Anal. Chim. Acta, 224 (1989) 243.
[25] J. Li and H.L. Pardue, Anal. Chem., 65 (1993) 1980.
[26] W.J. Blaedel and G.P. Hicks, Advances in Analytical Chemistry and Instrumentation, Vol. 3, Wiley, New York, 1964 pp. 105–142.
[27] J.D. Ingle, Jr. and S.R. Crouch, Anal. Chem., 43 (1971) 697.
[28] H.A. Baines, J. Chem. Soc. Perkin Trans., 49 (1930) 481T.
[29] E.B. Sandell and I.M. Kolthoff, J. Am. Chem. Soc., 56 (1934) 1426.
[30] M. Somogyi, J. Biol. Chem., 125 (1938) 399.
[31] H.V. Malmstadt and H.L. Pardue, Anal. Chem., 33 (1961) 1040.
[32] S. Siggia, Survey of Analytical Chemistry, McGraw-Hill, New York, 1968, p. 185.
[33] J. Ruzzicka, E.H. Hansen and H. Mosbaek, Anal. Chim. Acta, 92 (1977) 235.
[34] H.L. Pardue and B. Fields, Anal. Chim. Acta, 124 (1981) 39, 65.
[35] J.F. Tyson, Anal. Chim. Acta., 179 (1986) 131.
[36] H.L. Pardue and J.M. Jordan, Anal. Chim. Acta, 220 (1989) 23.
[37] R.E. Karcher and H.L. Pardue, Clin. Chem., 17 (1971) 214.
[38] J.G. Atwood and J.L. Di Cesare, Clin. Chem., 21 (1975) 1263.
[39] J.B. Landis, M. Rebec and H.L. Pardue, Anal. Chem., 49 (1977) 785.
[40] F.J. Holler, R.K. Calhoun and S.F. McClanahan, Anal. Chem., 54 (1982) 755.
[41] P.D. Wentzell and S.R. Crouch, Anal. Chem., 58 (1986) 2851.

[42] K. Sahlin, R.C. Harris and E. Hultman, Anal. Biochem., 63 (1975) 572.
[43] S.D. Hamilton and H.L. Pardue, Clin. Chem., 28 (1982) 2359.
[44] S.D. Hamilton and H.L. Pardue, Clin. Chem., 30 (1984) 226.
[45] L.C. Thomas and G.D. Christian, Anal. Chim. Acta, 77 (1977) 153.
[46] L.C. Thomas and C.L. Wood, Anal. Lett., 22 (1989) 989.
[47] L.C. Thomas and R.A. Othman, Talanta, 38 (1991) 773.
[48] G.E. Radke and L.C. Thomas, Anal. Chim. Acta, 161 (1984) 91.
[49] E.A. Cordos, S.N. Crouch and H.V. Malmstadt, Anal Chem., 40 (1968) 1812.
[50] G.P. Hicks, A.A. Eggert and E.C. Toren, Jr., Anal. Chem., 42 (1970) 729.
[51] J.D. Ingle, Jr. and S.R. Crouch, Anal. Chem., 42 (1970) 1055.
[52] I.B.C. Matheson, Anal. Instrum., 16 (1987) 345.
[53] C. Hsiech and H.L. Pardue, Anal. Chem., 65 (1993) 1809.
[54] C.E. Uhegbu, K.B. Lim and H.L. Pardue, Anal. Chem., 65 (1993) 2443.
[55] R.P.W. Scott, in H.A. Stobel and W.R. Heineman (Eds.), Chemical Instrumentation: A Sysematic Approach, Wiley, New York, 1989 pp. 892–894.
[56] J.F. Tyson, Anal. Chim. Acta, 214 (1988) 57.
[57] J.M. Jordan, M.D. Love and H.L. Pardue, Anal. Chim. Acta, 272 (1993) 125.
[58] C.E. Uhegbu and H.L. Pardue, Anal. Chem., 64 (1992) 2378.
[59] M.D. Love, H.L. Pardue and G. Pagan, Anal. Chem., 64 (1992) 1269.
[60] K.H. Mancey, D.A. Okum and C.N. Reilley, J. Electroanal. Chem., 4 (1962) 65.
[61] J. Janata, Anal. Chem., 62 (1990) 33R.
[62] I. Schechter, Anal. Chem., 64 (1992) 2610.
[63] I. Schechter, H. Schröder and K.L. Kompa, Anal. Chem., 64 (1992) 2787.
[64] I. Schechter, Anal. Chem., 64 (1992) 729.
[65] I. Schechter and H. Schröder, Anal. Chem., 64 (1992) 325.
[66] B.M. Quencer and S.R. Crouch, CRC Crit. Rev. Anal. Chem., 24 (3) (1993) 243.

ELSEVIER

Analytica Chimica Acta 299 (1994) 209–218

ANALYTICA CHIMICA ACTA

Systematic comparison of data-processing options for kinetic-based single-component determinations of non-catalysts Part 2. One-rate, two-point/fixed-time, two-rate, three-point/fixed-time options

Michael D. Love, Harry L. Pardue *

Department of Chemistry, 1393 Brown Bldg., Purdue University, West Lafayette, IN 47907-1393, USA

Received 28 April 1994; revised manuscript received 26 July 1994

Abstract

This paper describes and compares performance characteristics of four data-processing options for kinetic-based determinations. Options compared are two-point/fixed-time, one-rate, three-point/fixed-time and two-rate methods. Features evaluated are the effects of systematic changes in variables such as rate constants and reaction order as well as different levels of random noise. Both simulated and experimental data are used to evaluate effects of systematic changes in rate constants and simulated data are used to evaluate effects of random noise and systematic deviations from first-order behavior. All the options appear to be relatively independent of small changes (± 0.1) in reaction order. The two-point/fixed-time and one-rate options have no inherent ability to reject effects of systematic changes in rate constants but optimum conditions can be identified that reduce effects of such changes. The latter two methods have the inherent ability to reject effects of systematic changes in rate constants but appear to be more dependent on random noise than the two-point/fixed-time and one-rate options. Application of the optimized two-point/fixed-time and one-rate methods and the three-point/fixed-time and two-rate options to experimental data for uric acid demonstrate 40- to 100-fold improvements in ruggedness for changes in the rate constant relative to non-optimized two-point/fixed-time and one-rate methods.

Keywords: Kinetic methods; Data processing; Non-catalysts; Single-component determination

1. Introduction

Many different types of quantitative determinations are based on transient responses. Accordingly, many different measurement and data processing options for kinetic-based determinations have evolved [1–8]. As expected, these different options have different performance characteristics. For example, options such as one-rate and two-point/fixed-time methods [5–8] are very easy to implement but have no inherent ability to compensate for changes in kinetic behavior that result from unexpected changes in experimental conditions. However, these methods can be implemented in ways that reduce effects of experimental variables by selecting optimized measurement times such that effects of changes in variables are minimized [9–12]. Other more complex methods, such as the three-point/fixed-time [13], the two-rate [14] and the predictive [15] methods, automatically compensate for changes in experimental variables.

* Corresponding author.

SSDI 0003-2670(94)00363-7

A few studies have been designed to compare features of some examples of these many different data-processing options [5,7,16]. However, each of these studies has been limited to selected features of just a few of the many options available. The present study [17] was undertaken to better understand effects of random noise and systematic changes in kinetic parameters such as rate constants and reaction orders on results obtained with a wide range of data-processing options for kinetic-based determinations.

This is the second paper in a series in which results of this study will be reported. This paper focuses on four of the simpler options, namely the two-point/fixed-time, one-rate, two-rate [14] and three-point/fixed-time [13] options. This paper identifies more explicitly how to select optimum conditions for the optimized two-point/fixed-time method than was done in the original study [9]. It also compares effects of systematic changes in rate constants and reaction order on unoptimized and optimized two-point/fixed-time and one-rate methods, as well as the variable-compensating two-rate and three-point/fixed-time options by using both simulated and experimental data. Finally it compares effects of different levels of random noise on the four data-processing options.

2. Mathematical treatment

Mathematical treatments have been presented elsewhere for the optimized one-rate [10–12], two-rate [14] and three-point/fixed-time [13] methods, and these treatments are not discussed further here. Although the optimized two-point/fixed-time method was discussed previously [9], an explicit procedure for computing optimum times was not presented. Accordingly, that treatment is extended here.

The optimized two-point/fixed-time method, like the other options discussed herein, assumes first- or pseudo-first-order behavior. For a first-order process in which the time-dependent signal, S_t, varies linearly with the property of interest (e.g. product concentration), the signals, S_1 and S_2, at any two points, t_1 and t_2, in time are related as follows

$$\Delta S_{2,1} = S_2 - S_1 = \Delta S_\infty [\exp(-kt_1) - \exp(-kt_2)] \quad (1)$$

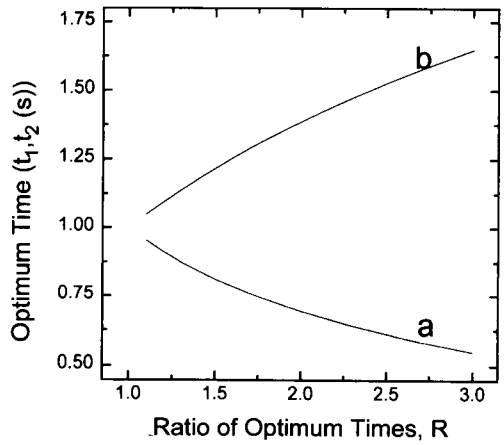

Fig. 1. Normalized optimum times vs. ratio of optimum times for two-point/fixed-time method. Both plots: $k = 1\ s^{-1}$; plot a: t_1 (Eq. 4); plot b: $t_2 = Rt_1$.

in which $\Delta S_{2,1}$ is the signal change between times t_1 and t_2, S_2, S_1, t_1 and t_2 are as defined above, ΔS_∞ is the total signal change when the process has gone from $t = 0$ to equilibrium ($\Delta S_\infty = S_\infty - S_0$) and k is the first-order rate constant.

To identify conditions that minimize the effects of changes in the rate constant on the results, we take the first derivative with respect to the rate constant and equate it to zero; the result is identified herein as the error coefficient for the rate constant (e.c.$_k$). The result for Eq. 1 is

$$\text{e.c.}_k = \frac{\partial(\Delta S_{2,1})}{\partial k} = \Delta S_\infty \{t_2[\exp(-kt_2)] - t_1[\exp(-kt_1)]\} \quad (2)$$

Setting Eq. 2 equal to zero to minimize the error coefficient and setting $R = t_2/t_1$, the result can be rearranged to give

$$t_2 - t_1 = (1/k)\ln(t_2/t_1) = (1/k)\ln R \quad (3)$$

in which R is assumed to be greater than unity. This equation is easily rearranged into the form

$$t_1 = (1/k)(\ln R)/(R-1) \quad (4)$$

Thus, for any value of k and R, it is easy to calculate the optimum value of t_1 and accordingly $t_2 = Rt_1$.

Fig. 1 shows how t_1 and t_2 vary with the ratio, R, for $1 < R \leq 3$ and k equal to unity. An interesting conclusion results from Eq. 4 when $R = 2$; for this situation, $t_1 = t_{1/2}$. For other values of R, values of t_1 and t_2 for

any value of the rate constants can be obtained by dividing ordinate values in Fig. 1 by the numerical value of k.

3. Experimental

3.1. Data processing

All data were processed on a supermicro computer (Masscomp MC-5500, Massachusetts Computer Corp., Westford, MA). All programs were written in the C language using the double-precision variable-class for numbers. Data were processed using a program designed to accommodate a wide variety of data-processing options; more details are presented elsewhere [17].

3.2. Simulated data

Signal vs. time data were generated by using both first-order and variable-order equations. The variable-order equation used was [18]

$$S_t = S_\infty - [k_s(n-1)t + (S_\infty - S_0)^{1-n}]^{1/1-n} \quad (5)$$

in which S_0, S_t and S_∞ are signals at times $t=0$, t and infinity (equilibrium), k_s is a signal-based rate constant [18] and n is the reaction order.

Random noise with a Gaussian distribution was superimposed upon some responses by using a random-number generator. Details of the process used to generate and test the random numbers are reported elsewhere [17]. Briefly, means and standard deviations of 10 sets of 10 000 numbers each agreed with expected values of zero and unity; an overlay of the 100 000 numbers with a Gaussian probability curve exhibited excellent agreement and the sample data set passed a chi-squared test for a Gaussian distribution at the 99% confidence level.

All results for simulated data are based on 100 simulated data sets for each set of conditions.

3.3. Experimental data

Experimental data from a previously reported study of the enzymatic determination of uric acid [19] were used. The data set consisted of absorbance vs. time data for duplicate runs on each of six uric acid standards spanning a concentration range of 0.100–0.250 mmol l^{-1}. The average rate constant for the data set was determined to be $k_{ref} = 0.0180\ s^{-1}$; the time scale for each of the kinetic data sets was varied by factors from 0.20 to 5.00 of the original data sets to simulate variations in the rate constant from 0.090 s^{-1} to 0.0036 s^{-1}, i.e. from $5k_{ref}$ to $0.2k_{ref}$. These modified data sets were used to evaluate the effects of variations of the rate constant on results obtained with different data-processing options with a fixed noise level.

3.4. Relative error coefficients

Relative error coefficients are use to quantify effects of systematic changes in rate constants and reaction orders. The relative error coefficient is defined as the change in concentration per unit change of the variable of interest divided by the true concentration [r.e.c. $(\%) = 100\ (dC/dV)/C_o$ in which dC and dV are the changes in concentration and the variable of interest and C_o is the true concentration]. Computed signal changes, $\Delta\hat{S}_\infty$, were converted to concentration by using assumed (simulated data) or real (experimental data) values of sensitivity factors (e.g. molar absorptivities and path lengths). Results were plotted as the ratio of computed to true concentrations, C/C_o, vs. the variable of interest. Solid curves in such plots represent fits of third-order cubic splines to the data for visualization purposes. Relative error coefficients were evaluated as the slopes of these plots at any desired value of the variable (usually the reference value). This is expressed mathematically as

$$\text{r.e.c.}(\%) = 100d(C/C_o)/dV \quad (6)$$

in which $d(C/C_o)/dV$ is the slope of a plot of C/C_o vs. the variable, V.

4. Results and discussion

The primary focus of this study is on effects of systematic changes in rate constants and reaction order on results obtained by using the different data-processing options. Both simulated and experimental data were used to evaluate effects of rate constants. Only simulated data were used to evaluate effects of reaction order and random noise.

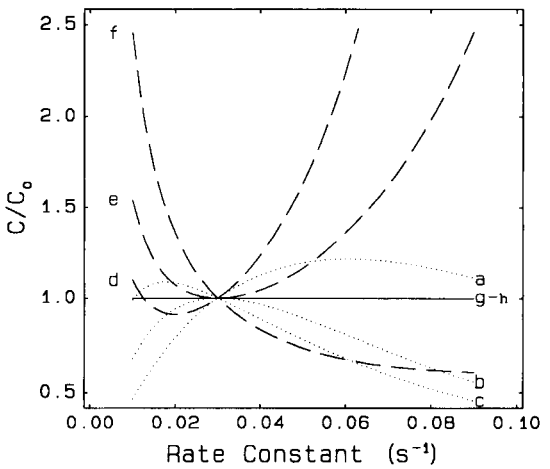

Fig. 2. Effects of rate constant on ratios of computed vs. true concentration for different data-processign options and conditions. Simulated data: $k_{ref}=0.0300\ s^{-1}$. a–c: Two-point/fixed-time option; measurement intervals: (a) 13.4–20 s, (b) 13.4–66.9 s*, (c) 13.4–150 s. d–f: One-rate method; measurement time: (d) 10 s, (e) 33.3 s*, (f) 50 s. g,h: Three-point/fixed-time and two-rate options; measurement times: (g) 10, 30 and 50 s, (h) 10 and 50 s.

Optimum measurement times are marked by an asterix in figure legends and tables. All imprecisions are reported at the level of one standard deviation (± 1 S.D.).

4.1. *Effects of rate constants.*

Simulated data

Fig. 2 shows effects of different values of rate constants on ratios of computed to true concentrations for each of the four data-processing options applied to responses without superimposed noise. Results for the two-point/fixed-time option (plots a–c) and the one-rate option (plots d–f) include measurement times below, at and above the optimum times for these methods. For the two-point/fixed-time method with $k=0.030\ s^{-1}$ and $R=5$, the optimum times computed with Eq. 4 are $t_1=(1/0.03\ s^{-1})\ (\ln 5)/(5-1)=13.4$ s and $t_2=5\ t_1=66.9$ s. The optimum time for the one-rate method is $t_{opt}=1/k_{ref}=1/0.030\ s^{-1}=33.3$ s.

As expected, results for the two-point/fixed-time and one-rate methods all cross the line corresponding to the ratio, $C/C_o=1$, at the true value of the rate constant. In other words, regardless of the measurement time used, all methods give the correct result for the correct value of the rate constant.

As noted earlier, the relative error coefficient in terms of the rate constant is the slope of the plot of C/C_o vs. the rate constant (see Eq. 6). It is noted that plots b and e, representing optimum measurement times for the two-point/fixed-time and one-rate methods, pass through a flat maximum and minimum near the true value of the rate constant. Thus, the slopes should approach zero, corresponding to small values of the relative error coefficients. On the other hand, plots a, c, d and f corresponding to non-optimum times have finite slopes at the intersection point, corresponding to larger relative error coefficients.

To quantify relative error coefficients for the two-point and one-rate methods, slopes of plots were computed from data in the range from $0.025\ s^{-1}<k<0.035\ s^{-1}$. Results for these simulated data are summarized in the first three columns of Table 1. Ideally, the relative error coefficients should be zero at the optimum times for both these methods. However, the finite values given are probably more realistic for finite changes in rate constants. Clearly, the use of optimum measurement times can yield manifold improvements in ruggedness for variables such as temperature, pH, enzyme activity, etc. that affect rate constants.

Plots g and h for the two-rate and three-point/fixed-time methods are superimposed and flat at $C/C_o=1.00$. This behavior, which represents relative errors coefficients of zero, is expected for these ideal data because these methods have the built-in ability to compensate for changes in rate constants [13,14].

Because of the curvature of the plots in Fig. 2, the relative error coefficients in Table 1 apply only for small deviations around expected values of the rate constant. It is apparent from slopes of plots in Fig. 2 that error coefficients could be different (both larger and smaller) for larger changes in rate constants.

Experimental data

Response curves for uric acid used in this study are illustrated in Fig. 3. The original data were offset by additive amounts needed to give each the same initial absorbance at $t=0$. As mentioned earlier, the average rate constant for these data was $0.018\ s^{-1}$ and the time scale was changed by different amounts to simulate rate constants from $0.0036\ s^{-1}$ to $0.090\ s^{-1}$.

Because these data were collected at 10-s intervals, it was not possible to select optimum times exactly; accordingly closest values were used.

Table 1
Relative error coefficients for changes in rate constant

Method	Relative error coefficients ($\%/s^{-1}$)					
	Simulated data [a]			Uric acid data		
	Low	Optimum	High	Low	Optimum	High
Two-point	17	0.26	−11	21 [b]	0.4 [b]	−17 [b]
One-rate	17	−0.26	−24	40 [c]	1.1 [c]	39 [c]
Three-point		0.00			−0.76 [d]	−1.2 [e]
Two-rate		0.00 [f]			−0.32 [g]	

[a] Times as in Fig. 2.
[b] Times as in Fig. 4.
[b,c] Times as in Fig. 5.
[d] Times: 10, 30, 50 s.
[e] Times: 20 ,40, 60 s.
[f] Times: 10, 50 s.
[g] Times: 25, 85 s.

Fig. 4 shows results for the two-point/fixed-time method for one near-optimum set of times (plot c, $k=0.018$, $R=2$, $t_1=t_{1/2}\simeq 40$ s and $t_2=2t_{1/2}=80$ s) and three non-optimum sets of times. As expected, the plot for the near-optimum times (plot c) passes through a flat maximum near $k=0.018\ s^{-1}$, whereas plots for other sets of times have steeper slopes in this region. Numerical values of the relative error coefficients are summarized in the first row of the last three columns of Table 1. The near optimum conditions yield a 50-fold improvement in ruggedness for changes in rate constants.

Fig. 5 shows analogous results for effects of changes in the rate constant on results by the one-rate method for the near-optimum time (plot b, $t_{opt}=1/k=1/0.018$ $s^{-1}\simeq 55$ s) and two non-optimum times(plots a and c). The scatter among the data reflects the degradation resulting from derivatives of data with noise. Even so, the slope of the plot for the optimized time (curve b) approaches zero near $k=0.018\ s^{-1}$. Quantitative val-

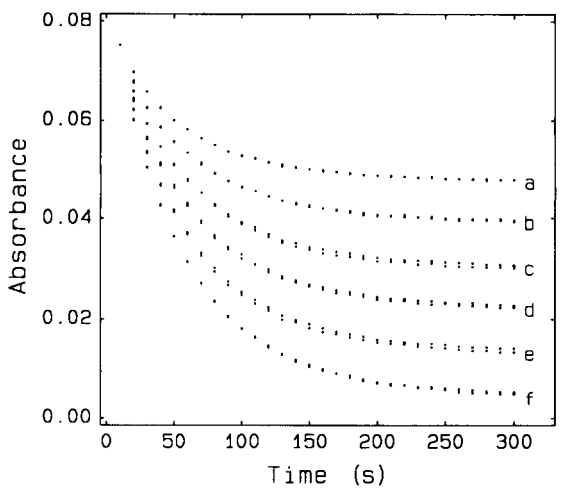

Fig. 3. Experimental data for duplicate uric acid standards, offset to start at the same initial absorbance. Conditions as described earlier [19]; Concentration (mmol l^{-1}): (a) 0.100, (b) 0.130, (c) 0.160, (d) 0.190, (e) 0.220, (f) 0.250.

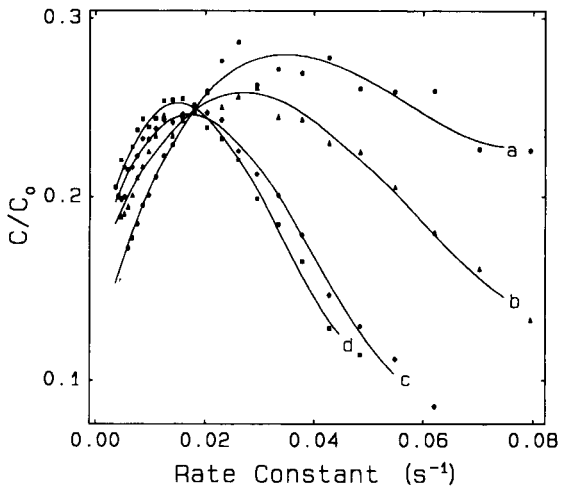

Fig. 4. Effects of rate constant on ratios of computed vs. true uric acid concentrations for two-point/fixed-time option with different measurement intervals. $C_o=0.250$ mmol l^{-1}; measurement intervals: (a) 10–50 s, (b) 20–60 s, (c) 40–80 s*, (d) 40–100 s.

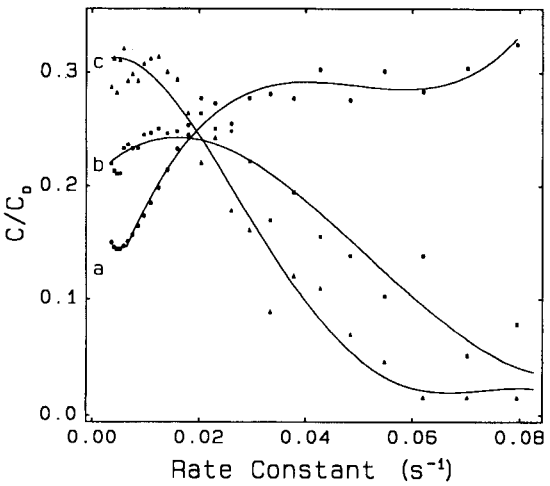

Fig. 5. Effects of rate constants on ratios of computed vs. true uric acid concentration for one-rate option with different measurement times. Measurement times: (a) 15 s, (b) 55 s*, (c) 95 s.

ues of relative error coefficients are included in Table 1 (second row, last three columns). There is roughly a 40-fold improvement in ruggedness relative to the non-optimized conditions.

Results for the two variable-compensating methods are also included in Table 1. In each case the ruggedness is significantly better than that for the non-optimized two-point and one-rate methods.

4.2. *Effects of reaction order*

This study was based solely on simulated data (Eq. 5) because it is very difficult to generate experimental data with controlled changes in reaction order. Some typical data on which the study was based are presented in Figs. 6A–C. Each frame contains plots for the ideal reaction orders ($n = 1$) and at the extremes of the range studied. Results are presented as absorbance although they should apply to any signal that varies linearly with the property (e.g. concentration) monitored. A surprising feature of the variable-order model is that the relative shapes of plots for different reaction orders depends upon the magnitude of the equilibrium signal changes, ΔS_∞. For signal changes less than or equal to unity (e.g. Figs. 6A and B) all plots approach the equilibrium value without crossing; for signal changes greater than unity (e.g. Fig. 6C), plots cross before reaching equilibrium. It should be noted that the equilibrium signal is the same for all plots within each frame of Fig. 6.

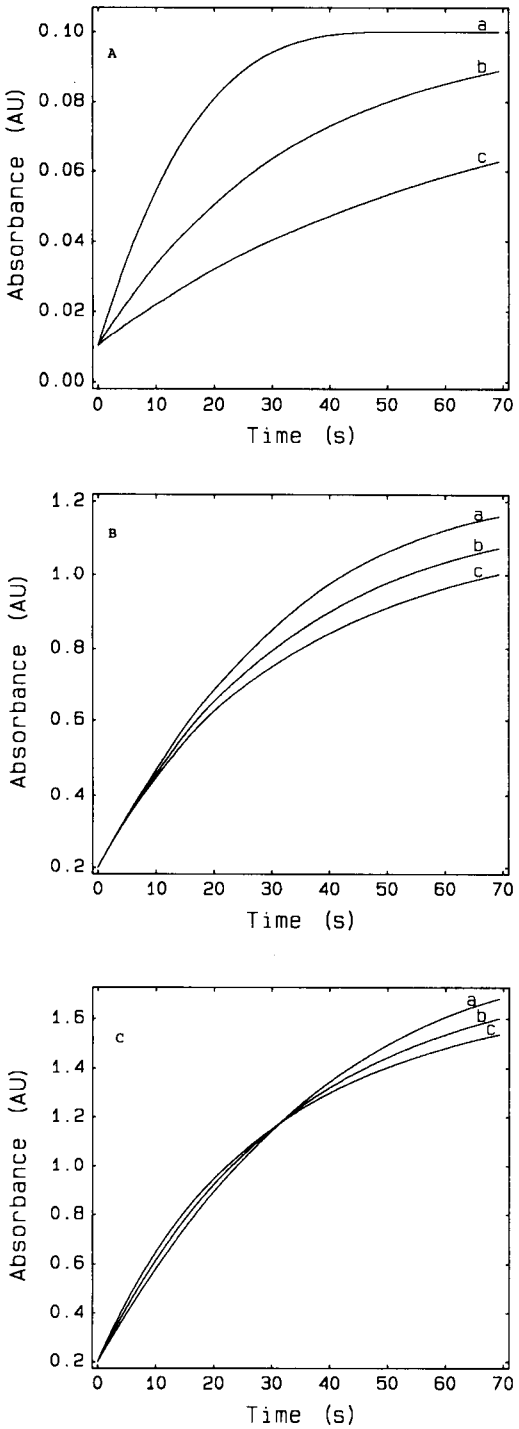

Fig. 6. Simulated data for different reaction orders and absorbance changes. All frames: $k = 0.030\ s^{-1}$; $\epsilon = 300\ l\ mol^{-1}\ cm^{-1}$; $b = 1.00$ cm; $C_o = 0.300$ mmol l^{-1}; reaction order: (a) 0.7, (b) 1.0 and (c) 1.3. (A) $A_o = 0.010$, $A_\infty = 0.100$, $\Delta A_\infty = 0.090$. (B) $A_o = 0.20$, $A_\infty = 1.20$, $\Delta A_\infty = 1.00$. (C) $A_o = 0.20$, $A_\infty = 1.80$, $\Delta A_\infty = 1.60$.

Figs. 7 and 8 show effects of reaction order on results obtained for the data sets in Fig. 6 by using the fixed-time (Fig. 7) and rate (Fig. 8) options. Measurement times are the same as those used to evaluate effects of rate constants. The goal here was to evaluate effects of reaction order for conditions selected to minimize effects of variables that affect rate constants and no attempt was made to select conditions to minimize effects of reaction order.

As expected, all plots intersect at a reaction order of unity and error coefficients were evaluated as the slopes of the plots in the range $0.92 \leq n \leq 1.08$. Results are summarized in Table 2.

Several observations can be made regarding these results. First, as a group, the error coefficients are smaller and depend less on data-processing conditions than those in Table 1 for changes in the rate constants. For example, the largest relative error coefficient in Table 2 is at least an order of magnitude smaller than the largest values in Table 1. Second, for the two-point/fixed-time and one-rate options, the measurement times corresponding to the smaller error coefficients are different for different signal amplitudes. For example, for the two-point option, the middle range (13.4–66.9 s) is best for the smallest signal change; the higher range (13.4–150 s) is best for the middle signal change and the lowest range (13.4–20 s) is best for the largest signal change. This behavior would make it very difficult to identify a single set of optimum conditions in regard to changes in reaction order and is the primary reason more effort was not expended in this area. Finally, it is noted that for changes in reaction order the three-point/fixed-time and two-rate options do not offer any significant advantages relative to the two-point and one-rate options. This is not surprising because the variable-compensating features of these options are based on the assumption of first-order behavior.

It is noted that the error coefficients in Table 2 apply only for small variations of reaction order about the expected value of unity. Error coefficients would be different for larger deviations.

4.3. Linearity

The uric acid data were used to compare the linearity of the various options. This was done by fitting a linear least-squares model to data for the computed signal

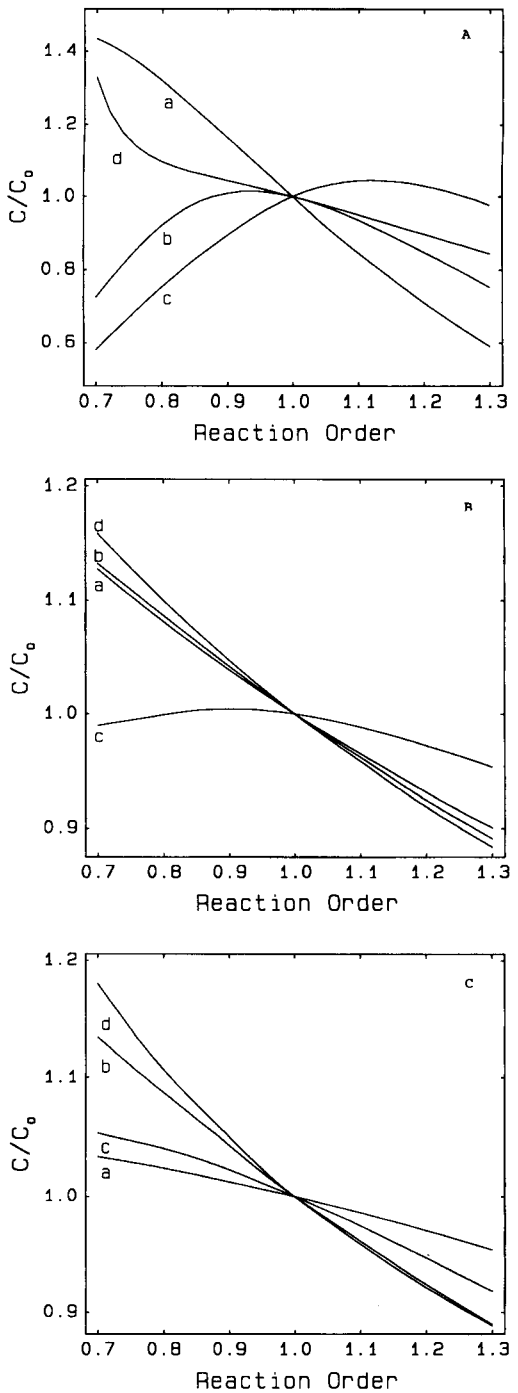

Fig. 7. Effects of reaction order on ratios of computed to true concentration for two-point and three-point/fixed-time options. Conditions as in Fig. 6 except for measurement times: (a) 13.4 and 20.0 s, (b) 13.4 and 66.9 s*, (c) 13.4 and 150 s, (d) 10, 30 and 50 s (three-point option).

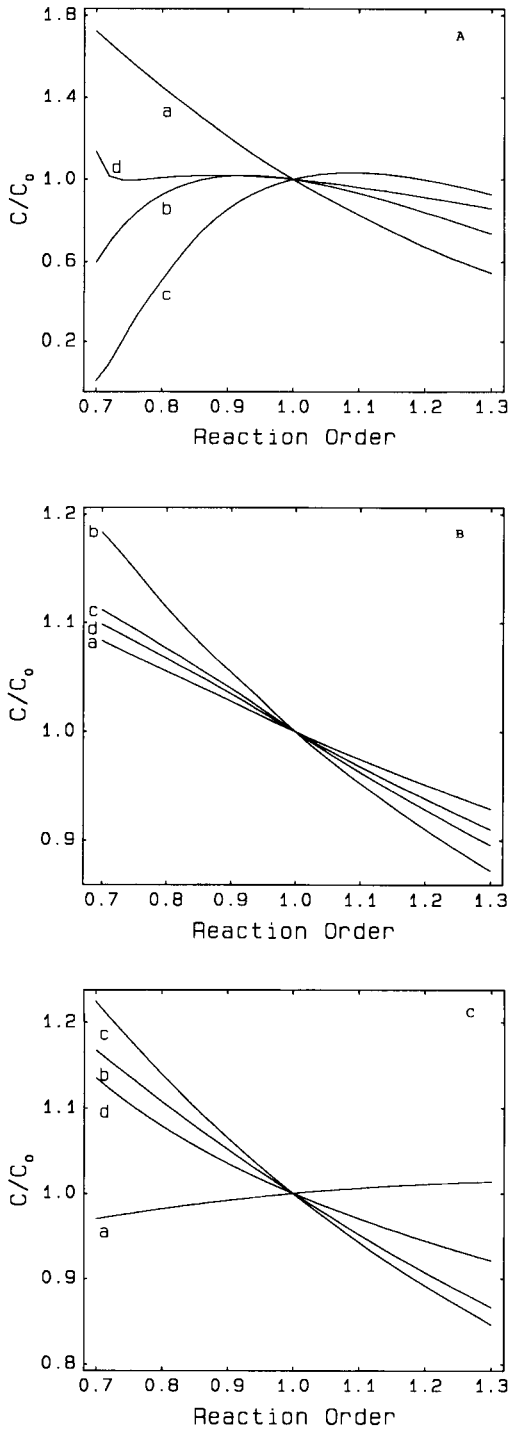

Fig. 8. Effects of reaction order on ratios of computed to true concentrations for one-rate and two-rate options. Conditions as in Fig. 6 except for measurement times: (a) 10 s, (b) 33.3 s*, (c) 50 s, (d) 10 and 50 s (two-rate option).

change vs. concentration. As expected, the measurement objective varied linearly with concentration for each of the data-processing options. However, as illustrated in Table 3, there were some differences among linear least-squares statistics.

The different data-processing options give different numerical values for absorbance changes (ΔA) and rates (dA/dt). Accordingly, to facilitate comparisons, results obtained with all the options were normalized to similar values by computing expected values of the equilibrium signal change, ΔA_∞, from measured values of ΔA and dA/dt, assuming first-order behavior. For ideal behavior, the values of ΔA_∞ should be the same for all options for each set of conditions. Least-squares statistics in Table 3 represent these computed values, $\Delta \hat{A}_\infty$, vs. concentration. Accordingly, ideal values of all least-squares parameters and statistics should be the same and any differences result from non-ideal behavior.

Our best estimate of the true value of the slope is 0.310 ± 0.0033 mmol^{-1} l, where the uncertainty is one standard deviation based on duplicates of each of six different concentrations. Thus, the ranges for ± 1 S.D. and ± 2 S.D. are 0.3067–0.3133 and 0.3034–0.3166, respectively. Two of the slopes are within one standard deviation of the expected value, five agree within two standard deviations of the expected value and five are outside two standard deviations. Interestingly, results for the optimized one-rate and two-point/fixed-time options as well as the three-point/fixed-time option are among the better values.

Because all the kinetic options should compensate for background signals, we have no reason to expect the intercept to be other than zero. From this point of view, the two-point/fixed-time option implemented at longer times and the two-rate option appear to be the best and the one-rate option and the two-point/fixed-time option implemented at short times appear to be the worst. However, the relatively large uncertainties that result from the narrow concentration range make it difficult to draw more meaningful conclusions from the intercepts because most numerical values are within ± 2 S.D.

The standard error of estimate which quantifies the scatter about the least-squares line through the data is one of the most useful statistics. There are only small differences among the two- and three-point fixed time options, slightly larger values for the two-rate option

Table 2
Relative error coefficients for simulated changes in reaction order

Method	Relative error coefficients (%/Δn) [a]								
	$\Delta S_\infty = 0.09$			$\Delta S_\infty = 1.00$			$\Delta S_\infty = 1.60$		
	Low	Optimum	High	Low	Optimum	High	Low	Optimum	High
Two-point [b]	−1.6	−0.39	0.73	−0.37	−0.41	0.08	−0.14	−0.40	−0.24
One-rate	−1.9	−0.47	0.87	−0.26	−0.50	−0.37	0.07	−0.50	−0.61
Three-point [b]	−0.45			−0.45			−0.45		
Two-rate	−0.31			−0.32			−0.32		

[a] Conditions/time ranges/times as in Figs. 6–8.
[b] Fixed-time options.

and significantly larger differences for the one-rate option. The best values for the one-rate option occur for the shortest measurement time at which the signal is changing most rapidly.

Correlation coefficients are poorest for the one-rate method applied at longer times.

4.4. Imprecision

The imprecision of each option was evaluated at different noise levels by using simulated data representing a first-order process with a rate constant of $0.028 s^{-1}$ and a total signal change of $\Delta S_\infty = 0.90$. The times at which the various options were implemented were as follows: two-point/fixed-time, $t_1 = 0$, $t_2 = t_{1/2}$; one-rate, $t_1 = 0$, $t_2 = 0.3t_{1/2}$; three-point/fixed-time, $t_1 = 0$, $t_2 = t_{1/2}$, $t_3 = 2t_{1/2}$; two-rate, first rate between $t = 0$ and $0.5t_{1/2}$ and second rate between $t = 0.5t_{1/2}$ and $t_{1/2}$.

Results from the studies are summarized in the last two columns of Table 3. Each relative standard deviation (R.S.D.) is the result of 100 simulated responses for a 3 mmol l^{-1} solution of analyte; the noise levels of 0.0005, 0.001 and 0.005 correspond to the one standard deviation levels of noise superimposed on each set of 100 simulated responses. The standard errors of estimates in the last column are averages for all five concentrations. For each data-processing option, the R.S.D. tends to increase in proportion to the noise level. The two-point/fixed-time option appears to be the least sensitive to signal noise with the one-rate method being next and the three-point/fixed-time and two-rate methods being most dependent on signal noise.

5. Conclusions

Given the options discussed in this paper, the method and experimental conditions one might choose will depend upon what features one wishes to emphasize. First, all options are relatively insensitive to small deviations from first-order behavior, so this is an important criterion only if one expects deviations of reaction order larger than ± 0.1. Second, if one wishes to reduce effects of variables that affect rate constants then one should choose one of the "variable-compensating" (three-point/fixed-time or two-rate) options or use one of the other options (two-point/fixed-time or one-rate options) under conditions that minimize effects of changes in rate constants. It should be noted that the optimum conditions depend on the value of the rate constant and accordingly the optimum conditions apply only for narrow ranges of the rate constant. If one wishes to minimize effects of random noise, then surprisingly, the results indicate that one should choose either the two-point/fixed-time or one-rate options. When all aspects of this study as well as other issues such as ease of implementation are considered, it appears that the optimized two-point/fixed-time option remains one of the more attractive choices considered here for situations in which experimental variables can be controlled within narrow limits economically. However, for situations in which it is difficult or expensive to control variables that affect kinetic behavior, then one of the variable-compensating options could be attractive.

Subsequent papers in this series will discuss and compare performance characteristics of a variety of

Table 3
Linear least-squares statistics [a] and imprecision [b] of the various data-processing options

Method	Linearity results [a]					Imprecision [b]		
	Times (s)	slope(S.D.) [a] (A.U. mmol^{-1}l)	Intercept(S.D.) (10^{-3}A.U.)	Std.Error Est- (10^{-4}A.U.)	Corr. coef.	Noise level [b]	Res. std. dev.(%) [b,c]	Std. error
Two-point	10, 50	0.368(0.003)	1.9(0.5)	4.9	0.99 94	0.00 05	0.17	0.00 5
	20, 60	0.327(0.004)	1.9(0.7)	6.7	0.99 87	0.00 1	0.3	0.01 0
	40, 80*	0.304(0.004)	0.4(0.7)	7.1	0.99 83	0.00 5	2.0	0.04 7
	40, 100	0.304(0.004)	0.5(0.8)	7.4	0.99 81	–	–	
One-rate	15	0.447(0.008)	2.9(1.4)	14	0.99 68	0.00 05	0.4	0.01 3
	55*	0.310(0.01)	4.0(2.5)	25	0.98 0	0.00 1	0.9	0.02 5
	95	0.306(0.03)	4.6(4.5)	44	0.93 8	0.00 5	4.0	0.13
Three-point	10, 30, 50	0.298(0.003)	0.73(0.5)	5.2	0.99 90	0.00 05	1.1	0.03 6
	20, 40, 60	0.306(0.005)	1.8(0.9)	9	0.99 72	0.00 1	2	0.17
Two-rate	25.85	0.334(0.006)	0.42(1.1)	11	0.99 66	0.00 05	1.0	0.03 5
						0.00 1	2.0	0.07 7
						0.00 5	14	0.74

A.U. = absorbance; Res. = residual.
[a] Experimental data for uric acid.
[b] Simulated data (see text).
[c] Based on 3 mmol l^{-1} solutions.
* Optimum times.

multipoint variable-compensating data-processing options.

Acknowledgements

This research was supported in part by Grant GM13326-25 from the National Institutes of Health.

References

[1] H. B. Mark, Jr. and G. A. Rechnitz, Kinetics in Analytical Chemistry, Interscience, New York, 1968.
[2] H. A. Mottola, Kinetic Aspects of Analytical Chemistry, Wiley-Interscience, New York, 1988.
[3] D. Perez-Bendito and M. Silva, Kinetic Methods in Analytical Chemistry, Ellis Horwood, Chichester, 1988.
[4] H. L. Pardue, Clin. Chem., 23 (1977) 2189.
[5] P. D. Wentzel and S. R. Crouch, Anal. Chem., 58 (1986) 2855.
[6] H. L. Pardue, Anal. Chim. Acta, 216 (1989) 69.
[7] J. D. Ingle and S. R. Crouch, Anal. Chem., 43 (1971) 697.
[8] M. L. Love and H. L. Pardue, Anal. Chim. Acta, Anal Chim. Acta, 299 (1994) 195.
[9] J. E. Davis, B. Renoe, Anal. Chem., 51 (1979) 526.
[10] J. G. Atwood and J. L. DiCesare, Clin. Chem., 21 (1975) 1263.
[11] J. B. Landis, M. Rebec and H. L. Pardue, Anal. Chem., 49 (1977) 785.
[12] F. J. Holler, R. K. Calhoun and S. F. McClanahan, Anal. Chem., 54 (1982) 755.
[13] R. C. Harris and E. Hultman, Clin. Chem., 29 (1983) 2079.
[14] P. D. Wentzel and S. R. Crouch, Anal. Chem., 58 (1986) 2851.
[15] G. E. Mieling and H. L. Pardue, Anal. Chem., 50 (1978) 1611.
[16] B. L. Bacon and H. L. Pardue, Clin. Chem., 37 (1991) 1338.
[17] M. D. Love, PhD Thesis, Purdue University, West Lafayette, IN, 1992.
[18] J. A. Larsson and H. L. Pardue, Anal. Chim. Acta, 224 (1989) 289.
[19] B. A. Dilena, M. J. Peake, H. L. Pardue and J. W. Skoug, Clin. Chem., 32 (1986) 486.

ELSEVIER

Analytica Chimica Acta 299 (1994) 219–229

ANALYTICA CHIMICA ACTA

Linear description of solute retention in reversed-phase liquid chromatography by a new mobile phase polarity parameter

Elisabeth Bosch, Pilar Bou, Martí Rosés *

Departament de Química Analítica, Universitat de Barcelona, Diagonal 647, 08028 Barcelona, Spain

Received 8 March 1994; revised manuscript received 5 July 1994

Abstract

Retention data (log k') for 14 benzene and 18 phenol derivatives have been obtained in a C_{18} column for the full range of methanol–water and acetonitrile–water mobile phase compositions. From the equations developed in an earlier work a new solvent parameter has been calculated from the retention data in the two mobile phases studied. General linear equations have been established which describe chromatographic retention in the full range of mobile phase compositions by a single solute parameter and the new solvent parameter. The applicability of the new solvent parameter to different solutes and C_{18} columns has been tested with literature data.

Keywords: Liquid chromatography; Benzenes; Phenols

1. Introduction

The description of solute retention in reversed-phase liquid chromatography by mobile phase parameters is a subject of great interest. Traditionally, linear plots of log k' (where k' is the solute capacity factor) vs. the volume fraction or percentage of organic modifier have been used for description of retention. Schoenmakers et al. [1] used the solubility parameter theory to explain retention in terms of the relative solubility parameters of the solute, mobile phase and stationary phase. From this theory they showed that at least a quadratic relationship is needed to relate log k' with the volume fraction of organic modifier. However, Johnson et al. [2] demonstrated linear relationships in a wide range of mobile phase compositions between the solute log k' and the mobile phase E_T (30) parameter, where E_T (30) is the Dimroth-Reichardt polarity parameter [3,4]. From multivariate regression of log k' with solute and mobile phase descriptors, we demonstrated [5] that linear relationships between log k' and the normalized E_T (30) parameter should be obtained

$$\log k' = q + pE^N_{Tm} \quad (1)$$

where E^N_{Tm} is the normalized E_T (30) value of the mobile phase and q and p the intercept and coefficient of the correlation, respectively.

Moreover, we observed that the q and p parameters for a series of solutes in the same column and mobile phase are linearly correlated, and therefore, Eq. 1 can be written as

$$\log k' = (\log k')_0 + p(E^N_{Tm} - E^N_{Ts}) \quad (2)$$

where E^N_{Ts} refers to the stationary phase. Eq. 2 adopts the form of the linear solvation energy relationships developed by Kamlet and co-workers [6–10], applied to the distribution of a solute between two phases.

* Corresponding author.

SSDI 0003-2670(94)00345-9

According to this formalism, based on the linear free energy relationships, any free energy related property (such as log k') can be calculated by the sum of a constant term ($(\log k')_0$ in our equation) and different solute–solvent interaction terms, which can be described by the product of a solute (p) and a solvent parameter. If the correlated property refers to distribution between two phases, then the solvent parameter becomes the difference between the solvent parameters of the two phases ($E^N_{Tm} - E^N_{Ts}$).

Therefore in Eq. 2, p (the solute parameter) depends only on the solute chromatographed and E^N_{Tm} (the mobile phase polarity) on the mobile phase organic modifier and composition. E^N_{Ts} is the E^N_T polarity of the stationary phase, supposed in first approximation to be constant. It is well known that the stationary phase is solvated by the mobile phase, and therefore its composition and properties change with the mobile phase composition, but it was demonstrated that if the polarity of the stationary phase is linearly related with the polarity of the mobile phase, Eq. 2 is kept. $(\log k')_0$ is the constant of the correlation and it should be the log k' value of any solute chromatographed using a hypothetical mobile phase with the same polarity than the stationary phase. Therefore, $(\log k')_0$ and E^N_{Ts} are constants depending only on the chromatographic system used (column and organic modifier), but not on the solute or the mobile phase composition. The most important conclusion drawn from Eq. 2 is that the retention of a solute in a particular chromatographic system can be described by only one single solute (p) and one single mobile phase composition (E^N_{Tm}) parameters.

However, the applicability of Eq. 2 is limited to the range of linearity of the log k' vs. E_T plots (40–100% and 0–80% of organic modifier for methanol–water and acetonitrile–water, respectively). An extension of Eq. 2 to the full range of mobile phase compositions would be very desirable, especially for application to gradient elution. In this paper, a new solvent parameter, partially related with E_T, is derived from the E_T correlations with chromatographic data by using Eq. 2 for the whole range of mobile phase compositions, and the applicability of this parameter to other solutes and chromatographic systems is investigated. By means of this new parameter, equations similar to Eq. 2, but that apply for the full range of mobile phase compositions, can be derived for any chromatographic system.

2. Experimental

2.1. Apparatus and procedure

Retention data for the solutes studied in methanol–water and acetonitrile–water mobile phases (1 ml min^{-1}) were measured at 25°C on a 25 cm × 4.0 mm i.d. Merck Lichrospher 100 RP-18 (5 μm) column with a precolumn of the same origin. For phenols the aqueous mobile phase solvent was 0.1 M in acetic acid to avoid ionization. The chromatographic equipment was the same as used previously [5], with the same 10-μl loop valve. The absorbance detector was set at 254 and 282 nm for benzene and phenols derivatives, respectively. A 0.01% potassium bromide solution measured at 200 nm was used as void volume marker.

2.2. Reagents

Methanol and acetonitrile (Merck, for chromatography), benzene (Panreac, >99%), toluene (Carlo Erba, RSE ACS, >99.5%), *p*-xylene, ethylbenzene and *n*-propylbenzene (Carlo Erba, RS standard for GC, >99%), *n*-butylbenzene (Aldrich, >99%), chlorobenzene (Aldrich, for HPLC, >99.99%), bromobenzene (Carlo Erba, RPE, >99.5%), nitrobenzene (Doesder), biphenyl (Aldrich, >99%), naphthalene (Scharlau), anthracene (Carlo Erba, RPE), pyrene (Aldrich, >99%), chrysene (Fluka, >95%) and the phenols reported elsewhere [5] were used. Triply distilled water was used throughout.

3. Results and discussion

The log k' values obtained for the benzene and phenol derivatives studied in methanol–water and acetonitrile–water mobile phases are presented in Tables 1 and 2 for the full range of mobile phase compositions. The log k' values have been correlated with the E^N_T values of the mobile phase presented in Table 3 through Eq. 1 in the range 40–100% of methanol and 0–80% of acetonitrile (all the percentages given as volume percentages, as usual in liquid chromatography). The results of these correlations are presented in Table 4.

As expected, the intercepts (q) and the slopes (p) obtained for each series of solutes are not independent. This can be observed in Fig. 1, where q is plotted

Table 1
Retention values ($\log k'$) of solutes in methanol–water mobile phase

N	Solute	$\log k'$										
		Methanol (%)										
		100	90	80	70	60	50	40	30	20	10	0
1	Phenol	−0.153	−0.093	0.022	0.134	0.296	0.477	0.712	0.945	1.147	1.359	1.586
2	4-Nitrophenol	−0.148	−0.073	0.063	0.210	0.389	0.635	0.907	1.177	1.453	1.692	2.034
3	3-Nitrophenol	−0.144	−0.062	0.049	0.233	0.432	0.684	0.961	1.238	1.491	1.751	2.083
4	2-Methylphenol	−0.117	−0.023	0.123	0.290	0.528	0.763	1.056	1.330	1.590	1.862	2.155
5	2-Chlorophenol	−0.130	−0.040	0.082	0.285	0.507	0.781	1.113	1.407	1.673	1.937	2.198
6	2,4-Dinitrophenol	−0.162	−0.085	0.031	0.239	0.453	0.725	1.009	1.301	1.569	1.867	–
7	2−Nitrophenol	−0.062	0.049	0.227	0.415	0.637	0.895	1.170	1.441	1.722	1.961	–
8	3-Chlorophenol	−0.109	−0.003	0.145	0.376	0.663	0.952	1.293	1.615	1.887	2.106	–
9	3-Bromophenol	−0.097	0.022	0.185	0.434	0.703	1.041	1.413	1.579	1.839	–	–
10	4-Bromophenol	−0.093	0.016	0.180	0.425	0.689	1.023	1.370	1.703	2.004	–	–
11	4-Chlorophenol	−0.117	−0.006	0.133	0.361	0.612	0.922	1.248	1.740	2.019	–	–
12	2,4-Dimethylphenol	−0.085	0.034	0.197	0.449	0.737	1.035	1.381	1.730	2.054	–	–
13	2,6-Dichlorophenol	−0.093	0.031	0.197	0.453	0.751	1.065	1.422	1.775	2.118	–	–
14	4-Chloro-3-methylphenol	−0.073	0.060	0.242	0.521	0.857	1.200	1.591	1.971	–	–	–
15	2,4-Dichlorophenol	−0.055	0.098	0.347	0.620	0.957	1.315	1.719	2.090	–	–	–
16	3,5-Dichlorophenol	−0.003	0.179	0.432	0.793	1.166	1.552	1.970	–	–	–	–
17	2,4,6-Trichlorophenol	0.028	0.244	0.559	0.885	1.274	1.663	2.092	–	–	–	–
18	Pentachlorophenol	0.230	0.563	0.967	1.463	1.971	–	–	–	–	–	–
19	Benzene	0.006	0.169	0.371	0.588	0.846	1.112	1.347	1.573	1.761	1.912	2.294
20	Nitrobenzene	−0.058	0.071	0.248	0.500	0.692	0.954	1.194	1.480	1.722	1.977	–
21	Toluene	0.063	0.273	0.522	0.811	1.125	1.437	1.726	2.023	–	–	–
22	Bromobenzene	0.068	0.280	0.553	0.858	1.206	1.566	1.888	–	–	–	–
23	Ethylbenzene	0.092	0.338	0.645	0.979	1.355	1.746	1.988	–	–	–	–
24	Chlorobenzene	0.043	0.243	0.503	0.793	1.117	1.473	2.085	–	–	–	–
25	Naphthalene	0.113	0.355	0.662	0.997	1.375	1.788	2.092	–	–	–	–
26	*p*-Xylene	0.127	0.387	0.698	1.042	1.417	1.789	2.129	–	–	–	–
27	Propylbenzene	0.137	0.455	0.801	1.202	1.638	2.087	–	–	–	–	–
28	Biphenyl	0.144	0.439	0.806	1.221	1.675	2.155	–	–	–	–	–
29	Butylbenzene	0.188	0.561	0.968	1.422	1.923	–	–	–	–	–	–
30	Anthracene	0.306	0.659	1.080	1.522	2.037	–	–	–	–	–	–
31	Pyrene	0.440	0.814	1.259	1.735	–	–	–	–	–	–	–
32	Chrysene	0.535	1.001	1.485	2.026	–	–	–	–	–	–	-

against p for the two studied mobile phases. The two parameters are correlated according to

$$q = -(0.512 \pm 0.042) - (0.735 \pm 0.002)p$$

$$s = 0.082,\ r^2 = 0.9997,\ n = 32 \qquad (3)$$

for methanol–water and

$$q = -(0.927 \pm 0.094) - (0.647 \pm 0.008)p$$

$$s = 0.122,\ r^2 = 0.9955,\ n = 32 \qquad (4)$$

for acetonitrile–water.

Substituting these equations in Eq. 1, we obtain:

$$\log k' = -0.512 + p(E^{N}_{Tm} - 0.735) \qquad (5)$$

for methanol–water and

$$\log k' = -0.927 + p(E^{N}_{Tm} - 0.647) \qquad (6)$$

for acetonitrile–water.

These expressions correspond to the general Eq. 2 applied to the two studied mobile phases in the particular chromatographic system studied. They show that $\log k'$ can be calculated from only one solute parameter (p) and one solvent parameter (E^{N}_{Tm}).

Figs. 2 and 3 present the $\log k'$ vs. E^{N}_{T} plots obtained

Table 2
Retention values ($\log k'$) of solutes in acetonitrile–water mobile phase

N	Solute	$\log k'$										
		Acetonitrile (%)										
		100	90	80	70	60	50	40	30	20	10	0
1	Phenol	−0.085	−0.106	−0.050	0.036	0.148	0.287	0.450	0.643	0.899	1.225	1.597
2	4-Nitrophenol	−0.110	−0.142	−0.078	0.030	0.172	0.334	0.546	0.811	1.172	1.581	2.044
3	3-Nitrophenol	−0.101	−0.115	−0.054	0.060	0.196	0.370	0.582	0.860	1.210	1.629	2.093
4	2-Methylphenol	−0.061	−0.058	0.023	0.136	0.287	0.481	0.663	0.937	1.271	1.691	2.165
5	2-Chlorophenol	−0.057	−0.046	0.023	0.128	0.278	0.461	0.678	0.976	1.348	1.781	2.208
6	2,4-Dinitrophenol	−0.123	−0.115	−0.035	0.089	0.256	0.450	0.700	1.000	1.370	1.767	–
7	2-Nitrophenol	−0.065	−0.010	0.091	0.231	0.394	0.593	0.843	1.099	1.418	–	–
8	3-Chlorophenol	−0.042	−0.050	0.036	0.160	0.329	0.553	0.771	1.109	1.519	–	–
9	3-Bromophenol	−0.021	−0.035	0.063	0.194	0.367	0.576	0.848	1.192	1.637	–	–
10	4-Bromophenol	−0.028	−0.031	0.054	0.178	0.349	0.550	0.811	1.159	1.612	–	–
11	4-Chlorophenol	−0.042	−0.058	0.026	0.148	0.306	0.500	0.751	1.071	1.496	–	–
12	2,4-Dimethylphenol	−0.021	−0.003	0.102	0.237	0.397	0.605	0.886	1.199	–	–	–
13	2,6-Dichlorophenol	−0.014	0.007	0.116	0.264	0.453	0.667	0.947	1.294	1.724	–	–
14	4-Chloro-3-methylphenol	−0.003	0.000	0.102	0.245	0.420	0.641	0.930	1.318	1.832	–	–
15	2,4-Dichlorophenol	0.023	0.023	0.131	0.291	0.482	0.723	1.038	1.443	–	–	–
16	3,5-Dichlorophenol	0.071	0.060	0.189	0.360	0.579	0.836	1.198	1.625	–	–	–
17	2,4,6-Trichlorophenol	0.096	0.137	0.284	0.462	0.694	0.996	1.312	1.772	–	–	–
18	Pentachlorophenol	0.263	0.316	0.511	0.748	1.033	1.371	1.828	–	–	–	–
19	Benzene	0.026	0.145	0.235	0.436	0.610	0.820	1.067	1.370	1.655	1.918	–
20	Nitrobenzene	−0.049	0.039	0.118	0.306	0.469	0. 689	0.926	1.224	1.547	1.884	–
21	Toluene	0.071	0.218	0.351	0.578	0.792	1.031	1.329	1.694	–	–	–
22	Bromobenzene	0.106	0.249	0.388	0.615	0.824	1.102	1.418	1.823	–	–	–
23	Ethylbenzene	0.111	0.289	0.447	0.705	0.947	1.226	1.575	–	–	–	–
24	Chlorobenzene	0.082	0.218	0.349	0.571	0.778	1.037	1.340	1.730	–	–	–
25	Naphthalene	0.109	0.284	0.429	0.677	0.909	1.199	1.562	–	–	–	–
26	*p*-Xylene	0.144	0.316	0.478	0.727	0.955	1.257	1.601	–	–	–	–
27	Propylbenzene	0.169	0.384	0.575	0.864	1.135	1.457	1.859	–	–	–	–
28	Biphenyl	0.141	0.327	0.513	0.798	1.067	1.413	1.837	–	–	–	–
29	Butylbenzene	0.232	0.485	0.710	1.027	1.323	1.685	–	–	–	–	–
30	Anthracene	−0.049	0.501	0.705	1.005	1.290	1.660	–	–	–	–	–
31	Pyrene	0.390	0.629	0.858	1.165	1.458	1.842	–	–	–	–	–
32	Chrysene	0.438	0.705	0.974	1.316	1.655	–	–	–	–	–	–

using Eqs. 5 and 6 for some representative solutes in the two mobile phases studied. All the regression lines intersect at the (E_{Ts}^{N}, $(\log k')_0$) coordinates, according to Eqs. 5 and 6.

Figs. 2 and 3 show that the range of linearity of Eqs. 5 and 6 is restricted to 20–100% of methanol and 0–80% of acetonitrile, approximately. Outside these ranges the plots exhibit a curvature, but in the same direction. Therefore, if the E_T^N values outside the linearity range were properly modified, linear relationships for all the solutes and for the full range of mobile phase compositions could be probably obtained. This has been tested by back calculation of the E_{Tm}^{N} value from the log k' data of each solute and mobile phase composition by using Eqs. 5 and 6 for methanol–water and acetonitrile–water, respectively. The series of E_T^N values obtained for each mobile phase composition (E_T^{N*}) has been averaged and the results are presented in Table 3. As expected, the E_T^{N*} values inside the linearity range agree very well with the E_T^N values used. Outside this range the calculated E_T^* values are concordant for the different solutes, but they deviate from the E_T^N values of methanol–water and acetonitrile–water binary solvents.

Table 3
Solvent parameters used and derived in this work

Methanol (%)	E_T^N [a]	E_T^{N*} [b]	P_m^N [c]	Acetonitrile (%)	E_T^N [a]	E_T^{N*} [b]	P_m^N [c]
100	0.764	0.767 ± 0.004	0.113	100	0.462	0.735 ± 0.012	0.138
90	0.777	0.777 ± 0.005	0.157	90	0.712	0.741 ± 0.010	0.158
80	0.792	0.791 ± 0.006	0.216	80	0.749	0.752 ± 0.010	0.193
70	0.809	0.808 ± 0.006	0.288	70	0.767	0.768 ± 0.012	0.244
60	0.827	0.827 ± 0.006	0.369	60	0.787	0.786 ± 0.012	0.302
50	0.848	0.849 ± 0.006	0.463	50	0.810	0.808 ± 0.013	0.373
40	0.870	0.872 ± 0.005	0.561	40	0.836	0.834 ± 0.014	0.457
30	0.896	0.897 ± 0.007	0.667	30	0.867	0.866 ± 0.015	0.559
20	0.926	0.920 ± 0.009	0.766	20	0.903	0.905 ± 0.014	0.685
10	0.960	0.944 ± 0.011	0.867	10	0.947	0.953 ± 0.014	0.839
0	1.000	0.975 ± 0.014	1.000	0	1.000	1.003 ± 0.013	1.000

[a] E_T^N values are the same used in Ref. [5].
[b] E_T^N values calculated from the log k' data and Eqs. 5 and 6 assuming validity for the full range of mobile phase composition.
[c] Calculated from Eqs. 11 and 12.

The E_T^{N*} values can be considered as a new solvent parameter linearly related with the log k' values. Although the complete physicochemical meaning of this new parameter is difficult to establish, it can be considered a polarity parameter (partially related with the E_T (30) polarity parameter) that integrates the relevant solvent properties that affect retention in reversed phase liquid chromatography. The E_T (30) solvatochromic parameter is supposed to measure the polarity and the hydrogen bond acidity of the solvent [4]. These are the solvent properties that mostly affect solute retention in reversed-phase liquid chromatography [5]. However, solvatochromic indicators can be preferentially solvated in binary solvents and the solvatochromic parameters derived from them (such as E_T (30)) do not measure the properties of binary solvents as well as the ones of pure solvents [11]. Fig. 4 compares the variation of E_T^N and E_T^{N*} with solvent composition for the two mobile phases studied. It can be observed that both parameters agree for most solvent compositions. They diverge for the solvent compositions where the preferential solvation of E_T indicator shows the strongest effect (water rich mixtures for methanol–water and acetonitrile rich mixtures for acetonitrile–water). The strong influence of preferential solvation is probably the reason that E_T does not show good correlations with retention in these composition ranges. Fig. 4 shows that these effects are minimized for E_T^{N*} and therefore the correlations with this parameter can be extended to the full range of compositions.

The log k' values are linearly correlated with E_T^{N*} and the intercepts (q) and slopes (p) obtained are also linearly correlated between them, according to

$$q = -(0.433 \pm 0.046) - (0.740 \pm 0.002)p$$
$$s = 0.095,\ r^2 = 0.9997,\ n = 32 \quad (7)$$

for methanol–water and

$$q = -(0.478 \pm 0.045) - (0.692 \pm 0.003)p$$
$$s = 0.080,\ r^2 = 0.9992,\ n = 32 \quad (8)$$

for acetonitrile–water.

Therefore, the retention of solutes in the full range of mobile phase compositions can be described by

$$\log k' = -0.433 + p(E_T^{N*} - 0.740) \quad (9)$$

for methanol–water and

$$\log k' = -0.478 + p(E_T^{N*} - 0.692) \quad (10)$$

for acetonitrile–water.

However, an inspection of Table 3 shows that the E_T^{N*} value is 0.975 for 0% of methanol, but 1.003 for 0% of acetonitrile, although both values refer to the same solvent (pure water). Therefore, some redefinition of this parameter in order to get the same value for this solvent is advisable. The most convenient is normalization of the parameter as it is usually performed with polarity parameters [4]. The reference points in these normalizations can be chosen arbitrarily, but they are usually chosen to obtain a variation from 0 to 1 for

Table 4
Correlations of log k' values with the E_T^N parameter of the mobile phase (Eq. 1) [a]

Solute [b]	Methanol–water					Acetonitrile–water				
	q	p	s	n	r^2	q	p	s	n	r^2
1	−6.43	8.17	0.034	7	0.9902	−5.05	6.62	0.032	9	0.9972
2	−7.84	10.00	0.041	7	0.9904	−6.60	8.61	0.193	9	0.9965
3	−8.29	10.58	0.044	7	0.9901	−6.65	8.71	0.183	9	0.9969
4	−8.71	11.18	0.037	7	0.9939	−6.49	8.62	0.039	9	0.9975
5	−9.24	11.83	0.054	7	0.9882	−6.78	8.98	0.045	9	0.9970
6	−8.88	11.32	0.049	7	0.9897	−7.03	9.27	0.159	8	0.9982
7	−9.08	11.76	0.020	7	0.9984	−6.43	8.68	0.012	7	0.9995
8	−10.50	13.50	0.050	7	0.9924	−7.23	9.63	0.042	7	0.9948
9	−11.19	14.43	0.053	7	0.9924	−7.66	10.23	0.050	7	0.9935
10	−10.92	14.07	0.050	7	0.9929	−7.58	10.10	0.057	7	0.9914
11	−10.19	13.10	0.048	7	0.9923	−7.17	9.53	0.050	7	0.9924
12	−10.92	14.10	0.042	7	0.9949	−6.95	9.38	0.031	6	0.9956
13	−11.29	14.57	0.046	7	0.9945	−7.76	10.46	0.038	7	0.9965
14	−12.40	16.04	0.052	7	0.9941	−8.34	11.17	0.069	7	0.9896
15	−13. 07	16.97	0.033	7	0.9978	−8.23	11.11	0.041	6	0.9945
16	−14.59	19.03	0.034	7	0.9982	−9.01	12.12	0.043	6	0.9950
17	−15.03	19.69	0.017	7	0.9996	−9.21	12.62	0.036	6	0.9966
18	−21.01	27.78	0.018	5	0.9995	−10.81	15.08	0.034	5	0.9968
19	−9.82	12.87	0.020	7	0.9987	−6.20	8.66	0.050	8	0.9939
20	−9.27	12.05	0.019	7	0.9986	−6.61	9.00	0.022	8	0.9989
21	−12.11	15.95	0.030	7	0.9980	−8.06	11.24	0.013	6	0.9994
22	−13.31	17.51	0.027	7	0.9988	−8.65	12.06	0.018	6	0.9991
23	−14.02	18.51	0.064	7	0.9933	−9.12	12.79	0.014	5	0.9993
24	−14.30	18.71	0.074	7	0.9912	−8.32	11.57	0.016	6	0.9992
25	−14.52	19.17	0.043	7	0.9971	−9.20	12.86	0.016	5	0.9990
26	−14.49	19.17	0.041	7	0.9974	−9.10	12.80	0.013	5	0.9994
27	−17.66	23.31	0.016	6	0.9996	−10.32	14.56	0.015	5	0.9993
28	−18.32	24.15	0.013	6	0.9998	−10.77	15.07	0.019	5	0.9990
29	−20.74	27.41	0.008	5	0.9999	−11.15	15.85	0.016	4	0.9990
30	−20.61	27.37	0.011	5	0.9998	−10.91	15.51	0.014	4	0.9992
31	−21.60	28.85	0.008	4	0.9999	−11.12	16.00	0.014	4	0.9993
32	−24.66	33.00	0.021	4	0.9993	−12.42	17.89	0.016	3	0.9989

[a] Correlation ranges: 40–100% of methanol and 0–80% of acetonitrile, s is the overall standard deviation and n the number of points correlated.
[b] See Tables 1 and 2.

the most common solvents (e.g., the E_T^N parameter is obtained from E_T (30) assigning unity and zero values to water and tetramethylsilane, respectively [4]). The solvent composition with a highest polarity is pure water and the most appropriate seems to be to assign unity value to this solvent (such as for E_T (30)). However, the other reference point is less clear. One possibility is to assign zero value to the pure organic solvent (methanol or acetonitrile), but with this procedure the same value is attributed to two different solvents (methanol and acetonitrile). Another possibility is to choose the polarity of the stationary phase as zero value. This polarity is measured by the E_{Ts}^N parameter (Eq. 2) obtained from the q against p correlations (Eqs. 7 and 8). This method offers the advantage of assigning different positive values to all the solvent compositions because they are always more polar than the stationary phase. Using these conventions, the normalized mobile phase parameter (represented by P_m^N) can be computed from E_T^{N*} according to

$$P_m^N = \frac{E_T^{N*} - 0.740}{0.975 - 0.740} \quad (11)$$

for methanol–water and

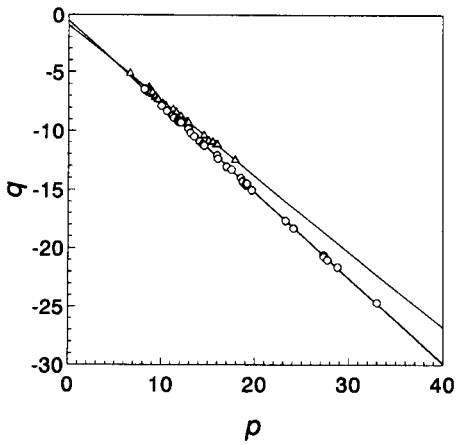

Fig. 1. Relationship between intercept (q) and slope (p) of Eq. 1. (○) methanol–water mobile phase, (△) acetonitrile–water mobile phase.

$$P_m^N = \frac{E_T^{N*} - 0.692}{1.003 - 0.692} \quad (12)$$

for acetonitrile–water.

The P_m^N values obtained are presented in Table 3 for each mobile phase composition, and they have been used for correlation with the log k' data. These P^N values can be easily calculated from the mobile phase composition by

$$P^N = 1.00 - \frac{1.33v}{1+0.47v} \quad s = 0.01 \quad (13)$$

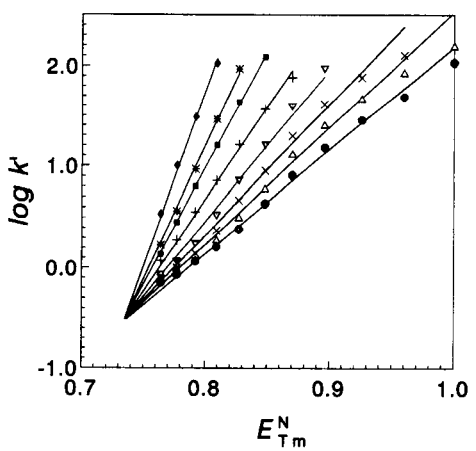

Fig. 2. Relationship between retention (log k') and mobile phase E_T^N polarity for some solutes in methanol–water mobile phase: (○) 4-nitrophenol, (△) 2-chlorophenol, (×) 3-chlorophenol, (▽) 4-chloro-3-methylphenol, (+) bromobenzene, (□) propylbenzene, (*) pentachlorophenol and (◇) chrysene.

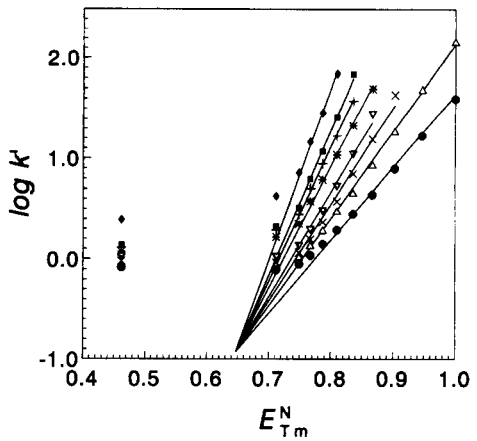

Fig. 3. Relationship between retention (log k') and mobile phase E_T^N polarity for some solutes in acetonitrile–water mobile phase: (○) phenol, (△) 2-methylphenol, (×) 3-bromophenol, (▽) 2,4-dichlorophenol, (*) toluene, (+) ethylbenzene, (□) biphenyl and (◇) pyrene.

for methanol–water and

$$P^N = 1.00 - \frac{2.13v}{1+1.42v} \quad s = 0.01 \quad (14)$$

for acetonitrile–water.

In these equations v is the volume fraction of organic modifier.

Eqs. 13 and 14 are similar to the ones used to calculate the E_T^N values of the mobile phases [5,11].

The correlation between the intercepts (q) and the slopes (p) obtained when the log k' values are corre-

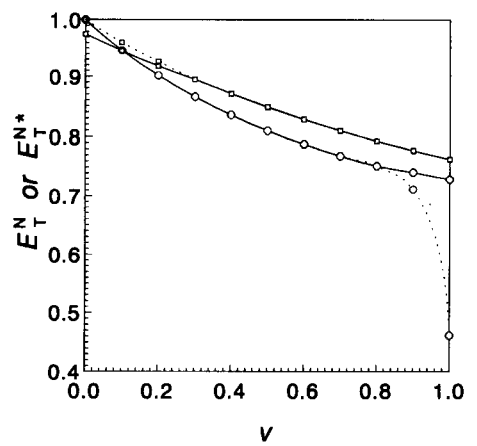

Fig. 4. Variation of E_T^N and E_T^{N*} parameters with solvent composition: (□) methanol–water, (○) acetonitrile–water. Dashed lines: E_T^N, continuous lines: E_T^{N*}. v is the volume fraction of organic solvent.

Table 5
Correlations of log k' with the P_m^N parameter of the mobile phase for the full range of mobile phase compositions (Eqs. 17 and 18)

Solute [a]	Methanol–water				Acetonitrile–water			
	p	n	s	r^2	p	n	s	r^2
1	2.04±0.03	11	0.025	0.9983	2.05±0.04	11	0.033	0.9966
2	2.42±0.03	11	0.030	0.9984	2.40±0.05	11	0.049	0.9956
3	2.49±0.03	11	0.023	0.9991	2.46±0.05	11	0.045	0.9965
4	2.62±0.02	11	0.021	0.9993	2.58±0.04	11	0.033	0.9981
5	2.68±0.04	11	0.042	0.9974	2.64±0.04	11	0.037	0.9977
6	2.57±0.03	10	0.027	0.9986	2.61±0.04	10	0.026	0.9985
7	2.82±0.01	10	0.011	0.9998	2.82±0.03	9	0.013	0.9993
8	2.98±0.05	10	0.039	0.9976	2.81±0.07	9	0.038	0.9953
9	3.06±0.09	9	0.060	0.9929	2.95±0.08	9	0.043	0.9946
10	3.15±0.04	9	0.023	0.9991	2.90±0.09	9	0.048	0.9930
11	3.07±0.09	9	0.056	0.9948	2.75±0.08	9	0.045	0.9932
12	3.20±0.03	9	0.017	0.9995	2.96±0.06	8	0.023	0.9974
13	3.27±0.03	9	0.018	0.9995	3.14±0.04	9	0.023	0.9985
14	3.52±0.04	8	0.023	0.9990	3.18±0.10	9	0.054	0.9928
15	3.76±0.03	8	0.014	0.9997	3.30±0.10	8	0.038	0.9945
16	4.24±0.05	7	0.020	0.9993	3.62±0.11	8	0.042	0.9946
17	4.51±0.07	7	0.028	0.9987	3.94±0.06	8	0.023	0.9986
18	6.46±0.10	5	0.021	0.9991	5.01±0.07	7	0.019	0.9989
19	2.92±0.09	11	0.080	0.9887	3.16±0.10	10	0.072	0.9879
20	2.87±0.04	10	0.029	0.9983	2.96±0.06	10	0.040	0.9964
21	3.92±0.11	8	0.060	0.9928	4.01±0.09	8	0.035	0.9962
22	4.30±0.10	7	0.039	0.9966	4.20±0.07	8	0.026	0.9982
23	4.61±0.19	7	0.076	0.9887	4.59±0.14	7	0.041	0.9938
24	4.29±0.14	7	0.056	0.9939	4.03±0.06	8	0.025	0.9981
25	4.73±0.14	7	0.057	0.9941	4.52±0.12	7	0.033	0.9959
26	4.80±0.15	7	0.060	0.9934	4.67±0.13	7	0.037	0.9950
27	5.53±0.14	6	0.043	0.9966	5.21±0.18	7	0.052	0.9927
28	5.63±0.11	6	0.033	0.9981	5.06±0.12	7	0.035	0.9966
29	6.35±0.19	5	0.039	0.9969	5.89±0.31	6	0.063	0.9863
30	6.75±0.16	5	0.033	0.9976	5.72±0.79	6	0.160	0.9298
31	7.65±0.23	4	0.030	0.9970	6.44±0.28	6	0.056	0.9891
32	8.68±0.36	4	0.047	0.9946	7.18±0.46	5	0.061	0.9840

[a] See Tables 1 and 2.

lated with P_m^N in the full range of mobile phase compositions is

$$q = -(0.432 \pm 0.046) - (0.001 \pm 0.010)p$$

$$s = 0.095,\ r^2 = 0.0001,\ n = 32 \qquad (15)$$

for methanol–water and

$$q = -(0.476 \pm 0.045) - (0.001 \pm 0.011)p$$

$$s = 0.080,\ r^2 = 0.0003,\ n = 32 \qquad (16)$$

for acetonitrile–water.

The slope of these correlations does not differ significantly from zero and hence the poor r^2 value, although the overall standard deviation is exactly the same as in Eqs. 7 and 8. The intercept of these correlations is the same as in Eqs. 7 and 8 because the log k' values correlated are the same.

From these correlations general equations which relate the retention of a solute over the full range of mobile phase compositions with a single solute (p) and a single solvent parameter (P_m^N) can be obtained

$$\log k' = -0.432 + p(P_m^N + 0.001) \qquad (17)$$

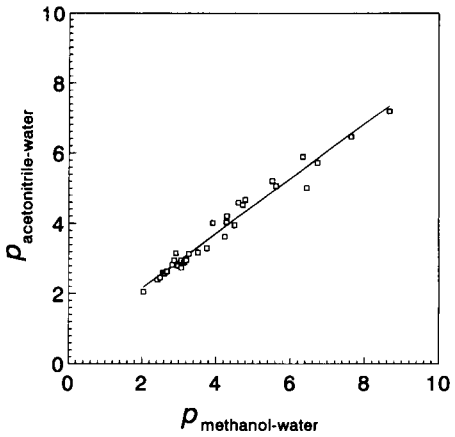

Fig. 5. Relationship between p values in methanol–water and acetonitrile–water mobile phases.

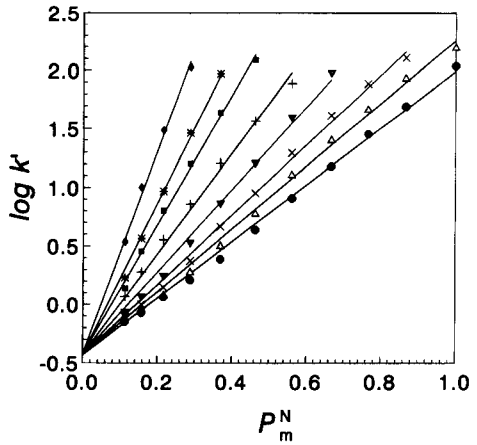

Fig. 6. Relationship between retention (log k') and mobile phase P^N_m polarity for some solutes in methanol–water mobile phase. Symbols as in Fig. 2.

for methanol–water and

$$\log k' = -0.476 + p(P^N_m + 0.001) \quad (18)$$

for acetonitrile–water.

These equations follow the model

$$\log k' = (\log k')_0 + p(P^N_m - P^N_s) \quad (19)$$

where the subscripts m and s indicate the mobile and stationary phases, respectively.

The P^N_s value for this particular column is zero because this has been the reference taken for P^N_m definition, although different P^N_s values are expected in other columns. The P^N_s for these columns would be positive or negative depending on if the column is more or less polar than our column.

The results obtained fitting the log k' values to Eqs. 17 or 18 are presented in Table 5. The p parameter (slope of the correlation) is a parameter which defines the sensitivity of the solute to the variation of the mobile phase polarity P^N_m, and therefore is characteristic of each solute. The p parameter of any solute in the two mobile phases studied has not the same value, but they are related (Fig. 5) according to

$$p_{acetonitrile—water} = (0.61 \pm 0.11) + (0.776 \pm 0.025) p_{methanol—water}$$
$$s = 0.23,\ r^2 = 0.969,\ n = 32 \quad (20)$$

Some examples of the straight lines obtained according to Eqs. 17 and 18 are presented in Figs. 6 and 7 for the same solutes as in Figs. 2 and 3. They show that the retention of the solutes studied can be linearly related with the new solvent parameter P^N_m over the full range of mobile phase compositions.

However, the validity of this new solvent parameter would be very limited if its applicability was restricted to the particular column studied. The general validity has been tested with literature data. Fig. 8 shows the plots obtained for retention of different drug compounds on a Hypersil ODS column [12] with methanol–water as mobile phase (20–50% of methanol). Straight lines are obtained for drugs of such different

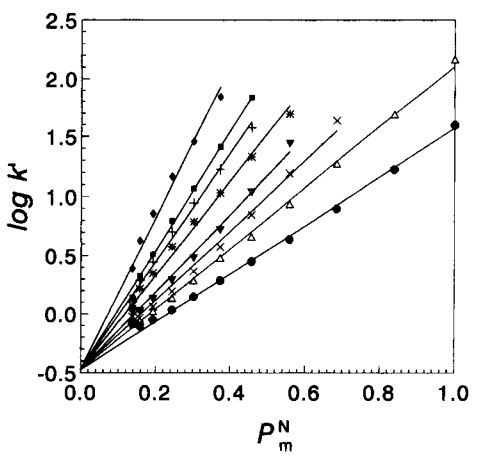

Fig. 7. Relationship between retention (log k') and mobile phase P^N_m polarity for some solutes in acetonitrile–water mobile phase. Symbols as in Fig. 3.

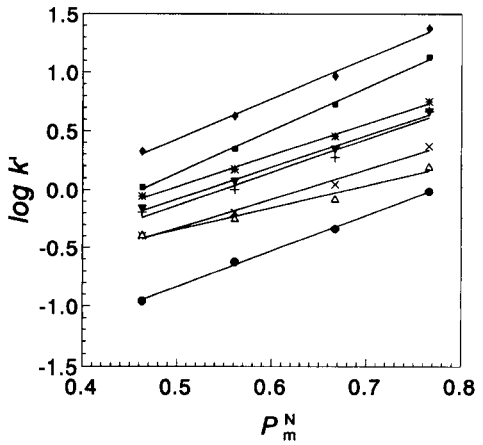

Fig. 8. Relationship between retention (log k') and mobile phase P_m^N polarity for some drug compounds from Ref. [11] in methanol–water mobile phase: (○) aspirin, (△) paracetamol, (×) theophylline, (+) caffeine, (▽) barbitone, (*) salicylamide, (□) phenobarbitone and (◇) phenacetin.

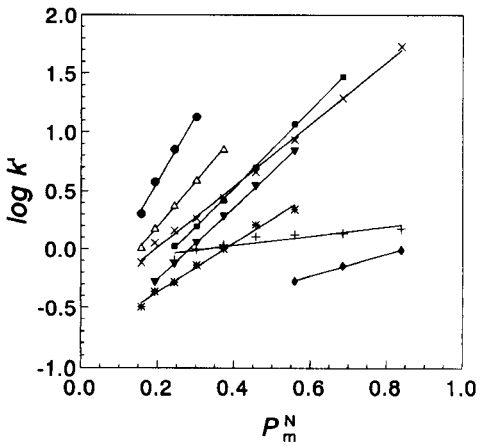

Fig. 9. Relationship between retention (log k') and mobile phase P_m^N polarity for diverse solutes in different columns from different references in acetonitrile–water mobile phase: (◇) acetone in Hypersil ODS [11], (+) nitromethane in Licrocart Superspher 100 RP 18 [17], (□) methyl benzoate in Chrompack Chromspher C_{18} [17], (*) aniline in Spherisorb ODS-2 [15], (▽) benzyl cyanide in Spherisorb ODS-2 [16], (×) 4-methylphenol in Unisil Q C_{18} [14], (△) octanol in ERC-1000 ODS [13] and (○) pentane in Develosil ODS [12].

structure as aspirin, paracetamol, theophylline, barbitone, salicylamide, caffeine, phenobarbitone and phenacetin. The usefulness of the proposed P_m^N parameter is confirmed in Fig. 9, where retention of compounds of diverse structure and functional groups in different C_{18} columns from different literature sources [12–18] with acetonitrile–water as mobile phase is plotted against P_m^N. Straight lines are obtained for all the solutes and columns in the range of mobile phase composition studied.

The general applicability of Eq. 19 can be demonstrated by the good correlations obtained for the retention of a wide variety of solutes (167 aromatic hydrocarbons, alcohols, phenols, anilines, nitriles, aldehydes, ketones, ethers, esters and amides for methanol–water and 168 for acetonitrile–water) studied by Smith and Burr [14,15,19–22] on the same C_{18} column (10 cm × 5.0 mm i.d. Spherisorb ODS-2, 5 μm). The same set of solutes has been studied by Smith and Burr from the retention index approach and by Abraham and Rosés [23] from the classical linear solvation energy relationships applied to solutes.

Correlation of Smith and Burr's data with the proposed P^N parameter gives:

$$\log k' = -(1.247 \pm 0.070) + p[P_m^N + (0.100 \pm 0.019)] \quad (21)$$

$s = 0.036$, $n = 783$ points for methanol–water, and

$$\log k' = -(1.092 \pm 0.035) + p[P_m^N + (0.063 \pm 0.010)] \quad (22)$$

$s = 0.030$, $n = 802$ points for acetonitrile–water.

The agreement between the experimental data and the calculated by Eqs. 21 or 22 is very good, although the points for low retentions are more scattered because

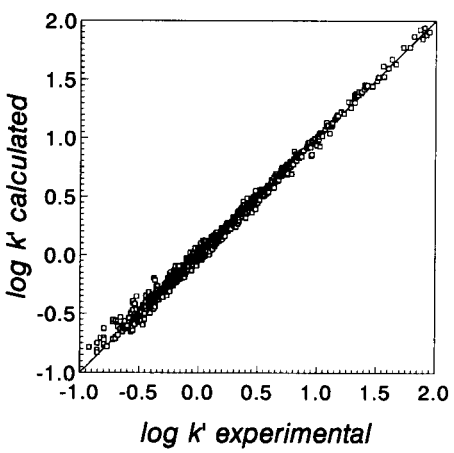

Fig. 10. Plot of log k' calculated (Eq. 22) vs. experimental in acetonitrile–water mobile phase for the retention of 168 solutes (802 log k' values) studied by Smith and Burr [14,15,19–22].

a small variation in retention time produces a high variation in log k' value. The example for acetonitrile–water (Eq. 22) is presented in Fig. 10.

The P_s^N values for the solvated stationary phase used by Smith and Burr are -0.10 (Eq. 21) for methanol–water and -0.06 (Eq. 22) for acetonitrile–water. Therefore, this particular C_{18} stationary phase seems to be slightly less polar than ours ($P_s^N = -0.01$ for both mobile phases). The $(\log k')_0$ values (-1.25 for methanol–water and -1.09 for acetonitrile–water) are lower than ours (-0.43 and -0.48, respectively, see Eqs. 17 and 18), probably because Smith and Burr's column is shorter than ours and therefore retention times are lower.

The correlations obtained demonstrate that the new P^N parameter can be successfully applied to the retention of a great variety of solutes in different C_{18} chromatographic columns. Therefore, it can be used for the estimation of the retention of other solutes in these systems in the same way the E_T^N parameter was used in the previous work [5]. The advantage of P^N over E_T^N is that it extends to the full range of mobile phase compositions.

Acknowledgements

Financial support from the DGICYT (project PB91-0262) is gratefully acknowledged.

References

[1] P.J. Schoenmakers, H.A.H. Billiet and L. de Galan, J. Chromatogr., 282 (1983) 107.
[2] B.P. Johnson, M.G. Khaledi and J.G. Dorsey, Anal. Chem., 58 (1986) 2354.
[3] K. Dimroth, C. Reichardt, T. Siepmann and F. Bohlmann, Justus Liebigs Ann. Chem., 661 (1963) 1.
[4] C. Reichardt, Solvents and Solvent Effects in Organic Chemistry, VCH, Weinheim, 2nd edn., 1988.
[5] M. Rosés and E. Bosch, Anal. Chim. Acta, 274 (1993) 147.
[6] M.J. Kamlet, J.L.M. Abboud and R.W. Taft, Prog. Phys. Org. Chem., 13 (1981) 485.
[7] M.J. Kamlet, J.L.M. Abboud, M.H. Abraham and R.W. Taft, J. Org. Chem., 48 (1983) 2877.
[8] R.W. Taft, J.L.M. Abboud, M.J. Kamlet and M.H. Abraham, J. Solut. Chem., 14 (1985) 153.
[9] M.J. Kamlet and R.W. Taft, Acta Chem. Scand., B39 (1985) 611.
[10] M.J. Kamlet, M.H. Abraham, P.W. Carr, R.M. Doherty and R.W. Taft, J. Chem. Soc., Perkin Trans. 2, (1988) 2087.
[11] E. Bosch and M. Rosés, J. Chem. Soc., Faraday Trans., 88 (1992) 3541.
[12] R.M. Smith and N. Finn, J. Chromatogr., 537 (1991) 51.
[13] M. Bogusz and R. Aderjan, J. Chromatogr., 435 (1988) 43.
[14] R.M. Smith and C.M. Burr, J. Chromatogr., 475 (1989) 57.
[15] R.M. Smith and C.M. Burr, J. Chromatogr., 481 (1989) 71.
[16] T. Hanai and J. Hubert, J. High Res. Chromatogr. Chromatogr. Commun., 6 (1983) 20.
[17] T. Hanai and J. Hubert, J. Chromatogr., 302 (1984) 89.
[18] T. Hanai and J. Hubert, J. Chromatogr., 290 (1984) 197.
[19] R.M. Smith and C.M. Burr, J. Chromatogr., 475 (1989) 75.
[20] R.M. Smith and C.M. Burr, J. Chromatogr., 481 (1989) 85.
[21] R.M. Smith and C.M. Burr, J. Chromatogr., 485 (1989) 325.
[22] R.M. Smith and C.M. Burr, J. Chromatogr., 550 (1991) 335.
[23] M.H. Abraham and M. Rosés, J. Phys. Org. Chem., in press.

ELSEVIER

Analytica Chimica Acta 299 (1994) 231–237

ANALYTICA CHIMICA ACTA

Isolation of the main organic acids from fruit juices and nectars for carbon isotope ratio measurements

M. Gensler, H.-L. Schmidt *

Lehrstuhl für Allgemeine Chemie und Biochemie der TU München, D-85350 Freising-Weihenstephan, Germany

Received 18 May 1994

Abstract

A method was developed for the quantitative separation and isolation of organic acids consisting of a three step clean-up procedure (C_{18} tube, cation exchange and anion exchange column) and subsequent liquid chromatographic separation on a reversed-phase column. The complete recovery of the total acids from standard juices (0.8–1 g per 20–100 ml) is between 72.6 (L-malic acid) and 73.3% (citric acid) and the $\delta^{13}C$ value difference between applied and isolated material does not exceed 0.3‰. An isotope discrimination of the eluted acids between begin and end of a peak in reversed-phase chromatography is between 1.3 and 2.2‰, while with ion exchange chromatography this is much larger (26.3–37.9‰). Upon the experiences obtained, isotope discriminations implied in chromatographic separations are discussed with regard to practical aspects.

Keywords: Chromatography; Citric acid; Fruit juices; L-Malic acid; Nectars; L-Tartaric acid

1. Introduction

Quality and authenticity control of fruit juices and wine demands reliable and reproducible methods for qualitative and quantitative analysis of various ingredients. An extremely powerful method, especially for origin assignments and adulteration proof, is isotope ratio mass spectrometry (IRMS) [1,2]. It additionally depends on the micro quantitative isolation of defined compounds from foodstuff. Isotope analysis has so far successfully been applied to pulp, sugars, the total acid fraction and ethanol in context with the authenticity check of the above mentioned beverages. Very typical and important for quality and organoleptic properties of juices are organic acids and sugars, and especially the sugar to acid ratio. The most abundant acids occuring in juices are citric acid (CA), L-malic acid (L-MA) and L-tartaric acid (L-TA); L-malic acid, for example, is predominant in cherry, apple and grape juices, citric acid in black currant, pineapple and citrus juices, L-tartaric acid is among the main organic acids in grape juice. However, in addition to the main acids, in any juice usually a second acid is present in noticeable amounts (Table 1).

Very recently we have described the principle of the external and internal standardization in isotope analysis [6], based on the experience that natural compounds from the same origin do not only have metabolic, but also isotopic correlations, and that a deviation from the normal δ value difference of two compounds from the same origin is highly indicative for the addition of one of these compounds from a foreign source. In this context the parallel occurance and the isotopic correlation of the above mentioned organic acids to each other and to sugar is of high interest. Their isotopic analysis

* Corresponding author.

SSDI 0003-2670(94)00338-6

Table 1
Amounts (g/l) of the main organic acids in different fruit juices [3–5] (CA = citric acid, L-MA = L-malic acid, L-TA = L-tartaric acid)

Species	CA	L-MA	L-TA
Apple	0.05–0.2	4.5–7.6	–
Black currant	25.6–42.8	1.0–5.4	–
Cherry	<0.7	>15.0	–
Grape	0.3–1.2	1.7–15.4	4.2–13.5
Grapefruit	9.5–20.0	0.3–1.1	–
Orange	7.6–11.5	1.1–2.9	–
Pineapple	4.0–10.0	1.0–4.5	–

demands a method for their micropreparative quantitative isolation.

Among the methods, predominantly liquid chromatography (LC), published for the analytical determination of these compounds [7,8], reversed-phase, anion exchange and ion exclusion chromatography should be most promising to meet the above mentioned prerequisites for isotopic analysis.

Very recently, Lee [9] has published a method for the separation and determination of the nonvolatile organic acids from orange juice by reversed-phase LC [9] as a means for quality assessment. We have independently developed a similar procedure, however, mainly with respect to the aim of an isotope effect free micropreparative isolation of the acids from fruit juice for their isotopic analysis. As this method has also general importance in the analysis of the acids, it will be reported in the present paper. Results of its application to isotopic analyses on fruit juices will be presented in an independent contribution.

2. Experimental

2.1. Materials

Fruit juices

Authentic fruit juices were kindly provided by the Schutzgemeinschaft der Fruchtsaftindustrie (SGF, Zornheim, Germany). A "Test Juice" was prepared as follows: 80 ml of an authentic orange juice were centrifuged (10 min, 5000 *g*), the supernatant was adjusted to pH 8.5 (25% NH_3), and 15 ml $CaCl_2$ solution (50 wt.-%) were added. Then the pH was again adjusted to 8.5, the solution was heated to 85°C, and the acids, precipitated as Ca salts, were eliminated by centrifugation. The pH value of the supernatant was readjusted to 8.5, then Na_2CO_3 solution (50 wt.-%) was added until complete precipitation of the excess of Ca^{2+}. After separation of the precipitated $CaCO_3$, the pH of the solution was adjusted to 3.5, and 1 g citric acid, 0.3 g L-malic acid and 0.023 g L-ascorbic acid of known $\delta^{13}C$ values were added.

Chemicals

All applied chemicals (purchased from Merck, Darmstadt and Aldrich, Steinheim, respectively) were of "analytical grade". Standard acids were purchased from Merck and Serva (Heidelberg), respectively. Enzyme kits for the determination of CA, L-MA and D-glucose were from Boehringer Mannheim. Water was purified using a Millipore system (Millipore, Bedford).

Column materials for clean up

A Mega Bond Elut C_{18} tube from ICT (Frankfurt), conditioned with 50 ml of methanol and 100 ml of water before each single sample, a cation exchange resin AG50W×8 (200–400 mesh, H^+ form) and an anion exchange resin AG1×8 (200–400 mesh, Cl^- form), both from Biorad (Munich) were employed. A 1.8 cm i.d. glass column was filled with cation exchange resin (10 g) and a 1 cm i.d. glass column was filled with anion exchange resin (10 g).

2.2. Methods

Isolation of the acids and carbon isotope ratio measurements

The procedure developed for the isolation of the pure acids from centrifuged juices (Fig. 1) comprised three chromatographic clean-up steps (1–3) and a subsequent liquid chromatographic separation (step 4).

The first clean-up was done to eliminate the nonpolar ingredients via a C_{18} tube, the second step separated the acids from amino acids by a cation exchange column, and the third step, an anion exchange process, supplied the pure acid fraction by eliminating the sugars. From the acid fraction of this procedure the individual acids were separated by reversed-phase LC.

Each step of the procedure was controlled by comparing it with a corresponding test solution. Detailed conditions, also in correlation with their evaluation are given below.

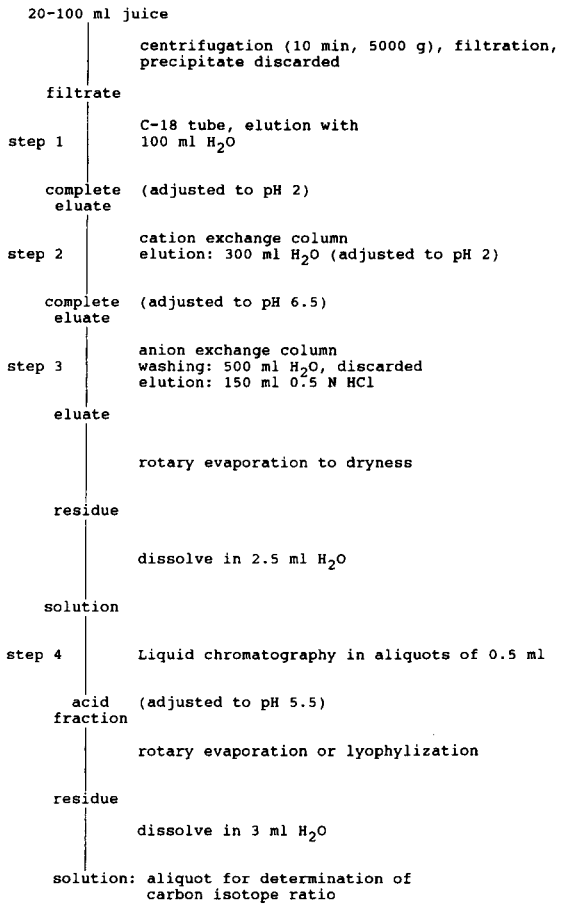

Fig. 1. Diagram for the isolation of the main organic acids (CA, L-MA, L-TA) from juices for carbon isotope ratio measurements. Step means chromatographic procedure.

(a) All juices and nectars were centrifuged (10 min, 5000 *g*) and filtered.

(b) Given aliquots of the supernatant (20–100 ml depending on juice species) or test solutions, respectively, were applied to the C_{18} tube. The polar fraction was eluted with 100 ml water and the eluate was adjusted to pH 2 (step 1, Fig. 1).

(c) The eluate from (b) was applied to the cation exchange column in the H^+ form, followed by elution with 300 ml water, adjusted to pH 2 with 5 M HCl (step 2, Fig. 1). The combined eluate was adjusted to pH 6.5.

(d) The eluate from (c) was applied to the anion exchange column, followed by a washing step with 500 ml of water and elution with 150 ml of 0.5 M HCl (step 3, Fig. 1). The eluate was brought to dryness by rotary evaporation (70°C, water-jet vacuum), and the residue was dissolved in 2.5 ml water.

(e) 0.5 ml of the residual solution (d) were injected into the LC column. A Varian liquid chromatograph (Model 5000, Varian, Palo Alto) with a Melz LCD 212 (Flowchem, Besigheim) RI detector was employed. The column used was a Lobar Li Chroprep RP-8 size 6 (440×37 mm, 40–60 μm) from Merck. Elution was performed with 0.02 M H_3PO_4 (5 ml/min) at 22°C (step 4, Fig. 1). The acid fractions were collected, adjusted to pH 5.5 and lyophilized to dryness. The residues were dissolved in 3 ml water.

(f) From an aliquot of the dissolved residues (e), the carbon isotope ratios were determined, as described by Winkler and Schmidt [10]. All $\delta^{13}C$ values were related to the PDB standard.

$$\delta^{13}C \text{ value} = \frac{R_{sample} - R_{standard}}{R_{standard}} \times 1000 \text{ (‰)}$$

$$R = [^{13}C]/[^{12}C]$$

The isotope ratio mass spectrometer was a VG Micromass 903 (VG Isogas, Middlewich) apparatus.

Evaluation of the method

The recovery was controlled by enzymatic methods (CA, L-MA, D-glucose) [11] or spectrophotometrically, as a complex of vanadate (L-TA) [12]; the isotopic abundances were analyzed after evaporation [10]. For the check on reproducibility several fruit juices were analyzed four times in sequence (according to Fig. 1).

Determination of the carbon isotope fractionation

The isotope fractionation was examined for two different resins. The Lobar RP-8 column was tested under conditions as described under Methods (e) with a standard mixture of 10 mg CA, L-MA and L-TA per 0.5 ml, pH 1 or 100 mg L-MA per 0.5 ml, pH 1, isolated from cherry juice, respectively. In the second column, an anion exchanger (glass column, 20×2 cm, filled with 10 g of Ag1×8 anion exchange resin, 200–400 mesh, formiate form (Biorad)) was used. Fractionation was performed with a gradient of 0–5 M formic acid in 330 min (1.5 ml/min) at 22°C. CA and L-MA were detected with enzymatic methods [11], L-TA photometrically, as a complex of vanadate [12]. A test

Table 2
Material recovery and isotope yield of acids from individual steps and from the complete separation method

Procedure according to Fig. 1	Acid	Recovery [a] (%)	$\delta^{13}C$ value $[‰]_{PDB}$	
			Found [b]	Deviation from original value
C_{18} tube	L-TA	98.2	−21.5	−0.1
(step 1)	L-MA	98.4	−24.9	+0.1
	CA	94.9	−24.1	−0.2
Cation exchange column	L-TA	93.6	−21.5	−0.1
(step 2)	L-MA	91.9	−24.9	+0.1
	CA	94.9	−24.0	−0.1
Anion exchange column	L-TA	91.5	−21.5	−0.1
(step 3)	L-MA	93.0	−24.8	+0.2
	CA	96.4	−24.0	−0.1
Liquid chromatography	L-TA	84.4	−21.5	−0.1
(step 4)	L-MA	93.7	−24.9	+0.1
	CA	87.9	−24.1	−0.2
Complete method	L-TA	76.2	−21.4	0.0
	L-MA	74.3	−25.0	0.0
	CA	78.4	−23.8	+0.1
Complete method on "Test-Juice"	L-MA	72.6	−25.3	−0.3
	CA	73.3	−23.9	0.0

Applied amounts for clean-up and complete method: mixture of 200 mg CA, 100 mg L-MA and L-TA per 20 ml or solutions of the individual acids of the same amounts, respectively; LC: mixture of 30 mg CA, 15 mg L-MA and L-TA per 0.5 ml; original $\delta^{13}C$ values: L-TA, −21.4; L-MA, −25.0; CA, −23.9.

[a] Mean value of 2 independent determinations.

[b] Mean value of 3 independent determinations (standard deviation always <0.2‰).

solution of 50 mg CA, 25 mg L-MA and L-TA per 0.5 ml, pH 7.9, was applied.

Acid peaks were divided into three parts. From each part the amount of acid and isotopic abundances were determined.

3. Results

The individual steps of the developed method (Fig. 1) as well as the complete method were controlled for mass and isotope recovery by the analysis of test mixtures and "Test Juices" (Table 2). Furthermore, the developed method was checked for reproducibility. Independently two column materials were tested in step 4 for isotope fractionation across the peaks.

3.1. Recovery and isotope discrimination

Clean-up (Step 1–3)

A standard mixture of isotopically analyzed acids (Table 2, recovery test), or solutions of the individual acids in the same amounts (isotope discrimination), respectively, were used throughout with individually adapted pH values (C_{18} tube: pH 3.5; cation exchange column: pH 2; anion exchange column: pH 6.5). From the test mixtures on the C_{18} tube, the cation and the anion exchange columns, a practically complete recovery of all acids was observed, and the shift of the measured $\delta^{13}C$ values from that of the applied acid was, even over all steps, within the standard error of carbon isotope determination, 0.1–0.2‰. Additionally, 12 g of D-glucose were applied to and completely eluted from the anion exchange column with 500 ml water (simulating corresponding amounts of sugars in juices); the recovery was more than 98% (not listed in Table 2).

Liquid chromatography (Step 4)

In the case of liquid chromatography the recovery of the acids from a standard mixture of isotopically analyzed compounds (30 mg CA, 15 mg L-MA and L-TA per 0.5 ml) was somewhat less than in the clean-up steps, but the measured $\delta^{13}C$ values were identical to those of the original acids.

Table 3
Isotope fractionation of acids across the peaks on reversed phase (RP) and anion exchange (AE) column, respectively

Column	Acid	Recovery (%)	Peak cuts		$\delta^{13}C$ values (‰)$_{PDB}$			
			Elution time (min)	Rel. amount [a] (%)	Peak fraction	Original substance	Mean value of fraction [b]	Deviation from original substance
RP-8	L-TA	93.0	55.0–59.5	11.8	−22.3	−21.4	−21.7	−0.9
			59.5–63.0	71.0	−21.7			−0.3
			63.0–69.0	17.2	−21.0			+0.4
	L-MA [c]	89.1	69.0–73.5	17.0	−24.0	−25.0	−25.1	+1.0
			73.5–77.0	57.4	−24.9			+0.1
			77.0–84.5	25.7	−26.2			−1.2
	CA	93.0	110.0–118.5	25.0	−25.0	−23.9	−24.4	−1.1
			118.5–124.0	52.2	−24.5			−0.6
			124.0–136.0	22.8	−23.3			+0.6
	L-MA [d]	90.2	70.0–74.0	10.0	−24.3	−25.6	−25.5	+1.3
			74.0–83.0	73.0	−25.5			+0.1
			83.0–94.0	17.0	−26.2			−0.6
AE	L-TA	96.1	140.0–154.0	23.1	−7.6	−21.4	−20.3	+13.8
			154.0–164.0	54.7	−19.6			+1.8
			164.0–174.0	22.2	−35.2			−13.8
	L-MA [c]	89.0	92.0–99.0	15.6	−5.5	−23.2	−24.8	+17.7
			99.0–109.0	67.4	−24.6			−1.4
			109.0–116.0	17.0	−43.4			−20.2
	CA	94.4	174.0–184.0	27.7	−12.4	−23.9	−24.4	+11.5
			184.0–199.0	56.0	−26.2			−2.3
			199.0–214.0	16.3	−38.7			−14.8

Applied amounts on RP-8 column: mixture of 10 mg CA, L-MA and L-TA per 0.5 ml or 100 mg L-MA from cherry juice per 0.5 ml, respectively; on AE column: Mixture of 50 mg CA and 25 mg L-MA and L-TA per 0.5 ml
[a] Total recovery was set to 100%.
[b] Calculated as sum of the individual fractions.
[c] Synthetic.
[d] Natural.

Complete separation

A standard mixture (200 mg CA, 100 mg L-MA and L-TA), pH 3.5, or "Test Juices" were submitted to the complete procedure.

The recovery was still very satisfactory and the $\delta^{13}C$ values were identical to those of the applied samples. Results obtained from the "Test Juice" agreed with those of the test mixture.

3.2. Reproducibility

The acids from a given juice were isolated and four times independently submitted to isotopic analysis. This was realized with one grape juice, four orange juice, three black currant juice and two apple juice samples. Maximum difference of the $\delta^{13}C$ values found for an acid from each juice was 0.2‰ (standard deviation 0.05–0.08‰).

3.3. Isotope fractionation across the LC peaks

In order to estimate the individual error on each acid implied by a possible chromatographic isotope discrimination combined to an incomplete recovery of the peaks, all acids were "fractionated" on the reversed phase and on an anion exchange column, respectively. Each elution peak was cut into three fractions, the first representing about 20%, the second about 60% and the third again about 20% of the total amount of the acid. From each fraction the exact yield and the $\delta^{13}C$ value of the acid were determined (see Table 3).

Table 4
Isotope fractionation of liquid chromatographic separations, published by other research groups

Stationary phase	Analyte	Break through sequence of isotopomers	Ref.
Cation exchanger	Mg^{2+}	$^{26}Mg^{2+} > {}^{25}Mg^{2+} > {}^{24}Mg^{2+}$	[13]
	Ca^{2+}	$^{48}Ca^{2+} > {}^{44}Ca^{2+} > {}^{43}Ca^{2+} > {}^{42}Ca^{2+} > {}^{40}Ca^{2+}$	[14]
	Sr^{2+}	$^{88}Sr^{2+} > {}^{87}Sr^{2+} > {}^{86}Sr^{2+}$	[13]
	Li^{+}	$^{7}Li^{+} > {}^{6}Li^{+}$	[15]
	K^{+}	$^{39}K^{+} > {}^{41}K^{+}$	[15]
	Rb^{+}	$^{85}Rb^{+} > {}^{87}Rb^{+}$	[15]
Polar phase	Plant hormones [a]	$^{1}H > {}^{2}H$	[16]
	Antidepressants [b]	$^{1}H > {}^{3}H$	[17]
	Aldehydes	$^{12}C > {}^{13}C$	[18]
Reversed-phase	Plant hormones [a]	$^{2}H > {}^{1}H$	[16]
	Leucine	$^{3}H > {}^{1}H$	[19]
	Leucine	$^{12}C > {}^{13}C$	[19]
	Antidepressants [b]	$^{1}H > {}^{3}H$	[17]
	Chlorophyll	$^{2}H > {}^{1}H$	[20]
	Chlorophyll	$^{12}C/{}^{13}C$ (not reproducible)	[20]
	Steroids	$^{13}C > {}^{12}C$	[21]
	FAME [c]	$^{13}C > {}^{12}C$	[21]
	L-TA, CA	$^{12}C > {}^{13}C$	o.r. [d]
	L-MA	$^{13}C > {}^{12}C$	o.r.
Anion exchanger	L-TA, CA, L-MA	$^{13}C > {}^{12}C$	o.r.
CP Sil 5 [e]	Terpenoids	$^{13}C > {}^{12}C$	[22]

[a] Plant hormones: indole-3-acetic acid, abscisic acid, phthalimido-1-aminocyclopropane-1-carboxylic acid.
[b] Antidepressants: imipramine, desmethylimipramine.
[c] FAME: fatty acid methyl esters.
[d] o.r.: own results.
[e] Gas chromatography: fused-silica capillary (non-polar).

From the reversed-phase column the light isotopomers of L-TA and CA were preferably eluted in the first fraction of the peak, while L-MA showed an inverse behaviour. On the anion exchange column the breakthrough of the ^{13}C isotopomers was prior for all acids. The extent of the isotope fractionation was in the same range for all acids on a given column, but was considerably larger on the AE column compared with the RP column. Total recoveries were 93.0 and 96.1% (L-TA), 89.1 and 89.0% (L-MA) and 92.0 and 94.4% (CA) on the reversed-phase and anion exchange column, respectively.

4. Discussion

Our results demonstrate that a well-adapted combination of chromatographic purification and separation steps, especially reversed-phase chromatography, is suitable for the purification and quantitative and pure isolation of acids from fruit juices, needed for their isotope analysis. They also prove that elution peaks must be completely compiled, as isotope effects are implied in the chromatographic procedure. This is well known from other compounds, but the direction of this isotope effect is obviously not always predictable (Table 4).

Summarizing the results shown in Table 4, the following conclusions can be drawn:

(1) The fractionation of inorganic cations on ion exchangers is obviously dependent on ion characteristics (ion radius, charge, etc.). It is noticeable that Li^{+} shows a reverse elution sequence when compared to the other alkali cations K^{+} and Rb^{+}. The results in the references cited [13–15] also indicate that the isotope fractionation is the larger, the higher the mass difference of two isotopes and the lower the atom mass of an element are.

(2) Polar phase (normal phase) chromatography of organic compounds with non-polar eluents is charac-

terized by a faster breakthrough of the light isotopomers, independent from the element in question (H, C), probably due to a reduced van der Waals interaction of the heavy isotopomers with the non-polar eluent [16].

(3) In reversed-phase chromatography of hydrogen isotopomers, normally the heavy individuals are less retained. Analogous results were obtained with gas chromatography (H and C isotopomers) [20,22]. This behaviour seems to be based on the same principle as above, with the difference that now the stationary phase is non-polar.

An exception, for example, is the separation of antidepressants, because their separation is probably not a pure reversed-phase process, but interfered by interactions between the polar OH groups of the silica matrix with complementary groups of the analyte [17].

In contrast to H isotopomers, the elution sequence of carbon isotopomers seems to be undefined ([19,20], and data reported here). In the case of L-TA and CA light isotopomers are enriched in the front part of the peak, as has been demonstrated for leucine, while L-MA is fractionated in reverse sequence. A satisfactory interpretation is not possible so far.

(4) Our results with an anion exchange column demonstrate the preferred elution of the heavy carbon isotopomers with all acids investigated, indicating their weaker interaction with the stationary phase. A possible explanation for this finding might be an isotope effect on the pK value.

For practical purposes the direction and mechanism of isotope fractionation is less important than its extent, as shown for LC, which is extremely dependent on the column material employed. In the present work, among two common materials for acid separation the isotope discrimination was very large for anion exchange (25–37‰, between the fractions of a peak, Table 3) but small for reversed-phase chromatography (1.3–2.2‰, Table 3); this is in line with results for chlorophyll [20].

For the separation of polar compounds, the isotope effect seems to increase from reversed phases over polar phases (normal phases) [18] to exchange phases, but will not generally be predictable. Because of the small isotope discrimination for the separation of organic acids and their isolation for carbon isotope ratio measurement, reversed-phase chromatography would be the most favourable method.

References

[1] A. Roßmann, W. Rieth and H.-L. Schmidt, Z. Lebensm. Unters. Forsch., 191 (1990) 259.
[2] R. Braunsdorf, U. Hener and A. Mosandl, Z. Lebensm. Unters. Forsch., 194 (1992) 426.
[3] Verband der deutschen Fruchtsaftindustrie (VdF) e.V., Bonn (Eds.), RSK-Werte. Die Gesamtdarstellung, 1. Edition, Flüssiges Obst GmbH, Schönborn, 1987
[4] S. Wallrauch, Flüssiges Obst, 60 (1993) 166.
[5] Fuleki et al., J. Assoc. Off. Anal. Chem., 76 (1993) 591.
[6] H.-L. Schmidt, M. Butzenlechner, A. Rossmann, S. Schwarz, H. Kexel and K. Kempe, Z. Lebensm. Unters. Forsch., 196 (1993) 105.
[7] R. Schwarzenbach, J. Chromatogr., 251 (1982) 339.
[8] J. Palmer and D.M. List, J. Agric. Food Chem., 21 (1973) 903.
[9] H.S. Lee, J. Agric. Food Chem., 41 (1993) 1991.
[10] F.J. Winkler and H.-L. Schmidt, Z. Lebensm. Unters. Forsch., 171 (1980) 85.
[11] Boehringer Mannheim, Methods of Biochemical Analysis and Food Analysis, 1989.
[12] Dtsch. Lebensmittel-Rdsch., 60 (1964) 140.
[13] T. Oi, H. Ogino, H. Kakihana and M. Hosoe, Sep. Sci. Technol., 27 (1992) 631.
[14] T. Oi, N. Morioka, H. Ogino, H. Kakihana and M. Hosoe, Sep. Sci. Technol., 28 (1993) 1971.
[15] T. Oi, K. Kawada, H. Kakihana and M. Hosoe, Sep. Sci. Technol., 26 (1991) 1353.
[16] B.H. Brown, S.J. Neill and R. Horgan, Planta, 167 (1986) 421.
[17] B.K. Kudelin, L.V. Gavrilina and Y.L. Kaminski, J. Chromatogr., 636 (1993) 243.
[18] R. Braunsdorf, U. Hener, G. Przibilla, S. Piecha and A. Mosandl, Z. Lebensm. Unters. Forsch., 197 (1993) 24.
[19] P.Q. Baumann, D.B. Ebenstein, B.D. O'Rourke and S.K. Nair, J. Chromatogr., 573 (1992) 11.
[20] R.R. Bidigare, M.C. Kennicutt, W.L. Keeney-Kennicutt and S.A. Macko, Anal. Chem., 63 (1991) 130.
[21] R.J. Caimi and J.T. Brenna, Anal. Chem., 65 (1993) 3497.
[22] A. Barrie, J. Bricout and J. Koziet, Biomed. Mass Spectrom., 11 (1984) 583.

ELSEVIER

Analytica Chimica Acta 299 (1994) 239–247

ANALYTICA CHIMICA ACTA

Preparation and characterization of bonded stationary phases of nitrogen-containing crown ether for high-performance liquid chromatography

Shi-Lu Da *, Wei-Ghua Yue, Yu-Feng Wen, Hui-Ling Da, Zhong-Hua Wang

Department of Chemistry, Wuhan University, Wuhan 430072, China

Received 7 July 1993; revised manuscript received 15 July 1994

Abstract

Silica gel bonded phases with a nitrogen-containing crown ether were synthesized via a three-step reaction on the surface of porous silica. The bonded molecular structure was characterized by chemical and instrumental analyses. The bonded phases possess complexing ability with copper ion and weak hydrophobicity. The retention behaviour of polar disubstituted benzene derivatives and amino acids on the bonded phases was studied using methanol and/or aqueous solution with acetate buffer and copper ion as mobile phases. When copper cations are added to the mobile phase at pH 5, positive charges are generated on the surface of the stationary phase and some electrostatic interaction occurs between polar organic compounds and the stationary phase. The chromatographic retention of the polar solutes is controlled mainly by dipolar and electrostatic interactions, and is less affected by hydrophobic interactions.

Keywords: High-performance liquid chromatography; Crown ethers

1. Introduction

The application of crown ethers in high-performance liquid chromatography (HPLC) is an important area of research in developing host–guest and multimodal stationary phase for LC [1–3]. Crown ethers have high complexing abilities not only with various metal ions, but also with ammonium ions. Highly lipophilic crown ethers have been used as stationary phases to be coated on octadecylsilane-bonded silica gel for the separation of alkali and alkaline earth metal cations [4]. Host–guest interaction between a crown ether and an amino group has been incorporated into reversed-phase HPLC for the separation of amino acids, peptides and substituted anilines, where crown ethers are involved as components of the mobile phases [5,6]. It has been reported that silica gel bonded crown ether packings have been mainly applied for separating metal ions selectively from mixtures [7].

The preparation of crown ether-bonded stationary phases has usually been accomplished by two routes: (1) first the synthesis of crown ethers and silanized silica gel containing organic reactive groups, then chemical reaction between the two as a condensation reaction [8]; (2) first the synthesis of organic silane monomers containing crown ether rings, then a covalent bonded reaction on silica gel [9]. Most of the

* Corresponding author.

SSDI 0003-2670(94)00336-X

bonded crown ethers that have been reported only contain oxygen. Nitrogen-containing crown ethers have a greater affinity for transitional metal, heavy metal and ammonium cations [10].

This paper reports the preparation of nitrogen-containing crown ether bonded phases via a successive reaction pathway on the surface of porous silica. The molecular structure of the bonded phases was characterized by elemental and functional group analyses, mass spectrometry (MS), Fourier transform infrared (FT-IR) spectrometry, differential thermal analysis, etc. The complexing capacity of the bonded phases for copper ion was determined by an extraction method. Polar disubstituted benzenes and amino acids were used to characterize the chromatographic properties of the bonded phases in reversed-phase HPLC.

2. Experimental

2.1. Reagents

All reagents were of analytical-reagent grade and were used as received unless indicated otherwise. Microparticulate silica (10 μm, surface area 320 m^2 g^{-1}, Qingdao Sea Chemical Plant) was refluxed in 0.5 M hydrochloric acid for 10 h, filtered, washed with neutral, doubly distilled water, dried at 120°C for 10 h and kept in a vacuum drier before use. 3-Glycidoxypropyltrimethoxysilane (Chemical Plant of Wuhan University) was redistilled under vacuum before use. 2-Aminoethanol, tetraethylene glycol, *p*-toluenesulphonyl chloride, sodium hydride and a diethyl ether solution of boron trifluoride ($BF_3 \cdot Et_2O$) were purchased from Shanghai General Chemical Reagent Factory. Amino acids were obtained from the Institute of Biochemistry, Academia Sinica.

2.2. Instrumentation

Elemental analysis was done using a MOD-1106 elemental analyser (Italy). For the FT-IR study, a Model 710 instrument (Nicolet Analytical Instruments) was used. A BT-30 thermal analyser system (Shimadzu) was used for thermogravimetric analysis (TGA) and differential thermal analysis (DTA). A UV-240 ultraviolet spectrophotometer (Shimadzu) was used for the determination of complexing capacities. For the MS study, an HP-5988 mass spectrome-

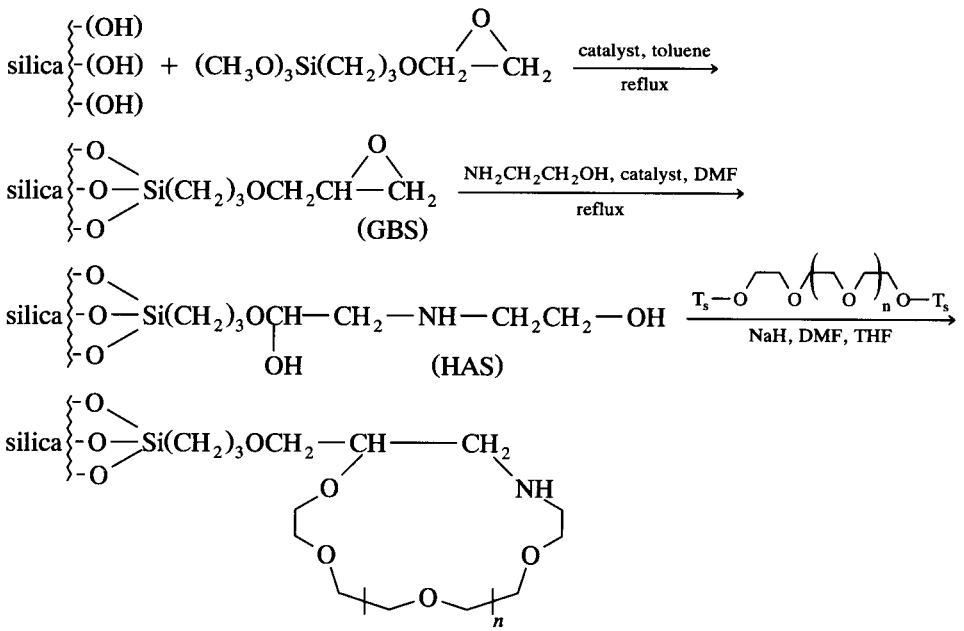

(BCN18-C-6 or BCN15-C-5) where $n = 1$ or 2

$T_s = p\text{-}CH_3C_6H_5SO_2$-

Fig. 1. Reaction sequence used to prepare the bonded phases.

ter (Hewlett-Packard) was used. The HPLC system consisted of an LC-6A pump (Shimadzu), a Model 7125 injector with a 20-μl loop (Rheodyne), a 150 × 4.6 mm i.d. or 250 × 4.6 mm i.d. stainless-steel column and an SPD-1 variable-wavelength UV detector (Shimadzu).

2.3. Preparation of bonded stationary phases

The reaction sequence used on the surface of porous silica gel for the preparation of nitrogen-containing crown ether bonded phases is shown in Fig. 1.

The precursor used in this study, 3-glycidoxypropyl-bonded stationary phase (GBS), was synthesized according to the literature [11]. The non-aqueous micro-titrimetric method with tetraethylammonium bromide–perchloric acid in glacial acetic acid established previously [12], was employed for the determination of α-epoxy groups on the surface of the GBS. The GBS with an epoxy end-group was treated with 2-aminoethanol to cleave the epoxy group, giving HAS with amino and hydroxy groups. The GBS (10 g) was placed in a flat-bottomed flask equipped with a reflux condenser, a magnetic stirrer and a heating mantle. 2-Aminoethanol, dimethylformamide (DMF) to be used as solvent and $BF_3 \cdot Et_2O$ as catalyst were added in that order. The mixture was heated and stirred under a stream of nitrogen for 4 h. The bonded material (HAS) was then filtered, washed with ethanol, acetone, doubly distilled water and acetone in that order and finally dried at 120°C.

The bonded phase of nitrogen-containing crown ether (BCN18–C-6) was synthesized in the presence of NaH by the reaction of HAS and oligoethylene glycol ditosylates, using tetrahydrofuran (THF) as solvent. The mixture was heated with stirring for 12 h. The solid product was filtered, washed with THF, methanol–water and acetone in that order and dried at 120°C. BCN18-C-6 should be capped by a silanization reaction with trimethylchlorosilane in dry toluene in order to remove residual Si–OH groups. The final bonded product was carefully filtered, washed with methanol, water and acetone, dried at 120°C and kept in a vacuum drier before packing the column.

2.4. Determination of complexing capacity of the bonded phases

The complexing capacities of the bonded phases were determined by the following procedure. The bonded phase, weighed accurately, was placed in a flat-bottomed flask with a ground-glass stopper. A solution of copper(II) in water or in acetic acid buffer (pH 5.7) was added. The flask was stoppered and placed in a shaker at constant temperature for 24 h, then the bonded phase was filtered. The concentration of Cu(II) before and after complexation was determined by UV spectrophotometry at 215 or 230 nm. The complexing capacities of the bonded phase were calculated according to the difference in Cu(II) concentration before and after complexation.

2.5. Chromatographic characterization of the bonded phases

Stainless-steel columns were packed with the bonded phases, HAS and BCN18-C-6 using the balanced-density slurry technique. The mobile phases used were methanol and acetate buffer solution containing Cu(II). Chromatography was performed at a flow-rate of 1.0 ml min^{-1}, aiding Cu(II) detection. The organic compounds used as the solutes were amino acids and disubstituted benzenes, namely nitrophenol, phenylenediphenol, phenylenediamine and aminophenol.

3. Results and discussion

3.1. Preparation of bonded stationary phases

Successive reactions on the silica surface were applied in order to prepare bonded phases with nitrogen-containing crown ether. In this way the tedious operation for the separation and purification of crown ether monomers was eliminated. The amount of bonded organic groups in the bonded product can be regulated in the range 500–1500 μm g^{-1}, which converts to a surface concentration of about 1.6–4.7 μm m^{-2}, by changing the reaction conditions. In each reaction the influence of the amount of reagent, the solvent used and the time and temperature of the

Table 1
Variation of α values of GBS with the time and temperature of the bonding reaction

Test No.	Temperature (°C)	Time (h)	Surface concentration ($\mu m\ m^{-2}$)
1	30	8.5	2.5
2	80	8.5	3.7
3	110	8.5	4.2
4	110	17.1	4.3
5	110	33.0	4.3

reaction on the surface concentration of bonded groups was investigated.

Table 1 shows the effect of time and temperature of the reaction on the α values of GBS, which were obtained by the determination of bonded α-epoxy groups. For the synthesis of HAS, the conversion efficiency of cleaving the epoxy group and the surface concentration α were higher using DMF than dioxane as solvent. For the synthesis of BCN18-C-6, the effect of the amount of NaH and oligoethylene glycol ditosylates on the conversion efficiency of closing the ring and the α value, which were estimated by FTIR spectrometry and elemental analyses, is highly important.

3.2. Characterization of the bonded stationary phases

The objective of sequental derivatization of the silica surface is to obtain bonded surface groups with the expected structure according to the reaction scheme shown. Information on the bonded molecular structure on the silica surface can be obtained by various techniques. Elemental analyses can be used to measure the C/H ratio for comparison with the expected ratio. Table 2 gives typical carbon, hydrogen and nitrogen contents and the surface concentration of the bonded groups. The C/H ratios determined are identical with the calculated ratios.

For GBS the α value obtained by the determination of epoxy groups is lower than that given by the carbon content. This is due to traces of water inducing opening of the ring of the epoxy group during the bonding reaction and subsequent treatment. For GBS, HAS and BCN18-C-6 packing with a carbon content of about 10–20%, α values of 3.7, 2.7 and 2.3 $\mu m\ m^{-2}$, respectively, can be calculated and correspond to about a 70% conversion rate for the bonding reaction assuming a stoichiometric reaction on the silica surface.

Thermal methods, such as TGA and DTA, have been widely applied to the study and characterization of inorganic and organic materials. Figs. 2 and 3 show the thermogram and differential thermogram, respectively, of the bonded material. The weight change and endothermic peak below 100°C result from the loss of physically adsorbed water. The temperatures of thermal decomposition for GBS, HAS and BCN18-C-6 are at 238, 296 and 326°C, respectively. Figs. 2 and 3 indicate that the bonded products obtained in each reaction step possess different structures and weight changes as a function of temperature. The α values obtained from the loss of weight at the decomposition temperature, given in Table 2, are the same as those obtained from the carbon contents.

Mass spectral data on the bonded phases are given

Table 2
Elemental and group analyses of the bonded material

Sample	Element (%)			Epoxy content ($\mu m\ m^{-2}$)	C/H ratio		Surface concentration ($\mu m\ m^{-2}$)		
	C	H	N		Calc.	Determined	A [a]	B [a]	C [a]
GBS	10.04	1.76		3.1	0.54	0.48	3.7	3.6	
HAS	9.43	1.79	1.06		0.44	0.44	2.7	2.5	2.3
BCN18-C-6	12.38	2.10	1.03		0.50	0.49	2.3	2.0	1.9
	(11.89	2.00	0.91) [b]						
BCN18-C-6 (capped)	12.71	2.26	0.96						
	(12.02	2.10	0.91) [b]						

[a] Surface concentration of bonded groups. Calculated according to (A) carbon content, (B) TG and DTA curves and (C) nitrogen content.
[b] Values in parentheses were determined for the bonded material 3 months of use in HPLC.

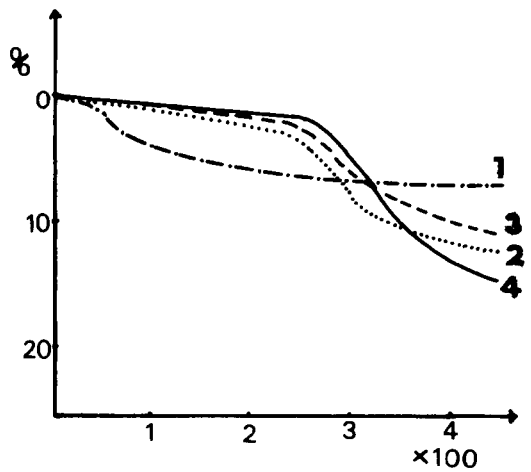

Fig. 2. Thermogram for decomposition of the bonded material. 1 = SiO_2; 2 = GBS; 3 = HAS; 4 = BCN18-C-6.

in Table 3. Most of fragment ions formed can be explained by fragmentation rules for ether, polyfunctional alcohol and crown ether groups [13]. For GBS and HAS, fragment ions at m/z 115 and 176, respectively, are obtained by cleaving the Si–C bond. The fragmentation of the bonded crown ether in BCN18-C-6 can be approximately illustrated by Fig. 4. The base peak ion $[C_4H_7N]^+$ (m/z 69) can be formed by loss of CH_2 and H from the fragment ion at m/z 84. The fragment ion at m/z 276 formed by cleaving the Si–C bond is important evidence for the

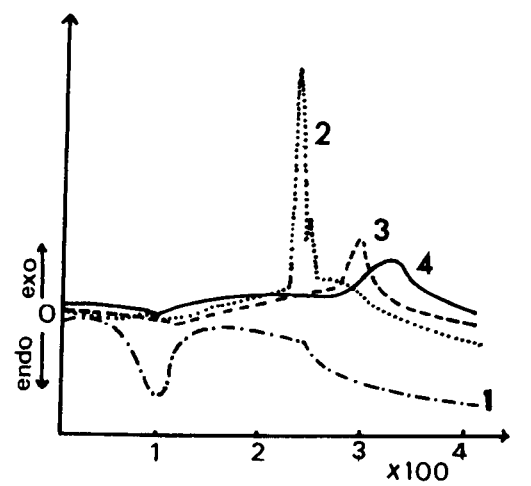

Fig. 3. Differential thermogram of the bonded material. Curves 1–4 as in Fig. 1.

Table 3
Mass spectra of the bonded material

Sample	m/z (relative intensity, %)
GBS	236(11), 185(24), 149(58), 129(56), 115(31), 87(38), 73(100), 71(77), 57(71), 43(41)
HAS	176(23), 155(24), 129(30), 91(64), 87(25), 86(100), 84(42), 58(73), 56(38), 55(33), 44(38)
BCN18-C-6	276(13), 188(26), 129(13), 128(14), 127(14), 117(14), 115(32), 114(13), 101(11), 100(28), 85(73), 84(37), 83(67), 71(64), 70(28), 69(100), 60(24), 58(13), 57(71), 56(32), 44(26)

Operating conditions: source, electron impact; temperature of source, 200°C; temperature of sample probe, 30–320°C; filament electric current, at 300 μA; mass range of scan, 10–600 u; scanning rate, 0.75 s per decade.

presence of a crown ether structure in the BCN18-C-6 bonded phase.

FT-IR spectra, after subtraction of the blank silica spectrum, are shown in Fig. 5. The spectra of the bonded product GBS in the first step of the bonding reaction shows the disappearance of a strong absorption band around 3600–3700 cm^{-1}, which is characteristic of the Si–OH stretching frequency for bare silica. All of the bonded materials display a readily identifiable peak around 2900 cm^{-1} due to C–H aliphatic CH_2 stretching. The spectra of GBS offer evidence that the epoxy group was attached to silica because of the characteristic epoxy peaks at 810, 918 and 1250 cm^{-1} and the C–O stretch around 1100 cm^{-1}. Strong absorption in the spectra of HAS is shown by three peaks around 3500, 1600 and 1100 cm^{-1}, which were identified as follows: 3500 cm^{-1} as O–H and C–N stretches, 1100 cm^{-1} as C–O and

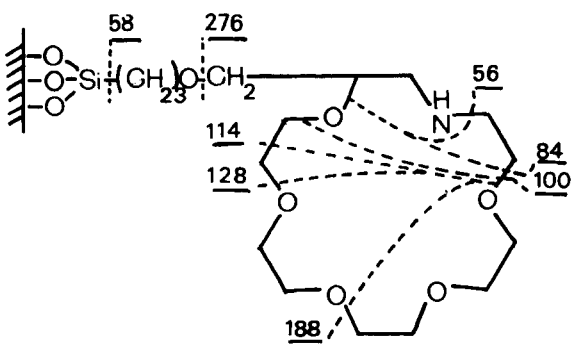

Fig. 4. Interpretation of mass spectral fragmentation process of BCN18-C-6 bonded phase.

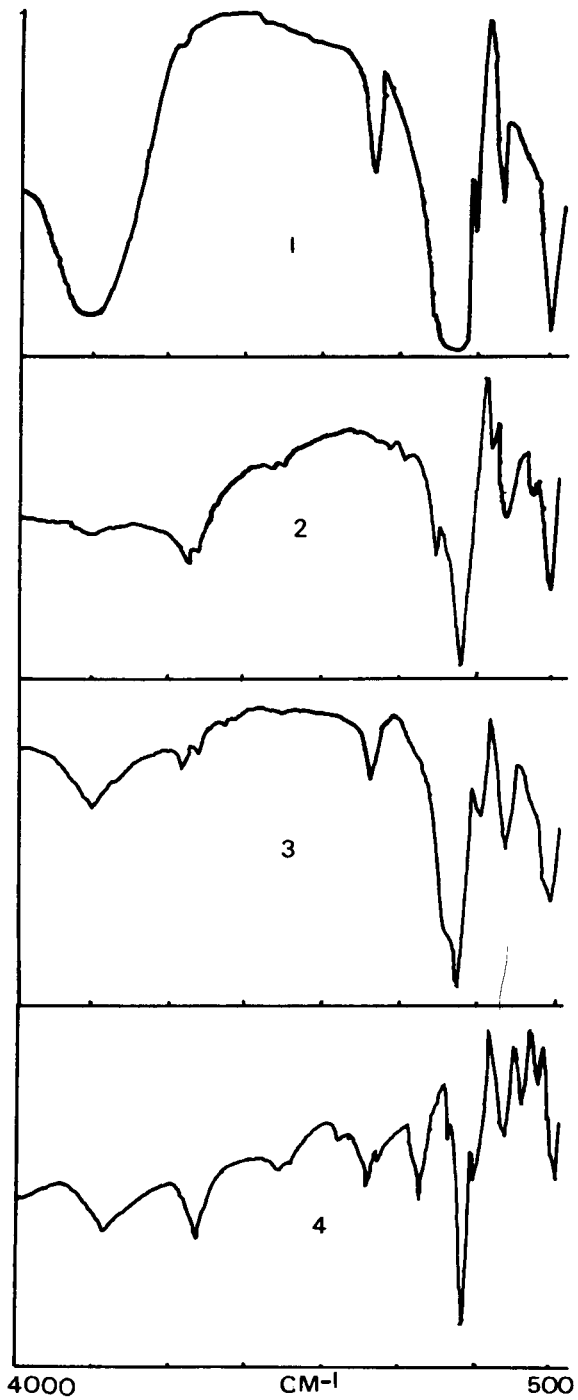

Fig. 5. FT-IR spectra of the silica and the bonded material. 1 = Bare silica; 2 = GBS; 3 = HAS; 4 = BCN18-C-6. For 2–4, the bare silica was used as a blank.

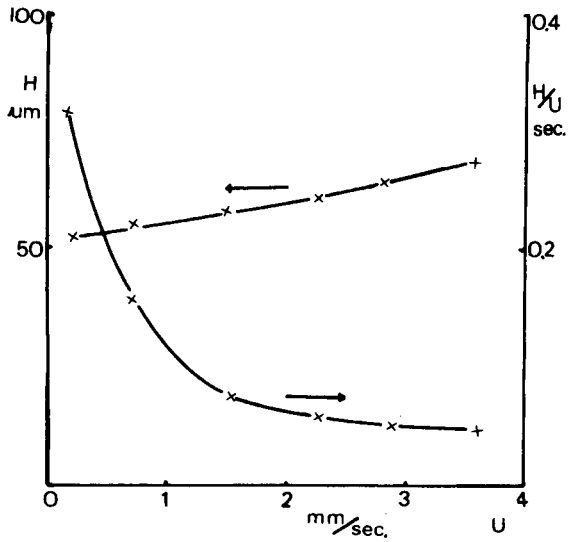

Fig. 6. Dependence of H and H/U on the velocity (U) of the mobile phase. Mobile phase, methanol–buffer solution at pH 5 (80 + 20, v/v); solute, *p*-nitrophenol.

C–N stretches and 1600 cm^{-1} as NH aliphatic RNH bending.

For BCN18-C-6 characteristic absorption is seen of ether and $-CH_2-O-$ groups around 2900 and 1100 cm^{-1}. The strength and broadness of the absorption peaks of BCN18-C-6 around 1100 cm^{-1} obviously differs from those for GBS and HAS. Most prominent are the successive absorption peaks in the fingerprint region of 1300–500 cm^{-1}, which are characteristic frequencies of macrocyclic polyethers [14].

3.3. Chromatographic characterization of the bonded phases

The column efficiency of the BCN18-C-6 bonded phase was determined with methanol or methanol–buffer solution as mobile phases. The theoretical plate heights (H) were 78, 65 and 68 μm using biphenyl, *p*-nitrophenol and phenylalanine as solutes, respectively. Typical plots of H and H/U versus the mobile phase velocity (U) for the BCN18-C-6 column are shown in Fig. 6. Only a slight increase in H with increasing velocity of the mobile phase was observed. The results indicate that the mass transfer term for the chromatographic column is small and suitable for high-speed separations.

Table 4
Effect of methanol content in eluent on the retention of disubstituted benzenes (capacity factors, k')

Solute	Methanol content (%, v/v)											
	100		80		60		40		20		0	
	HAS	BCN	HAS	BCN	HAS	BCN	HAS	BCN	HAS	BCN	HAS	BCN
o-Aminophenol	0.10	0.32	0.14	0.36	0.16	0.45	0.22	0.55	0.30	0.80	0.42	1.02
m-Aminophenol	0.10	0.40	0.14	0.44	0.17	0.48	0.23	0.61	0.35	0.88	0.46	1.24
p-Aminophenol	0.08	0.40	0.09	0.42	0.11	0.45	0.16	0.50	0.22	0.76	0.28	1.11
o-Phenylenediphenol	0.10	0.30	0.13	0.57	0.16	0.74	0.25	1.02	0.38	1.78	0.60	2.55
m-Phenylenediphenol	0.10	0.32	0.13	0.54	0.15	0.70	0.25	0.98	0.45	1.65	0.53	2.24
p-Phenylenediphenol	0.10	0.34	0.14	0.61	0.16	0.77	0.30	1.12	0.48	1.88	0.72	2.95
o-Phenylenediamine			0.08	0.25	0.14	0.40			0.28	0.47	0.64	0.81
m-Phenylenediamine			0.08	0.12	0.14	0.30			0.20	0.44	0.58	0.62
p-Phenylenediamine			0.08	0.12	0.14	0.26			0.20	0.42	0.52	0.56
o-Nitrophenol	0.12	0.41	0.18	0.45	0.20	0.75	0.26	1.29	0.48	1.80	0.56	2.95
m-Nitrophenol	0.14	0.53	0.20	0.68	0.22	1.13	0.36	1.81	0.70	2.61	0.84	4.33
p-Nitrophenol	0.14	0.58	0.25	0.81	0.30	1.58	0.40	2.52	0.78	3.94	1.19	6.25

Mobile phase: methanol–acetate buffer solution containing 2 mmol Cu(II).

In order to carry out the separation by ligand-exchange chromatography and Cu(II)-aided detection [15], the complexing capacities of the bonded phases with Cu(II) were determined. The complexing capacities of HAS and BCN18-C-6 with Cu(II) in water are 28 and 49 mmol mol^{-1}, respectively, and those in acetate buffer are 18 and 32 mmol mol^{-1}, respectively. Owing to the competing coordination of acetic acid to Cu(II), the complexing capacities in acetate buffer are lower than those in water. Under the same conditions the complexing capacity of BCN18-C-6 is higher than that of HAS, showing that the bonded phase containing a crown ether possesses a higher complexing ability to copper ion.

The retention data of some disubstituted benzenes on HAS and BCN18-C-6 columns using methanol–acetate buffer solution containing Cu(II) as the mobile phase are given in Table 4. The retention of the solutes increases slightly with decrease in methanol content of the mobile phase, which indicates a weak hydrophobicity of the bonded phases. The retentions of the amino acids are shown in Table 5. Fig. 7 illustrates the dependence of the retention of disubstituted benzenes on Cu(II) concentration using the BCN18C-6 bonded phase. A considerable retention enhancement for the acidic nitrophenol on addition of a certain concentration of Cu(II) to the mobile phase at pH 5 was observed. From Tables 4 and 5, it can be seen that the retentions of the polar disubstituted benzenes and amino acids on BCN18-C-6 are greater than those on the HAS bonded phase using the same mobile phase.

The retention enhancement may be explained by Cu(II) in the mobile phase being complexed strongly by the crown ether moiety on the bonded phase, which is thus positively charged. Therefore, an electrostatic attractive force between the positive charge and the polar group of solutes is generated, which in turn enhances the retention of polar compounds. Because of electrostatic interaction, the retention of acidic nitrophenol is higher than that of basic phenylenediamine. For disubstituted benzenes the or-

Table 5
Retention of amino acids on the bonded phases

Bonded phase	Solute											
	Lys	Arg	His	Gly	Ser	Ala	Val	Ileu	Leu	Tyr	Phe	Asp
HAS	0.32	0.45	0.63	1.09	1.85	2.12	2.07	2.91	3.36	4.15	4.92	5.88
BCN	0.54	0.97	2.06	3.03	3.63	4.30	5.23	6.62	7.60	13.60	11.40	17.68

Mobile phase: acetate buffer solution containing copper [Cu(II) 1 mM, acetic acid 5 mM, pH 5.50]. Detection: UV at 254 nm.

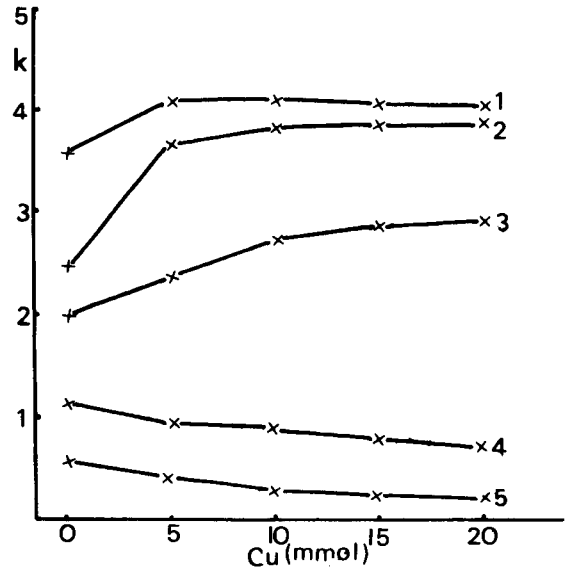

Fig. 7. Dependence of retention of disubstituted benzenes and amino acids on Cu(II) concentration in the chromatographic system using of BCN18-C-6. Mobile phase: methanol–buffer solution at pH 5 (50+50, v/v). Solutes: 1 = Ser; 2 = *p*-nitrophenol; 3 = *o*-nitrophenol; 4 = Arg; 5 = *p*-phenylenediamine.

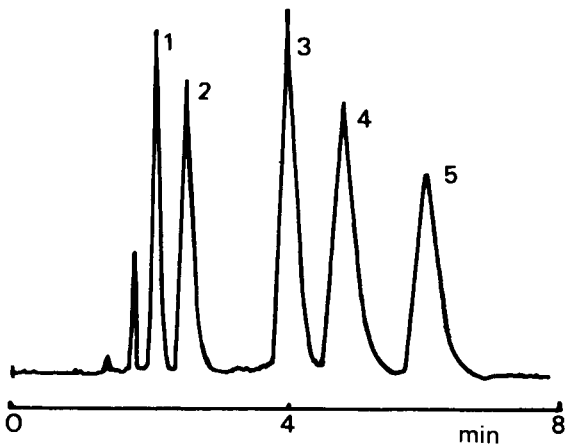

Fig. 8. Chromatographic separation of disubstituted benzenes on BCN16-C-6. Mobile phase: methanol–acetate buffer solution at pH 5 (65+35, v/v). Solutes: 1 = *p*-phenylenediamine; 2 = *m*-phenylenediphenol; 3 = *o*-nitrophenol; 4 = *m*-nitrophenol; 5 = *p*-nitrophenol.

der of retention is roughly nitrophenol > phenylenediphenol > aminophenol > phenylenediamine, which is similar to the order of decrease in acidity. For amino acids the retention of acidic amino with two carboxy groups, such as aspartic acid, is much greater than that of basic amino acids with two amino groups, such as lysine and arginine. With the mobile phase at pH 5, the amino group of organic compounds is easily protonated, thus becoming positively charged. The electrostatic repulsive force between the positive charges of the cationic solutes and the crown ether-complexed cation on the bonded

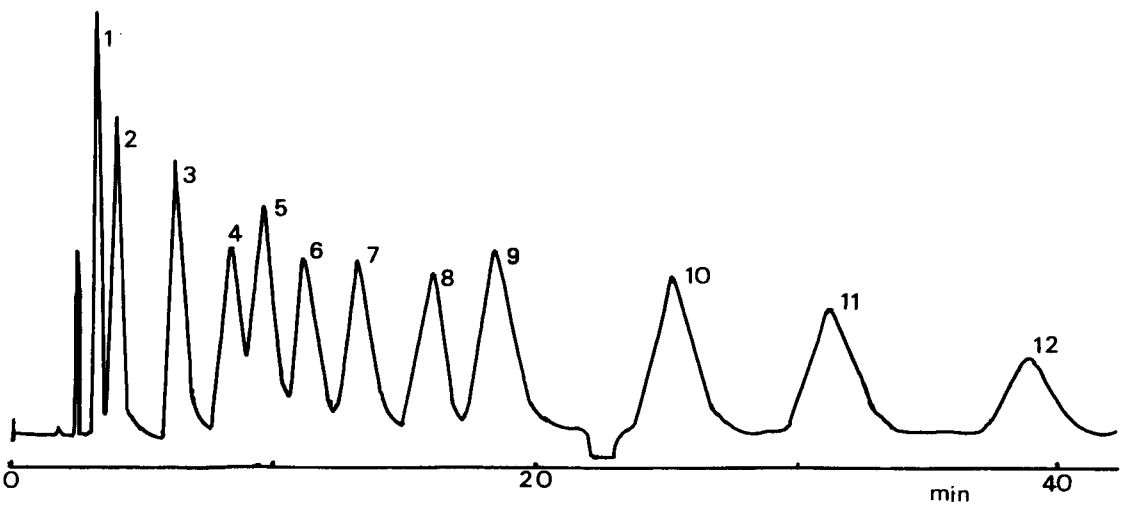

Fig. 9. Chromatographic separation of amino acids on BCN18-C-6. Mobile phase: methanol–acetate buffer solution at pH 5.5 containing 1 mM Cu(II) (5:95, v/v). Detection: UV at 254 nm. Solutes: 1 = Lys; 2 = Arg; 3 = His; 4 = Gly; 5 = Ser; 6 = Ala; 7 = Val; 8 = Ile; 9 = Leu; 10 = Phe; 11 = Tyr; 12 = Asp.

phase decreases their retention. The decreased retention of basic phenylenediamine on addition of Cu(II) is illustrated in Fig. 7. This shows that the crown-complexing cation affects the chromatographic retention considerably.

Based on the results described above and the fact that the elution order of amino acids on BCN18-C-6 differ from their elution from a reversed-phase ODS column [15], it is suggested that the retention of the polar solutes on BCN18-C-6 is derived from electrostatic interaction and ligand exchange with Cu(II) as the central ion and acetic acid group as the elution ion. The effect of hydrophobic interaction on the retention of the polar solutes is of less importance.

The isomers of nitrophenol and amino acids were separated successfully by reversed-phase HPLC on the BCN18-C-6 bonded phase. Figs. 8 and 9 show typical chromatograms of the disubstituted benzene and amino acids.

4. Conclusions

A nitrogen-containing crown ether bonded phase was prepared by successive reactions on the surface of porous silica gel. Information of the bonded molecular structure was obtained by chemical and instrumental analyses. The formation of a crown ether on the bonded phase was demonstrated by mass data and the cation-complexing ability of the bonded material. Acidic organic compounds in the chromatographic system with the bonded phase with Cu(II) in the mobile phase exhibit greater retentions than basic compounds, owing to an electrostatic attractive force between the positive charge and polar groups, such as carboxy and phenolic hydroxy groups. The isomers of nitrophenol and twelve amino acids were separated successfully by reversed-phase HPLC on the bonded phase.

Acknowledgment

The authors thank the National Natural Science Foundation Committee of China for their financial support of this project.

References

[1] K. Kimura and T. Shono, J. Liq. Chromatogr., 5, Suppl. 2 (1982) 223.
[2] T. Shinbo, T. Yamaguchi, K. Nishmura, M. Sugur and J. Chromatogr., 405 (1987) 145.
[3] P.R. Brown, Anal. Chem., 62 (1990) 995A.
[4] K. Kimura, T. Shono and E. Hayata, J. Chem. Soc., Chem. Commun., (1984) 271.
[5] T. Nakaguwar, A. Shibukawa, A. Kaihara and H. Tanka, J. Chromatogr., 353 (1986) 399.
[6] A. Shibukawa, T. Nakaguwa, A. Kaihara, K. Yagi and H. Tanaka, Anal. Chem., 59 (1987) 2496.
[7] M.K. Nakajima, K. Kimura and T. Shono, Bull. Chem. Soc. Jpn., 56 (1983) 3052.
[8] M. Lauth and P. Gramain, J. Chromatogr., 395 (1987) 153.
[9] J.S. Bradshaw and R.L. Bruening, J. Chem. Soc., Chem. Commun., (1988) 812.
[10] R.M. Izatt, R.L. Bruening and J.S. Bradshaw, Anal. Chem., 60 (1988) 1825.
[11] H. Engehardt, J. Liq. Chromatogr., 10 (1987) 1999.
[12] S.L. Da, G.L. He and Z.G. Wang, Chin. J. Chromatogr., 11 (1993) 232.
[13] D. Yan, T.H. Wang, G.H. Wan and C.T. Wu, Chin. Org. Chem. (Youji Huaxue), 1 (T.55) (1986) 47.
[14] K. Nakanshi and P.H. Solomon, Infrared Absorption Spectroscopy, Holden-Day, San Francisco, 1977, pp. 25–44.
[15] S. Levin and E. Grushka, Anal. Chem., 53 (1985) 1830.

ELSEVIER

Analytica Chimica Acta 299 (1994) 249–256

ANALYTICA CHIMICA ACTA

A new approach for the simultaneous determination of inorganic cations and anions using ion chromatography

Wenzhi Hu [a,*], Hiroaki Tao [a], Mamoru Tominaga [a], Akira Miyazaki [a], Hiroki Haraguchi [b]

[a] *National Institute for Resources and Environment, 16-3 Onogawa, Tsukuba-shi, Ibaraki 305, Japan*

[b] *Department of Applied Chemistry, School of Engineering, Nagoya University, Furo-cho, Chikusa-ku, Nagoya 464-01, Japan*

Received 21 December 1993; revised manuscript received 20 July 1994

Abstract

A new approach for the simultaneous determination of inorganic cations and anions using ion chromatography was proposed. In this study, a zwitterionic stationary phase was employed with water as the eluent. With the ion separation achieved under these conditions, each anion species of the analytes could be separated from the others and eluted together with the analyte cations. The combination of the analyte anions with the analyte cations can be considered as an "ion-pairing-like" form and is briefly denoted as "ion pair". If we determine all the ion pairs, the concentrations of the anions and the cations in the original solution can be calculated. This new approach for the simultaneous determination of inorganic cations and anions was investigated in this study.

Keywords: Ion chromatography; Ion exchange; Simultaneous determination; Waters; Zwitter ions

1. Introduction

Inorganic cations and the counter-ions (anions) must simultaneously be present because of electroneutrality. In the procedure of separation (including the simultaneous cation and anion separations [1–8]) achieved by conventional ion chromatography (IC) [9], the analyte cations could be separated from the analyte anions, and independently eluted from the column. This was because the new counter-ions for the analyte ions could be provided by the mobile phase. If the ion separation could be achieved with a non-ionic mobile phase, in other words, if the mobile phase does not have the ability to provide the counter-ions, the analyte cations and the analyte anions must be eluted together to maintain electroneutrality.

In 1977, Blasius et al. [10] published a paper dealing with a unique separation method. They initially introduced crown ethers as a stationary phase in a liquid chromatographic system, and demonstrated that the inorganic ions could be separated with water and/or methanol as the mobile phase. In this case, the analyte cations and anions were always eluted together. Methanol is a non-ionic eluent, and water is a very weak ionic eluent ($[H^+] = [OH^-] = 1 \times 10^{-7}$), and as a result, cannot provide the counter-ions for the analyte ions. Since the analyte ions eluted as combinations of cations with anions, their concentrations may be evaluated by the determination of the prevailing cation–anion combinations. Later Igawa et al. [11] introduced

* Corresponding author.

SSDI 0003-2670(94)00347-5

crown-ether-coated stationary phases into liquid chromatography (LC), and tried to determine both ions with water as the eluent, but they failed, because the separation efficiency obtained under these conditions was not good enough. Currently, LC using crown-ether-coated stationary phases with water as the eluent is commonly used for the separation of anions and/or cations. A review prepared by Lamb and Smith [12] deals with the details of its applications.

It was demonstrated recently by the present authors that when a strong positively–negatively charged zwitterionic stationary phase was used in LC, ion separations could also be achieved with water as the eluent [13]. Moreover, various cation–anion combinations could be base-line separated by this method. Since the separation efficiency of the zwitterionic stationary phase is superior to the one with crown ethers we decided to use LC with the zwitterionic stationary phase and try to determine both ions, by the determination of the cation–anion combinations.

2. Experimental

2.1. Apparatus

The liquid chromatography system used in this study was a conventional LC system, obtained from Shimadzu (Kyoto, Japan). It consisted of a pump (LC-7A), an auto-injector (SIL-6A, sample injection volumes, 20 μl), a system controller (SCL-6A), a conductivity detector (CDD-6A), and a photodiode array UV–visible detector (SPD-M6A). The ODS columns (L-Column, 4.6×250 mm) used as the support columns to form the zwitterionic stationary phases, were obtained from the Chemical Inspection and Testing Institute (Tokyo, Japan). The procedure for the preparation of the zwitterionic stationary phases was the same as described previously [13]. An inductively coupled plasma atomic emission spectrometer (ICP-AES), (Model 075 Plasma Atomcomp MKII, Thermo Jarrell-Ash, Franklin, MA) was also used as an on-line detector for the identification of cations.

2.2. Reagents

Inorganic salts used as the standard analytes were obtained from Wako (Osaka). The zwitterionic surfactant reagents used to form the stationary phases {3-[(3-cholamidopropyl)dimethylammonio]-1-propanesulphonate (CHAPS), 3-[(3-cholamidopropyl)dimethylammonio]-2-hydroxy-1-propanesulphonate (CHAPSO), and Zwittergent-3-14} were obtained from Dojin (Kumamoto, Japan). All reagents were of analytical-reagent grade and were used as received. The pure water used as the mobile phase and used to dissolve the reagents was prepared in the laboratory using a Milli-Q system (Nihon Millipore Kogyo, Tokyo).

3. Results and discussion

3.1. Behaviour of ion combinations

An aqueous solution containing 16 mM Na^+ and 4 mM each of Cl^-, Br^-, I^- and SCN^- was separated by IC using the CHAPS micelle-coated stationary phase with water as the eluent. The combinations of cations with anions, i.e., Na^+–Cl^-, Na^+–Br^-, Na^+–I^-, and Na^+–SCN^-, were observed. The four ion pairs were base-line separated. Another mixed aqueous solution containing 16 mM Ca^{2+} and 8 mM each of Cl^-, Br^-, I^-, and SCN^- was also prepared and separated under the same conditions. Four ion pairs, Ca^{2+}–$2Cl^-$, Ca^{2+}–$2Br^-$, Ca^{2+}–$2I^-$, and Ca^{2+}–$2SCN^-$, were also observed and base-line separated. The cations and anions in the ion pairs were identified by using the ICP-AES and the photodiode array UV–visible detectors, respectively. We then mixed the two solutions together, and then separated this mixed solution under the same conditions. Accordingly, eight ion pairs, Na^+–Cl^-, Na^+–Br^-, Na^+–I^-, and Na^+–SCN^- and Ca^{2+}–$2Cl^-$, Ca^{2+}–$2Br^-$, Ca^{2+}–$2I^-$, and Ca^{2+}–$2SCN^-$, were expected. The actual results (chromatogram shown in Fig. 1), however, show that only six ion pairs were observed. The possible ion pairs Ca^{2+}–$2Cl^-$ and Na^+–SCN^- were not observed.

To explain the behaviour of the ion combinations for the formation of ion pairs, the *molal energies* ΔG of the hydrated ions were considered. We suppose an aqueous solution containing only two cation species, A and C, and only two anion species, B and D (the simplest case). When separating this aqueous solution, four ion pairs, i.e., A–B, A–D, C–B, and C–D are expected. We further suppose that no chemical inter-

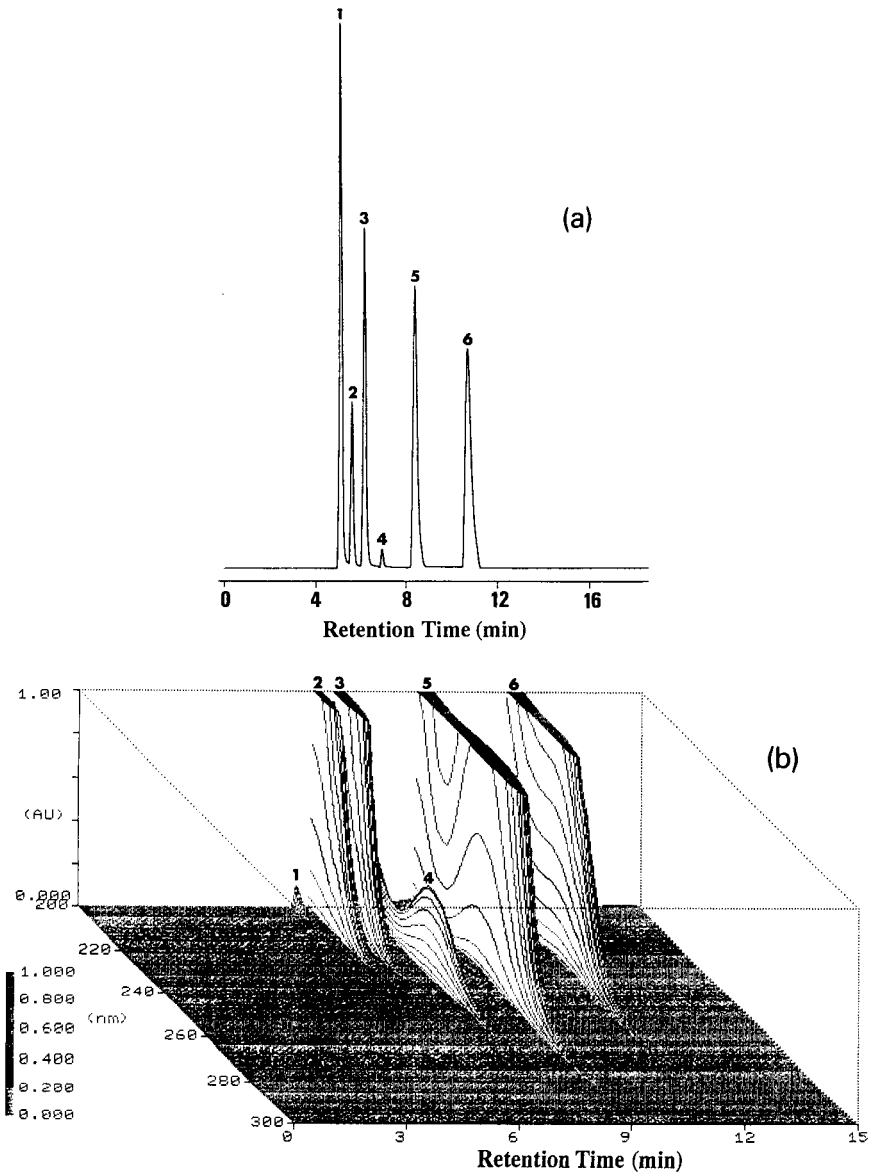

Fig. 1. Chromatogram of a mixed aqueous solution containing Na^+, Ca^{2+}, Cl^-, Br^-, I^-, and SCN^-. Column: ODS column (4.6×250 mm) coated with CHAPS micelles; mobile phase: pure water; flow-rate: 0.5 ml/min; detectors: (a) conductivity and (b) photodiode array UV–visible. (1) Na^+–Cl^-; (2) Na^+–Br^-; (3) Ca^{2+}–$2Br^-$; (4) Na^+–I^-; (5) Ca^{2+}–$2I^-$; and (6) Ca^{2+}–$2SCN^-$.

actions happened among these ions (no energy loss), and the order of molal energies for the cations is $\Delta G_A > \Delta G_C$, and for the anions is $\Delta G_B > \Delta G_D$. The redistribution of the analyte ions in the formation of the ion pairs A–B, A–D, C–B, and C–D, therefore, is a kind of energy redistribution. The combination of A–B ($\Delta G_{\text{max-cation}}$ with $\Delta G_{\text{max-anion}}$) is the least-stable ion pair, the combinations of A–D ($\Delta G_{\text{max-cation}}$ with $\Delta G_{\text{min-anion}}$) and C–B ($\Delta G_{\text{min-cation}}$ with $\Delta G_{\text{max-anion}}$) are the medium-stable ion pairs, and the combination of C–D ($\Delta G_{\text{min-cation}}$ with $\Delta G_{\text{min-anion}}$) is the most-stable ion pair. If the most-stable ion pair C–D was produced to the greatest extent, the least-stable ion pair A–B must simultaneously preferably be produced. This is clearly less probable. To avoid production of A–B (the least-stable ion pair), the ions A, B, C, and D must

produce the medium-stable ion pairs (A–D and C–B), as much as possible.

The results in Fig. 1 show that the most-stable ion pair Ca^{2+}–$2Cl^-$ and the least-stable ion pair Na^+–SCN^- were not observed. This was because no Ca^{2+}, Na^+, Cl^-, and SCN^- did remain (according to Born's equation, the molal energy orders for the cations are $\Delta G_{Na+} > \Delta G_{Ca^{2+}}$, and for the anions are $\Delta G_{SCN-} > \Delta G_{I-} > \Delta G_{Br-} > \Delta G_{Cl-}$). The values of Na^+–Cl^-, Na^+–Br^-, Na^+–I^-, Ca^{2+}–$2Br^-$, Ca^{2+}–$2I^-$, and Ca^{2+}–$2SCN^-$ were found to be 6.0, 1.92, 0.08, 2.04, 2.96, and 3 mM, respectively, from the calibration graphs of the standard solutions (concentration ranges from 0.01 to 10 mM) of NaCl, NaBr, NaI, $CaBr_2$, CaI_2, and $Ca(SCN)_2$, respectively.

3.2. *The efficiencies of the stationary phases*

In an attempt to separate more ion pairs, an aqueous solution containing Na_2SO_4, NaCl, $NaNO_2$, NaBr, $NaNO_3$, NaI, and NaSCN was also prepared and separated under the same conditions as in Fig. 1. The ion pair Na^+–NO_2^- was not base-line separated from Na^+–NO_3^-. Na^+–Br^- and Na^+–NO_3^- were eluted at the same time. The separation efficiency of IC is determined by the stationary phase and the mobile phase. In this study, we decided to change the stationary phase in order to improve the separation efficiency. It was demonstrated in our previous study [13] that the ion separations could also be achieved with water as the eluent, when using a microcolumn coated with Zwittergent-3-14 micelles. In this study, we also prepared a conventional column coated with Zwittergent-3-14 micelles, and tried to separate more ion pairs. Fig. 2 shows a chromatogram of a mixed aqueous solution containing Na_2SO_4, NaCl, $NaNO_2$, NaBr, $NaNO_3$, NaI, and NaSCN, obtained using the conventional ODS column coated with Zwittergent-3-14 micelles. The ion pairs Na^+–NO_2^-, Na^+–Br^-, and Na^+–NO_3^- were base-line separated when using this column. However, $2Na^+$–SO_4^{2-} was not base-line separated from Na^+–Cl^-. Na^+–I^- eluted with a long retention time, and the ion pair Na^+–SCN^- was not eluted at all from the column.

Zwittergent-3-14 and CHAPS are two different types of surfactants. Zwittergent-3-14 is a linear surfactant with a long alkyl chain, while CHAPS is a steroidal one. Previous study [13] demonstrated that the

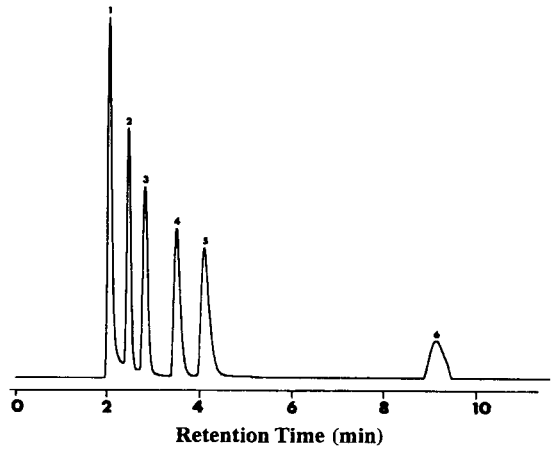

Fig. 2. Chromatogram of a mixed aqueous solution containing Na_2SO_4, NaCl, $NaNO_2$, NaBr, $NaNO_3$, NaI, and NaSCN obtained using Zwittergent-3-14 micelle-coated stationary phase. Column: ODS column (4.6×250 mm) coated with Zwittergent-3-14 micelles; mobile phase: pure water; flow-rate: 1.0 ml/min; detector: conductivity. (1) $2Na^+$–SO_4^{2-}; (2) Na^+–Cl^-; (3) Na^+–NO_2^-; (4) Na^+–Br^-; (5) Na^+–NO_3^-; (6) Na^+–I^-. Na^+–SCN^- was not eluted from the column.

CHAPS micelle-coated stationary phase does not show reversed-phase activity. This is due to the fact that the ion-separation sides are present at the inside of the CHAPS micelles, and the inside of the micelle is the hydrophilic phase. As a result, the ion pairs M–I^- and M–SCN^- (M denoting the cations) could be rapidly eluted from the column. On the contrary, the ion-separation sides (positive and negative charge) are present at the top of the long alkyl chain. In other words, the Zwittergent-3-14 micelle-coated stationary phase also show reversed-phase activity, and strong affinity of the M–I^- and M–SCN^- ion pairs can be expected.

The above experimental results indicate that the CHAPS micelle-coated stationary phase is effective for the rapid base-line separation of M–SO_4^{2-}, M–Cl^-, M–I^-, and M–SCN^- ion pairs, while the Zwittergent-3-14 micelle-coated stationary phase is suitable for the base-line separation of M–NO_2^-, M–Br^-, and M–NO_3^-. If we mix the CHAPS and the Zwittergent-3-14 together, to form a CHAPS–Zwittergent-3-14 mixed micelle-coated stationary phase, the advantages of each can be combined on one stationary phase. A mixed aqueous solution containing 20 mM CHAPS and 20 mM Zwittergent-3-14 was passed through a conventional ODS column (L-column, 4.6×250 mm) for at least 50 min at a flow-rate of 1.0 ml/min. This was

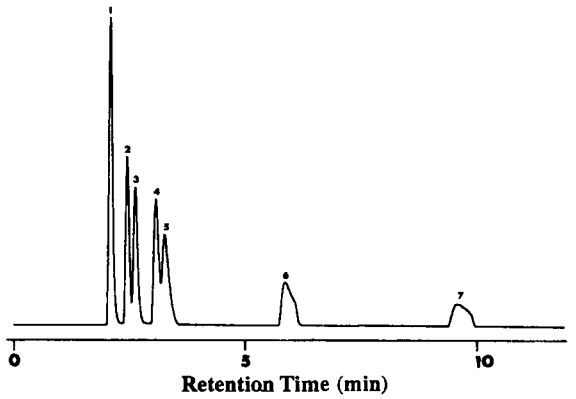

Fig. 3. Chromatogram of a mixed aqueous solution containing Na_2SO_4, NaCl, $NaNO_2$, NaBr, $NaNO_3$, NaI, and NaSCN, obtained using the CHAPS–Zwittergent-3-14 mixed micelle-coated stationary phase. Column: ODS column (4.6 × 250 mm) coated with CHAPS–Zwittergent-3-14 mixed micelles; mobile phase: pure water; flow-rate: 1.0 ml/min; detector: conductivity. (1) $2Na^+$–SO_4^{2-}; (2) Na^+–Cl^-; (3) Na^+–NO_2^-; (4) Na^+–Br^-; (5) Na^+–NO_3^-; (6) Na^+–I^-; (7) Na^+–SCN^-.

followed by a pure water rinse for at least 40 min at the same flow-rate. The column was then conditioned with the water eluent for the separations. Fig. 3 shows a chromatogram of an aqueous solution containing 1 mM each of Na_2SO_4, NaCl, $NaNO_2$, NaBr, $NaNO_3$, NaI, and NaSCN, obtained using the CHAPS–Zwittergent-3-14 mixed micelle-coated stationary phase. The efficiency for the separation of Na^+–NO_2^-, Na^+–Br^- and Na^+–NO_3^- was improved, compared with using the CHAPS micelle-coated stationary phase, while it was reduced compared with using the Zwittergent-3-14 micelle-coated stationary phase. On the contrary, the efficiency for the separation of $2Na^+$–SO_4^{2-} and Na^+–Cl^- ion pairs was improved, compared with using the Zwittergent-3-14 micelle-coated stationary phase. Na^+–SCN^- could also be eluted from the column although the peak was not sharp. A mixed aqueous solution containing more cation-species and anion-species was also prepared and separated using the CHAPS–Zwittergent-3-14 mixed micelle-coated stationary phase. Seven ion pairs ($2Na^+$–SO_4^{2-}, Na^+–Cl^-, Ca^{2+}–$2Cl^-$, Na^+–Br^-, Ca^{2+}–$2Br^-$, Ca^{2+}–$2I^-$, and Ca^{2+}–$2SCN^-$) were base-line separated (chromatogram shown in Fig. 4).

We also tried to use the CHAPS–Zwittergent-3-14 mixed micelle-coated stationary phase for the separation of ion pairs having the same anion-species as well as the same cation charge. It was found in our previous experiments that this type of ion pairs are always eluted with the same retention time (i.e., could not be separated) when using the CHAPS and the Zwittergent-3-14 micelle-coated stationary phases. Fig. 5 shows a chromatogram of an aqueous solution containing 1 mM each of $Mg(NO_3)_2$ and $Ca(NO_3)_2$, obtained using the CHAPS–Zwittergent-3-14 mixed micelle-coated stationary phase. Mg^{2+}–$2NO_3^-$ could also be separated from Ca^{2+}–$2NO_3^-$. The two components were only

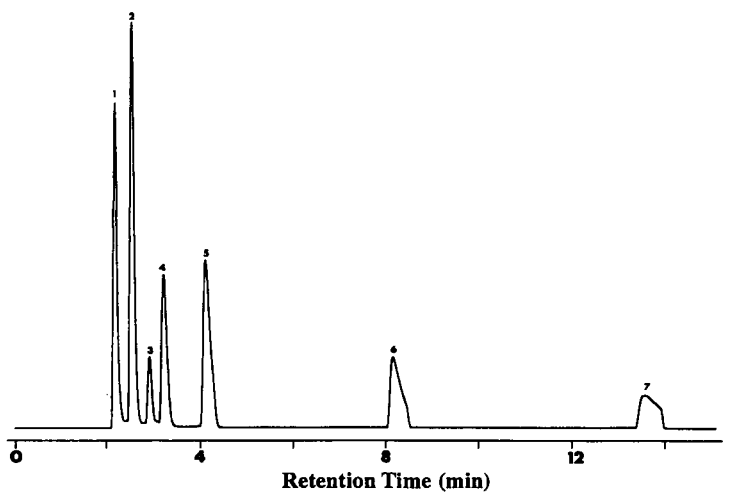

Fig. 4. Chromatogram of a mixed aqueous solution containing Na^+, Ca^{2+}, SO_4^{2-}, Cl^-, Br^-, I^-, and SCN^- obtained using the CHAPS–Zwittergent-3-14 mixed micelle-coated stationary phase. Separation conditions are the same as shown in Fig. 3. except for the flow-rate. Flow-rate: 1.0 ml/min for 5 min and then changed to 2.0 ml/min. (1) $2Na^+$–SO_4^{2-}; (2) Na^+–Cl^-; (3) Ca^{2+}–$2Cl^-$; (4) Na^+–Br^-; (5) Ca^{2+}–$2Br^-$; (6) Ca^{2+}–$2I^-$; and (7) Ca^{2+}–$2SCN^-$.

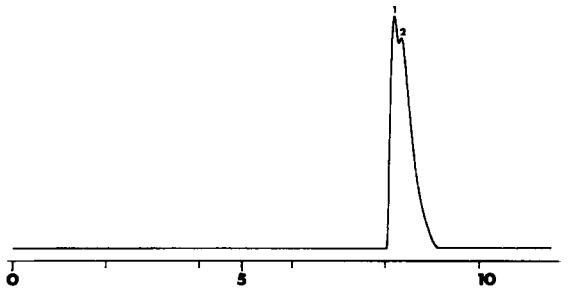

Fig. 5. Chromatogram of an aqueous solution containing $Mg(NO_3)_2$ and $Ca(NO_3)_2$ obtained using the CHAPS–Zwittergent-3-14 mixed micelle-coated stationary phase. Separation conditions are the same as shown in Fig. 3 except for the flow-rate of the water eluent. Flow-rate: 0.5 ml/min. (1) Mg^{2+}–$2NO_3^-$; (2) Ca^{2+}–$2NO_3^-$.

slightly separated, but it shows the possibility for the separation of any type of ion pairs.

3.3. Practical application

In order to demonstrate the possibility of the new method for the determination of both ions, a simple real sample, tap water, was chosen and analyzed. Na^+, Ca^{2+}, SO_4^{2-}, Cl^-, and NO_3^- are the main inorganic ions contained in tap water. Artificial tap water containing 2 mM each of Na_2SO_4, NaCl, $NaNO_3$, $CaCl_2$, and $Ca(NO_3)_2$ was prepared and separated, the chromatogram being shown in Fig. 6. The least-stable ion pair, Na^+–NO_3^-, and the most-stable ion pair, Ca^{2+}–SO_4^{2-}, were also observed along with the medium-stable ion pairs (the molal energy orders for the cations are $\Delta G_{Na^+} > \Delta G_{Ca^{2+}}$, and for anions are $\Delta G_{NO_3^-} > \Delta G_{Cl^-} > \Delta G_{SO_4^{2-}}$). This was because the Na^+, Ca^{2+}, SO_4^{2-}, and NO_3^- ions were left after most of the medium-stable ion pairs were formed. The values of $2Na^+$–SO_4^{2-}, Na^+–Cl^-, Na^+–NO_3^-, Ca^{2+}–$2Cl^-$, and Ca^{2+}–$2NO_3^-$ were found to be 1.906, 4.00, 0.188, 1.00, and 2.906 mM, respectively, from the calibration graphs of the pure components. The value of Ca^{2+}–SO_4^{2-} was found from the remaining Ca^{2+} and SO_4^{2-} ions, which was 0.094 mM. Fig. 7 shows the chromatogram of a tap water sample (A), and the tap water with addition of 0.2 mM each of Na_2SO_4, NaCl, $CaCl_2$, and $Ca(NO_3)_2$ (B), obtained under the same conditions as in Fig. 6. The results shown in Fig. 7 indicate that the four peaks observed in the chromatogram of the tap water are due to the ion pairs $2Na^+$–SO_4^{2-}, Na^+–Cl^-, Ca^{2+}–$2Cl^-$, and Ca^{2+}–$2NO_3^-$. The ion pairs Ca^{2+}–SO_4^{2-} (most-stable) and Na^+–NO_3^- (least-stable) were not observed because under the concentration condition of tap water, all the Ca^{2+}, Na^+, SO_4^{2-}, and NO_3^- ions were used for the formation of the medium-stable ion pairs.

Tap water was also analyzed using the CHAPS micelle-coated stationary phase because tap water does not contain NO_2^- and Br^- ions (NO_2^- could not be base-line separated from NO_3^-, and Br^- and NO_3^- eluted together when using the CHAPS micelle-coated stationary phase). The chromatograms are shown in Fig. 8.

The concentrations of $2Na^+$–SO_4^{2-}, Na^+–Cl^-, Ca^{2+}–$2Cl^-$, and Ca^{2+}–$2NO_3^-$ found in tap water are 0.20, 0.30, 0.18, and 0.021 mM, respectively, from the calibration graphs of the pure components. Consequently, the concentrations of the cations and the anions in tap water were provided, as summarized in Table 1.

To confirm the results obtained by the present method, the same tap water was also examined using ICP-AES and conventional IC, for the determination of cations and anions, respectively. The results are sum-

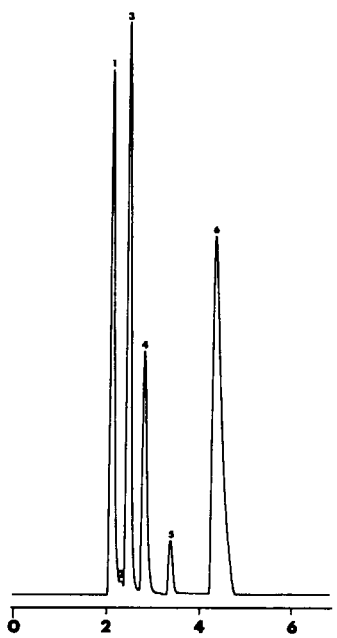

Fig. 6. Chromatogram of artificial tap water obtained using the CHAPS–Zwittergent-3-14 mixed micelle-coated stationary phase. Separation conditions are the same as shown in Fig. 3. (1) $2Na^+$–SO_4^{2-}; (2) Ca^{2+}–SO_4^{2-}; (3) Na^+–Cl^-; (4) Ca^{2+}–$2Cl^-$; (5) Na^+–NO_3^-, (6) Ca^{2+}–$2NO_3^-$.

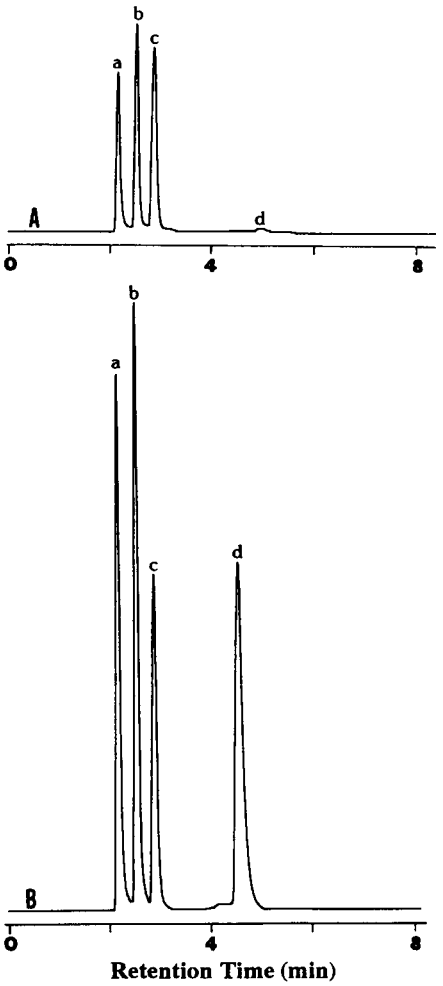

Fig. 7. Chromatogram of (A) tap water and (B) tap water with addition of Na_2SO_4, NaCl, $CaCl_2$, and $Ca(NO_3)_2$. Separation conditions are the same as shown in Fig. 6. (a) $2Na^+$–SO_4^{2-}; (b) Na^+–Cl^-; (c) Ca^{2+}–$2Cl^-$; (d) Ca^{2+}–$2NO_3^-$.

marized in Table 1. Good agreements for the anions were obtained. For the cations, however, the results obtained using ICP-AES indicate that the K^+ and Mg^{2+} ions were also present in tap water. The concentrations of Na^+ and Ca^{2+} obtained by the present method, therefore, are the total concentrations of Na^+ and K^+, and the total concentrations of Ca^{2+} and Mg^{2+}.

The ion pair K^+–X^- could not be recognized from Na^+–X^-, as did Mg^{2+}–$2Y^-$ and Ca^{2+}–$2Y^-$ (X and Y being the anions). This is because the efficiency of the stationary phases (even the CHAPS–Zwittergent-3-14 mixed micelle-coated stationary phase) for the

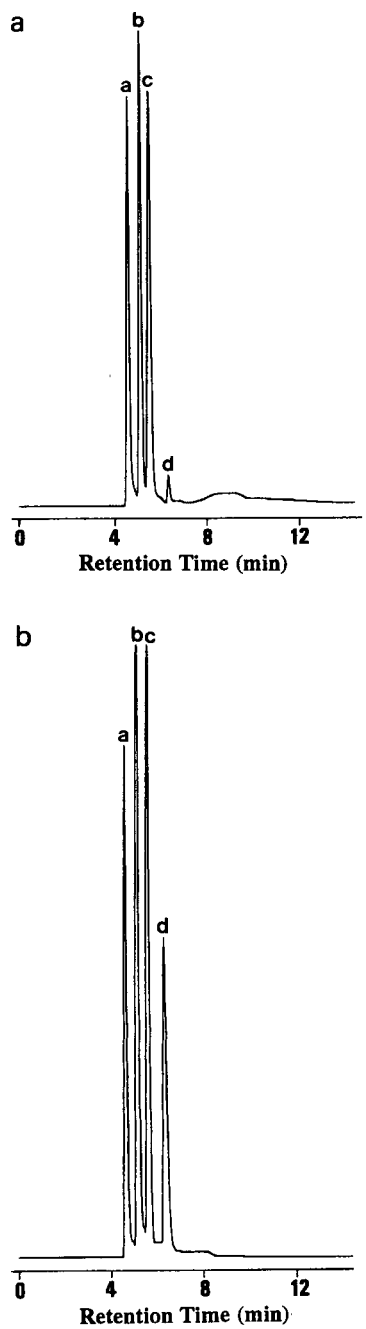

Fig. 8. Chromatogram of (a) tap water and (b) tap water with addition of Na_2SO_4, NaCl, $CaCl_2$, and $Ca(NO_3)_2$. Separation conditions are the same as shown in Fig. 1. (a) $2Na^+$–SO_4^{2-}; (b) Na^+–Cl^-; (c) Ca^{2+}–$2Cl^-$; (d) Ca^{2+}–$2NO_3^-$.

Table 1
Comparison of the concentrations (mM) of the cations and anions in tap water determined by using ICP-AES and conventional IC, respectively

Present method					Conventional IC			ICP-AES			
Na^+	Ca^{2+}	Cl^-	NO_3^-	SO_4^{2-}	Cl^-	NO_3^-	SO_4^{2-}	Na^+	K^+	Mg^{2+}	Ca^{2+}
0.70	0.201	0.66	0.042	0.20	0.64	0.04	0.21	0.53	0.16	0.08	0.13

separation of this type of ion pairs is so poor. This problem can be overcome by the development of a more suitable stationary phase.

References

[1] D.J. Pietrzyk and D.M. Brown, Anal. Chem., 58 (1986) 2554.
[2] J.G. Tarter, J. Chromatogr. Sci., 27 (1989) 463.
[3] D. Yan and G. Schwedt, J. Chromatogr., 516 (1990) 383.
[4] R. Saari-Nordhaus and J.M. Anderson, Jr., J. Chromatogr., 549 (1991) 257.
[5] S. Matsushita, J. Chromatogr., 312 (1984) 327.
[6] V.K. Jones and J.G. Tater, J. Chromatogr., 312 (1984) 456.
[7] M. Yamamoto, H. Yamamoto, T. Yamamoto, S. Matsushita, N. Baba and T. Ikushige, Anal. Chem., 56 (1984) 832.
[8] I. Iskandarani and T.E. Miller, Jr., Anal. Chem., 57 (1985) 1591.
[9] H. Small, T.S. Stevens and W.C. Banman, Anal. Chem., 47 (1975) 1801.
[10] E. Blasius, K.-P. Janzen, W. Adrian, G. Klautke, R. Lorscheider, P.-G. Maurer, V.B. Nguyen, T. Nguyen Tien, G. Scholten and J. Stockemer, Z. Anal. Chem., 284 (1977) 337.
[11] M. Igawa, K. Saito, J. Tsukamoto and M. Tanaka, Anal. Chem., 53 (1981) 1942.
[12] J.D. Lamb and R.G. Smith, J. Chromatogr., 546 (1991) 73.
[13] W. Hu, T. Takeuchi and H. Haraguchi, Anal. Chem., 65 (1993) 2204.

ELSEVIER

Analytica Chimica Acta 299 (1994) 257–268

ANALYTICA CHIMICA ACTA

Flow-injection analysis applied to the kinetic determination of reactive (toxic) aluminium: comparison of chromophores

D.J. Hawke, H.K.J. Powell *

Department of Chemistry, University of Canterbury, Private Bag 4800, Christchurch, New Zealand

Received 29 March 1994; revised manuscript received 25 July 1994

Abstract

A comparison of chrome azurol S (CAS), eriochrome cyanin R (ECR) and pyrocatechol violet (PCV) was made for the estimation of kinetically-labile Al(III) in a series of complexes with model ligands. Flow-injection analysis was used with short reaction times (ca. 10 s). All chromophores differentiated between Al(III) bound in strong and weak complexes, and were suitable for ordering soil solutions and natural waters for relative Al(III) toxicity. By analysing solutions at an isosbestic point at $\lambda > \lambda_{max}$, measurements of "kinetically-labile" (10 s reaction) and "equilibrium-reactive" (10 min reaction) Al(III) were obtainable from a single injection into ECR or CAS. A method is proposed using 0.05 M KCl carrier and CAS (35 μM at the detector) at pH 5.50 in a low sample-dispersion manifold. Kinetically-labile and equilibrium-reactive Al(III) can be determined with a detection limit of 60 nM. The response is linear to 30 μM. The determination of Al(III) in soil solution samples is reported.

Keywords: Flow injection; Chrome azurol S; Eriochrome Cyanin R; Pyrocatechol violet; Aluminium; Soils

1. Introduction

Although Al^{3+} is generally more toxic to plants than H^+ [1], soil pH frequently gives an equal or better correlation with plant growth parameters [2]. Acid precipitation has led to large pH decreases in waters within poorly-buffered catchments. Again, it is Al^{3+} rather than H^+ which is biologically active. These observations emphasise the need to improve analytical methods for Al(III). Measurement of toxic Al, rather than total Al, is of prime importance in soils and natural waters. In particular, $Al^{3+}(aq)$ and $Al(OH)_n^{(3-n)+}$ strongly inhibit root development [3,4] and are toxic to fish [5].

A frequently used approach combines colorimetric assays with short reaction times (e.g., 15 s [6], or 60 s [7]) to minimise stripping of Al(III) from comparatively stable, non-toxic Al complexes. Short reaction times can discriminate between "free" and complexed Al^{3+}, because water bound to Al^{3+} exchanges with colorimetric chromophores more quickly than do other Al^{3+}-bound ligands (see review in [8]).

These short reaction times may give reproducibility problems in conventional assays. Flow-injection analysis (FIA) offers closely reproducible mixing parameters and reaction times. FIA has previously been applied to Al analysis in environmental samples using spectrophotometric [9,10] and amperometric [11] detection. Clarke et al. [12] recently published a solvent extraction method using oxine in a flow-injection system with an 8 s reaction time. However, solvent

* Corresponding author.

SSDI 0003-2670(94)00335-1

extraction and other speciation processes based on separation procedures can lead to partial re-equilibration of the Al–ligand system [13,14], particularly where ligands of weak or intermediate strength are involved [8].

In this paper, we compared three chromophores (chrome azurol S (CAS), eriochrome cyanin R (ECR) and pyrocatechol violet (PCV)) using FIA with short reaction times, for their potential to determine toxic Al in soil solutions. The effects of pH, ionic strength, buffer composition and reagent concentration were investigated. These studies led us to further comparisons at fixed pH (5.50), ionic strength (0.05 M) and buffer (acetate) of the lability of Al bound to synthetic and natural ligands and of Al in soil solution.

2. Experimental

A fundamental aim of our work was to minimise the chance for sample re-equilibration. We therefore aimed at constructing a manifold with the minimum reaction time and dispersion. We wanted to minimise pH and ionic strength changes during the analysis; in particular, we wished to avoid Al(III) hydrolysis. Care in these areas is likely to assist in defining reactive aluminium.

2.1. Instruments and apparatus

Consistent with the above, our manifold was constructed to minimise buffer and chromophore flows while maintaining adequate buffer capacity and chromophore concentration. Following the results of experiments on Fe oxyhydroxide colloids (see Results and discussion), no masking agent for Fe^{3+} interference was used for most experiments. This was of no significance in model ligand studies. In aerobic soils, soluble Fe^{3+} is commonly $<2\%$ of soluble Al^{3+} [15]. The manifold in Fig. 1 was used for all experiments. It had a sample dispersion of 1.26. Microline (Cole Palmer) tubing of 0.51 mm i.d. was used to connect Ismatec tygon pump tubing and for reaction coils. Flow was controlled by an Alitea XV peristaltic pump. The sample injection volume was 250 μl.

A GBC Model 918 UV–visible spectrophotometer with a 10 mm light path flow cell (3 mm i.d., 70 μl volume) was used as the detector. Absorbance was

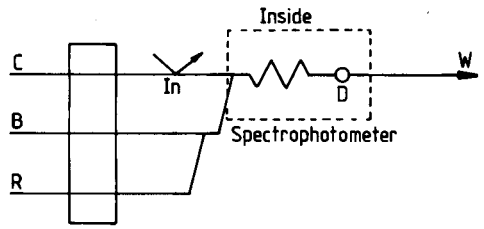

Fig. 1. Schematic diagram for the flow-injection manifold. C = Carrier (1.09 ml min^{-1}); B = buffer (0.27 ml min^{-1}); R = chromophore (0.07 ml min^{-1}); W = waste; D = spectrophotometric detector (1 cm path length); In = sample injector (250 μl). The final merging zone and the 280 mm reaction coil are inside the spectrophotometer cell compartment.

measured as the FIA peak height using the instrument's computer software.

Temperature control was essential to obtain reproducible standard curves from day-to-day, the analysis being kinetically controlled. A temperature of 25°C was chosen, consistent with the thermodynamic database used for calculating speciation in model ligand solutions (see below). This was achieved by placing all reagents in a thermostatted water bath (25 ± 0.1°C) and by thermostatically controlling the ambient room temperature (25 ± 0.5°C). The spectrophotometer was run for 1 h to thermally stabilise the cell compartment before daily measurements. Finally, FIA effluent temperature was continually monitored; this was normally 24.8–25.8°C.

Measurement of pH was performed with a laboratory-built pH meter and using temperature-adjusted 0.05 m potassium hydrogenphthalate standard buffer (pH 4.008).

2.2. Reagents

Chemicals were analytical grade and used as supplied except as follows. Al^{3+} solutions were prepared from $AlCl_3 \cdot 6H_2O$ (Alfa, 99.9995%); the acidified (0.01 M HCl) stock solution was standardised gravimetrically using 8-hydroxyquinoline [16]. Al^{3+} standards for analysis (1–40 μM) prepared from this solution were not further acidified and were prepared 1–2 weekly. No deterioration was found within this time. Standards were prepared in electrolyte to give the same ionic strength as the carrier and buffer lines. CAS (Aldrich) was purified by double recrystallisation from 50% HCl [17]. PCV (Koch-Light) was dried to constant weight at 100°C under vacuum (to remove acetic

acid), prior to dissolving in dilute acid to prevent oxidation. Stock CAS and PCV solutions were standardised potentiometrically and diluted as required. ECR (Merck) was used as supplied and solutions prepared daily. Acetate buffers were prepared by titrating acetic acid with KOH. Hexamine buffers were prepared daily by titrating hexamine with HCl.

2.3. Reaction coil, buffer, pH, and ionic strength effects

Two reaction coil lengths were evaluated: 40 mm and 280 mm. The time taken for solution to travel from the final merging zone to the light path was measured by timing a bubble and was found to be 6.5 s (40 mm coil) and 7.9 s (280 mm coil). The 40 mm coil gave a small decrease in contact time between reagents, but led to a less stable baseline and lower reproducibility. For ECR, a tendency for a non-zero standard curve intercept was increased. Therefore, all subsequent experiments used the 280 mm reaction coil.

Buffer, pH and ionic strength effects were measured at a chromophore concentration of 223 μM (11 μM at the detector). All comparisons were based on the slope of the standard curves (absorbance μM^{-1}). Buffer effects were measured in 0.6 M KCl at pH 5.80 over a range of buffer concentrations (0.05–0.25 M). Two buffers were compared; acetate and hexamine. The effect of pH was measured in 0.1 M KCl containing 0.05 M acetate buffer (for pH < 5.8) or 0.10 M hexamine buffer (for pH > 5.4). For these experiments total ionic strength was maintained at $I = 0.1$ M in all reagent lines.

Ionic strength effects were measured over the range 0.005–1.1 M, in 0.05 M acetate buffer at pH 5.0 (CAS) or pH 5.5 (ECR and PCV). The desired ionic strength was maintained in all lines using KCl. The experiment at $I = 0.005$ M was carried out by using water in the carrier line and as diluent for the standards.

2.4. Kinetic studies

The time dependence of Al^{3+}–chromophore formation was observed by stopping the flow when the absorption maximum was recorded at the detector. The wavelength was set at an apparent isosbestic point for the chromophore–Al^{3+} interaction (see below). Because the sample volume was much larger than the flow cell light path volume (250 μl vs. 70 μl), maximal reactant concentrations were trapped in the cell. The increase in absorbance after stopping the flow was measured for 10 min and the rate and extent of reaction compared between ligands and between chromophores.

2.5. Model ligand experiments

We chose model ligands with a wide range of Al affinities. Literature stability constant data for Al hydrolysis [18] and Al interactions with salicylate [19], malonate [20], oxalate [21], fluoride [22] and citrate [23] and the program SOLGASWATER [24] were used to calculate speciation. For each binary Al–ligand system, the minimum ligand concentration required to complex > 98% of 5.5 μM total Al at pH 5.50 was calculated. The calculated ligand concentrations were 500 μM (salicylate), 40 μM (malonate and oxalate), 40 μM (fluoride) and 20 μM (citrate).

Solutions containing 5.5 μM total Al, one of the model ligands at the above concentration and 10.0 ml 0.05 M acetate buffer (pH 5.50) were prepared in 25 ml volumetric flasks to a total ionic strength of 0.05 M (KCl). They were equilibrated in a water bath at 25 ± 0.1°C for 1–2 h prior to analysis. Either a 300 μM or 700 μM chromophore concentration (16 μM and 35 μM respectively at the detector) was used for these experiments.

2.6. Experiments on humic substances

Fulvic acid was isolated from IHSS reference peat by the acid pyrophosphate–XAD-7 method [25]. Humic acid was isolated from the same source by extraction with pyrophosphate (pH 9.0–9.5) and repetitive acid precipitation/pyrophosphate dissolution until a low ash product (< 2%) was achieved [26]. The humic acid had 0.25% w/w Fe and 0.085% w/w Al content, or 350 nM Fe and 250 nM Al in solution at the humic concentration used. The fulvic acid had 0.1% w/w Fe and 0.05% w/w Al content, or 140 nM Fe and 150 nM Al in solution.

Humic and fulvic acids were mixed with 5.5 μM Al^{3+} at $I = 0.05$ M in the same way as the model ligand solutions above. A blank (no added Al) was also prepared. The concentration of humic substance used was such that the Al^{3+} concentration was equal to the Cu^{2+} complexation capacity (0.7 mmol Cu g^{-1}; [26]). We

assumed that this would give 100% complexed Al^{3+} at equilibrium. Equilibrium was for ca. 2 days. Samples were filtered (0.025 μM) immediately prior to injection. Because of the appreciable Fe content of the humic substances, 0.05% w/v ascorbic acid was weighed into each reaction flask immediately prior to filtration and analysis. Labile Al was calculated by subtracting the signal arising from the blank. Blank values were lower for fulvic acids (10–30% of sample signal, depending on the chromophore) than humic acids (35–80% of sample signal). Blanks were similar to that predicted from the ash content (based on ICP measurements) and were $<5\%$ of total added Al^{3+}.

2.7. Experiments on model colloids

Ferrihydrite was prepared by adding 50 ml 0.01 M HCl–0.1 M KCl to 0.21 g $Fe(NO_3)_3 \cdot 9H_2O$. This was titrated at 0.39 ml min^{-1} with carbonate-free 0.1 M KOH to pH 7.5. The resulting solution was aged overnight at 25°C. This was diluted and mixed with Al^{3+} at $I=0.05$ M in the same way as the model ligand solutions above. Final concentrations were 10 mg l^{-1} ferrihydrite and 5.5 μM Al^{3+}. A blank (no added Al) was also prepared.

A second ferrihydrite was prepared in the same way, except that 1.58 ml of 1.59 mM Al^{3+} was included to give coprecipitated Al at a Fe:Al ratio of 4:1. Final concentrations were 8.8 mg l^{-1} ferrihydrite and 4.9 μM Al^{3+}. To evaluate the effect of Fe^{3+} reductant on reactive Al in this colloid, ascorbic acid was added at 0%, 0.046%, and 0.11% w/v prior to equilibration for 1 h.

2.8. Measurements on soil solutions

Soil solutions were extracted by centrifugation (4000 g, 60 min) from sieved (4 mm) field-moist soils (0–10 cm depth) then filtered (0.2 μm). Two of the soils were Brown soils under grazed ryegrass pasture (Belmont silt loam, pH ca. 5.2). The other two were a Pumice soil under *Pinus radiata* (Oruanui sandy loam, pH ca. 4.8) and a Podzol under native podocarp/tawa forest (Tihoi sandy loam, pH ca. 4.6). These soils were chosen to cover a range of likely reactive Al concentrations. Analysis was by the same method as for ligand solutions, with dilution as required. Following results of the model colloid experiments, no attempt was made to mask Fe^{3+} interference.

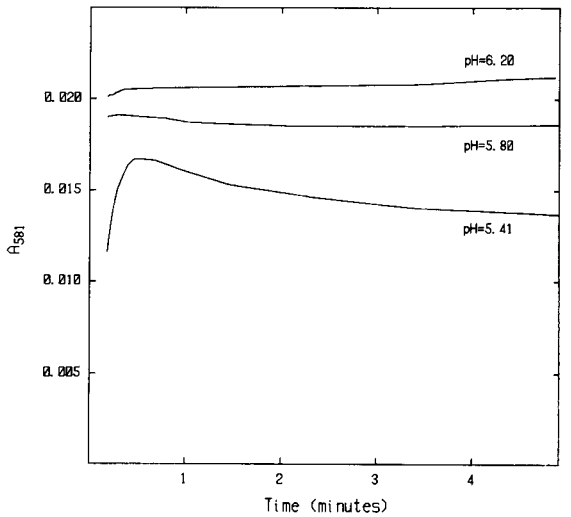

Fig. 2. Plot of absorbance (at 581 nm) vs. time for the reaction of 2.76 μM Al^{3+} standard and 223 μM PCV at $I=0.10$ M (KCl) using 0.10 M hexamine buffer under pH conditions shown. Zero time corresponds to the time of first contact between reagent and sample, at the final merging zone in Fig. 1.

3. Results and discussion

3.1. Time dependence of Al^{3+}–chromophore spectra

Response to Al^{3+} standards at fixed wavelength

Initial experiments used λ_{max} wavelengths from previous equilibrium and FIA studies (CAS, 545 nm [27]; ECR, 540 nm [9]; PCV, 581 nm [10]). Results showed that PCV reacted substantially faster than the other chromophores. At 220 μM chromophore (11 μM at the detector), $I=0.05$ and pH 5.5, percentages of Al^{3+} reacted in 10 s were CAS, 45%; ECR, 48%; and PCV, 90%. These results were measured relative to equilibrium absorbance ($t=10$ min; CAS and ECR), or maximum absorbance ($t<10$ min; PCV), at λ_{max}.

Time effects on λ_{max}

PCV showed a tendency for the peak absorbance at 581 nm to subsequently decrease with time, especially as the pH was lowered (Fig. 2). Absorbances for ECR also decreased with time, but to a lesser extent.

Further, literature results [28] obtained from conventional PCV spectrophotometry indicated an extinc-

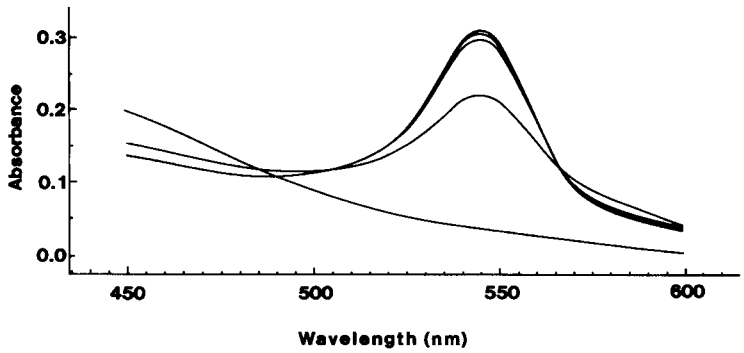

Fig. 3. Absorbance scans vs. time for 5.5 μM Al^{3+} and CAS at pH 5.5 in $I = 0.05$ M (KCl), showing the formation of an isosbestic point at 567 nm. Scan times (relative to turning off pump), in order of increasing absorbance at 550 nm: ligand only; 0 min; 2 min; 5 min; 22 min.

tion coefficient of 4.8×10^4 at 585 nm and pH 6, rather greater than the value of 9.6×10^3 at pH 6.4 calculated from Fig. 4 (corrected for dispersion). Our value is similar to the FIA result obtained by Røyset [10] (1.0×10^4).

Experiments were carried out at two pH values to elucidate the unexpectedly low PCV extinction coefficient. For these experiments an Al^{3+} standard in 0.05 M KCl was pumped in the carrier line. Once a stable absorbance was attained, the pump was stopped and the spectrum scanned rapidly as a function of time. At pH 5.9 λ_{max} decreased from 590 nm at the time the pump was turned off (10 s reaction time), to 576 nm after 35 min. It remained unchanged for the rest of the 160 min observation time. The extinction coefficient (576 nm) was still increasing slowly at 160 min. Its value (3.4×10^4) is in reasonable agreement with the literature [28] (4.8×10^4), considering the incomplete nature of the reaction. In contrast, at pH 5.5 there was no change in absorption maximum, but a slow decrease in absorbance over the extent of the Al–PCV spectrum (ca. 550–700 nm) was observed. This may be caused by adsorption of the coloured complex on the walls of the spectrophotometer cell.

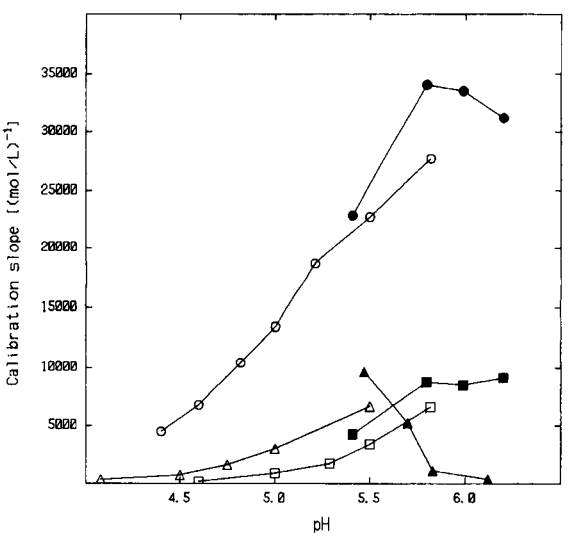

Fig. 4. Dependence of FIA assay on pH. Measured at 545 nm (○; CAS); 540 nm (△; ECR); and 581 nm (□; PCV), in (open symbols) 0.05 M acetate, $I = 0.05$ M (KCl); and (closed symbols) 0.10 M hexamine, $I = 0.10$ M (KCl). Calibration slopes are as recorded, and not corrected for dispersion. [Chromophore] = 223 μM (11 μM at detector).

ECR showed qualitatively similar results, with a small shift in λ_{max} from 536 nm (10 s) to 533 nm (42 min). CAS showed no significant change in λ_{max} on this timescale. However, subsequent experiments at shorter reaction times (< 10 s) showed a shift in λ_{max} similar to that observed with ECR.

Isosbestic point formation

The time-dependent development of the CAS spectrum is shown in Fig. 3. This shows 2 isosbestic points. At the first isosbestic point ($\lambda < \lambda_{max}$), the first scan crossed the ligand-only spectrum at a shorter wavelength than subsequent scans, which all crossed to form the isosbestic point reported in [17]. At $\lambda > \lambda_{max}$, an isosbestic point (excluding the ligand-only spectrum) was observed at 567 nm.

ECR showed a similar isosbestic point at $\lambda > \lambda_{max}$, at 548 nm. For PCV at pH 5.5, there was no isosbestic point at $\lambda > \lambda_{max}$ but at pH 5.9 a poorly defined isosbestic point formed at 608 nm.

Interpretation and implications

The changes in λ_{max} and the formation of an isosbestic point at $\lambda > \lambda_{max}$ indicate a sequence of reactions. We interpret the spectral features for CAS (Fig. 3) as

follows. In the 10 s following contact between Al^{3+} and CAS, an intermediate species forms rapidly. This subsequently rearranges to give the complex with $\lambda_{max} = 545$ nm. The isosbestic point at 567 nm therefore represents the transition from the initial intermediate to the final complex. At the time of the first scan (10 s reaction), the initial intermediate is still present to a substantial extent, thus accounting for the slightly different crossover point with the ligand-only spectrum near 490 nm. We suggest that the intermediate may be an outer sphere complex between Al^{3+} and CAS, although complexation at another site on CAS is also conceivable. An outer-sphere complex would absorb at longer wavelength than the final, equilibrium complex, as implied by λ_{iso} at 567 nm.

A similar explanation is likely for the formation of an isosbestic point with ECR, at 548 nm. The additional feature for ECR, a change in λ_{max}, could be due to polymerisation of the 1:1 complex. Polymerisation has been reported [17] for CAS (which is structurally very similar to ECR).

For PCV the experiments at pH 5.9 showed changes in λ_{max} and isosbestic point formation. The isosbestic point at 608 nm can be explained in the same way as for CAS, i.e., rapid formation of an initial intermediate, followed by conversion to the 1:1 complex. The relatively large shift in λ_{max} for PCV is consistent with the initial formation of a 1:1 complex (λ_{max} 590 nm) followed by the slow coordination of a second ligand to give the 2:1 complex found at pH 5–6 under millimolar equilibrium conditions [31]. The long equilibration time is probably due to low reagent concentrations at the detector. The absence of λ_{max} changes at pH 5.5 is consistent with the absence of the 2:1 complex at this pH.

By monitoring FIA peak absorbance with time at the CAS and ECR isosbestic points, an estimate of both the Al^{3+}–chromophore-competing ligand equilibrium ($t = 10$ min), and the measurement of kinetically-labile Al ($t = 10$ s) can be obtained. No analytical use was made of the PCV isosbestic point, because the pH required for its formation was too high. Kinetically-labile Al measurements do not need correction for the extent of reaction in the absence of competing ligand if the isosbestic point reflects the initial rapid formation of an intermediate. This correction would be necessary if the analyses were carried out at λ_{max}.

For measurements on synthetic metal–ligand systems or on soil solutions the Al^{3+} concentration determined from the isosbestic point corresponds to 100% of free monomeric Al (Al^{3+}, $Al(OH)^{2+}$) plus Al^{3+} formed by dissociation of metal complexes within the 10 s reaction time. The rate of dissociation of the organic complexes will be inversely related to complex stability.

3.2. Kinetic measurements

Optimum conditions for rapid, sensitive analyses were established by considering the effect of pH, buffer and ionic strength. These experiments used λ_{max}.

Effect of pH

For all chromophores the Al^{3+}–chromophore sensitivity (expressed as the slope of the calibration graph) showed a strong pH dependence (Fig. 4). A limitation on ECR data was the non-linearity of standard curves at $[Al^{3+}] \ll [ECR]$ and pH > 5.5. At these pH values extrapolation of the linear segment of the standard curve, corresponding to higher $[Al^{3+}]$, gave a negative intercept. CAS and ECR showed pH optima of 5.7–6.0 (CAS) and 5.5 (ECR). PCV showed approximately constant sensitivity above pH 5.8, consistent with the pH optimum selected in other work (pH 6.0) [28].

The observed pH dependence will result from several contributing factors. Firstly Al^{3+} complexation will increase as chromophore donor groups are deprotonated with increasing pH. Secondly, hydrolysis of Al^{3+} to monomeric species $Al(OH)^{2+}$ and $Al(OH)_2^+$ (pH 4.5–5.5) increases the rate of metal–ligand complex formation. At higher pH this effect will be offset by formation of less labile polymeric hydrolysis products, $Al_x(OH)_y^{(3x-y)+}$. Thirdly, at higher pH the stoichiometry of the complex (and therefore λ_{max}) may change.

Effect of buffer

Hexamine buffer gave better sensitivity than acetate for all chromophores at pH 5.8 (Fig. 4). This may indicate competitive complexation by acetate. However, sensitivity was not significantly affected by buffer concentration. The exception was for CAS, where sensitivity in hexamine almost doubled over the buffer concentration range of 0.1 M to 0.25 M. The basis for this latter result is not clear, although it is broadly anal-

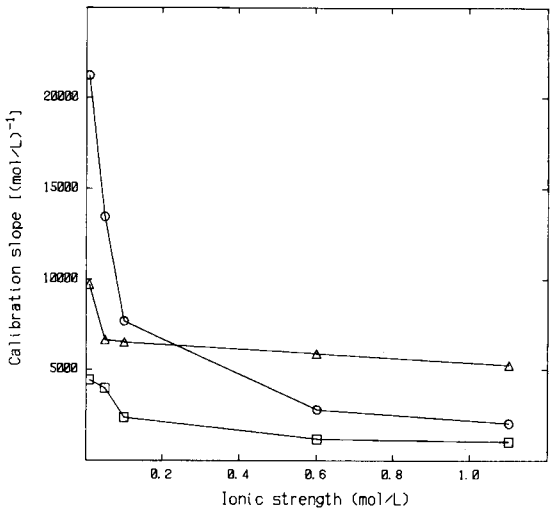

Fig. 5. Dependence of FIA assay on ionic strength at pH values indicated, and measured at 545 nm (○; CAS, pH 5.0); 540 nm (△; ECR, pH 5.5); and 581 nm (□; PCV, pH 5.5). Calibration slopes are as recorded, and not corrected for dispersion. [Chromophore] = 223 μM (11 μM at detector).

ogous to the enhancement of sensitivity of chromogenic reagents by surfactants [9].

Hexamine has been widely used [10] to control pH in Al analysis by chromogenic reagents, but suffers from pH drift. We have measured (upward) drift of ca. 0.5 pH over 24 h for a pH 6 buffer. Acetate does not suffer appreciable pH drift; its lower sensitivity was regarded as preferable to the instability of hexamine.

Effect of ionic strength

The ionic strength study was carried out below the pH optimum for sensitivity, since a low analysis pH will minimise speciation disruption, especially Al hydrolysis, in naturally acidic samples. Sensitivity decreased significantly with increasing ionic strength for all chromophores at pH 5.0 or 5.5 (Fig. 5). CAS showed the greatest effect, with sensitivity decreasing by an order of magnitude over the range $I = 0.005$–1.1 M. These kinetic effects are qualitatively those predicted [29] for reactions involving ions of opposite charge or polar molecules and could be due to decreasing activity coefficients of ionic species. For example, the activity coefficient of Al^{3+} calculated according to [30] decreases from 0.518 at $I = 0.005$ M to 0.056 at $I = 1.1$ M. However, deprotonation of CAS increases with ionic strength [17], which would increase the rate of reaction if the rate limiting step(s) involve deprotonated chromophore. Unlike CAS and ECR, PCV showed little change from $I = 0.005$–0.05 M. Kinetic experiments showed that this was because the reaction being monitored (formation of a 1:1 complex) was nearly complete at these low ionic strengths, within the 10 s reaction time.

Lability of Al complexed to model ligands and humic substances

For CAS and ECR, these measurements were carried out at the isosbestic points rather than the λ_{max}. The PCV measurements were carried out at the λ_{max} identified by the kinetic measurements (578 nm). All measurements were carried out consecutively with the equilibrium measurements described below. The percent of complexed Al rapidly reactive with each chromophore is given for each ligand in Table 1. For each ligand > 98% of Al^{3+} was calculated to be complexed prior to injection in the FIA manifold. Due to the low sample dispersion (1.26) and constant pH, similar complexation would be expected at the detector. At a chromophore concentration of 330 μM (16 μM at detector), reactive Al^{3+} ranged from 38% (salicylate, PCV) to less than the detection limit (citrate, all chromophores). The FIA technique combined with a short reaction time therefore discriminated well between Al complexes of different stability. A measurement on a soil solution or natural water will give 100% of Al^{3+} plus (using 330 μM chromophore) 0 to ca. 30% of organic-bound Al^{3+} in the sample.

Increasing chromophore concentration to 700 μM (35 μM at the detector) increased the reactive Al to a maximum of 54% (salicylate, PCV); citrate complexes were again unreactive. This dependence on chromophore concentration implies that the rate of dissociation of Al–ligand complex does not alone control formation of Al^{3+} or the formation of Al–chromophore intermediate. The chromophore therefore must directly attack the Al–ligand complex. To minimise the contribution to the signal from this source it is necessary to minimise chromophore concentration. However, this must be balanced against the required linear range.

In general, Al complexed to model ligands was reactive in the order salicylate > malonate > fluoride > oxalate > fulvic acid > humic acid > citrate at both chromophore concentrations. The exceptions were that fluoride and oxalate, and humic acid and fulvic acid complexes were similarly labile to PCV; and Al com-

Table 1
Percentage of complexed Al reactive to each chromophore in 10 s

Ligand	ECR		PCV		CAS	
	330 μM	700 μM	330 μM	700 μM	330 μM	700 μM
Salicylate	20	47	42	60	32	50
	nd	(66)	nd	(65)	nd	(75; 92)
Malonate	22	36	29	50	33	54
	(62)	(85)	(55)	(73)	(84)	(111; 72)
Fluoride	15	24	23	33	23	29
	nd	(42)	nd	(48)	nd	(74; 71)
Oxalate	9	19	20	38	15	27
	(17)	(31)	(38)	(52)	(28)	(60; 71)
Fulvic acid [a]	nd	10	nd	9	nd	20
		(29)		(17)		(42)
Humic acid [a]	–	7	–	11	–	7
		(18)		(19)		(29)
Citrate	<2	<2	<5	<4	<1	1
					(nd)	(nd; 8)

Absorbances were measured at 567 nm (CAS), 548 nm (ECR), and 578 nm (PCV). PCV results were corrected for fractional reaction of Al^{3+} standard under the same conditions. Results in parentheses give 10 min equilibrium values; the second number in the CAS results gives the calculated equilibrium value. Model ligand concentrations were calculated to give <2% free Al at equilibrium at pH 5.50. They were: salicylate, 500 μM; malonate, oxalate, and fluoride, 40 μM; citrate, 20 μM; fulvic and humic acids, 7.9 mg/l.
[a] 0.05% ascorbic acid added to sample to suppress Fe^{3+} interference.

plexed with malonate was more labile to CAS than Al complexed with salicylate.

Aggressiveness of the chromophores to the complexes (as measured by the extent of reaction in 10 s) was: PCV > CAS > ECR (salicylate, oxalate); PCV > CAS ≈ ECR (humic acid); CAS > PCV ≈ ECR (fulvic acid); and PCV ≈ CAS > ECR (malonate, fluoride). Even though ECR was the least aggressive, it was no more discriminating than CAS and PCV. These changes in order for different ligands imply that thermodynamic effects do not dominate the observed reaction.

There is a qualitative inverse correlation between kinetically-labile Al determined by FIA (Table 1) and the effect of organic acids in ameliorating Al toxicity in sensitive plants. For example, for cotton root growth in hydroponic solution, Al–citrate gave 0%, Al–oxalate 1%, Al–malonate 17% and Al–salicylate 31% decrease in relative root length (RRL) compared to an Al-free control at pH 4.75 [32]. The low lability of Al bound to humic substances is consistent with many qualitative field studies (e.g., [33]) showing amelioration of Al toxicity by "soil organic matter". The relatively high lability of fluoride-bound Al contrasts with the complete removal of Al toxicity by fluoride at $[F^-]:[Al^{3+}]$ ca. 1.0 in nutrient solution studies [1,34]. It suggests that these chromophores over-estimate the "reactive" fraction of Al^{3+} complexed to F^-. However, our results are qualitatively consistent with recent fish studies [35,36] showing significant toxicity of Al–F species.

The different reaction rates for the chromophores are shown in Fig. 6, using the reaction with oxalate-bound Al as an example. For both ECR and PCV the reaction was essentially complete within 2 min. In contrast, the reaction with CAS was incomplete after 10 min. The relatively slow kinetics for CAS qualitatively explain its slightly lower aggressiveness compared with PCV in the kinetic experiments (despite the ability of CAS to sequester a higher proportion of Al^{3+} under equilibrium conditions, see below).

3.3. *Equilibrium measurements*

Monitoring absorbance at the isosbestic point for ca. 10 min after turning off the pump at the peak of the 10

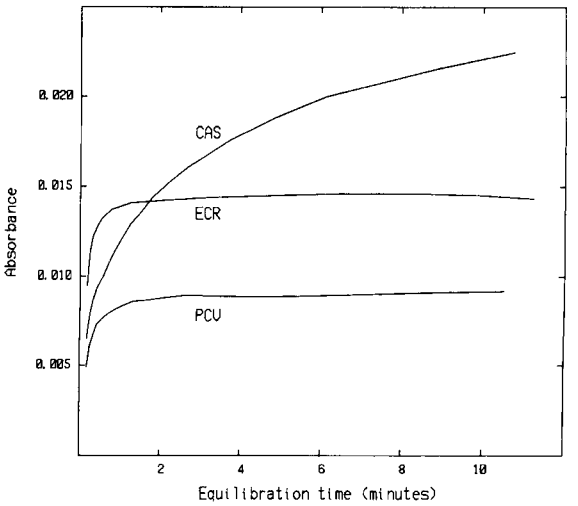

Fig. 6. Rate of colour development for 5.5 μM Al^{3+} + 50 μM oxalate with 330 μM chromophore, at isosbestic point wavelengths (567 nm (CAS); 548 nm (ECR); and 578 nm (PCV)).

s reaction gave a "10 min equilibrium" value for the Al^{3+}–chromophore complex as well as the 10 s kinetically-labile result. The equilibrium-reactive result depended on competition for Al between the chromophore and sample ligand. Using this method with Al^{3+} standards established no change in absorbance with time after the pump was turned off for CAS (λ_{iso} 567 nm). The result was acceptable for ECR, with a change of ca. 5% (λ_{iso} 548 nm). As PCV did not show an isosbestic point at the pH of our analyses (pH 5.5), we monitored the change of absorbance with time at λ_{max} (578 nm). As shown in Fig. 2, PCV showed an unacceptable decrease with time when measuring standards. However, in the presence of model ligands and soil solutions this decrease was either minimal or not observed. We therefore proceeded with the PCV experiments, conscious of the limitations.

The equilibrium displacement of Al from model ligands by each chromophore is given in parentheses in Table 1. The observed stabilities of Al–ligand complexes toward CAS were citrate > humic acid > fulvic acid > oxalate > fluoride > salicylate > malonate. Humic and fulvic acids gave similar results with ECR. The kinetic measurements gave the same sequence for all chromophores except for the reversal of salicylate and malonate. Where 2 chromophore concentrations were used, the higher concentration gave the higher concentration of Al–chromophore complex.

In contrast to the kinetic results, CAS was always the most aggressive chromophore (CAS > ECR > PCV for malonate, fulvic acid; CAS > PCV > ECR for fluoride, oxalate; and CAS > PCV = ECR for salicylate, humic acid). However, the PCV results may be compromised by the analysis problems mentioned earlier. The lack of stability constants for Al–ECR and Al–PCV complexes prevents comparison with these results. Although a literature Al–PCV study exists [37], the proposed constants are anomalously large for an Al^{3+}–"catecholate" complex. For the Al–CAS system stability constants have been determined at $I = 0.10$ M KCl [17]. As shown in Table 1, the agreement between experimental and calculated Al–CAS results is acceptable, especially considering that no stability constants are available for $I = 0.05$ M for the ligands or the chromophore. The major discrepancies were with malonate and salicylate. Salicylate was substantially less reactive than predicted from stability constants. The malonate result is unclear; our determination of the Al–CAS system [17] found no evidence for complicating features such as ternary complex formation with malonate.

Kinetic vs. equilibrium stability effects are shown for CAS in Fig. 7. The salicylate complex reached an apparent equilibrium most rapidly (ca. 3 min), but the malonate complex had a faster initial rate. The smaller initial reaction rate of the salicylate complex could be

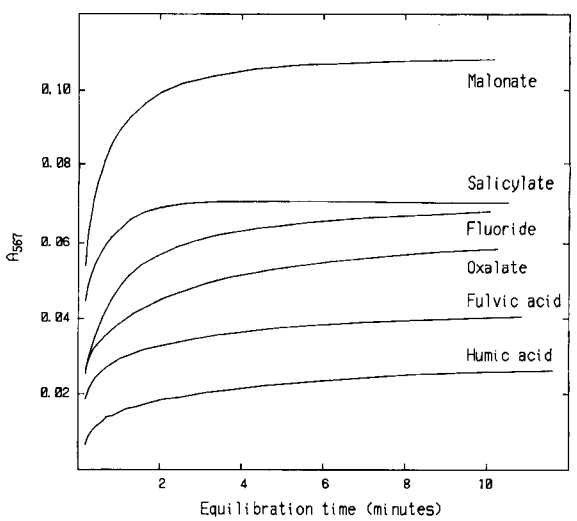

Fig. 7. Plot of absorbance vs. time for 5.5 μM Al^{3+} + model ligands with 700 μM CAS, at the isosbestic point wavelength (567 nm).

Table 2
10 s-reactive Al (μM) (or Fe equivalent) for Fe–Al colloid study

Colloid	ECR	PCV	CAS
Ferrihydrite, no Al^{3+}	0.3	0.5	0.2
Ferrihydrite, +5.5 μM Al^{3+}	0.9	1.6	0.3
Al–ferrihydrite, 0% ascorbic acid	0.3	1.5	0.5
Al–ferrihydrite, 0.046% ascorbic acid	1.7	1.4	2.4
Al–ferrihydrite, 0.11% ascorbic acid	3.0	1.1	4.0

Absorbances were measured at 567 nm (CAS), 548 nm (ECR), and 578 nm (PCV). PCV results were corrected for fractional reaction of Al^{3+} standard under the same conditions. Chromophore concentration was 700 μM. The colloid concentrations were 10 mg l^{-1}. The Al–ferrihydrite suspension would have given 4.9 μM Al^{3+} had total dissolution occurred.

due to formation of a metastable species that reacts slowly at the low chromophore concentrations of the FIA system. Oxalate and fluoride required ≥ 10 min to reach an equilibrium absorbance.

Detection limit and working range

The detection limits (3×S.D. of instrument noise) for each chromophore at 330 μM (700 μM) using the isosbestic wavelengths at $I = 0.05$ M (KCl) in 0.05 M acetate buffer pH 5.50 were: CAS, 80 nM (70 nM); ECR, 90 nM (70 nM). The detection limit for PCV at λ_{max} was 300 nM (200 nM). Under the same measurement conditions, the CAS detection limit at 545 nm is 50 nM. Under kinetic conditions (FIA peak absorbance at 10 s), the response was linear for Al^{3+} standards up to: CAS, 15 μM Al^{3+} (30 μM); ECR, 7 μM (12 μM); and PCV, 12 μM (20 μM).

3.4. Interactions with Fe colloids

All colloid solutions were analysed using 700 μM chromophore. The results for all chromophores (Table 2) indicated little reaction in the absence of added Al^{3+}. This shows that colloidal Fe^{3+} is essentially unavailable on the time scale of the assay. In the presence of added Al^{3+} (adsorbed onto the colloid), CAS was the least aggressive, recovering a negligible amount of the added Al^{3+}. At 10 mg l^{-1} ferrihydrite, 10 min equilibrium values could not be obtained due to chromophore adsorption onto the colloid.

The experiments on coprecipitated Al^{3+} showed that reactive Al in the absence of ascorbate was < 10% for CAS and ECR. Increasing the ascorbate concentration led to corresponding increases in reactive Al. PCV results showed the reverse trend, with substantial Al reactivity at all ascorbic acid concentrations. This could be due to Al-induced surface changes rendering the colloid more reactive to PCV. To determine the time scale for the labilising of coprecipitated Al, the experiment was repeated for ECR and CAS with ascorbic acid added 60 s prior to sample injection. The results showed that > 80% of the effect occurred within this time.

These experiments show that colloidal Fe^{3+} is essentially unreactive to all chromophores but that addition of ascorbate labilises coprecipitated Al^{3+} (to CAS and ECR). Al in this form is unlikely to be toxic. We therefore conclude that using ascorbate (or similar reductant) is likely to be counterproductive in assays for toxic Al using ECR or CAS. The situation is less clear for PCV, and requires further investigation.

3.5. Analysis of soil solutions

The four soil solutions were analysed by the same protocol as the model ligands, using a chromophore concentration of 700 μM. A 5× sample dilution of the pumice-podzol soils was made, to match the linear working range. The results (Table 3) show that 10 min equilibrium values were approximately double the kinetic (10 s) values, which is similar to the result for model ligands (Table 1). The chromophores showed no clear trends for either kinetic or equilibrium aggressiveness. However, the kinetic plots showed that CAS

Table 3
Reactive Al (μM) in soil solution samples, using 700 μM chromophore

Soil solution	ECR	PCV	CAS
1. Belmont silt loam	1.5 (2.9)	2.4 (3.6)	1.8 (3.8)
2. Belmont silt loam	3.7 (7.7)	3.6 (6.6)	3.9 (8.4)
3. Tihoi sandy loam	17 (40)	22 (43)	20 (57)
4. Oruanui sandy loam	8.0 (14)	5.1 (10)	5.7 (8.8)

All results were calculated relative to Al^{3+} standards measured under the standard kinetic conditions. Analyses on samples 3 and 4 were obtained on 5× dilutions. Values in parentheses give 10 min equilibrium results. Absorbances measured at 567 nm (CAS), 548 nm (ECR) and 578 nm (PCV).

always reacted more slowly than the other chromophores. This is the same trend as observed with the model ligands (Fig. 6) and Al^{3+} solutions.

4. Conclusions

Previous work emphasised the utility of short reaction times via manual methods in assessing toxic Al. Using FIA and an isosbestic point, we were able to analyse both 10 s kinetically-labile and 10 min equilibrium-reactive Al with a single sample injection. All chromophores differentiated between free Al^{3+}, Al^{3+} bound to strongly complexing ligands and Al^{3+} bound to weaker ligands. Our method therefore gives the ability to order soils or natural waters for Al toxicity, based on either (or both) kinetic and equilibrium criteria.

PCV was slightly more aggressive kinetically, while CAS was rather more aggressive under equilibrium conditions. However, CAS provides greater sensitivity than ECR and (particularly) PCV. PCV analysis of Al^{3+} standards also showed a decrease in absorbance with time at pH 5.5, which complicates interpretation of equilibrium-labile Al^{3+}.

Our recommendation is that CAS be used with the manifold shown in Fig. 1 to measure kinetically-labile Al^{3+} in environmental samples. For routine use we recommend acetate buffer, rather than hexamine, because of its pH stability. A pH of 5.5 maintains good sensitivity while minimising disturbance of sample speciation.

For Al initially bound to organic ligands, equilibrium-reactive Al was greater than kinetically-labile Al by a factor of 2–3 (depending on chromophore concentration). This prompts the question as to whether kinetic methods are better than equilibrium methods as predictors of Al toxicity, or merely different. Previous manual methods probably stripped too much Al^{3+} from soil solution ligands because of the use of high chromophore concentrations. However, it is clear that kinetic measurements, using the shortest possible reaction times, will give the best indication of free Al^{3+} (100% reactive) with the least contribution from organically bound Al^{3+} ($<$ca. 30% reactive).

Acknowledgements

We are grateful to R.L. Parfitt (Landcare Research Ltd.) for provision of soil solutions and helpful discussions. E. Fenton isolated the humic substances, and determined Cu complexation capacities. This paper is a partial fulfilment of Contract UOC315 from the New Zealand Foundation for Research, Science and Technology to the University of Canterbury.

References

[1] R. Cameron, G.S.P. Ritchie and A.D. Robson, Soil Sci. Soc. Am. J., 50 (1986) 1231.
[2] L.M. Shuman, E.L. Ramseur and R.R. Duncan, Agron. J., 82 (1990) 313.
[3] F.P.C. Blamey, D.G. Edwards and C.J. Asher, Soil Sci., 136 (1983) 197.
[4] J. Lee and M.W. Pritchard, Plant Soil, 82 (1984) 101.
[5] C.S. Cronan and C.L. Schofield, Science, 204 (1979) 304.
[6] B.R. James, C.J. Clark and S.J. Riha, Soil Sci. Soc. Am. J., 47 (1983) 893.
[7] G.L. Kerven, D.G. Edwards, C.J. Asher, P.S. Hallman and S. Kokot, Aust. J. Soil Res., 27 (1989) 91.
[8] J.G. Hering and F.M.M. Morel, in W. Stumm (Ed.), Aquatic Chemical Kinetics, Wiley, New York, 1990.
[9] O. Røyset, Anal. Chim. Acta, 178 (1985) 223.
[10] O. Røyset, Anal. Chim. Acta, 185 (1986) 75.
[11] A.J. Downard, H.K.J. Powell and S. Xu, Anal. Chim. Acta, 251 (1991) 157.
[12] N. Clarke, L.-G. Danielsson and A. Sparén, Int. J. Environ. Anal. Chem., 48 (1992) 77.
[13] C.T. Driscoll, Int. J. Environ. Anal. Chem., 16 (1984) 267.
[14] J.L. Means, D.A. Crerar and J.L. Amster, Limnol. Oceanogr., 22 (1977) 957.
[15] H.K.J. Powell, unpublished results.
[16] J. Basset, R.C. Denney, G.H. Jeffery and J. Mendham (Eds.), Vogel's Textbook of Quantitative Inorganic Analysis, Longman, New York, 1978.
[17] D.J. Hawke, H.K.J. Powell and S. Sjöberg, Polyhedron, in press.
[18] P.L. Brown, R.N. Sylva, G.E. Batley and J. Ellis, J. Chem. Soc., Dalton Trans., (1985) 1967.
[19] L.-O. Öhman and S. Sjöberg, Acta Chem. Scand., 37A (1985) 875.
[20] H.K.J. Powell and R.M. Town, Aust. J. Chem., 46 (1993) 721.
[21] S. Sjöberg and L.-O. Öhman, J. Chem. Soc., Dalton Trans., (1985) 2665.
[22] C. Brosset and J. Orring, Sven. Kem. Tidskr., 55 (1943) 101.
[23] L.-O. Öhman, Inorg. Chem., 27 (1988) 2565.
[24] G. Eriksson, Anal. Chim. Acta, 112 (1979) 375.
[25] J.E. Gregor and H.K.J. Powell, J. Soil Sci., 37 (1986) 577.
[26] E. Fenton and H.K.J. Powell, in preparation.
[27] P. Pakalns, Anal. Chim. Acta, 32 (1965) 57.

[28] W.K. Dougan and A.L. Wilson, Analyst, 99 (1974) 413.
[29] E.S. Amis, Kinetics of Chemical Change in Solution, Macmillan, New York, 1949.
[30] F.J. Millero and D.R. Schreiber, Am. J. Sci., 282 (1982) 1508.
[31] S. Simpson, S. Sjöberg and H.K.J. Powell, unpublished results.
[32] N.V. Hue, G.R. Craddock and F. Adams, Soil Sci. Soc. Am. J., 50 (1986) 28.
[33] R.J. Bartlett and D.C. Riego, Plant Soil, 37 (1972) 419.
[34] A.D. Noble, M.E. Sumner and A.K. Alva, Soil Sci. Soc. Am. J., 50 (1986) 1231.
[35] K.J. Wilkinson, P.M. Bertsch, C.H. Jagoe and P.G.C. Campbell, Envir. Sci. Technol., 27 (1993) 1132.
[36] K.J. Wilkinson, P.G.C. Campbell and P. Couture, Can. J. Fish. Aquat. Sci., 47 (1990) 1446.
[37] L. Havelkova and M. Bartuske, Collect. Czech. Chem. Commun., 34 (1969) 3722.

ELSEVIER

Analytica Chimica Acta 299 (1994) 269–275

ANALYTICA CHIMICA ACTA

Convenient and sensitive chemiluminescent detection system for 2-furancarboxylic acid using a continuous-flow method

Mikita Ishii *, Kyoichi Itoh, Yoshiro Yoshihiro, Toshihiro Nakamura

Department of Industrial Chemistry, School of Science and Technology, Meiji University, Higashimita, Tama-ku Kawasaki, Kanagawa 214, Japan

Received 27 July 1993; revised manuscript received 8 July 1994

Abstract

A sensitive and convenient detection system for 2-furancarboxylic acid (2-FA) was developed using a three-channel continuous-flow manifold with chemiluminescence (CL) detection. The CL reaction involves hydrogen peroxide, alkali, alcohol and 2-FA methyl ester. 2-FA is first esterified to methyl 2-furancarboxylate (2-FM) with 70% efficiency. Analytical figures of merit for 2-FM were as follows: detection limit, 1.0×10^{-6} M (signal-to-noise ratio = 2): determination range, 1.0×10^{-6}–0.1 M; sampling frequency, 60 h^{-1}; and reproducibility ($n = 10$), 4.1% R.S.D. for 1×10^{-6} M 2-FM. A correlation between the present method and a gas chromatographic method as a standard was good with a correlation coefficient of 0.999 ($n = 5$). The selectivity towards 2-FA compared with the related species, e.g., furyl methyl ketone, was also good. The recovery for normal human sera was 97–110%.

Keywords: Chemiluminescence; Flow system; 2-Furancarboxylic acid

1. Introduction

Recently, some furan compounds harmful to humans, such as furancarboxylic acid (FA) and polychlorodibenzofuran, have been actively investigated in relation to biomedicine [1–4] and the environment [5,6]. For example, 2-furancarboxylic acid (2-FA) and its derivatives cause albuminoses (e.g., albumin-deficient disease) with a decrease in the so-called albumin bindability owing to their strong affinities. Also, 3-carboxy-4-methyl-5-propyl-2-furanpropionic acid (FPA), which is related to uraemia [4], exists at 15 ± 10 μmol l^{-1} in normal human serum. In cases of uraemia, however, its content increases to 196 ± 63 μmol l^{-1} because of a lack of sedimentation ability; in addition, as the compound cannot be removed from the body even by blood dialysis, a major operation such as an organ transplant needs to be performed. Thus, although some biomedical information on these compounds such as concentrations have been provided for a few of human body fluids and organs, we were confronted with some problems to be clarified concerning the compounds in our studies, e.g., the distribution and/or the role in other body fluids or organs and means for therapy and/or prevention of diseases.

In order to facilitate further FA studies, the development of a highly sensitive and convenient detection tool for 2-FA, which has the core structure for

* Corresponding author.

SSDI 0003-2670(94)00337-8

various kinds of 2-FAs, is essential. The compounds in body fluids exist as unstable species and at low concentrations. Some 2-FAs have been successfully determined by gas chromatography (GC) with flame ionization detection [3], liquid chromatography (LC) with UV detection [4] and GC–mass spectrometry (GC–MS) [2,4]. Although GC and GC–MS are convenient and sensitive for determination with the detection limits of ca. 10^{-3} and ca. 10^{-6} M, respectively, these techniques need to be improved with respect to sensitivity and convenience in use in order to contribute to further FA studies.

As chemiluminescence (CL) analysis has some advantages such as sensitivity, ease of use and simple instrumentation, it has been actively investigated for the highly sensitive detection of small amounts of chemical species at ultra-trace levels [7–14]. Also, it is well known that CL analysis can be further improved with respect to reproducibility and selectivity by combination with a flow-injection method.

Prior to developing a sensitive and convenient CL detection technique for a wide variety of FAs, commercially available 2-FA was investigated for CL production. A new CL reaction system applicable to the determination of small amounts of 2-FA was developed consisting of hydrogen peroxide–alkali–alcohol–2-FA ester. As this CL reaction system can be also easily combined with a flow-injection technique, the combined system is promising as an economical, sensitive, convenient and rapid detection method for 2-FA which is operatable at room temperature with satisfactory reproducibility.

In this paper, the instrumentation and analytical characteristics for a sensitive and convenient 2-FA detection system using a continuous-flow (CF) method combined with the new CL detection system (CF–CL) is described in relation to FA studies.

2. Experimental

2.1. Apparatus

An HP5890A capillary gas chromatograph (Yokogawa, Tokyo) was employed according to Spiteller's method [3]. An H-11N centrifuge was obtained from Kokusan Enshinki (Tokyo). A Z-8000 Zeeman atomic absorption spectrometer from Hitachi (Tokyo) was used. Water was purified using an RO-10C system (Tokyo Rikakikai, Tokyo).

2.2. Reagents and samples

Analytical-reagent grade reagents as follows were used as received: sulfuric acid was obtained from Nakai Kagaku (Tokyo), nitroblue tetrazolium (NBT), potassium superoxide (KO_2) and some other compounds except for the alcohols listed in Table 1 from Sigma (St. Louis, MO), toluene, 2-furancarboxylic acid and the organic compounds listed in Table 3 from Wako (Osaka), hydrogen peroxide and sodium hydroxide from Tokyo Kasei (Tokyo) and C_1–C_4 alcohols from Kanto Kagaku (Tokyo).

Distilled, deionized water was used throughout; it was checked by AAS that metallic cations such as copper(II) were not present down to the 1×10^{-8} M level.

A 1.0 M stock standard solution of sodium hydroxide was prepared and was diluted as appropriate just before use.

Stock standard sample solutions (0.1 M) such as methyl 2-furancarboxylate (2-FM) esterified from 2-FA were prepared with alcohols and the solutions were stable for at least 1 week; these samples were used as standards; the solutions were also diluted with alcohols as appropriate before use.

Unstable reagents such as hydrogen peroxide, NBT and KO_2 were freshly prepared each time; the solutions were used after dilution with water.

The cross-check samples were prepared as 0.01 M and 1×10^{-3} M 2-FM solutions in methanol as the detection limit of GC was low [3].

Some normal human serum samples for recovery tests were prepared as follows. Normal human blood collected with a commonly used, commercially available vacuum-type blood sampler was centrifuged for 15 min at 3000 rpm. The supernatant obtained was mixed 1 + 1 with methanol and the solution was filtered with a Millipore filter (Sumitomo, Tokyo). The solution thus obtained was mixed with the 2-FM standard solution for the recovery test.

2.3. CF–CL system

A flow diagram of the CF–CL system for 2-FA is shown in Fig. 1. The components employed in previ-

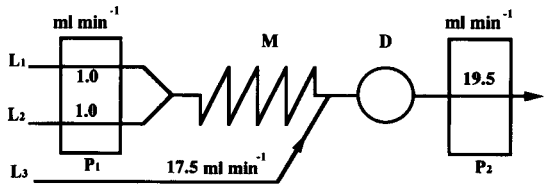

Fig. 1. Schematic diagram of the flow system. L_1–L_2 = flow manifold; D = detector; M = 1-m mixing coil; P = peristaltic pump. Optimum operating conditions: L_1, 1 M NaOH; L_2, 2.1% H_2O_2; L_3, sample.

ous work [15] were used. The continuous sample feeding method was also selected to improve the sensitivity. As the coexistence of hydrogen peroxide with alkali causes consumption of hydrogen peroxide by the reaction, they were separately placed in the manifolds L_1 and L_2 (made of 1 mm i.d. and 2 mm o.d. PTFE tubing) connected with a peristaltic pump (P_1 = SJ-1220; Atto, Tokyo; Tygon pump tubing, 2 mm i.d. and 3 mm o.d.), and they were mixed in a 1 m × 1 mm i.d. × 2 mm o.d. PTFE mixing coil (M). The system consisted of a three-channel manifold including a sample feeding manifold (L_3) connected to the outlet of the mixing coil. The distance from the sample introduction point to the inlet point of the detector was set at about 5 cm, as short as it could possibly be, as the rate of the CL reaction was very high. The spiral flow cell (1 m × 1 mm i.d. × 2 mm o.d.) for the detector was made of poly (vinyl chloride). The cell and pump P_2 (AP-7000; Atto, Tokyo) tubing was also protected from organic solvents such as acetone by dilution with water from the manifolds L_1 and L_2; as 2-FA ester is insoluble in water, it should be dissolved in an organic solvent such as an alcohol. The CF–CL system with suction-type sample feeding was designed as described previously [16].

3. Results and discussion

3.1. Preliminary experiments with a batch system

Concerning the new CL reaction system, two CL responses (current intensity) of methanol and 2-FM–methanol as shown in Fig. 2 were obtained with a commonly used batch system [17]. Fig. 2A shows the CL for a hydrogen peroxide–alcohol–alkali reaction (so-called background CL; BG-CL) and Fig. 2B the CL of 2-FM along with the BG-CL.

The BG-CL is produced by the reaction of hydrogen peroxide, alkali and small amounts of metallic species such as copper(II) in the reagents and/or water [18]; the CL is especially enhanced in methanol solution. As the BG-CL should be lower in order to increase the sensitivity [the signal-to-noise ratio (S/N)], methanol should be isolated from other reagents. Since, as described later, the proposed CL reaction was related to active oxygen produced by the reaction of hydrogen peroxide and sodium hydroxide, mixing of the two reagents should be performed for the sufficient production of active oxygen.

A sharp CL response for 2-FM was observed; this CL profile shows that the rate of the CL reaction is higher than that of BG-CL. Therefore, it was required for the design of the CF–CL system that the sample should be fed at a higher speed. In addition, a higher rate of the CL reaction can contribute to a decrease in BG-CL intensity.

These observations were utilized for the optimum design of the flow system as shown in Fig. 1.

3.2. Esterification of 2-FA to 2-FM

The esterification was performed by the methanol–sulfuric acid–toluene reaction according to Fischer's esterification method [19]. The esterifi-

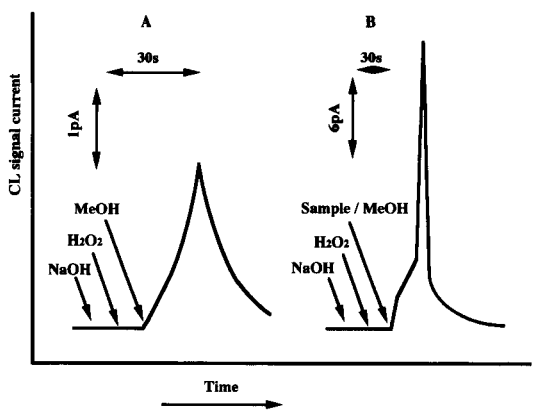

Fig. 2. CL signals obtained with the batch system. Operating conditions: introduction of 2 ml of each reagent solution, 1 M NaOH, 0.9% H_2O_2; solvent, CH_3OH; sample, 1×10^{-2} M 2-FM in CH_3OH. (A) Background; (B) sample.

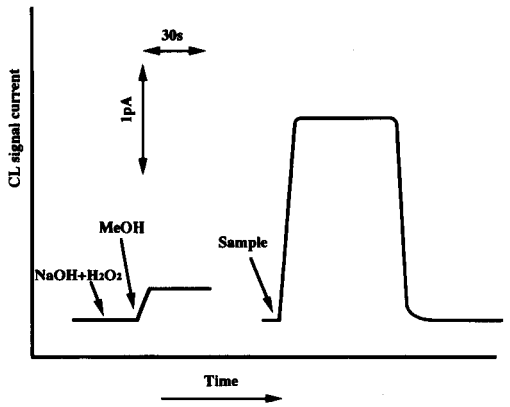

Fig. 3. CL signals obtained with the flow system. Operating conditions: 1 M NaOH, 0.9% H_2O_2; Solvent, CH_3OH; sample, 1×10^{-4} M 2-FM in CH_3OH.

cation ratio of 2-FA to 2-FM was determined by GC for 2-FA concentrations ranging from 0.1 to 1×10^{-3} M. The result for each test sample showed a value of 70.5–70.6% (average 70.5%) at room temperature for 10 min with a 1.5–1.8% R.S.D. ($n = 5$).

3.3. CL profile for the proposed flow system

The CL profile obtained with the flow system is shown in Fig. 3. The low signal on the left is the background CL (BG-CL), wherein methanol was introduced from the manifold L_3. The higher CL signal on the right is for the 2-FM solution in methanol; it shows a rising signal from the BG-CL level. Quenching of the signal is caused by consumption of the sample solution. A stable and strong CL signal was obtained, which was usable for the sensitive detection of 2-FM.

3.4. Effect of organic solvents on the CL intensity

Organic solvents such as alcohols sometimes contribute to CL enhancement [16,18]. According to a previous report [18], C_1–C_4 alcohols and six another organic solvents such as acetonitrile were examined to increase the CL intensity.

The results are shown in Table 1 in terms of relative molar CL intensity; methanol showed the strongest CL intensity. Some polar organic solvents, especially alcohols, contributed to the CL enhancement: in our judgement, alcohols can play an important role as trappers of OH radicals for the sufficient production of the active oxygen required for the CL [16]. As methanol produced the strongest CL for 2-FM of all the alcohols tested, the role of alcohols was examined in detail in relation to chemical structure between 2-FA esters and alcohols. The results are given in Table 2.

Effective CL production was obtained when the same functional groups were present in the 2-FA esters and alcohols, e.g., the combinations of 2-MF–methanol, ethyl 2-furancarboxylate (2-FE)–ethanol and propyl 2-furancarboxylate (2-FP)–propanol. Although the reason is not clear, it is presumed that the homology may be related to the production of oxygen-linking hyper-compounds. In subsequent experiments, the homology was adopted for the sensitive CL detection of 2-FM.

Table 1
Effect of various organic solvents on CL intensity of 2-FM

Solvent	Relative molar CL intensity (%)
Methanol	100
Ethanol	95.4
n-Propanol	72.8
n-Butanol	64.1
Acetone	33.4
N,*N*-Dimethylformamide	30.1
Acetonitrile	17.4
Benzene	9.5
n-Hexane	5.4
Cyclohexane	1.5

Operating conditions: 1 M NaOH for manifold L_1, 0.9% H_2O_2 for manifold L_2, 1×10^{-4} M 2-FM in various organic solvents for manifold L_3.

Table 2
Effect of C_1–C_4 alkanols on the CL intensity for 2-FE and 2-FP

Solvent	Relative molar CL intensity (%)	
	2-FE	2-FP
Methanol	20.5	41.0
Ethanol	100	89.7
n-Propanol	72.8	100
n-Butanol	24.3	16.8

Operating conditions: 1 M NaOH for manifold L_1, 0.9% H_2O_2 for manifold L_2, 1×10^{-2} M 2-FE or 1×10^{-2} M 2-FP in C_1–C_4 alkanols for manifold L_3.

3.5. Optimization of concentration and flow-rate of CL reagents

Sodium hydroxide was first characterized for the optimization. Under the conditions of 1×10^{-4} M 2-FM and 0.9% hydrogen peroxide at flow-rates of 1.0 ml min^{-1} for L_1 and L_2 and 15.0 ml min^{-1} for the L_3, sodium hydroxide was examined at concentrations ranging from 1×10^{-3} to 4 M. The CL response was first observed at 1×10^{-2} M and increased with an upward convex rising curve until 1 M. Above 1 M, the CL intensity decreased rapidly owing to quenching.

Next, under the conditions of 1 M sodium hydroxide and 1×10^{-4} M 2-FM, the concentration of hydrogen peroxide was optimized. The strongest CL was obtained at 2.1% hydrogen peroxide with a homogeneous result in the case of sodium hydroxide.

Finally, the flow-rate of the manifolds was optimized under the conditions of 1×10^{-4} M 2-FM, 2.1% hydrogen peroxide and 1 M sodium hydroxide. As the flow-rate of L_1 and L_2 was fixed at 1.0 ml min^{-1} in order to minimize the consumption of CL reagents, L_3 was tested at flow-rate of 1.0–20 ml min^{-1}; the total flow-rate obtained at the detector outlet ranged from 3.0 to 22.0 ml min^{-1}. The CL response was first observed at a total flow-rate of 10.5 ml min^{-1}; the response was maximum at a flow-rate of 19.5 ml min^{-1}, with an upwards convex curve up to the maximum point. Above the maximum point, the CL response decreased because of the too high flow-rate. Therefore, a total flow-rate of 19.5 ml min^{-1} ($L_3 = 17.5$ ml min^{-1}) was adopted as the optimum. The optimum operating conditions for the system were selected as shown in Fig. 1.

3.6. Calibration data

Under the optimum operating conditions, analytical characteristics such as reproducibility and detection limit were investigated for 2-FM.

A calibration graph of 2-FM was constructed on a logarithmic scale between the CL intensity (current intensity, Y, pA) and the molar concentration of 2-FM (X, M). Linearity was obtained for concentrations ranging from 1.0×10^{-6} to 0.1 M with the relationship in $Y = 1.0X + 4.0$; the detection limit was 1.0×10^{-6} M ($S/N = 2$). The detectability at higher concentrations and the wide linear range may be due to the use of highly concentrated sodium hydroxide at a lower flow-rate than that of the sample. The detection limits for 2-FE and 2-FP were similar to that for 2-FM.

The R.S.D.s for ten repeated runs with 1×10^{-2} and 1×10^{-6} M 2-FM were 3.9% and 4.1%, respectively. The reproducibility is good over the wide range of concentration in comparison with the ca. 3% r.s.d. of GC.

The analysis time for one 2-FM determination was less than 1 min with a sampling rate of 60 h^{-1}; the analysis time including the esterification to 2-FM was 15 min, which is 30 min shorter than that using GC.

Table 3
Effect of coexsisting substances on the CL intensity for 1×10^{-4} M 2-FM

Species (1×10^{-3} M in CH_3OH)	Relative error (%)
2-FE	233
2-FP	225
Furyl methyl ketone	756
Methyl crotonate	20.3
Furfurylamine	−27.3

Operating conditions as in Fig. 1 with a 1×10^{-4} M 2-FM solution in methanol. Ethyl acetate, vinyl acetate, *n*-butyl acrylate, methyl benzoate, 2-furancarboxylic acid, furfuryl alcohol, methyl methacrylate, tetrahydrofuran and thiophene did not interfere with the CL signal for 2-FM.

3.7. Effect of coexisting substances on the CL intensity

In order to observe the CL behaviour of the proposed CL reaction system in the presence of different substances, fifteen kinds of organic compounds as listed in Table 3 were examined under the optimum operating conditions and their relative molar CL intensities were compared. 2-FM provided the strongest CL; the next was furyl methyl ketone with 8.7% CL intensity compared with the 2-FM standard (100%). Other FA esters, 2-FE and 2-FP gave rise to a weak CL intensity of about 2.8% compared with the standard; this result is due to the difference in homogeneity between the ester and its corresponding alcohol. Other compounds were within ca. 1% com-

pared with the standard, except for ca. 0.2% quenching by methyl methacrylate. Although a clear relationship between the chemical structure and the CL intensity was not revealed, some compounds having a saturated hydrocarbon, methyl ester and/or furyl structure in the molecule seem prone to give rise to CL.

Next, the interference in 2-FM determination of the coexistent substances listed in Table 3 was examined at concentrations of 1×10^{-2}, 1×10^{-3} and 1×10^{-4} M. The effects of foreign substances were expressed in terms of the relative error with respect to the CL intensity of 1×10^{-4} M 2-FM alone. The results are given in Table 3. The test substances at 1×10^{-3} and 1×10^{-4} M concentrations did not interfere with the CL signal of 1×10^{-4} M 2-FM. Some substances, such as furyl methyl ketone, first interfered with the CL signal of 2-FM at concentrations over 0.01 M; the results showed the same tendency as those in the study of their CL production behaviour. Although interference was observed from 2-FE, 2-FP, furyl methyl ketone, methyl crotonate and furfurylamine, the concentration of 2-FM was 100 times lower than that of the coexisting substances. As interfering substances such as furyl methyl ketone are not known to coexist with FA esters in organs and body fluids at high levels, the present CL system is sufficiently specific for 2-FM detection.

3.8. Correlation with GC data and recovery

The correlation between the present method and the convenient standard GC method [3] was evaluated. The correlation was good with correlation coefficients of 99.9% ($n = 5$) for both 0.01 and 1×10^{-3} M sample solutions.

The result of the recovery test are given in Table 4. The recovery was good, 97–110% (R.S.D. $\approx$ 4%).

Table 4
Recovery of 2-FM from normal human serum

Sample No.	Taken (10^{-6} M)	Found (10^{-6} M)	Recovery (%)	R.S.D. (%)
1	0	6.8±0.3	–	4.2
	1.0	7.9±0.3	110	4.0
	5.0	12.0±0.5	104	4.1
	10.0	16.5±0.7	97	3.8
	20.0	26.9±1.1	101	3.0
2	0	7.2±0.3	–	3.8
	1.0	8.3±0.4	110	4.2
	5.0	12.3±0.5	102	3.6
	10.0	16.9±0.6	97	3.5
	20.0	27.0±1.3	99	3.4
3	0	6.7±0.3	–	3.9
	1.0	7.8±0.4	110	3.7
	5.0	11.8±0.6	102	3.7
	10.0	16.7±0.8	100	3.5
	20.0	26.8±1.0	101	3.3
4	0	6.8±0.3	–	4.0
	1.0	7.9±0.4	110	4.1
	5.0	11.7±0.5	98	3.7
	10.0	16.9±0.8	101	4.1
	20.0	26.5±1.1	99	3.1
5	0	7.0±0.3	–	4.0
	1.0	8.1±0.4	110	4.3
	5.0	11.9±0.6	98	3.9
	10.0	17.2±0.8	102	3.5
	20.0	27.2±0.9	101	3.1

Operating conditions as in Fig. 1; five repeated runs for each sample.

3.9. Mechanism of the CL reaction

Furan compounds such as tetrahydrofuran easily produce some hyper-compounds by reaction with active oxygen [16]. Especially concerning the proposed CL reaction, alcohols play a key role in the CL enhancement; it has been reported [18,20] that alcohols play an important role as trappers of OH radicals. As OH radicals are produced by the reaction of hydrogen peroxide with alkali in the present CL system, the CL reaction will be accelerated by trapping OH radicals with alcohols. Therefore, the reverse reaction to the trapping of OH radicals, i.e., the reaction to produce superoxide anion radicals ($O_2^{-\cdot}$) is presumed to be the key to CL production. The 2-FM CL mechanism was investigated in relation to active oxygen.

In order to examine the effect of $O_2^{-\cdot}$ on the present CL, NBT (an $O_2^{-\cdot}$ trapper) and potassium superoxide (KO_2: an $O_2^{-\cdot}$-producing reagent) were added to the CL reaction system. The CL intensity on NBT addition decreased until it was about one third in comparison with that with no addition. The result of the KO_2 effect is shown in Fig. 4; the pH of the test solution was controlled with sodium hydroxide as dissolution of KO_2 in water produces hydroxy anions and changes pH of the solution. The addition

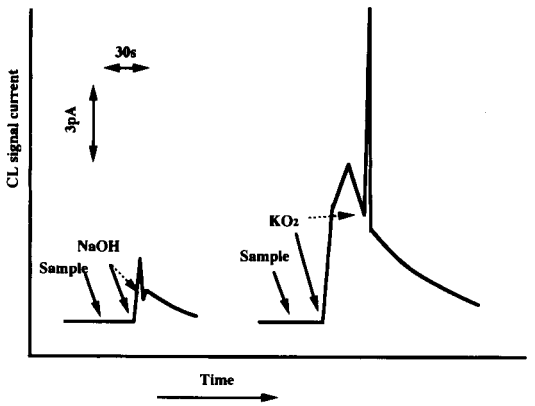

Fig. 4. Comparisons of CL intensity and profile obtained with the batch system, with and without KO_2 addition. Operating conditions: introduction of 2 ml of each reagent solution, 10^{-2} M KO_2 or none (NaOH, pH. 11.7); sample, 1×10^{-2} M 2-FM in CH_3OH.

of KO_2 gave rise to stronger CL than in its absence. These two results show that $O_2^{-\cdot}$ is related to the present CL. On the other hand, the effect of thiophene (an S-heterocyclic compound) on the CL was examined since S-compounds sometimes act as radical scavengers which may quench or decrease the CL; the addition of thiophene gave rise to no emission. These results show that the CL is related to active oxygen and a radical reaction. Further studies on the CL mechanism are in progress.

4. Conclusions

A sensitive and convenient 2-FM detection technique was established by a continuous-flow method combined with a new CL detection system. The present CL technique is more sensitive than GC and more economical and convenient in use than GC–MS. The present technique is also usable for the easy and rapid detection of 2-FA. However, concerning the selective detection among related 2-FA compounds such as 2-FM and 2-FE, combination of a separation technique such as LC with the present technique may be preferable. Studies on further selective detection are in progress with a view to the application of the present CL technique to some biomedical and environmental studies.

References

[1] A. Roger, T. Kariya, J. Martin and V. Petrow, J. Med. Chem., 20 (1983) 781.
[2] D.M. Sand, H. Schlenk, H. Thoma and G. Spiteller, Biochim. Biophys. Acta, 751 (1983) 455.
[3] M. Spiteller and G. Spiteller, J. Chromatogr., 164 (1987) 253.
[4] T. Niwa, N. Takeda, K. Maeda, M. Shibata and A. Tatematsu, Clin. Chim. Acta, 173 (1988) 127.
[5] R. Watanuki and H. Kawamura, Dokubutu-Daiokishin, Gizyutu to Ningen, Tokyo, 1986, p. 1.
[6] T. Yamagishi, Chemosphere, 10 (1981) 1137.
[7] L.J. Kricka and G.H.G. Thorpe, Analyst, 108 (1983) 1274.
[8] H. Hoshino and W.L. Hinze, Anal. Chem., 59 (1987) 496.
[9] K. Hool, T.A. Nieman, Anal. Chem., 60 (1988) 834.
[10] M. Ishii and M. Yamada, Bunseki, (1989) 442; (1994) 452.
[11] A. Townshend, Analyst, 115 (1990) 495.
[12] M. Ishii, Y. Ohno and T. Hobo, Anal. Sci., 7 (1991) 873.
[13] M. Ishii and M. Shirai, Bunseki Kagaku, 41 (1992) 125.
[14] K. Robards and P.J. Worsfold, Anal. Chim. Acta, 266 (1992) 147.
[15] M. Ishii, Anal. Sci., 7 (1991) 703.
[16] M. Ishii and K. Itoh, Bunseki Kagaku, 41 (1992) 433.
[17] M. Ishii, T. Takahashi and S. Babasaki, in Proceedings of the 52nd Symposium on Analytical Chemistry, Obihiro, May 1991, p. 415.
[18] M. Ishii, M. Yamada and S. Suzuki, Bunseki Kagaku, 35 (1986) 373.
[19] Kagaku Daijiten Hensyu Iinkai (Chemical Society of Japan), Encyclopaedia Chimica, No. 7, Kyoritsu Syuppan, Tokyo, 1962 p. 650.
[20] N. Ueda and N. Kaneda, Kasankasisitsu Zikkenhou, Ishiyaku Syuppan, Tokyo, 1983, p. 119.

ELSEVIER

Analytica Chimica Acta 299 (1994) 277–284

ANALYTICA CHIMICA ACTA

Determination of lactate by the intrinsic fluorescence of lactate oxidase

J. Galbán *, S. de Marcos, P. Segura, J.R. Castillo

Department of Analytical Chemistry, Faculty of Sciences, University of Zaragoza, E-50009 Zaragoza, Spain

Received 26 April 1994; revised manuscript received 19 July 1994

Abstract

A fluorimetric method for the determination of lactate based on its enzymatic reaction with lactate oxidase (LOx) is proposed. The method relies on the relationship between the decrease in the enzyme intrinsic fluorescence during the reaction and the lactate concentration, which is shown to be the result of a primary internal filter effect on the enzyme by the pyruvate formed in the reaction. A mathematic model for predicting the effect of some parameters on the magnitude of the analytical signal was developed that provided good correlations with the experimental results. All those experimental variables affecting the analytical signal were optimized. Under the best possible conditions, the method features a linear determination range from 4 to 25 mg/l lactate and a reproducibility of 3.5%, as the relative standard deviation. The proposed method allows lactate and pyruvate to be determined simultaneously. The predictions of the proposed model were also quite consistent with the experimental results obtained for synthetic samples containing both species.

Keywords: Enzymatic methods; Fluorimetry; Lactate

1. Introduction

Instrumental methods of analysis based on enzyme reactions feature a high selectivity resulting from the specificity of the enzyme used to a single substrate: the analyte. Redox enzyme reactions are of special interest in this context, particularly those involving the coenzyme NAD (and a dehydrogenase) or dissolved oxygen (and an oxidase). Because the participants of these enzyme reactions are typically substances involved in various biological processes, methods for the determination of any such participant are potentially of high interest.

Enzyme reactions can be monitored by optical methods based on the properties of one of the reaction participants [1]. However, when none of the species involved in some reactions exhibits appropriate spectroscopic properties, such reactions must be coupled to a second reaction (whether enzymatic or otherwise) involving a spectroscopically active species. An example involving oxygen and an oxygenase is

$$L + O_2 \overset{LOx}{\rightleftharpoons} P + H_2O_2 \qquad (1)$$

where L denotes lactate, P pyruvate and LOx lactate oxidase. In order to determine lactate (or, in general, the substrate), the reaction is usually coupled to another one in which the hydrogen peroxide formed gives a chemiluminescent oxidation reaction with reagents such as lucigenin or luminol [2], or oxidizes a spectroscopically active organic dye [3]. Alternatively, the hydrogen peroxide can be monitored by means of an

* Corresponding author.

SSDI 0003-2670(94)00349-1

enzyme electrode [4], where the typically low sensitivity of this type of determination can be increased by using an amplification reaction [5,6].

One scarcely explored alternative to monitoring the above reactions relies on optical properties. Thus, some enzyme species exhibit intrinsic fluorescence that can be altered by various external factors (e.g., quenching effects) [7], use of which avoids the need to introduce a coupled reaction.

Following previous research, in this work a new method was developed for the enzymatic determination of lactate based on the proportionality between the decrease in the intrinsic fluorescence of the enzyme lactate oxidase (LOx) during the reaction (1) and the lactate concentration. The method also allows lactate and pyruvate to be determined simultaneously in mixtures, thereby opening up new avenues for approaching this type of determinations.

2. Experimental

2.1. Apparatus and reagents

All measurements were made on a Perkin-Elmer LS 50 luminometer.

The reagents used included the following:

- A buffer of pH 7.0 made from 0.1 M citric acid and 0.1 M disodium hydrogenphosphate.
- A lactate oxidase solution containing 20 IU/ml of the enzyme in the previous buffer, made from a Sigma L-0638 (50 IU/ml) chemical. The solution was prepared freshly before use and kept in an ice bath during experiments. Under these conditions, it remained stable for at least one day.
- A 100 mg/l L-(+)-lactate solution prepared from lithium lactate (Sigma L-2250) in the same buffer.
- A 100 mg/l pyruvate solution made from sodium pyruvate (Sigma P-2256) in the above buffer immediately prior to use.
- A 30%, w/v, stock solution of H_2O_2 from which working-strength solutions were prepared by dilution as required. The stock was periodically iodometrically standardized.

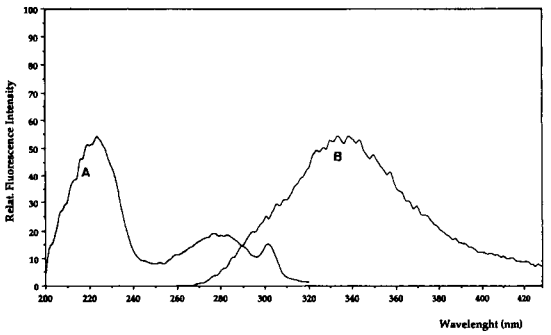

Fig. 1. (A) Excitation ($\lambda_{em}=335$ nm) and (B) emission ($\lambda_{ex}=225$ nm) spectra of (0.10 IU/ml) lactate oxidase (LOx) in phosphate buffer.

2.2. Procedure

A 2-ml aliquot of the buffered lactate solution containing between 4 and 25 mg/l was placed in the luminometer cuvette and supplied with 0.050 ml of 20 IU/ml LOx under continuous stirring. After 10 s, the fluorescence intensity of the solution was measured at $\lambda_{exc}=225$ nm and $\lambda_{em}=335$ nm. A new measurement was made after a further 30 s. The data thus obtained were used to calculate the reaction rate (measurement parameter), given by

$$\Delta I/I_0=(I_0-I_{30})/I_0 \qquad (2)$$

where I_0 and I_{30} denote the initial fluorescence intensity ($t=0$) and that after 30 s ($t=30$ s).

3. Results and discussion

3.1. Recording and origin of the analytical signal

Many enzymes show native fluorescence that can be attributed to tyrosine and tryptophan groups present in their molecules; in general, tyrosine's contribution is very low because of both its low molecular absorptivity and the existence of quenching by tryptophan groups (normally by a energy transfer process). As a result of that, fluorescence spectra of enzymes are more similar to the tryptophan spectrum [8]. Fig. 1 shows the excitation and emission spectra for LOx. It exhibit two excitation maxima at 225 and 280 nm, as well as an emission maximum at 335 nm; essentially consistent with the spectra for other enzymes. While the shape of both spectra was found to be independent of the type

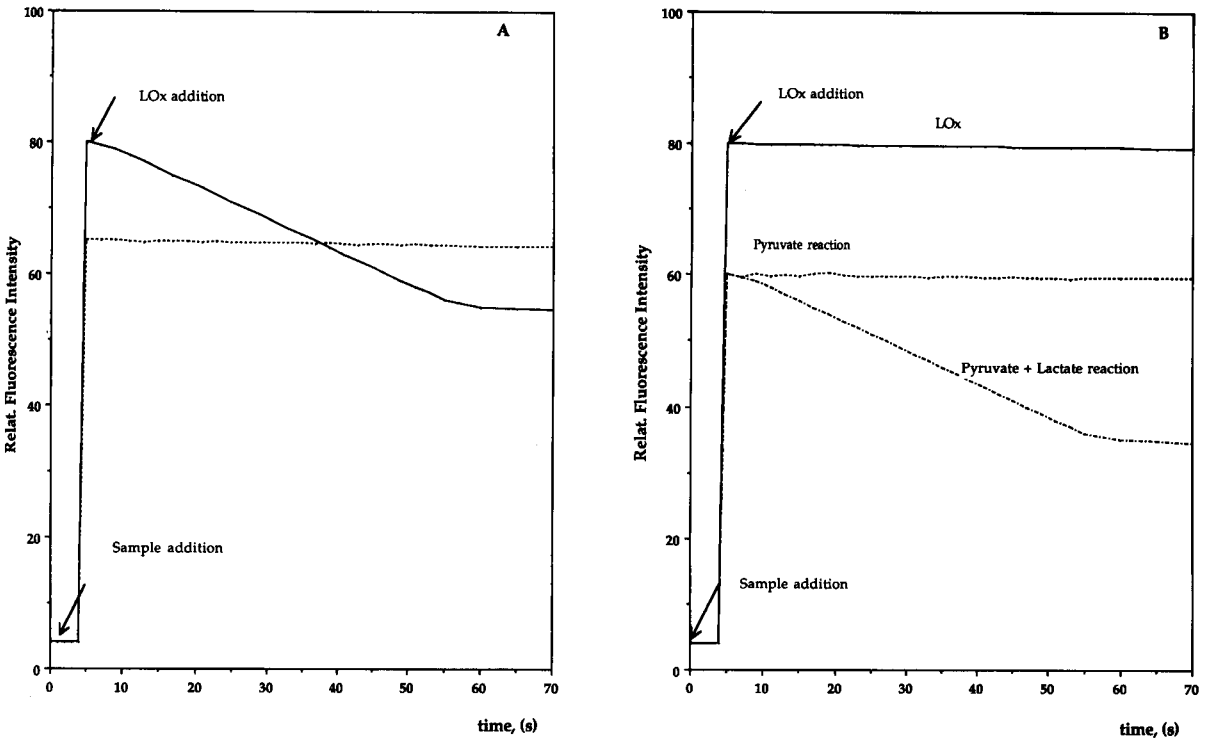

Fig. 2. (A) Fluorescence intensity variation during the enzymatic reaction: (——) 225–335 nm and (·····) 280–335 nm, [LO] = 0.15 IU/ml and [lactate] = 1.0×10^{-4} M. (B) Variation of LOx (0.15 IU/ml) fluorescence intensity (225–335 nm) with pyruvate [2.9×10^{-4} M] (·····) and pyruvate + lactate [2.9×10^{-4} M and 1.0×10^{-4} M, respectively] (-·-·-) addition.

of buffer used, their intensity was markedly affected by the choice; thus, a glycine–hydrazine–EDTA buffer (frequently used in this type of determination) had a strong quenching effect on the fluorescence, whereas a phosphate buffer ensured constancy of the fluorescence intensity at considerably high levels. The enzyme fluorescence intensity in this latter buffer was found to vary linearly with its concentration in the cuvette up to 0.75 IU/ml according to the following equation:

$$I_0' = 492.7[\mathrm{LOx}] + 9.3$$

$r = 0.998$ (note that I_0' is used to term the fluorescence intensity obtained when only LOx is present in the solution).

As can be seen from Fig. 2A, addition of the enzyme to a lactate solution gradually decreased its fluorescence intensity to an extent proportional to the lactate concentration in solution; the variation was different for the two excitation–emission line pairs for the enzyme, viz. 225–335 and 280–335 nm; in fact, changes in the former were much more pronounced than in the latter, so the 225–335 nm line was chosen for further experiments. The original fluorescence intensity was not regained with time, but rather levelled off at a much lower level relative to the initial value at the end of the reaction.

In order to account for this variation, one should take account of the effect of the different reaction ingredients on the LOx fluorescence. In this respect, one should consider that, because it involves an oxygenase, the enzyme reaction (1), takes place in three steps, namely:

$$\mathrm{LOx} + \mathrm{O_2} \underset{k_{-1}}{\overset{k_1}{\rightleftharpoons}} \mathrm{LOx \cdot O_2} \qquad (1a)$$

$K_1 = k_1/k_{-1}$.

$$\mathrm{LOx \cdot O_2} + \mathrm{L} \underset{k_{-2}}{\overset{k_2}{\rightleftharpoons}} \mathrm{LOx \cdot H_2O_2} + \mathrm{P} \qquad (1b)$$

$K_2 = k_2/k_{-2}$.

$$\mathrm{LOx \cdot H_2O_2} \overset{k_3}{\rightarrow} \mathrm{LOx} + \mathrm{H_2O} \qquad (1c)$$

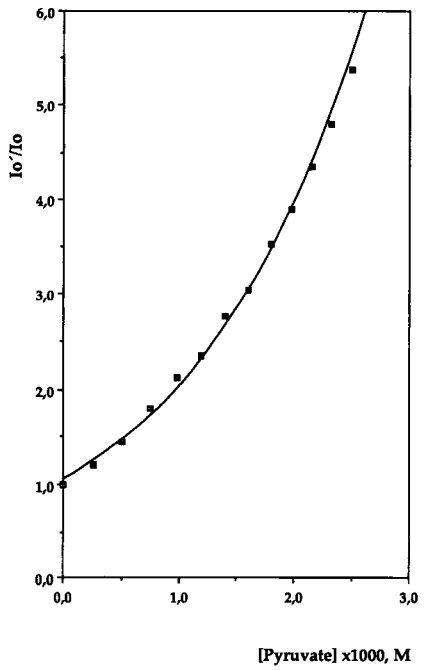

Fig. 3. Variation of I_0'/I_0 fluorescence intensity (225–335 nm) with pyruvate concentration.

(rds).

Contrary to the expectations, the enzyme fluorescence was not affected by oxygen. Thus, the fluorescence intensity of LOx in a normal and an oxygen-saturated aqueous solution was quite similar. Therefore, the formation of the $LOx \cdot O_2$ complex in reaction (1a) does not affect the enzyme fluorescence.

Adding various amounts of pyruvate to an enzyme solution caused a sharp decrease in its fluorescence intensity; the effect was instantaneous and invariable over time (i.e., $I_0 = I_{30}$) (Fig. 2B). The effect of the pyruvate concentration on the enzyme fluorescence intensity did not occur conform to the ordinary Stern-Volmer equation, but rather to an exponential equation of the following type (Fig. 3):

$$I_0'/I_0 = \exp(292.7[P]_0) \qquad (3)$$

($r = 0.994$) where $[P]_0$ is the pyruvate concentration at $t = 0$.

This equation accounts for two rather different types of quenching effects, namely: (a) action sphere quenching [9], and (b) quenching by a primary internal filter effect [7]. Calculations based on the action sphere model led to an inconsistent enzyme molecular size. On the other hand, based on the primary internal filter effect approach, the multiplication factor of 292.7 in Eq. 3, was consistent with the molar absorptivity for pyruvate at the working wavelength (Fig. 4) taking into account that, as shown by Henderson [10], the pathlength of the fluorimeter cuvette does not coincide with its physical length (1 cm).

Finally, addition of various amounts of H_2O_2 to an LOx solution also decreased the fluorescence intensity to a low level that remained essentially invariable with time ($I_0 = I_{30}$) (Fig. 5), as with pyruvate. The effect did not occur conform to the ordinary Stern-Volmer equation either, but fitted the following exponential equation:

$$I_0'/I_0 = \exp(38.9[H_2O_2]_0)$$

($r = 0.997$) the multiplication factor being consistent with the molar absorptivity of H_2O_2 (Fig. 4) at the working wavelength (225 nm). Accordingly, the formation of the $LOx \cdot H_2O_2$ complex has an additional quenching effect.

In summary, the decrease in the LOx fluorescence for the 225–335 nm line during the enzyme reaction can be ascribed to the formation of pyruvate and hydrogen peroxide, which exert a primary internal filter effect and the disappearance of lactate, which has no such effect (Fig. 4). It should be noted that the quenching effect from pyruvate is more marked than that exerted by H_2O_2 (the molar absorptivity of the former is ca. eight-fold that of the latter); taking into account that the amounts of the two species formed in the reaction

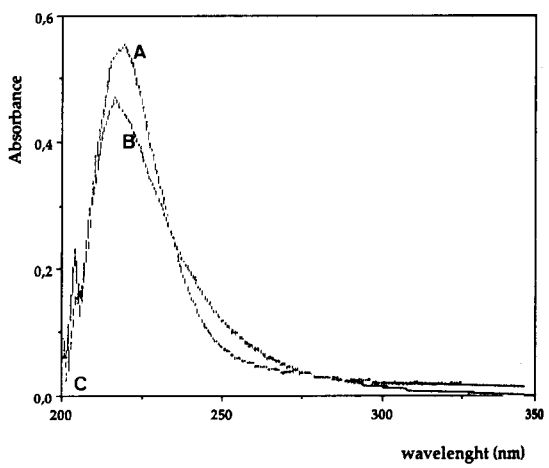

Fig. 4. Molecular absorption spectra of (A) 4.8×10^{-4} M pyruvate, (B) 4.7×10^{-3} M hydrogen peroxide and (C) 1.0×10^{-4} M lactate.

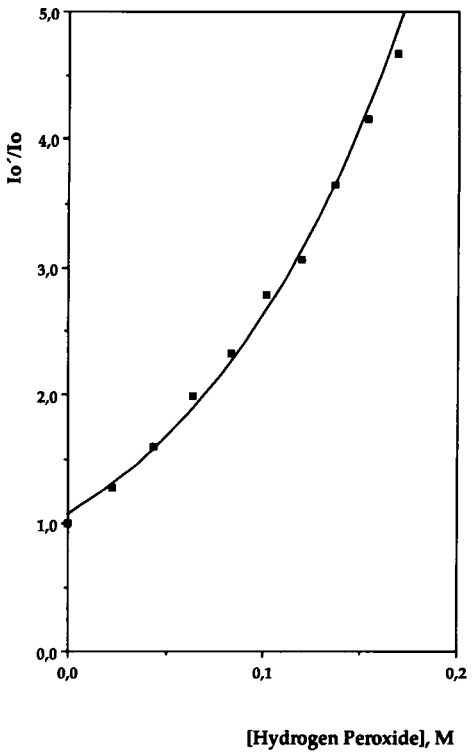

Fig. 5. Variation of I_0'/I_0 (225–335 nm) with H_2O_2 concentration.

are identical, the loss of enzyme fluorescence during the reaction can be virtually exclusively assigned to the formation of pyruvate. This is also the reason why no appreciable fluorescence loss was observed in the 280–335 nm line.

3.2. Mathematical model

As noted earlier, the reaction rate [Eq. (2)] was chosen as the measurement parameter. Taking into account that the fluorescence loss was due to the internal filter effect from pyruvate [Eq. (3)],

$$\Delta I/I_0 = 1 - \exp(-292.7[P]_{30}) \quad (4)$$

In order to better model $\Delta I/I_0$, $[P]_{30}$ should be expressed as a function of the initial lactate and enzyme concentrations ($[L]_0$ and $[LOx]_0$, respectively). This entails considering some aspects of the process, namely:

(a) The oxygen used in the reaction is that dissolved in water, the concentration of which remains constant throughout the process since the solution is in continuous contact with the atmosphere. Therefore, the starting enzyme solution actually contains the $LOx \cdot O_2$ complex. All the enzyme released in step (1c) above reacts with the oxygen to give $LOx \cdot O_2$, so

$$[LOx \cdot O_2]_{30} = [LOx \cdot O_2]_0 = [LOx]_0 \quad (5)$$

(b) This enzyme reaction allows for several assumptions applicable to other enzyme reactions to be made, namely:

- The lactate concentration remains virtually constant at its initial value during the first 30 s of reaction, so:

$$[L]_{30} = [L]_0 \quad (6)$$

- The pyruvate concentration formed in the first few seconds of reaction is very small, so

$$k_{-2}[P] + k_3 = k_3 \quad (7)$$

- The steady-state approximation ($d[LOx \cdot H_2O_2]/dt = 0$) holds, so

$$d[LOx \cdot H_2O_2]/dt = 0$$
$$= k_2[LOx][L] - k_{-2}[LOx \cdot H_2O_2][P] - k_3[LOx \cdot H_2O_2]$$

which, taking into account the implications of Eqs. (5)–(7), can be simplified to

$$[LOx \cdot H_2O_2] = k_2[LOx]_0[L]_0/k_3 \quad (8)$$

By calculating the rate of formation of pyruvate [reaction (1b) above], substituting $[LOx \cdot H_2O_2]$ from Eq. (8) and integrating between $t = 0$ and $t = 30$, one obtains

$$[P]_{30} = (k_3/k_{-2})(1 - \exp[-(30k_{-2}k_2/2.302k_3) \times [LOx]_0[L]_0]) \quad (9)$$

substitution of which into Eq. (1b) yields the sought relationship. This equation admits two general simplifications, namely:

(i) If $[L]_0$ or $[LOx]_0$ is small enough, then Eqs. (4) and (9) can be expanded into two mathematical series as follows: at small x values, the second-order and higher terms can be considered negligible,

$$1 - 10^{-x} = 2.302x - (2.302x)^2/2! + (2.302x)^3/3..... \quad (10)$$

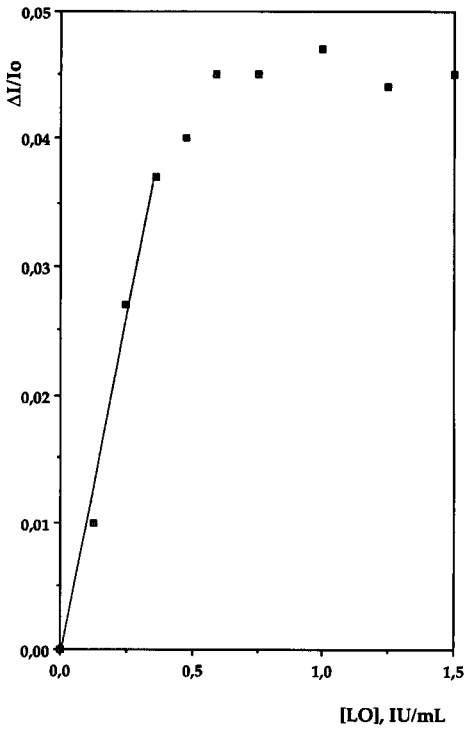

Fig. 6. $\Delta I/I_0$ variation, (225–335 nm), with LOx concentration, [lactate] = 2.1×10^{-4} M.

so Eqs. (4) and (9) can be simplified and rearranged to

$$\Delta I/I_0 = 3811 k_2 [\mathrm{LOx}]_0 [\mathrm{L}]_0 \qquad (11)$$

(ii) At large $[\mathrm{L}]_0$ or $[\mathrm{LOx}]_0$ values, the following assumption can be made:

$$1 - 10^{-x} = 1$$

which, based on Eqs. (4) and (9), yields

$$\Delta I/I_0 = k_3/k_{-2} \qquad (12)$$

3.3. Optimization of parameters

The parameters most markedly influencing the reaction rate and hence $\Delta I/I_0$ were found to be the type of buffer used, the pH and the enzyme concentration. A careful study of the effect of the enzyme concentration on the analytical signal revealed 0.75 IU/ml to result in the maximum possible rate (Fig. 6). This is essentially consistent with the predictions of the proposed model that $\Delta I/I_0$ should be linearly related to the enzyme concentration at low values [Eq. (11)], but independent of it at high values [Eq. (12)]. The maximum $\Delta I/I_0$ value was found to be 0.55, which supports the simplification made in Eq. (7).

As noted earlier, the buffer used influenced the initial fluorescence intensity of the enzyme, as well as $\Delta I/I_0$. A careful study of the effect (Table 1) revealed the optimum buffer solution to be one consisting of citric acid and disodium hydrogenphosphate at pH 7.00; in fact, the reaction hardly developed at very low or very high pH values due to the denaturation of the enzyme, which is reflected in a sharp increase in the fluorescence intensity arising from the release of tyrosine and tryptophan residues from the LOx molecule. We tested other procedures in order to improve the sensitivity of the analytical signal including the use of various surfactants and several enzyme species. Surfactants are known to enhance fluorescence signals by formation of stable micellar aggregates. We tested both cationic (hexadodecyltrimethylammonium bromide, HDTAB), anionic (lauryl sulphate, LS) and neutral surfactants (Triton X-100). The ionic surfactants had no appreciable effect on the shape of spectra or the reaction rate, and only HDTAB caused a slight absolute increase in the enzyme signal, with no alteration to the analytical signal. Triton X-100 caused a spectral shift arising from its own fluorescence properties and an increase in the

Table 1
Variation of the $\Delta I/I_0$ ratio with the pH of various buffers ([LOx] = 0.50 IU/ml and [lactate] = 1.0×10^{-4} M)

Buffer	pH								
	4.0	5.0	6.0	6.5	7.0	7.5	8.0	9.0	10.0
Citric acid—HPO_4^{2-}	0.009	0.010	0.015	0.016	0.017	0.015	0.009		
Tris—HCl					0.009	0.011	0.010		
$H_2PO_4^-$–HPO_4^{2-}				0.009	0.012	0.012	0.009		
Glycine–NaOH						0.010	0.010	0.009	0.009

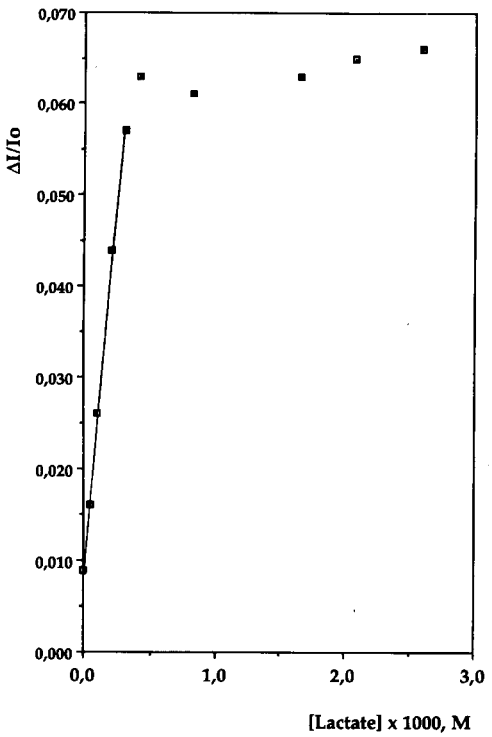

Fig. 7. $\Delta I/I_0$ (225–335 nm) variation with lactate concentration, [LOx] = 0.50 IU/ml.

overall signal intensity, but had an adverse effect on the rate of the enzyme reaction that remained constant at various pH values. As regards the use of additional enzymes potentially enhancing the fluorescence of LOx, we tested mixtures of this and lactate dehydrogenase (LDH), which exhibits fluorescent properties similar to those of LOx. The spectra for various mixtures of the two enzymes in different proportions, but having the same overall enzyme activity, exhibited an increased initial fluorescence that was accompanied by a decrease in the reaction rate with increase in the proportion of LDH in the mixture.

3.4. Analytical figures of merit

Fig. 7 shows the variation of the $\Delta I/I_0$ ratio as a function of the lactate concentration. The results are consistent with the predictions of the proposed model (a linear relationship was observed at low lactate concentration that disappeared at higher concentrations). As can be seen, the linear response range was from 5.2×10^{-5} to 3.1×10^{-4} M of lactate (4–25 mg/l), which follows the equation (obtained by the least squares regression method)

$$\Delta I/I_0 = 0.009 + 158.1[\mathrm{L}]_0$$

$$(r = 0.997). \qquad (13)$$

The reproducibility, expressed as the relative standard deviation, was 3.5% ($n=8$), and the detection limit, calculated as twice the standard deviation for the blank ($n=8$), was 1.0 mg/l lactate.

3.5. Simultaneous determination of lactate and pyruvate

As shown above, addition of pyruvate to an LOx solution caused a sharp decrease in the enzyme fluorescence that was proportional to the pyruvate concentration added and given in mathematical terms by Eq. (3). This was exploited for developing a method for the simultaneous determination of lactate and pyruvate in the same sample. Pyruvate shows a moderately high molecular absorptivity that ensures a certain selectivity in the determination.

Fig. 2B shows the effect of adding the enzyme to a solution containing a mixture of lactate and pyruvate; as can be seen, the enzyme fluorescence initially dropped to a very low level and then continued to decrease (more gradually) with time. From the figure it also follows that the initial drop observed was due to the presence of pyruvate, whereas the subsequent decrease was produced by lactate. In order to determine both analytes simultaneously in a mixture it suffices to obtain I_0', I_0 and I_{30} and substitute them into the Eqs. 3 and 13 for pyruvate and lactate determination, respectively. Note that the effect of the pyruvate initially present in the sample has already been subtracted when I_0 and I_{30} are used for lactate determination, and that the presence of this species requires no modification of the proposed mathematical model since the low pyruvate concentrations involved ensure that the approximation of Eq. (7) still holds.

The accuracy of the above is apparent from Tables 2 and 3, which give the I_0'/I_0 and $\Delta I/I_0$ values obtained by using different pyruvate concentrations and a constant lactate concentration (Table 2), and vice versa (Table 3). These results are consistent with the predicted equations; consequently, lactate and pyruvate

Table 2
Variation of I_0'/I_0 and $\Delta I/I_0$ with the pyruvate concentration in the presence of 1.0×10^{-4} M lactate ([LOx] = 0.50 IU/ml)

[Pyruvate] (M)	I_0'/I_0	$\Delta I/I_0$
0.0	0.000	0.017
2.9×10^{-4}	1.213	0.017
5.6×10^{-4}	1.459	0.016
8.2×10^{-4}	1.741	0.016
1.4×10^{-3}	2.552	0.016

Table 3
Variation of I_0'/I_0 and $\Delta I/I_0$ with the lactate concentration in the presence of 2.9×10^{-4} M pyruvate ([LOx] = 0.50 IU/ml)

[Lactate] (M)	I_0'/I_0	$\Delta I/I_0$
0.0	1.213	0.008
1.0×10^{-4}	1.215	0.017
2.1×10^{-4}	1.216	0.027
3.1×10^{-4}	1.214	0.058

Table 4
Results obtained in the determination of lactate and pyruvate in synthetic samples, expressed in mg/l ($n=5$)

Sample	[Lactate]		[Pyruvate]	
	Added	Found	Added	Found
1	20	18±1	15	16±1
2	8	10±0	40	38±2
3	14	13±0	20	20±1

can be determined in mixtures with no interference from each other.

Finally, Table 4 gives the results obtained by using the proposed method to determine three synthetic mixtures of lactate and pyruvate. As can be seen, the concentrations found were quite consistent with those added.

4. Conclusions

The proposed mathematical treatment can be used as the basis for development of a general procedure for enzyme reactions involving a large difference between the molar absorptivity of the analyte and reaction product. Also, the proposed methodology can be extended to the simultaneous determination of species involved in this type of reaction.

In summary, enzyme fluorescence is a useful tool for the determination of enzyme species.

Acknowledgements

Cables de Comunicaciones S.A. (General Cable Group) are acknowledged for their financial support (Project CEDETI-OTRI 90/0076).

References

[1] J.R. Castillo, G. Ceprià, S. de Marcos, J. Galbán, J. Mateo and E. García Ruiz, Sensors Actuators A, 37–38 (1993) 582.
[2] N. Niklajsen, J. Nielsen and J. Villadsen, Anal. Chim. Acta, 214 (1988) 137.
[3] N. Shimojo, K. Nada, C. Nakajima, C. Yoshikawa, K. Okuda and K. Okada, Clin. Chem., 35 (1989) 1992.
[4] D. Weigelt, F. Schubert and F. Scheller, Analyst, 112 (1987) 1112.
[5] E.H. Hansen, A. Arnald and L. Noergoard, Anal. Lett., 23 (1990) 225.
[6] E.H. Hansen, L. Noergoard and M. Pederson, Talanta, 38 (1991) 275.
[7] J. Galbán, S. de Marcos and J.R. Castillo, Anal. Chem., 65 (1993) 3076.
[8] E.A. Permyakov, Luminescent Spectroscopy of Proteins, CRC Press, Boca Raton, FL, 1993, Chap. 3, pp. 35–55.
[9] J.R. Lakowicz, Principles of Fluorescence Spectroscopy, Plenum Press, New York, 1983, Chap. 9, pp. 258–297.
[10] G.J. Henderson, J. Chem. Educ., 54 (1977) 57.

ELSEVIER

Analytica Chimica Acta 299 (1994) 285–290

ANALYTICA CHIMICA ACTA

Application of a wavelength dispersive x-ray fluorescence spectrometric technique for the analysis of tantalum in titanium–tantalum alloys

G. Radha krishna, H.R. Ravindra *, B. Gopalan, S. Syamsundar

Control laboratory, Nuclear Fuel Complex (DAE), Hyderabad- 500762, India

Received 28 February 1994; revised manuscript received 20 July 1994

Abstract

Titanium–tantalum alloys show high corrosion resistance and are the materials of choice for some of the structural components in nuclear industry. This paper describes a procedure to determine tantalum present in the range of 0.75–5.0% in a titanium alloy by x-ray fluorescence spectrometry based on a solution technique. The method is fast, reliable and does not involve prior separation of tantalum from titanium. Various samples were analysed and the values obtained were compared with those obtained by atomic absorption spectrometry. The precision of the method is 1.68% R.S.D. This method can be used for routine analysis of samples.

Keywords: X-ray fluorescence spectrometry; Atomic absorption spectrometry; Tantalum; Titanium alloys; Corrosion resistant; Background correction

1. Introduction

Titanium has been reported to possess excellent corrosion resistant properties in concentrated nitric acid and hence has become a material of choice especially in the nuclear industry. It is used for (a) dissolvers wherein hot/boiling nitric acid is used, (b) vessels meant for solvent extraction for separating fission products like plutonium and uranium, (c) evaporators to concentrate products in hot nitric acid and (d) storage tanks in reprocessing units of nuclear reactors for holding the radioactive materials in nitric acid medium. β-Titanium and tantalum are part of a continuous series of solid solutions [1], however, the solubility of α-tantalum in titanium is limited to about 5%. In this Ti–5 Ta alloy, corrosion during electrolysis in 12 M nitric acid is low and is comparable to that of zircaloy-2. The conventional choice of stainless steel is not favourable under highly oxidising conditions in the fuel reprocessing units as they undergo intergranular corrosion even in non-sensitised conditions. Titanium, however, in weakly oxidising medium as that encountered in the vapour and condensate regions of the evaporators, shows a high corrosion rate and forms a white non-adherent hydrated oxide film. The addition of materials like tantalum improves the film-forming ability by improving the kinetics of the cathodic reduction reaction and further improves the oxide film stability and corrosion resistance in nitric acid medium.

The separation and determination of tantalum in titanium by chemical methods is rather difficult and cumbersome [2]. Tantalum cannot be determined directly

* Corresponding author.

SSDI 0003-2670(94)00348-3

Table 1
Optimised conditions

	Tantalum (analyte)	Tantalum Background	
		1, −offset factor	2, +offset factor
Line	$L\alpha_1$		
Wavelength (Å)	1.5220		
Energy (keV)	8.11		
Crystal	LIF(200)		
Angle (2ϕ) (after peaking)	44.42	44.055	44.855
Detector	Flow proportional and scintillation counter used in tandem		
Collimator	Fine		
Spacing (m)	0.15×10^{-3}		
Voltage (kV)	60		
Current (mA)	40		
Medium	Helium		
Counting time (s)	60		

by gravimetry in the presence of titanium and as such it has to be separated either by an ion exchanger [3] or by solvent extraction systems like methyl isobutyl ketone (MIBK) in HCl–HF medium [4], tributyl phosphate (TBP)–kerosene in H_2SO_4–HF medium [5] or by column chromatography [6] in which ammonium fluoro salts of tantalum can be eluted from a cellulose column with a mixture of 85:15 methyl ethyl ketone and 40% HF. Tantalum can also be separated from titanium by the hydrolysis of tantalum by dilute hydrochloric acid [7] or by an oxalate–salicylate method [8] in which a solution containing tantalum and titanium is treated with sodium salicylate followed by treatment with calcium chloride to separate tantalum leaving titanium complexed with the salicylate. After effecting the separation of tantalum from titanium, the former is estimated by precipitation with tannin in ammonium chloride–oxalic acid medium. However, these methods are time consuming. Some of the instrumental methods for the determination of tantalum in titanium are atomic absorption spectrometry (AAS) using the 2714 Å line, which incidentally has been adopted at the authors laboratory. Inductively coupled plasma atomic emission spectrometry (ICP-AES) is among the most powerful and versatile methods for elemental analysis in trace levels. However, at the concentration range studied, the samples have to be severely diluted to avoid errors. Hence, the advantage of an extended dynamic range cannot be utilised in this case. Berge et al. [9] have analysed tantalum in tantalum–niobium alloys by differential pulse polarography with 0.02 M oxalic acid, 0.10 M H_2SO_4 and 5% H_2O_2 as a supporting electrolyte at a peak potential of −0.20 V vs. SCE. Tantalum has also been determined spectrophotometrically by pyrogallol [10] or with dyes such as morin [11] and methyl violet [12]. The spectrophotometric methods are difficult to perform and require highly skilled personnel, since the analytical parameters and state of reagents required for the analysis are very rigorous. To overcome the above analytical difficulties an x-ray fluorescence spectrometric method has been developed using a solution technique for the determination of tantalum in Ti–Ta alloys. The method is more versatile and is advantageous because prior separation of tantalum from titanium is not involved.

2. Experimental

2.1. Instrumentation

X-ray fluorescence spectrometric measurements were made on a Philips 1404 (Eindhoven) wavelength dispersive sequential x-ray spectrometer using X44 software supported by a micro PDP 11/23 computer. The spectrometer is equipped with a 3 kW side window rhodium anode source. The measurement of standards and samples was carried out in a specially designed PTFE liquid cell with a 6-μm mylar window. The

instrumental parameters for measurement of analyte line intensity are shown in Table 1.

2.2. Reagents and apparatus

High-purity tantalum and titanium metal were used for the preparation of standards. All reagents were of analytical grade. Distilled water was used throughout for preparation of the solutions. The pipettes and the volumetric flasks used were of polythene (Nalgene).

2.3. Standard preparation

Tantalum and titanium stock solutions were prepared by dissolving the respective metals in 5 ml of 40% HF and 2 ml of 16 M nitric acid in a PTFE beaker. After dissolution the solution was made up to 100 ml to give a stock solution of 5 mg/ml of tantalum and 50 mg/ml titanium, respectively. From the above stock solution suitable standards in the range 0.75–5.0% tantalum in titanium were made by diluting the stock solution maintaining a total concentration at 0.3 g with respect to titanium and tantalum. 2 ml 40% HF and 5 ml 16 M nitric acid, together with 10 ml of saturated boric acid were added. The volume was carefully made up to 50 ml with distilled water.

2.4. Sample preparation

For the analysis of samples 0.15–0.25 g of alloy is weighed into a clean PTFE beaker. Titanium metal is added to the sample to bring the total amount of tantalum and titanium exactly to 0.3 g. 10 ml of water followed by 5 ml of nitric acid and 2 ml of HF were added and the beaker was heated on a water bath in a well-ventilated fumehood for dissolution. After complete dissolution 10 ml of saturated boric acid was added and the volume was made up to 50 ml with distilled water.

2.5. Measurement

A portion of the standard was transferred into the liquid cell, loaded into the spectrometer and excited by primary x-rays. The fluorescent intensities for tantalum ($L\alpha_1$) were measured. A calibration graph was generated by correlation of the Ta line intensities with concentrations of the element present. The X44 software was used for this purpose. The samples were measured in a similar manner.

3. Results and discussion

The calibration graph of tantalum in the concentration range of 0.75–5.0% in titanium vs. fluorescent intensity (Kcps) is linear with D and E values of 1.9902 and 0.08861, respectively (see below). In the present work the regression analysis was done applying the de Jongh calibration model supplied by M/s Philips in the X44 software package. The mathematical expression is

$$C_i = D_i - \Sigma[L_l \times C_l] + E_i \times \frac{r_i}{r_s} \times \left[1 + \Sigma_{a,j} \times \frac{c_j}{100}\right]$$

in which C_i is the concentration (in wt.%) of element i; r_i the count rate (in Kcps) for element i; r_s the count rate for the internal ratio channel if any or $r_s = 1$ as in the present case; D_i the calibration constant representing the intercept; E_i the calibration constant representing the inverse slope of the calibration line for element i; L_l the constant representing the spectral correction for element l upon i; and a_{ij} is the constant representing matrix correction for element j on element i.

The direct x-ray fluorescence spectrometric technique is more rapid for the determination of many elements, but the success of the method is dependent upon the availability of standard samples with very accurately known concentrations. Since certified solid matching tantalum standards with a titanium matrix were not available, a simpler method for the preparation of standards in solution has been adopted for this investigation. The solution technique has an advantage in that the analytical results are representative of the bulk sample and not just of the surface, and hence the effects of non-representative surface composition, surface texture and particle size are eliminated. Day to day instrumental drifts are controlled and corrected for, by measuring the intensity of the analyte in a reference material. Although Ta $L\alpha_1$ with 44.42° 2Θ LiF200 and Ta $L\beta_1$ 38.48° 2Θ LiF200 have identical line intensities, Ta $L\alpha_1$ is preferred for the determination of tantalum in titanium because of its lower background compared to that of the $L\beta_1$ line. To realise higher overall measured intensities and to improve the peak to background ratio for a longer wavelength region as that

used in this work, the helium path is made use off. A counting time of 60 s together with flow proportional and scintillation counter were employed in tandem to get large net accumulated intensities so that the statistical error in counting is reduced to the bare minimum. Various elements like hafnium, cobalt and copper have been cited as reference internal standard elements for estimation of tantalum. However, this being a two component system with no interelement effects, and also as no substantial gain in sensitivity or accuracy was achievable by using an internal standard, no internal standard has been added. As evident from the mass absorption coefficient data, [13] titanium does not appreciably effect the tantalum line intensity, hence no mathematical corrections were required either for enhancement or absorption. From the qualitative scan (Fig. 1) it is evident that there is a substantial background at the analyte peak position and hence background correction was applied. The background at the analytical line mainly arises due to scattering of (a) primary radiation by the low effective atomic number of liquid matrices, (b) cell windows and (c) the adjoining copper $K\alpha$ peak at 45.03° 2Θ LiF200 arising from the spectrometer component. However, the background as observed is not constant and is varying in nature. The background correction is effected by measuring the intensity at the respective offset angles. If both the offsets have the same value, that is, if they are at the same 2Θ angular distance from the peak, the background can be automatically subtracted without any special correction. However, in this case the difference between the negative offset and the peak is not the same as the difference between the positive offset and the peak. Hence it becomes necessary to multiply the background using the correction factor calculated from the equation (see Fig. 2)

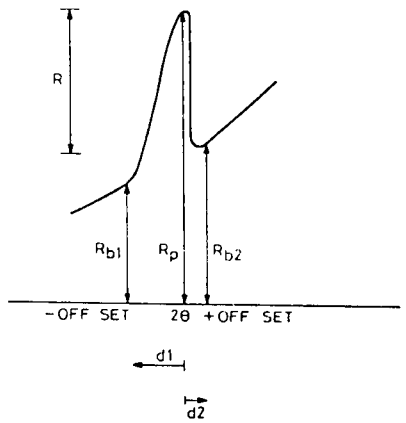

Fig. 2. Sloping background correction. R_{b1} = Count rate at the − background position; R_{b2} = count rate at the + background position; R_p = count rate at the element position; R = element of interest nett count rate.

$$OC_1 = \frac{d_1}{d_1 + d_2} = -\textit{offset factor}$$

$$OC_2 = \frac{d_2}{d_1 + d_2} = +\textit{offset factor}$$

The background at the peak position then would be $R_{bs} = OC_1 \times R_{b1} + OC_2 \times R_{b2}$. In this study, it can be seen from Fig. 1 that

Angle at $R_p = 44.42°$

Angle at $R_{b1} = 44.055°$

Angle at $R_{b2} = 44.855°$

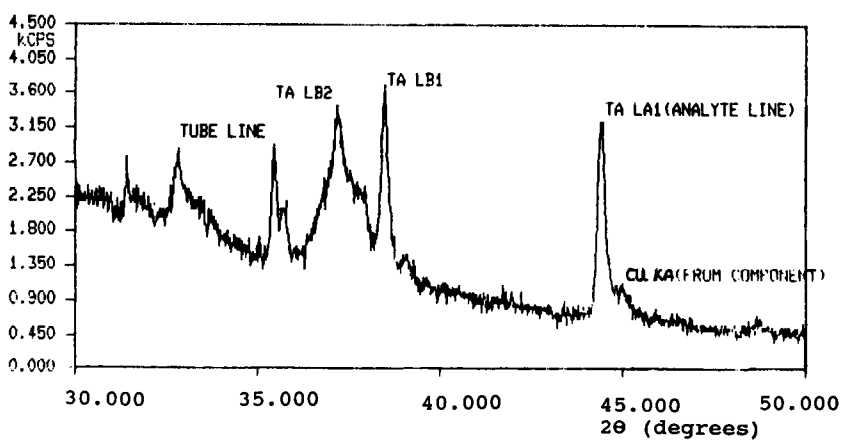

Fig. 1. Qualitative scan.

Hence,

$$OC_1 = -\text{offset factor} = \frac{0.365}{0.365 + 0.435} = 0.456$$

$$OC_2 = +\text{offset factor} = \frac{0.435}{0.365 + 0.435} = 0.544$$

From the respective offset factors the background count at the peak position is calculated as per the above equation. The net intensity is then given by the expression

$$\text{Net intensity (Kcps)} = R_p - R_{bs}$$

The effective x-ray absorption coefficient and scatter of the solvents and other reagents used must be as low as practicable. Keeping this in view, conditions with respect to sample preparation were regulated by holding the sample in fluoride medium in which tantalum exhibits a very high stability coupled with a considerably low background compared to mediums like tartrate, citrate or oxalate. Since hydrofluoric acid is corrosive the excess fluoride present is selectively complexed as fluoroboric acid by controlled addition of boric acid. As the Philips titanium liquid cells used for measurements were susceptible to fluoride attack, even though they were complexed with boric acid, specially designed PTFE liquid cells with specifications matching those supplied by Philips were fabricated and used.

In order to illustrate the potentials of the proposed x-ray fluorescence spectrometric method, ten synthetic samples were analysed and the values obtained by the method show an excellent recovery rate (Table 2). A single sample which was measured ten times on different days gave an R.S.D. of 1.68%. Table 3 gives the comparative values for samples analysed by XRFS and AAS technique which are in good agreement. For higher concentrations of tantalum in titanium, suitable standards can be. From the results obtained it is seen that tantalum in titanium can be easily determined by wavelength dispersive x-ray fluorescence spectrometry which is fast, accurate and needs no matrix separation.

Table 2
Tantalum recovery with the proposed method

Sample No.	Tantalum added to titanium (%)	Tantalum recovered by XRF (%)
1	0.64	0.64
2	0.89	0.88
3	1.45	1.45
4	3.92	3.92
5	2.68	2.69
6	3.21	3.18
7	4.85	4.86
8	0.98	0.95
9	0.72	0.74
10	5.08	5.12

Table 3
Comparision of values obtained by the proposed method with those by AAS for actual samples

Sample No.	Tantalum (%)	
	XRFS	AAS
1.	3.90	4.10
2.	4.10	4.00
3.	4.28	4.07
4.	5.02	5.06
5	1.62	1.59
6.	2.70	2.79

Acknowledgements

The authors are grateful to V.A. Chandramouli, Dy. Chief Executive (QA), for his keen interest and constant encouragement. Thanks are due to S. Raju for providing the AAS data and to G. Satyanarayana for technical assistance.

References

[1] B.W. Gonser, Ind. Eng. Chem., 42 (1950) 222.
[2] R.A. Mercer and R.A. Wells, Analyst, 17 (1954) 339.
[3] J.W. Cobble, T.W. Gilbert Jr., S. Kallmann, B.R.F. Kjellgren, E.S. Melick, C.W. Schwenzfeier and J. Sedlet, in I.M. Kolthoff and P.J. Elving (Eds.), Treatise on Analytical Chemistry, Part II, Vol. 6, Interscience, New York, 1964, p. 254.
[4] G.W.C. Milner and A.J. Wood, U.K. at Energy Auth. Report c/R, (1952) 895.
[5] D.I. Ryabehikov and M.P. Volynets, Zh. Anal. Khim., 4 (1959) 700.

[6] N.H. Furman, in Standard Method of Chemical Analysis, Vol. 1, 6th edn., Van Norstand, Princeton, NJ, 1968, p. 723.
[7] W.R. Schoeller and C. Jahn, Analyst, 54 (1929) 321.
[8] W.R. Schoeller and C. Jahn, Analyst, 57 (1932) 75.
[9] H. Berge, T.X. Gian and L. Bruegmann, Z. Chem., 27 (1987) 416.
[10] B. Sarry and A.Z. Lange, Anal. Chem., 241 (1968) 186.
[11] O. Tomicek and V. Holecek, Chem. Listy, 46 (1952) 11.
[12] W. Rutkowski and S. Wasowicz, Chem. Anal. (Warsaw), 11 (1966) 971.
[13] E.P. Bertin, in Principles and Practice of X-Ray Spectrometric Analysis, 2nd edn., Plenum Press, New York, 1984, p. 972.

ELSEVIER

Analytica Chimica Acta 299 (1994) 291–298

ANALYTICA CHIMICA ACTA

Coprecipitation behaviour of 5,8-polyquinolyl polydisulphide for trace element preconcentration from aqueous solution

Magnuss Vircavs [a,*], Vallija Rone [b], Agrida Pelne [b], Daina Vircava [b]

[a] *Nuclear Research Centre, Latvian Academy of Sciences, 31 Miera St., Salaspils, LV-2169, Latvia*
[b] *Institute of Inorganic Chemistry, Latvian Academy of Sciences, 34 Miera St., Salaspils LV-2169, Latvia*

Received 7 December 1993; revised manuscript received 8 July 1994

Abstract

The oxidation product of SH-containing reagent such as 5,8-dimercaptoquinoline was used for the coprecipitation of traces of non-transition and transition *d*-element from aqueous solution. The coprecipitation behaviour of 5,8-polyquinolyl polydisulphide (PQPD) for the preconcentration of V(IV), Cr(III), Mn(II), Fe(III), Co(III), Ni(II), Cu(II), Zn(II), Ga(III), As(III), Se(IV), Mo(VI), Ru(III), Pd(II), Cd(II), In(III), Au(III), Hg(II), Ir(III), Os(III) and Pt(II) is discussed. In special cases the coprecipitation of the inner complex of 5,8-dimercaptoquinoline is compared with that using quinoline-8-thiol. The formation of the PQPD solid phase and the coprecipitation of inner complex compounds of 5,8-dimercaptoquinoline occur over a wide range of acidity from 1.5 mol l^{-1} HCl to pH 12. For all the above elements the recovery is more than 95%, with the exception of Ir(III), for which it is 85%. For the coprecipitation it is sufficient to use 60 mg of 5,8-dimercaptoquinoline for 1 l of aqueous solution, in contrast to quinoline-8-thiol, where 100 mg are needed.

1. Introduction

On oxidation of organic reagents whose molecules contain an SH group, disulphides are obtained. The latter are used as analytical reagents for the selective liquid–liquid extraction of various ions, e.g., Cu(I), Te(IV), Se(IV), Pd(II) and Pt(II, IV) and for their spectrophotometric determination. Mostly the disulphides of dithiocarbamates (tetramethyl- and tetraethylthiuram disulphides [1,2]), the disulphides of dithiophosphates and dithiophosphinates [1] and the disulphides of quinoline-8-thiol and some of its derivatives [3] have been investigated. The reaction between Cu(I) ions and these organic disulphides is the most frequently studied and applied in analytical practice.

In the aqueous chemistry of trace elements, another application of organic disulphides is their use as collectors for the coprecipitation of inner complex compounds formed after the reaction with non-transition and transition *d*-elements. This application has already been described using bis(8-quinolyl) [4–7], tetraethylthiuram [8], bis(pyrrolidin-1-ylthiocarbonyl) [9], bis(pentamethylenedithiocarbonyl) [10,11], bis-(benzylbismuthiol) and bis(naphthylbismuthiol) disulphides [12].

The coprecipitation with organic disulphides is based on two reactions: the formation of water-in-

* Corresponding author.
Present address: Board of Environment Impact Assessment, Ministry of Environmental Protection and Regional Development of Latvia, 25 Peldu St., Ríga LV-1494, Latvia.

SSDI 0003-2670(94)00344-0

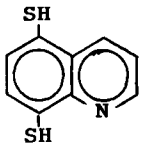

DMQ

soluble inner complex compounds of non-transition and transition *d*-elements and the formation of the collector owing to the possibility of the SH groups being easily oxidized to disulphide.

In aqueous solution, during the formation of the solid phase of the organic disulphide, inner complex compounds coprecipitate with the collector, i.e., a distribution of inner complex compounds between water and the solid phase of disulphide occurs.

This paper reports results for the coprecipitation of inner complex compounds of V(IV), Cr(III), Mn(II), Fe(III), Co(III), Cu(II) and others using 5,8-dimercaptoquinoline (DMQ) for the formation of chelate complex compounds and 5,8-polyquinolyl polydisulphide (PQPD) as their coprecipitator. In addition, the coprecipitation behaviours of some elements (Mn, Se, Cr, As, platinum metals) with the oxidation product of quinoline-8-thiol are compared and discussed.

2. Experimental

2.1. Instrumentation

The study of the coprecipitation was carried out by using radiotracers. Radioactivity measurements were effected with a gamma-ray spectrometer equipped with a Ge(Li) crystal coupled to an LP-4900 multi-channel analyser (Nokia, Helsinki, Finland). The system has an energy resolution of 2.8 keV for 1332.5-keV ^{60}Co gamma-rays.

A precision pH meter (Type OP-205/l; Radelkis, Budapest, Hungary) was used. The absorbances of PQPD and of Rh(III) quinoline-8-thiolate in chloroform were measured with a Specord ultraviolet–visible spectrophotometer (Carl Zeiss, Iena, Germany).

For neutron activation analysis (NAA) of the concentrates of trace elements obtained, a vertical ($F_{th} = 1.2 \times 10^{13}$ and $F_{res} = 2.1 \times 10^{11}$ neutrons cm^{-2} s^{-1}) channel of an ordinary water–water pool reactor (IRT-M) was used; the nominal thermal power is 5000 kW.

A U-10 thermostat (VEB MLW Prüfgerate-WERR Medingen/SITZ Freistal, Germany) was used. All laboratory glassware was washed with 6 mol l^{-1} nitric acid and rinsed with triply distilled water.

Coprecipitation was carried out in a composite filtration equipment constructed of Plexiglas. Nuclear filters of pore size 0.46 μm (Joint Institute for Nuclear Research, Dubna, Russian Federation) and Filtrak-90 filter-papers were used.

2.2. Reagents

The synthesis of DMQ has been described previously [13]. Solutions of DMQ in ethanol and the sodium salt of quinoline-8-thiol in triply distilled water were prepared daily.

The following radionuclides in microgram and submicrogram amounts were used: ^{48}V, ^{51}Cr, ^{54}Mn, ^{57}Co, ^{59}Fe, ^{64}Cu, ^{65}Ni, ^{65}Zn, ^{72}Ga, ^{74}As, ^{75}Se, ^{99}Mo, ^{103}Ru, ^{109}Pd, ^{115}Cd, ^{116m}In, ^{191}Os, ^{192}Ir, ^{197}Pt, ^{198}Au and ^{203}Hg. Radionuclides of ^{51}Cr, ^{54}Mn, ^{57}Co, ^{59}Fe, ^{103}Ru, ^{109}Pd, ^{191}Os, ^{192}Ir, ^{197}Pt, ^{198}Au were used in the form of chlorides; radionuclides of ^{64}Cu, ^{65}Zn, ^{72}Ga, ^{115}Cd, ^{116m}In, ^{203}Hg in the form of nitrates; radionuclide of ^{48}V in the form of vanadium oxychloride; radionuclide of ^{65}Ni in the form of acetate; radionuclides of ^{74}As and ^{75}Se in the form of arsenite, selenite and selenate, respectively; and radionuclide of ^{99}Mo in the form of molybdate.

A 1% (w/v) aqueous solution of hydrogen peroxide was prepared daily. All solutions of acids and salts were prepared using triply distilled water and analytical-reagent grade chemicals (chemically pure and especially pure) according to the classification in the former USSR. Aqueous solutions with defined pH were prepared using hydrochloric acid, acetic acid, sodium acetate, sodium borate and sodium hydroxide.

2.3. Procedures

The procedures for the determination of the pH ranges for the formation of coprecipitator solid phase and the pH ranges and recoveries of the coprecipita-

tion of inner complex compounds have been described in previous papers [5,9]. The only difference here is connected with the solution of the organic reagent indicated above.

Sorption of Mn(II) on bis(8-quinolyl) disulphide

Take 100 ml of triply distilled water acidified to pH 1 with concentrated nitric acid. Add 1 ml of radionuclide solution of ^{54}Mn (0.5 μg). After 15 min, add 10% of ammonia solution by stirring to adjust the pH to 6–8 and add 5 ml of an acetone solution of bis(8-quinolyl) disulphide (30 mg). After 5, 10, 30 and 45 min, filter the solution.

In order to investigate the sorption of Mn(II) quinoline-8-thiolate, the procedure is the same with the following exception. Before the pH adjustment, add 0.2 ml of sodium quinoline-8-thiolate (4 μg) solution. After 15 min adjust the pH to 6–8. Using obtained filtrate, performed the pH measurement. Determine the recovery of the sorption as described previously for coprecipitation.

NAA of the concentrates

The samples (concentrates) with standards were packed in an aluminium container for neutron irradiation. The irradiation time of the samples and standards was 17 h, the delay time was 21 d and the measurement time was 15 min. The standards SSB-1 and SSB-2 (Institute of Nuclear Physics, Georgia) [14] were used. The limit of detection of the elements was calculated as $3N_f^{1/2}$, where N_f is the background level under the photopeak.

3. Results and discussion

3.1. Characteristics of disulphide solid phase

In aqueous solution, the oxidation product of DMQ precipitates in the form of tiny crystals. In contrast to the previously studied bis(8-quinolyl) disulphide [5], PQPD exists in the solid phase over a wider range of acidity. Further, the oxidation product of DMQ forms its own solid phase in acidic solution. This can be explained by a stronger acid behaviour of the organic reagent used here in comparison with that of quinoline-8-thiol, which is related to the presence of the substituent (SH) in the 5-position of the DMQ molecule. The maximum formation of the solid phase of PQPD occurs from 1.5 mol l^{-1} HCl to pH 12. In contrast, the formation of the bis(8-quinolyl) disulphide solid phase occurs in the pH range 2.5–12 [5].

3.2. Coprecipitation of inner complex compounds

Inner complex compounds of DMQ with non-transition and transition *d*-elements coprecipitate with the corresponding disulphide over a wide range of conditions in aqueous solution. It should be noted that the feasibility of coprecipitating the elements in acidic media is due to fact that in acidic media the competition of interfering reactions, e.g., the formation of hydroxo complexes, is insignificant and the greatest part of the elements exists in the cationic form. Most of all, however, it promotes the formation of stable inner complex compounds.

The dependence of the coprecipitation of inner complex compounds of DMQ on the acidity of aqueous solution is shown in Table 1 and Figs. 1 and 2. The coprecipitation of V(IV), Fe(III), Ni(II), Cu(II), Zn(II), Mo(VI), Pd(II), Cd(II), Pt(II), Au(III) and Hg(II) in the form of 5,8-dimercaptoquinolinates with PQPD occurs completely within acidity ranges that are shifted to more acidic values than the pH ranges of the coprecipitation maxima of quinoline-8-thiolates of the same elements with bis(8-quinolyl) disulphide [5].

The coprecipitation behaviour of the DMQ inner complex compounds of Cr(III), Mn(II), As(III), Se(IV, VI) and platinum metals with PQPD in comparison with bis(8-quinolyl) disulphide is discussed below.

3.3. Chromium(III)

In aqueous solution, Cr(III) ions exist in the form of kinetically inert aqua-complex compounds Cr(III) slowly forms inner complex compounds with quinoline-8-thiol and its derivatives at 18–22°C, but at 90°C the complex formation reaction occurs in 1 min [3]. Therefore it is necessary to heat the solution to be analysed at 90°C for 10 min. The effectiveness of the coprecipitation of Cr(III) quinoline-8-thiolate and 5,8-dimercaptoquinolinate with bis(8-quinolyl) disulphide and PQPD, respectively, is shown in Fig. 3. It

Table 1
pH ranges and maximum recovery of inner complex compounds of 5,8-dimercaptoquinoline with 5,8-polyquinolyl polydisulphide

Elements and added amounts of radiotracers (μg)			pH range	Recovery (%) [a]
V(IV),	0.001		1.7–6.7	97±3
Cr(III),	0.01 [b]		4.2–9.0	95±2
Mn(II),	0.04		4.7–7.7	97±3
			8.5–10	90±4
Fe(III),	0.14		2.3–8.1	98±3
Co(III),	0.03		2.4–7.8	97±2
Ni(II),	3.0		1.5–10	97±3
Cu(II),	0.2–0.5	1.5 mol l^{-1}	HCl–pH 9	97±2
Zn(II),	0.13		1.3–8.0	98±2
			8.5–10	90±3
Ga(III),	0.84		0.2–8.5	98±2
As(III),	0.8		0.2–7.5	98±3
Se(IV),	0.5	1 mol l^{-1}	HCl–pH 7.5	96±4
Se(VI),	0.5	1 mol l^{-1}	HCl–pH 7.5	8±2
Mo(VI),	2.6		0.2–8.8	94±3
Ru(III),	3.3		3.7–9.0	95±4
Pd(II),	20.1	0.5 mol l^{-1}	HCl–pH 10	98±2
Cd(II),	0.8		0.3–7.9	98±2
In(III),	0.1–0.8		0.6–8.5	95±3
Au(III),	0.02	1 mol l^{-1}	HCl–pH 9.2	95±4
Hg(II),	0.9	1 mol l^{-1}	HCl–pH 8.5	98±2
Ir(III),	0.05 [c]		7.0–8.5	85±3
Os(III),	27.0 [b]		5.8–7.3	98±2
Pt(II),	26.3 [b]	1 mol l^{-1}	HCl–pH 10.5	97±3

Filtration time, 15 min.
[a] recovery is given as the mean of five replicates (± standard deviation at a significance level of 0.05).
[b] Heating at 90°C for 10 min.
[c] Heating at 90°C for 1 h.

follows that under identical conditions (see curves 2 and 3 in Fig. 3) it is necessary to use 60 mg of sodium quinoline-8-thiolate and 30 mg of DMQ to coprecipitate completely the Cr(III) inner complex compounds. This demonstrates that PQPD is a more effective coprecipitator than bis(8-quinolyl) disulphide. The formation of Cr(III) quinoline-8-thiolate at 20°C and the subsequent coprecipitation do not occur completely even after waiting for 2 h (curve 1 in Fig. 3). On the other hand, from the data obtained, it is possible to conclude that bis(8-quinolyl) disulphide as an organic coprecipitator does not coprecipitate Cr(III) in the form of aquo complexes, hydroxo complexes or mixed complex compounds, i.e., the recovery obtained of 70% reflects the coprecipitation of Cr(III) quinoline-8-thiolate.

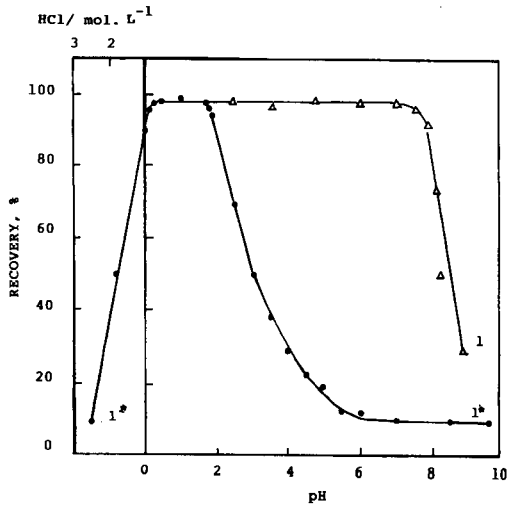

Fig. 1. Effect of pH on the recovery of As(III) with 5,8-polyquinolyl polydisulphide. Amount of added radiotracer ^{74}As taken, 0.8 μg. For explanation of curves 1 and 1*, see text.

In contrast to the coprecipitation of Cr(III) 5,8-dimercaptoquinolinate with PQPD, the coprecipitation of Cr(III) quinoline-8-thiolate with bis(8-quinolyl) disulphide occurs within a narrow pH range of 3.8–5.2 with a recovery of 94 ± 2%.

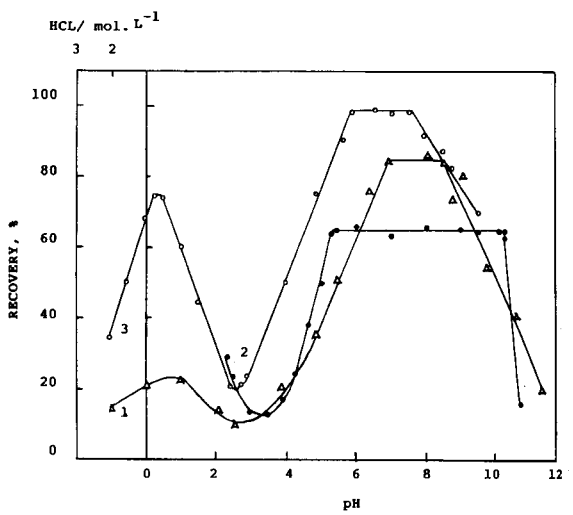

Fig. 2. Effect of the pH on the coprecipitation of Ir(III) with (1) 5,8-polyquinolyl polydisulphide and (2) bis(8-quinolyl) disulphide and of Os(III) with (3) 5,8-polyquinolyl polydisulphide.

3.4. Manganese(II)

Manganese (II) in the form of quinoline-8-thiolate and 5,8-dimercaptoquinolinate coprecipitates with the corresponding disulphides from weakly acid media up to pH 10. In contrast to the formation and coprecipitation of the Mn(II) inner complex compound of DMQ, the formation and coprecipitation of Mn(II) quinoline-8-thiolate occurs slowly, within 45 min (see Table 2). Further, it is necessary to use double the amount (30 mg) of the reagent (sodium quinoline-8-thiolate) compared with that of DMQ under analogous conditions. Heating the analyte solution at 90°C for 15 min promotes the complete coprecipitation of Mn(II) (recovery 93 ± 3%) with bis(8-quinolyl) disulphide.

The data summarized in Table 2 show that sorption possibilities of bis(8-quinolyl) disulphide are insignificant with regard to Mn(II) in the forms of aquo complex, mixed complex compounds and quinoline-8-thiolate.

3.5. Arsenic(III)

In aqueous solution, As(III) in the form of AsO_3^{3-} forms an unstable compound with quinoline-8-thiol which is not extracted into chloroform (the recovery is ca. 10%) [3]. In acidic media, AsO_4^{3-} oxidizes quinoline-8-thiol and its derivatives to the corresponding disulphides and As(V) is reduced to As(III). The latter forms stable inner complex compounds with derivatives of quinoline-8-thiol such as DMQ. The data obtained show (Fig. 1) that the coprecipitation of As(III) occurs with PQPD over a wide range of pH. In Fig. 1, two curves, which characterize the effect of pH on As(III) coprecipitation, are represented. Curve 1* is obtained when the formation and coprecipitation of the As(III) complex compound of DMQ occur at the same pH. In spite of the acidic behaviour of the reagent, it has no possibility of forming an inner complex of As(III) from weakly acidic media up to pH 7–8. This is due to the stable anions of As(III) that exist within this pH range. If the inner complex compound of As(III) is formed in acidic media (pH 1), but the coprecipitation is performed at pH > 1, then the disulphide used coprecipitates As(III) completely up to pH 7–8 (curve 1 in Fig. 1). In the range up to pH 1.5 As(III) coprecipitation is the same in both cases. The difference between both coprecipitation possibilities is observed best of all at pH > 1.5. In the first case (curve 1*), the coprecipitation recovery decreases, which can be explained by the competition between As(III) 5,8-dimercaptoquinolinate and As(III) oxo-anions. In contrast, in the second case (curve 1), the coprecipitation recovery does not change in the presence of As(III) oxo-anions. The latter do not influence the coprecipi-

Table 2
Dependence of Mn(II) coprecipitation and sorption with bis(8-quinolyl) disulphide on the effect of waiting time at 20°C

Waiting time (min)	Recovery (%) [a]	
	Coprecipitation [b]	Sorption [c]
0	39 ± 3	
5		17 ± 4
10	48 ± 2	6 ± 3
15	53 ± 3	
30	78 ± 3	5 ± 2
45	94 ± 2	13 ± 3 [d]

Coprecipitation and sorption were carried out at pH 6.0–7.6.
[a] Recovery is given as the mean of five replicates (± standard deviation at a significance level of 0.05).
[b] 30 mg of sodium quinoline-8-thiolate were used.
[c] The first three values were obtained in the abscence of sodium quinoline-8-thiolate.
[d] Sorption in the presence of 4 μg of sodium quinoline-8-thiolate.

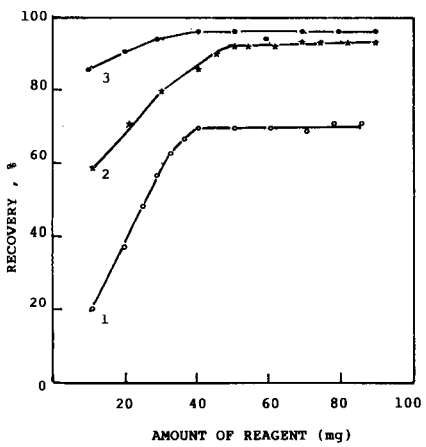

Fig. 3. Effect of the temperature and amount of organic reagent on the coprecipitation of Cr(III) inner complex compounds with (1 and 2) bis(8-quinolyl) disulphide and (3) 5,8-polyquinolyl polydisulphide. (1) At 20°C; (2 and 3) at 90°C. Waiting time, 2 h at 20°C; pH of triply distilled water, 5.0; volume, 100 ml; amount of added radiotracer ^{51}Cr taken, 0.01 μg.

tation recovery if the As(III) inner complex compound of DMQ is formed at pH 1.

3.6. Selenium(IV)

The data that characterize the formation and existence of Se(IV) quinoline-8-thiolate in aqueous solution are contradictory. Se(IV) forms an inner complex compound with quinoline-8-thiol, which, on standing, decomposes [3]. In addition, Se(IV) is reduced to Se^0 by simultaneously oxidizing the reagent to bis(8-quinolyl) disulphide. Véveris et al. [15] found that in the presence of a 100-fold excess of quinoline-8-thiol, Se(IV) is extracted into chloroform in the form of its inner complex compound with a recovery of 90% within the pH range 3–7. Previous studies showed that Se(IV) quinoline-8-thiolate does not coprecipitate with bis(8-quinolyl) disulphide. These facts are the main negative factors influencing the coprecipitation. Further, these factors are interdependent. On the other hand, liquid–liquid extraction of Se(IV) quinoline-8-thiolate into chloroform occurs immediately after the formation of the inner complex compound [15]. DMQ forms Se(IV) 5,8-dimercaptoquinolinate, which is a stable compound and coprecipitates with PQPD within a wide range of pH (Table 1). The results show that Se(VI) coprecipitates insignificantly with PQPD. The fact that the pH values of the coprecipitation maxima of Se(IV) and Se(VI) (Table 1) are equal demonstrates that under the experimental conditions used Se(VI) is hardly reduced to Se(IV). The latter coprecipitates with PQPD. Considering the difference in the coprecipitation of Se(IV) and Se(VI), it is possible to determine the concentrations both of Se(IV) and Se(VI) in aqueous solutions.

3.7. Ruthenium(III), rhodium(III), palladium(II), osmium(III), iridium(III) and platinum(II)

In aqueous solution, platinum metals form different inorganic complex compounds such as chloro, aquochloro, chlorooxy and polynuclear complexes that exist within a wide range of acidity. The formation of platinum metal inner complex compounds of quinoline-8-thiol and its derivatives occurs only on heating of the aqueous solution in the presence of the organic reagents. In this connection, the formation of the Pd(II) inner complex compounds of DMQ and quinoline-8-thiol is an exception, i.e., Pd(II) forms stable inner complex compounds with the mentioned organic reagents at 18–20°C and their coprecipitation occurs within a wide range of acidity (Table 1). Bis(8-quinolyl) disulphide coprecipitates Pd(II) quinoline-8-thiolate from pH 2 to 12 [5].

Rh(III) quinoline-8-thiolate coprecipitates completely with bis(8-quinolyl) disulphide from pH 4.2 to 7.0 on heating the analyte solution at 90°C for 30 min.

However, not in all cases do heating and the presence of the organic reagent provide complete formation and coprecipitation of inner complex compounds. For instance, the recovery of the coprecipitation of Ru(III) and Ir(III) quinoline-8-thiolates does not exceed 65% even when 100 mg of the organic reagent (volume of aqueous solution 100 ml) are present and the aqueous solution is heated for up to 1 h. An analogous result was obtained by coprecipitating Ir(III) 5,8-dimercaptoquinolinate with the corresponding disulphide (Table 1). In acidic media from 1 mol l^{-1} to pH 1 and from pH 2 to 4, maxima and minima were observed in the coprecipitation of Os(III) and Ir(III) 5,8-dimercaptoquinolinates with PQPD (Fig. 2). As the bis(8-quinolyl) disulphide solid phase exists only at pH > 2, Ir(III) quinoline-8-thiolate shows a minimum coprecipitation at pH 3.3. A tendency is observed for the recovery of the coprecipitation to increase from pH 3.3 to 2.2. In acidic media the mentioned coprecipitation behaviour is probably connected with the formation of different complex compounds with different compositions. Besides, in the molecule of DMQ the mercapto group at the 5-position is ionized first [16]. Therefore, it is possible to consider that mercaptides are formed in the interaction with ionized mercapto groups.

3.8. Comparison of the coprecipitation techniques

Previously, it was found [17] that high concentrations (1 mol l^{-1} and more) of different inorganic and organic salts such as fluorides, nitrates, chlorides, sulphates, citrates and tartrates of alkali and alkaline earth metals and aluminium do not influence the coprecipitation of Mn(II), Fe(III), Co(III), Cu(II), Zn(II), Ag(I), Cd(II) and Hg(II) in the form of

quinoline-8-thiolate with bis(8-quinolyl) disulphide. However, the present investigations show that this is not true in all cases. For instance, the recovery of Au(III) quinoline-8-thiolate coprecipitation from 2 mol l^{-1} NaCl solution is 97 ± 3% but for 3 mol l^{-1} it is 86 ± 2% and for 4 mol l^{-1} it is 69 ± 4%. For complete coprecipitation of V(IV) (recovery 95 ± 3%) with bis(8-quinolyl) disulphide from 3 mol l^{-1} $NaNO_3$ solution, it is necessary to use 80 mg of sodium quinoline-8-thiolate (volume 100 ml).

In this connection, the coprecipitation of inner complex compounds of DMQ with PQPD proceeds more effectively from aqueous solutions of salts in comparison with the coprecipitation using quinoline-8-thiol.

On the basis of the investigations described, a coprecipitation technique for traces of elements from aqueous solutions has been developed. Contrast to the previously elaborated coprecipitation technique [5], it is sufficient to use 60 mg of DMQ for complete preconcentration of an element from 1 l of water sample.

The elaborated technique was used for NAA and atomic emission analysis of high-purity $AlCl_3$ (concentration of the salt 100 g l^{-1}) including the coprecipitation of the impurities (V, Fe, Co, Ni, Cu, Zn, Pb and Bi) in the form of their 5,8-dimercaptoquinolinates with PQPD [18]. Considering the hydrolysis of $AlCl_3$, the coprecipitation is possible for pH up to 3.0. Limits of detection of the mentioned impurities of 10^{-6}–10^{-8}% were obtained.

In order to compare the effectiveness of coprecipitation using different organic reagents and their oxidation products such as bis(8-quinolyl) disulphide [5], PQPD, tetraethylthiuram disulphide [8] and bis(pyrrolidin-1-yldithiocarbonyl) disulphide [9], pond water was analysed by NAA. The coprecipitation of traces of elements was carried out from the same water sample. The data obtained are given in Table 3. Statistical evaluation shows that the concentrations of the determined elements are equal at a significance level of 0.05. Among the indicated collectors, PQPD and bis(pyrrolidin-1-yldithicarbonyl) disulphide are to be preferred. According to the previously discussed chemical behaviour of quinoline-8-thiol using the coprecipitation with bis(8-quinolyl) disulphide, it is not possible to concentrate As and Se. The drawback of coprecipitation with tetraethylthiuram disulphide is related to the instability of sodium diethyldithiocarbamate and the narrow pH ranges of inner complex compound coprecipitation [8,9].

In spite of the selectivity of the organic reagents used, the mentioned collectors after the coprecipita-

Table 3
Comparison of data for pond water obtained by coprecipitation with organic disulphides and neutron activation analysis

Element determined	QD [a]	Concentration ($\mu g\ l^{-1}$) [b]			
		PQPD	TETD [c]	DPTD [d]	LOD [e]
Cr	0.18 ± 0.03	0.18 ± 0.01	0.15 ± 0.03	0.20 ± 0.03	0.04
Fe	65.9 ± 4.5	76.4 ± 2.6	59.4 ± 3.1	61.3 ± 4.9	0.8
Co	0.10 ± 0.01	0.13 ± 0.0005	0.09 ± 0.01	0.11 ± 0.01	0.007
Ni	0.26 ± 0.03	0.28 ± 0.02	NI [f]	NI	0.01
Zn	39.2 ± 5.0	38.7 ± 3.5	41.3 ± 4.4	35.8 ± 3.8	0.1
As	DNR [g]	1.0 ± 0.1	0.9 ± 0.1	1.1 ± 0.1	0.1
Se	DNR	0.06	0.07	0.06	0.06
Sb	0.09 ± 0.01	NI	0.12 ± 0.02	NI	0.002
Hg	0.05 ± 0.007	0.03 ± 0.004	0.05 ± 0.008	0.04 ± 0.008	0.009

Volume of water sample analysed = 500 ml.
[a] QD = bis(8-quinolyl) disulphide.
[b] Concentration is given as the mean of five replicates (± standard deviation of the mean).
[c] TETD = tetraethylthiuram disulphide.
[d] DPTD = bis(pyrrolodin-1-ylthiocarbonyl) disulphide.
[e] LOD = Limit of detection.
[f] NI = not investigated.
[g] DNR = does not react with quinoline-8-thiol.

tion contain both major and trace elements which do not react with these reagents, i.e., they adsorb on the disulphides. The concentrations of the adsorbed elements are decreased by washing the collectors after the filtration, but not completely. Therefore, the concentrates obtained are not radiochemically pure. The concentration ranges have been determined for the following adsorbed elements by analysing the disulphide precipitates (in $\mu g\ g^{-1}$): Na 393–512, Cl 1267–1354, Sc 0.01–2.25, Br 89–118, Rb 0.7–1.8, Cs 0.03–0.09, Ba 0.15–0.37, Hf 0.07–0.08, Ce 0.4–2.4 and Th 0.2–0.5. The mass of the coprecipitator (PQPD) was 73-75 mg.

The description of the coprecipitation behaviour of bis(8-quinolyl) disulphide and particularly PQPD shows that these organic disulphides can satisfactorily achieve the preconcentration of non-transition and transition *d*-elements from aqueous solution.

References

[1] N.G. Vanifatova, I.V. Serjakova and Yu, A. Zolotov, in Extraction of Metals with Neutral Sulphur Containing Compounds, Nauka, Moscow, 1980.
[2] A.I. Busev, V.M. Byr'ko and A.I. Dikusar, Zh. Anal. Khim., 26 (1971) 1380.
[3] Yu.A. Bankovsky, in The Chemistry of Mercaptoquinoline Chelates and Their Derivatives, Zinátne, Ríga, 1980.
[4] M.V. Vircavs, Thesis, Institute of Inorganic Chemistry of Latvian Academy of Sciences, Ríga, 1980.
[5] Yu.A. Bankovsky, M.V. Vircavs, O.E. Véveris, A.R. Pelne and D.K. Vircava, Talanta, 34 (1987) 179.
[6] M.V. Vircavs, A.R. Pelne and L.L. Djemina, Geokhimiya, (1988) 1037.
[7] M.V. Vircavs and S.M. Fazlullin, Vulkanol. Seismol., (1990) 101.
[8] M.V. Vircavs, A.R. Pelne, D.K. Vircava, V.F. Rone and O.E. Véveris, in Transactions of the 3rd Meeting of the USSR, Tomsk, Gidro-meteoizdat., Leningrad, 1987, p. 151.
[9] M.V. Vircavs, A.R. Pelne, V.F. Rone and D.K. Vircava, Analyst, 117 (1992) 1013.
[10] E. Beinrohr and J. Garaj, Analyst, 111 (1986) 979.
[11] E. Beinrohr, H. Hofbauerova and M. Cakrt, Mikrochim. Acta, 11 (1987) 209.
[12] M.V. Granda, Summary of Thesis, University of Havana, Havana, 1987.
[13] Ya. V. Ashaks and Yu.A. Bankovsky, Proc. Latv. Acad. Sci., Ser. Khim., (1972) 592.
[14] L.M. Mosulihvili, V.Yu. Dundua, N.E. Kharabadze and E. Yu. Efremova, J. Radioanal. Nucl. Chem., 83 (1984) 13.
[15] O.E. Véveris, G.G. Mihelson, Z.E. Peléke, L.L. Pelékis and I. Ya. Taure, Proc. Latv. Acad. Sci., Ser. Phys. Technol., (1969) 25.
[16] Ya. Ashaks, S. Rapiova, M. Zikmund and Yu. Bankovskii, Chem. Zvesti, 36 (1982) 65.
[17] M.V. Vircavs, A.R. Pelne, O.E. Véveris, V.F. Rone and D.K. Vircava, Vysokochistye Vechestva, (1991) 76.
[18] M.V. Vircavs, V.F. Rone, A.M. Garbar, V.G. Pimenov, D.K. Vircava, M.B. Kozlova and I.V. Mednis, Vysokochistye Vechestva, (1992) 138.

PUBLICATION SCHEDULE FOR 1995

	O'94	N'94	D'94	J	F	M	A	M	J	J	A	S
Anal. Chim. Acta	296/2 296/3 297/1–2	297/3 298/1 298/2	298/3 299/1 299/2	299/3 300/1–3 301/1–3	302/1 302/2–3 303/3							
Vib. Spec.		8/1		8/2		8/3		9/1		9/2		9/3

INFORMATION FOR AUTHORS

Detailed "Instructions to Authors" for *Analytica Chimica Acta* was published in Volume 289, No. 3, pp. 381–384. Free reprints of the "Instructions to Authors" of *Analytica Chimica Acta* and *Vibrational Spectroscopy* are available from the Editors or from: Elsevier Science B.V., P.O. Box 330, 1000 AH Amsterdam, The Netherlands. Telefax: (+31-20) 4852 459.

Manuscripts. The language of the journal is English. English linguistic improvement is provided as part of the normal editorial processing. Authors should submit three copies of the manuscript in clear double-spaced typing on one side of the paper only. *Vibrational Spectroscopy* also accepts papers in English only.

Rapid publication letters. *Letters* are short papers that describe innovative research. Criteria for letters are novelty, quality, significance, urgency and brevity. Submission data: max. of 2 printed pages (incl. Figs., Tables, Abstr., Refs.); short abstract (e.g., 3 lines); *no* proofs will be sent to the authors; submission on floppy disc; *no* revision will be possible.

Abstract. All papers, reviews and letters begin with an Abstract (50–250 words) which should comprise a factual account of the contents of the paper, with emphasis on new information.

Figures. Figures should be suitable for direct reproduction and as rich in contrast as possible. One original (or sharp glossy print) and two photostat (or other) copies are required. Attention should be given to line thickness, lettering (which should be kept to a minimum) and spacing on axes of graphs, to ensure suitability for reduction in size on printing. Axes of a graph should be clearly labelled, along the axes, outside the graph itself.

All figures should be numbered with Arabic numerals, and require descriptive legends which should be typed on a separate sheet of paper. Simple straight-line graphs are not acceptable, because they can readily be described in the text by means of an equation or a sentence. Claims of linearity should be supported by regression data that include slope, intercept, standard deviations of the slope and intercept, standard error and the number of data points; correlation coefficients are optional.

Photographs should be glossy prints and be as rich in contrast as possible; colour photographs cannot be accepted. Line diagrams are generally preferred to photographs of equipment. Computer outputs for reproduction as figures must be good quality on blank paper, and should preferably be submitted as glossy prints.

Nomenclature, abbreviations and symbols. In general, the recommendations of IUPAC should be followed, and attention should be given to the recommendations of the Analytical Chemistry Division in the journal *Pure and Applied Chemistry* (see also *IUPAC Compendium of Analytical Nomenclature, Definitive Rules*, 1987).

References. The references should be collected at the end of the paper, numbered in the order of their appearance in the text (*not* alphabetically) and typed on a separate sheet.

Reprints. Fifty reprints will be supplied free of charge. Additional reprints (minimum 100) can be ordered. An order form containing price quotations will be sent to the authors together with the proofs of their article.

Papers dealing with vibrational spectroscopy should be sent to: Dr J.G. Grasselli, 150 Greentree Road, Chagrin Falls, OH 44022, U.S.A. Telefax: (+1-216) 2473360 (Americas, Canada, Australia and New Zealand) or Dr J.H. van der Maas, Department of Analytical Molecular Spectrometry, Faculty of Chemistry, University of Utrecht, P.O. Box 80083, 3508 TB Utrecht, The Netherlands. Telefax: (+31-30) 518219 (all other countries).

0003-2670/94/$07.00

Flow-Through (Bio)Chemical Sensors

By **M. Valcárcel** and **M.D. Luque de Castro**, Department of Analytical Chemistry, University of Córdoba, 14004 Córdoba, Spain

Techniques and Instrumentation in Analytical Chemistry Volume 16

Flow-through sensors are more suitable than classical probe-type sensors for addressing real (non-academic) problems. The external shape and operation of flow-through (bio)chemical sensors are of great practical significance as they facilitate sample transport and conditioning, as well as calibration and sensor preparation, maintenance and regeneration, all of which result in enhanced analytical features and a wider scope of application. This is a systematic presentation of flow-through chemical and biochemical sensors based on the permanent or transient immobilization of any of the ingredients of a (bio)chemical reaction (i.e. the analyte, reagent, catalyst or product) where detection is integrated with the analytical reaction, a separation process (dialysis, gas diffusion, sorption, etc.) or both.

The book deals critically with most types of flow-through sensors, discussing their possibilities and shortcomings to provide a realistic view of the state-of-the-art in the field. The large numbers of figures, the wealth of literature references and the extensive subject index complement the text.

© 1994 332 pages Hardbound
Price: Dfl. 355.00 (US$ 202.75)
ISBN 0-444-89866-2

ELSEVIER SCIENCE

ORDER INFORMATION
ELSEVIER SCIENCE B.V.
P.O. Box 330
1000 AH Amsterdam
The Netherlands
Fax: (+31-20) 5862 845
For USA and Canada
P.O. Box 945
Madison Square Station
New York, NY 10159-0945
Fax: (212) 633 3680
US$ prices are valid only for the USA & Canada and are subject to exchange rate fluctuations; in all other countries the Dutch guilder price (Dfl.) is definitive. Customers in the European Union should add the appropriate VAT rate applicable in their country to the price(s). Books are sent postfree if prepaid.

0003-2670(19941230)299:2;1-#